Polycomb-like 2 (Mtf2/Pcl2) mediated epigenetic regulation of hematopoiesis and refractory leukemia

Harinad Maganti

This thesis is submitted to the Faculty of Graduate and Postdoctoral Studies
as a partial fulfillment of the Ph.D. program in Microbiology and Immunology.

Department of Biochemistry
Faculty of Medicine
University of Ottawa
Ottawa, Ontario
Canada

Abstract

The Polycomb Repressive Complex 2 (PRC2) epigenetically regulates gene expression by methylating lysine 27 on histone 3 (H3K27me3). While the role of PRC2 core members during hematopoiesis has been elucidated, the role of PRC2 accessory protein, Mtf2, has not been well characterized outside of mouse embryonic stem cells.

To investigate the role of Mtf2 *in vivo*, we created a gene-targeted knockout mouse model. Using this model, we discovered that Mtf2 was a critical regulator of hematopoiesis and its loss within the hematopoietic cells leads to loss of global H3K27me3 levels at the transcriptional start sites (TSS) therefore leading to the overexpression of multiple signalling networks. These findings presented in the first part of my thesis place Mtf2 as a critical regulator of hematopoiesis and expand the role of Mtf2 beyond a canonical accessory PcG protein.

While our murine studies revealed that the loss of Mtf2 did not cause leukemia in mice, our studies of MTF2 in human cells demonstrated that MTF2 deficiency within human Hematopoietic Stem and Progenitor Cells (HSPCs) causes a myelo-proliferative phenotype that is reminiscent of pre-leukemia. Furthermore, when we screened *MTF2* expression within leukemic stem cell (LSC) enriched $CD34^{+}CD38^{-}$ cells isolated from primary Acute Myeloid Leukemia (AML) patient samples at diagnosis, we observed that *MTF2* is miss-regulated in AML and its loss predicted refractory AML. Using *MTF2* knockdown (KD) transcriptomic and ChIP-seq data, we drafted *MTF2*-PRC2 Gene Regulatory Network (GRN) in human HSPCs and LSC enriched cells. Finally, using the *MTF2*-PRC2 GRN, we uncovered a direct mechanism by which *MTF2* regulates chemoresistance in AML and show that targeting this mechanism via MDM2 inhibitors sensitizes refractory AML to standard induction therapy. These findings presented in second part of my thesis

demonstrate MTF2 as a novel prognostic marker for refractory AML and provide a novel therapy that helps target MTF2 deficient refractory AML.

List of Tables

List of Figures

Tables of Contents

List of Abbreviations

AGM	aorta-gonadal-mesonephros
AML	acute myeloid leukemia
B-AML	acute myeloid leukemia with basal levels of MTF2
BasoE	basophilic erythroblast
BFU-E	burst forming-unit, erythroid
BM	bone marrow
CDKs	cyclin-dependent kinases
CFU	colony forming unit
CFU-E	colony forming unit-erythroid
CFU-G	colony forming unit-granulocyte
CFU-GEMM	colony forming unit-granulocyte, erythrocyte, macrophage, megakaryocyte
CFU-GM	colony forming unit-granulocyte, macrophage
CFU-M	colony forming unit-macrophage
ChIP	chromatin immunoprecipitation
CKIs	cyclin-dependent kinase inhibitors
CLP	common lymphoid progenitor
CML	chronic myeloid leukemia
CMP	common myeloid progenitor
Dnmts	DNA methyl transferases
ENU	N-ethyl-N-nitrosourea
Epo	erythropoietin
EryC	BM-derived orthochromatic erythroblasts

ESC	embryonic stem cell
FL	fetal liver
GMP	granulocyte-macrophage progenitor
GRN	gene regulatory network
GO	gene ontology
H2AK119ub1	ubiquitination on lysine 119 of histone 2A
H3K27me3	trimethylation on lysine 27 of histone 3
H3K36me3	trimethylation on lysine 36 of histone 3
HMTase	histone methyltransferase
Hox	homeotic
HSC	hematopoietic stem cell
HSPCs	hematopoietic stem and progenitor cells
LSC	leukemic stem cell
LSK	lineage-Sca1+cKit+
LT-HSC	long-term repopulating hematopoietic stem cell (LSK CD48-CD150+)
LTC-IC	long-term culture – initiating cell
MD-AML	MTF2 deficient acute myeloid leukemia
mESCs	mouse embryonic stem cells
MEP	megakaryocyte-erythroid progenitor
MLL	mixed lineage leukemia gene
Mtf2/Pcl2	Polycomb-like 2
PcG	Polycomb protein
Pcl	Polycomblike

PHD	plant homeodomain
PRC1	Polycomb Repressive Complex 1
PRC2	Polycomb Repressive Complex 2
PRE	Polycomb Response Element
RBC	red blood cell
ST-HSC	short-term repopulating hematopoietic stem cell (LSK CD48-CD150-)
TFs	transcription factors
TSS	transcriptional start site
YS	yolk sac

Acknowledgements

My accomplishments as a scientist are in great part due to the team of people I have the privilege of working alongside, both in the lab and behind the scenes.

First, I would like to thank my mentors Dr. William Stanford and Dr. Caryn Ito. Being new to the field, Bill and Caryn took a chance on me and helped motivate me to learn all there is about the field of HSC research. They taught me to think things through, write scientifically, and understand the mechanisms behind experiments so that I could work independently. Caryn, thank you for taking the time to teach me the various complex *in vitro* and *in vivo* experiments presented in this thesis. Bill, thank you for inspiring me to work hard and meticulously. I will always be indebted to both of you for the encouragement and counseling you continue to provide and which has helped me make the appropriate career choice.

Next, I would like to, thank all of our collaborators who made this project possible. I would like to thank Dr. Mitchell Sabloff without whom this project would not have been possible. Special thanks to the patients at the TOH who generously consented to be part of our study. I would also like to thank all of our collaborators at the Ottawa Hospital Research Institute including members of the Stem Core Facility, the Flow Cytometry Facility, the Ottawa Bioinformatics Core Facility, and the staff at the University of Ottawa Animal Care and Veterinary Services. Thank you to my advisory committee members Dr. David Allan, Dr. Marjorie Brand and Dr. Harry Atkins for their insightful discussions, helpful advice and constant support on the project. Thank you to my thesis advisory panel for taking the time to evaluate this thesis and participate in the defense examination.

Third, I would like to thank the members of the Stanford lab, past and present: I have had the pleasure to be able to work with and learn from not one, but many amazing people. Thanks Janet for being patient and teaching me the various molecular techniques presented in this thesis

as well as helping me better develop my presentation skills. I would like to thank Hani for being a great friend/colleague. Thanks to Chris and Hannah for their continued work on this project. Julien, I greatly appreciate all your help with molecular assays and statistics.

Forth, I would like to thank my parents - Subbamma and Sreenivas for inspiring me to pursue my dreams and work hard. Thank you to Ram (my brother) for being an inspirational figure in my life. I can never forget your love and support. Special thanks to Revathi (my sister in law) and to my mother for your patience and love in taking care of me and ensuring that I had everything at my disposal (especially amazing food) at all times of the day/night.

Last, but never least, thanks to my lovely wife Liliane, for your incredible support and love throughout the last 5 years of my PhD. Thank you for your support in reaching for my dreams. Your unwavering support and positive outlook continues to play an important role in helping me deal with the insanity one comes across after long hours of lab work. The unconditional love provided by you and Spotty continues to inspire me to be a better human being. I couldn't be happier to experience our next adventure together.

Chapter 1

Introduction

Epigenetics and stem cell fate decisions

Stem cells are defined by their unique ability to self-renew and differentiate into specialized, functional cells (e.g., blood cells). Tissue –resident (a.k.a., somatic or adult) stem cells are responsible for tissue homeostasis, where they divide and differentiate to replace damaged or dying cells in the various tissues, while at the same time ensuring their own self-renewal to maintain the stem cell pool. In addition to the intrinsic properties of stem cells, the stem cell decision-making processes are also influenced by external signals from their microenvironment (Drummond-Barbosa 2008, Orkin and Zon 2008). The external signals provide cues to control stem cell fate decisions in terms of proliferation or differentiation into a desired, differentiated cell. The progression from a stem cell to a terminally differentiated cell is often accompanied by significant changes in both cellular morphology and function. These changes are determined at each stage by unique gene expression patterns. Importantly, genes associated with self-renewal are repressed, while genes associated with specific cell type function are activated (Walker, Chang et al. 2010, Cabezas-Wallscheid, Klimmeck et al. 2014). Interestingly, the transcriptional activation, repression and maintenance of these cell type specific genes are regulated through an epigenetic program including chromatin modifications and covalent DNA modifications that control the accessibility of the DNA (Chronis, Fiziev et al. 2017). Therefore, epigenetics plays an important role in the controlled differentiation and maintenance of stem cells.

Transcriptional repression and Polycomb group proteins

Polycomb Group (PcG) proteins are critical epigenetic regulators that are responsible for establishing and maintaining an epigenetic program that governs cell fate decisions. The PcG proteins form complexes to regulate stem cell differentiation, cell cycle progression and other cell

functions via transcriptional repression through histone modifications (Sauvegeau and Sauvegeau 2010, Surface, Thornton et al. 2010, Radulovic, de Haan et al. 2013). PcG complexes are also responsible for the maintenance of histone modifications in differentiated cells (first described by (Struhl and Akam 1985), therefore providing epigenetic memory and ensuring terminal differentiation in fully committed cells.

The *Polycomb* gene (*Pc*) was first discovered in Drosophila melanogaster (Lewis 1978). Loss of function mutations in the *Pc* gene were shown to cause homeotic phenotypes including increased number of sex combs therefore, suggesting that multiple Hox genes were becoming activated in body regions where they should be normally silenced (Lewis 1978). Subsequently more genes with similar phenotypes were identified and collectively these genes were suggested to belong to group of repressors and were collectively termed the Polycomb group (PcG) (Kennison and Tamkun 1988). In addition to the homeotic gene repressors, genes encoding proteins which promoted the expression of Hox genes were also identified belonging to the Trithorax (*Trx*) gene family. In contrast to Pc proteins, Trx proteins were shown in Drosophila to promote the expression of *Hox* genes (Ingham, Pinchin et al. 1985). Thus, the highly conserved PcG and Trx group (TrxG) proteins work antagonistically and regulate several hundred developmentally important genes (Kennison and Tamkun 1988, Simon and Kingston 2013, Steffen and Ringrose 2014). The repertoire of target genes regulated by PcG and TrxG are well conserved in flies and mammals.

The Polycomb Repressive Complex 2 (PRC2)

In mammals, the PcG complexes are broadly classified into two groups, Polycomb Repressive Complex 1 (PRC1) and Polycomb Repressive Complex 2 (PRC2). The PRC2 complex

consists of core and accessory complex proteins. The core complex proteins are found in 1:1:1 ratio (Smits, Jansen et al. 2013) and they include Ezh1/2, Suz12 and Eed (Faust, Schumacher et al. 1995, O'Carroll, Erhardt et al. 2001, Kuzmichev, Nishioka et al. 2002, Pasini, Bracken et al. 2004) (Figure 1.2). Ezh1/2 proteins contain the SET domain which make them the catalytic subunit of the PRC2 complex. Ezh1 and Ezh2 are mutually exclusive within the PRC2 complex and play a complementary role in stem cells. The loss of Suz12 within stem cells leads to post-translational loss of Ezh1/2 and Eed (Pasini, Bracken et al. 2004, Xie, Xu et al. 2014). Taken together these results show that Suz12 helps maintain the PRC2 complex stability (Cao and Zhang 2004).

The PRC2 complex mediates tri-methylation of lysine 27 on histone 3 (H3K27me3) by its enzymatic core component Ezh1/2 (Levine, King et al. 2004, Lund and van Lohuizen 2004) (Figure 1.1). Once the H3K27me3 repressive marks are laid down, the PRC1 complex recognizes the H3K27me3 mark via its Cbx subunit and then uses its Ring (2,3,6-8) subunit to ubiquitinate H2A Lysine119 (H2AK119u1), leading to chromatin compaction and repression of downstream target genes (de Napoles, Mermoud et al. 2004, Wang, Wang et al. 2004) (Figure 1.2). Recent evidence suggests that multiple non-cononical PRC1 complexes exist. In these PRC1 variants, the Cbx protein is replaced with Rybp/Yap2 protein. Interestingly, the Rybp/Yap2 containing non-cononical PRC1 complexes deposit H2AK119ub1 marks independent of PRC2-mediated H3K27me3 marks (Tavares, Dimitrova et al. 2012), which then leads to the recruitment of the PRC2 (Blackledge, Farcas et al. 2014).

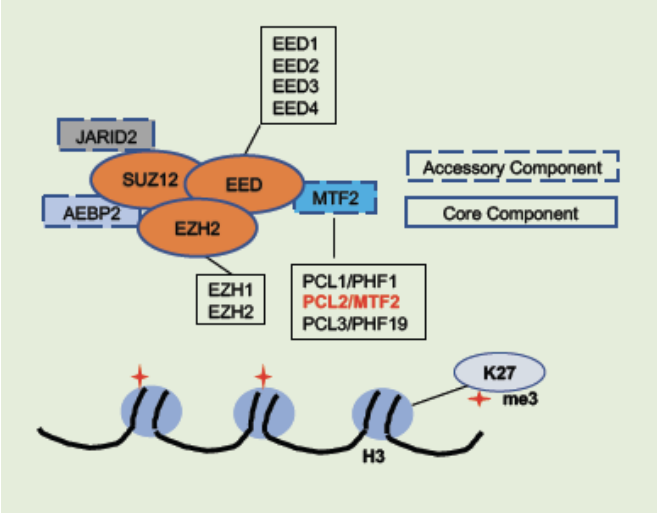

Figure 1.1. The Polycomb Repressive Complex 2 (PRC2) consists of several core and accessory proteins. *The core proteins include Ezh2, Suz12 and Eed and are required for the stability and functioning of the PRC2 complex. Multiple isoforms of each protein exist giving rise multiple PRC2 complex variants that may have unique functions. (adapted from Sauvageau and Sauvageau 2010))*

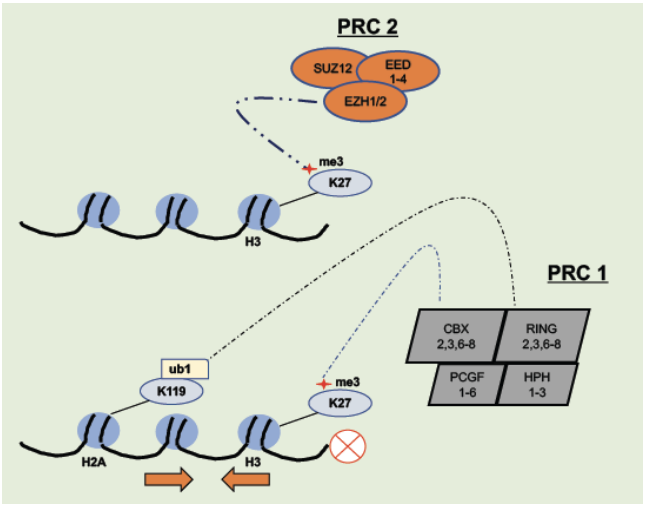

Figure 1.2. PRC2 mediated recruitment of PRC1*. Once Polycomb Repressive Complex 2 (PRC2) is bound to DNA, EZH2 lays down H3K27 marks, that act as a signal for the recruitment of Polycomb Repressive Complex 1 (PRC1). The RING protein then lays down the H2AK119ub1 marks that ultimately lead to gene repression. (adapted from Sauvageau and Sauvageau 2010))*

Polycomb accessory proteins

In addition to PRC2 core members, mass spectrometry studies have identified several proteins including Pcl2/Mtf2, Jarid2 and Aebp2 that associate with PRC2 at sub-stoichiometric ratios (Figure 1.1). Since these proteins are not found in all PRC2 complexes they have been termed as PRC2 accessory proteins. While the knock down of PRC2 core proteins (Ezh1/2, Suz12 and Eed) prevents PRC2 complex formation and triggers global loss of H3K27me3 levels, studies to date have shown that the knock down of the accessory proteins does not affect the PRC2 complex formation or affect the global H3K27me3 levels within ESCs (Walker, Chang et al. 2010, Grijzenhout, Godwin et al. 2016). Interestingly, several studies have revealed that core complex members such as Ezh2, Suz12 and Eed, do not have DNA-binding capacity. Therefore, PRC2 accessory proteins with DNA binding capacity, such as Jarid2 and members of the Polycomb-like (Pcl) family (Kim, Kraus et al. 2003, Walker, Ohishi et al. 2007) are thought to play a critical role in the recruitment of the PRC2 complex to chromatin and help increase the Histone Methyl Transferase (HMTase) activity of the complex (Peng, Valouev et al. 2009, Pasini, Cloos et al. 2010, Sauvegeau and Sauvegeau 2010, Surface, Thornton et al. 2010, Walker, Chang et al. 2010, Walker, Manias et al. 2011).

Aebp2

Adipocyte Enhancer-Binding Protein 2 (Aebp2) is a Zinc-finger protein that was identified via mass spectrometry and was found to be in complex with Ezh2, Suz12 and Eed within mouse embryonic stem cells (ESCs) (Cao and Zhang 2004, Grijzenhout, Godwin et al. 2016). The homozygous deletion of Aebp2 leads to embryonic lethality and the mice die at embryonic 15.5 (e15.5). Knocking out Aebp2 in mice leads to a Trithorax phenotype (anterior homeotic

transformations) in the embryos and chromatin immunoprecipitation-coupled with next generation sequencing (ChIP-seq) results showed that Aebp2 is enriched at PRC2 targets. However, loss of Aebp2 within ESCs did not affect global loss of H3K27me3 levels (Grijzenhout, Godwin et al. 2016).

Jarid2

Jarid2/*Jumonji* was discovered in 1995 as a regulator of neural development via a gene trap mutagenesis screen in mice (Takeuchi, Yamazaki et al. 1995). The gene was named *Jumonji* because of the cruciform shape of neural grooves (Jumonji means cruciform in Japanese) observed in *Jarid2*-targeted embryos. Jarid2 is required for ESC differentiation and its depletion leads to loss of PRC2 biding at target sites (Shen, Kim et al. 2009, Landeira, Sauer et al. 2010). Outside of the ES model system Jarid2 has been implicated in epidermal and muscle cell differentiation (Mejetta, Morey et al. 2011, Londhe and Davie 2013). In mice *Jarid2* is expressed in multiple tissues including the brain, heart, spinal cord, liver and thymus (Takeuchi, Yamazaki et al. 1995, Jung, Mysliwiec et al. 2005). Mouse models with *Jarid2* deficiency show multiple range of phenotypes and the severity is dependent on the mouse background in which chimeras were made and backcrossed. For example, embryos generated from Jarid2 null cells show defects in liver, thymus, neural, heart and definitive hematopoiesis (Motoyama, Kitajima et al. 1997, Takeuchi, Kojima et al. 1999, Toyoda, Shirato et al. 2003, Takahashi, Kojima et al. 2004, Takahashi, Kojima et al. 2007). Depending on the mouse strain, loss of *Jarid2* causes embryonic lethality between 10.5 – 15.5 days of gestation. In humans, genetic mutations within *JARID2* have been associated with nonsyndromic cleft lip (Scapoli, Martinelli et al. 2010), spina bifida and congenital heart defects (Liu, Chen et al. 2009), leukemia and schizophrenia (Pedrosa, Ye et al. 2007). Interestingly,

Jarid2 appears to be contained in PRC2 complexes devoid of Polycomblike accessory proteins, these results suggest that Jarid2 and Polycomblike proteins may be mutually exclusive (Peng, Valouev et al. 2009, Landeira, Sauer et al. 2010, Li, Margueron et al. 2010).

Polycomblike proteins

The Polycomblike (*Pcl*) gene was identified during a polycomb mutation modifier screen in Drosophila melanogaster (Duncan 1982). In Drosophila, similar to the gene *Polycomb (Pc), Pcl* is a transcriptional repressor. *Pcl* is required for the recruitment of Enhancer of zeste and the loss of *Pcl* leads to altered body patterning in flies (Duncan 1982, Nekrasov, Klymenko et al. 2007, Savla, Benes et al. 2008). In mammals, there are three mammalian homologs of *Pcl*: *Phf1*/*Pcl1*, *,Mtf2*/*Pcl2 and Phf19*/*Pcl3*. All the Pcl proteins contain TUDOR domains (facilitate protein-protein interactions and bind to H3K27me3 marks) and PHD domains (DNA-binding domains) and have been shown to play a vital role in recruitment of PRC2 to target sites (Casanova, Preissner et al. 2011; Cai, Rothbart et al. 2013, (Ballare, Lange et al. 2012, Brien, Gambero et al. 2012, Hunkapiller, Shen et al. 2012, Musselman, Avvakumov et al. 2012).

Phf1/Pcl1and Phf19/Pcl3

PHD finger protein 1 (*Phf1*) is an accessory member of the PRC2 complex. *Phf1*/*Pcl1* deficiency has been shown to result in reduction in H3K27me3 levels and PRC2 occupancy at specific HOX gene loci (Cao, Wang et al. 2008, Sarma, Margueron et al. 2008). While the other *Pcl* proteins are highly expressed within cycling cells, *Phf1*/*Pcl1* is highly expressed within quiescent cells, where it has been shown to directly interact and stabilize p53 via a chromatin-independent function (Brien, Healy et al. 2015). Furthermore, *Phf1*/*Pcl1* has also been implicated

in DNA damage response, where it has been shown to be recruited to site of double strand breaks (DSBs) and promote non-homologous end joining (NHEJ) repair pathway (Hong, Jiang et al. 2008). The PRC2-independent and dependent roles of *Phf1*/*Pcl1* are yet to be completely deciphered and further study is required.

Phf19/*Pcl3* is over-expressed in many cancers and has been shown to mediate PRC2 complex targeting and H3K27me3 spreading (Sauvegeau and Sauvegeau 2010, Cai, Rothbart et al. 2013). Promoter occupancy data have revealed that *Phf19* binding significantly overlaps with *Suz12* and H3K27me3 binding and its loss causes loss of *Suz12* and H3K27me3 binding (Hunkapiller, Shen et al. 2012). Furthermore, in ESCs Phf19/Pcl1 has been shown to directly interact with the methylated histone H3 Lys36 (H3K36me) marks and recruit the PRC2 complex to target sites. H3K36me3 is an active mark laid down by TrxG proteins at sites of active chromatin (Ballare, Lange et al. 2012, Brien, Gambero et al. 2012).

Pcl2/Mtf2

Polycomb like 2 (*Pcl2*/*Mtf2*) is the third homolog of the *Pcl* encoded in vertebrates and mammals (Coulson, Robert et al. 1998, Kawakami, Mitsunaga et al. 1998, Kitaguchi, Nakata et al. 2001, Ballare, Lange et al. 2012). In mammals, *Pcl2*/*Mtf2* is alternatively spliced into 3 isoforms (Mtf2A, Mtf2B and Mtf2C), which are differentially expressed within distinct tissues (Wang, He et al. 2007). While Mtf2A and Mtf2B contain a Tudor domain and two tandem Plant homeodomain (PHD) fingers, the shortest isoform Mtf2C lacks the TUDOR domain (Walker, Chang et al. 2010) (Figure 1.3).

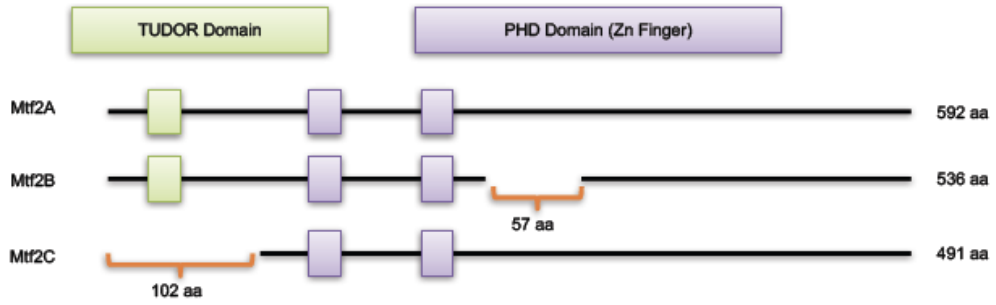

Figure 1.3. Mtf2 is alternatively spliced into 3 isoforms: Mtf2A, Mtf2B and Mtf2C. *While the two longest isoforms of Mtf2 (A and B) contain both the TUDOR and PHD domains, the shortest isoform (C) only contains the PHD domain. The Tudor domain is responsible for targeting associated protein towards targeted sites, while the PHD domain is associated with DNA binding.*

Pcl2/Mtf2 is a critical regulator of embryonic stem cell fate

In ESCs, Pcl2/Mtf2 recruits and facilitates the binding of PRC2 at target gene loci using its C-terminal PHD domain (Casanova, Preissner et al. 2011). The Stanford lab discovered *Pcl2/Mtf2* as a critical regulator of mouse ESC (mESC) fate. Loss of *Pcl2/Mtf2* in mESCs led to enhanced self-renewal and increased proliferation. Using *Pcl2/Mtf2* knockdown transcriptomic and ChIP-seq data, we drafted a Mtf2-PRC2 gene regulatory network in mESCs that showed that Mtf2 was directly repressing a core set of pluripotency and self-renewal factors within mESCs and its loss led to the constitutive activation of the core pluripotency (*Oct4*, *Sox2* and *Nanog*) and self-renewal (*Klf4*, *Foxd3* and *Tbx3*) factors (Figure 1.4) (Walker, Chang et al. 2010). Loss of Pcl2/Mtf2 within ESCs does not affect the global levels of H3K27me3 (Walker, Chang et al. 2010) thus reflecting its role as an accessory PRC2 member within mESCs. Interestingly although Pcl2/Mtf2 and Phf19/Pcl3 exist in different PRC2 complexes, they bind to many of the same PRC2 targets within ESCs (Hunkapiller, Shen et al. 2012). Since *Phf19/Pcl3* is abnormally expressed in many cancers, this raises many important questions relating to the potential role of *Pcl2/Mtf2* in

cancer. While *Pcl2/Mtf2* has been well studied within ESCs, its role outside of this model system is not known.

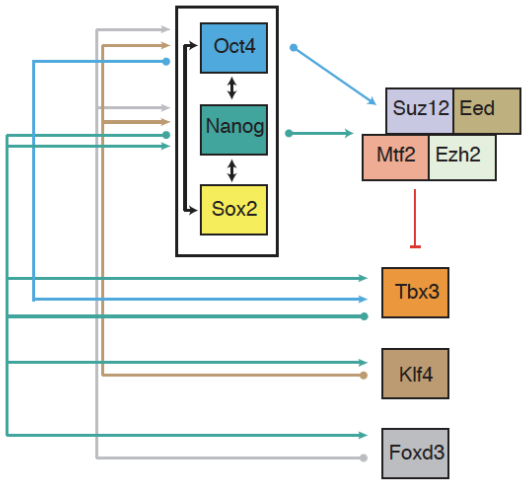

Figure 1.4. Pcl2/Mtf2 regulated pluripotency gene regulatory network in mESCs*. Mtf2/Pcl2-PRC2 represses genes critical for self-renewal (such as Klf4, Foxd3 and Tbx3) that are activated by the core pluripotency factors Oct4, Sox2 and Nanog, and in turn activate the core pluripotency factors in a feed-forward network (Walker, Chang et al. 2010).*

Gene Regulatory Networks (GRNs)

Gene expression is a well-regulated dynamic intracellular process that is controlled by GRNs. GRNs are hardwired genetic regulatory circuits that control the expression of genes both spatially and temporally. GRN are constituted by many simple recurring patterns of interactions between factors and their target genes called 'network motifs'. The frequencies of these 'network motifs' are significantly higher than those found in randomized interactions and have been shown to be recurrent amongst widely varying organisms. The feed-forward motif is an example of a 'network motif' that has been well characterized (Milo, Shen-Orr et al. 2002). The Stanford lab drafted a feed-forward circuit of Mtf2 in mESC (Walker, Chang et al. 2010). Within the feed-

forward loop in mESCs the Mtf2-PRC2 complex acts as a rheostat switch, fine-tuning the expression of core self-renewal and pluripotency factors (Figure 1.4). Loss of Mtf2 constitutively turns on the feed-forward loop that results in the continuous expression of the core self-renewal and pluripotency factors thus making the cells refractory to differentiation.

The role of *Pcl2/Mtf2 In vivo*

While chicken *Pcl2/Mtf2* is essential for the left-right asymmetry of the developing embryo, partial loss of function (hypomorphic) *Pcl2/Mtf2* gene trap mice exhibit pleiotropic defects such as posterior transformation of axial skeleton, growth retardation, hydrocephaly, hunchback and incisor abnormalities (Wang, Yu et al. 2004, Wang, He et al. 2007, Li, Isono et al. 2011). These skeletal transformations have been attributed to changes in master cell cycle regulators such as Cdkn2a and hometotic gene expression. The Stanford lab had previously generated a hypomorphic *Pcl2/Mtf2* gene trap mutant mouse which displayed severe growth impairment, loss of subcutaneous fat, situs inversus, hair cycling defects (Stanford Lab, unpublished). Furthermore, these mice died by 3 months of age and showed lymph node enlargement, bordering on lymphoma.

Polycomb Response Elements mediated targeting of PRC2

Recruitment of the PRC2 complex to target genes has been well studied in *Drosophila* and Polycomb response elements (PREs) have been identified in DNA loci where PRC2 members are recruited. Invertebrate PREs are not a simple conserved sequence, but contain multiple PHO, Zeste and GAGA binding sites. Despite the abundance of genome-wide promoter occupancy data for each of the PRC2 proteins, identification of PREs in mammalian cells has proven unsuccessful. One potential mammalian targeting factor is YY1 (PHO homolog) has been previously shown to

have some success in predicting PRC2 binding (Sing, Pannell et al. 2009, Woo, Kharchenko et al. 2010). However, only two instances have been identified and hence it is difficult to decipher any rules for mammalian PREs or conclude whether this is a general mechanism of recruitment.

Accessory proteins mediated targeting of PRC2

Recent evidence suggests that the PRC2 accessory proteins such as Jarid2, Phf1/Pcl1, Phf19/Pcl3, Mtf2/Pcl2 play an important role in recruiting the PRC2 complex to target sites within the mammalian cells. Analysis of the ChIP-sequencing data of Phf19/Pcl3 and Jarid2 in ESCs revealed that the binding of both these proteins are enriched at CpG-rich regions (Pereira, Piccolo et al. 2010, Hunkapiller, Shen et al. 2012). Furthermore, *in vitro* peptide pull down assays have shown that the TUDOR domain in Phf1/Pcl1 and Phf19/Pcl3 binds to H3K36me3 marks (Brien, Gambero et al. 2012) with high affinity (but not Mtf2/Pcl2). This interaction has been shown to be required for the deposition and spreading of PRC2 mediated H3K27me3 marks within ESCs (Ballare, Lange et al. 2012, Cai, Rothbart et al. 2013). It is important to note that most of these studies had been performed in ESCs and whether these mechanisms are conserved within other mammalian cells is yet to be tested.

Hematopoiesis

Hematopoiesis is a dynamic process that provides continuous replenishment of mature blood cells through controlled differentiation and expansion of a hierarchical array of multi-potential, bi-potential and committed progenitors. This developmental cascade is maintained by a heterogeneous hematopoietic stem cell (HSC) pool comprised of subpopulations with varying multi-lineage differentiation and self-renewal potential (Dykstra, Kent et al. 2007, Benveniste,

Frelin et al. 2010, Challen, Boles et al. 2010). HSCs are usually quiescent but can be activated to self-renew or differentiate by specific signaling cues that are not well understood but involve a complex regulation of cell autonomous (transcription and epigenetic factors) and non-cell autonomous (cytokines, chemokines) mechanisms reviewed in (Orkin and Zon 2008). The phenotype and function of distinct stages of hematopoietic differentiation have been well characterized and can be isolated at high purity by multi-color fluorescence activated cell sorting (FACS) (Kondo, Weissman et al. 1997, Doulatov, Notta et al. 2010). While hematopoietic development is well characterized, the mechanisms governing differentiation are far from being fully understood and disruption of this tightly regulated process by genetic or epigenetic alterations results in hematopoietic dysfunctions manifested as cytopenia, anemia, polycythemia, leukemia, or lymphoma.

Hematopoiesis during development

During development in mammals, hematopoiesis occurs in two waves: the primitive wave and the definitive wave. A common model suggests that hematopoiesis begins in the extraembryonic yolk sac (YS). Cell derived from the YS then enter circulation and colonize aorta-gonada-mesonephros (AGM) followed by the placenta, fetal liver and finally the bone marrow (Galloway and Zon 2003). In mice, during e7-7.5 the mesoderm progenitors in the YS differentiate to form multipotent precursor cells that can differentiate into both hematopoietic and endothelial cells. These multipotent precursor cells are called hemangioblasts or hemogenic endothelial cells and they form blood islands including the endothelium, monocytes and primitive erythroblasts. The primitive erythroblasts undergo asymmetric cell divisions and predominantly give rise to erythrocytes and macrophages. The primitive erythroblasts are not pluripotent and have a limited

time span and their primary purpose is to produce erythroid cells to provide oxygen to the developing tissues (Yoder and Hiatt 1997, Yoder, Hiatt et al. 1997). By e8.5-9 the maturing erythroid cells enter embryonic circulation and colonize other sites of hematopoiesis.

Definitive hematopoiesis in the mouse starts between e10-11. During e10 the first set of definitive HSCs emerge from the dorsal aortic endothelium in the AGM (Muller, Medvinsky et al. 1994, Boisset, van Cappellen et al. 2010). Between e10-11 the HSCs colonize the AGM, placenta and umbilical arteries and begin to give to rise to pluripotent precursor cells. The HSCs along with the precursor cells colonize the fetal liver and by e11, the fetal liver is the primary site of hematopoiesis in the developing embryo. These HSCs are characterized by the expression of cell surface markers $CD45^+$, $Sca1^+$, $c\text{-}kit^+$, $CD34^+$ and are capable of long-term self-renewal and multi-lineage differentiation and can repopulate the adult mice (Sanchez, Holmes et al. 1996, Sanchez, Bockamp et al. 2001, North, de Bruijn et al. 2002, Ling, Ottersbach et al. 2004). Just prior to the birth of the mouse fetus, HSCs colonize the bone marrow. The fetal liver HSCs continue to cycle rapidly until 4 weeks after homing to the bone marrow upon which a marked reduction in expression of *Sox17* occurs, upon which 95% of the bone marrow HSCs become quiescent (Cheshier, Morrison et al. 1999, Bowie, McKnight et al. 2006, Kiel, Radice et al. 2007). The HSCs within the bone marrow undergo both differentiation and self-renewal processes, thereby ensuring their own self-renewal and giving rise to progenitor cells that become increasingly lineage restricted and ultimately differentiate into all lineages of mature blood cells (erythrocytes, platelets, myeloid and lymphoid cells).

PRC2 mediated cell cycle regulation of hematopoiesis

The activity of HSCs over the life time of an organism is dynamic and reflects the needs of the organism at various developmental stages. For example, during fetal life, the role of HSCs is to provide large number of red blood cells for oxygen transport. In line with this 95% of the fetal liver HSCs are cycling. In contrast only 5% of the HSCs within the adult bone marrow are cycling (defined as S,G_2, or M phases) at any one time (Cheshier, Morrison et al. 1999, Bowie, McKnight et al. 2006, Kiel, Radice et al. 2007). Despite the great difference in the frequency by which fetal and adult HSCs cycle, once the cells enter cell cycle, they transit through it at the same rate (Nygren, Bryder et al. 2006). The disruption of HSC quiescence within adult bone marrow leads to defects in HSC self-renewal and results in HSC exhaustion (Orford and Scadden 2008). These findings taken together underscore the importance of complex network regulatory mechanisms that enforce the balance between HSC quiescence and proliferation.

HSC quiescence at the molecular level is controlled by cyclin dependent kinases (CDK). The CDKs are further controlled by cyclin dependent kinase inhibitors (CKI). Members belonging to both the CDKs and CKIs are transcriptionally regulated by PRC2 in HSCs. Recent studies have revealed that Cdk4/6 control the progression of HSCs through G1 phase, while *Cdk2* activation occurs in late G1. While single knockouts of *Cdk4* and *Cdk6* does not affect HSCs, the dual knock out of Cdk4/6 leads to erythropoiesis and embryonic lethality (Malumbres, Sotillo et al. 2004). Interestingly, the same phenotype is also achieved upon triple knockdown of CCND1/2/3 (Malumbres, Sotillo et al. 2004). The overexpression of *Cdk6* has been shown to prime quiescent HSCs towards cycling. These results taken together suggest that several components of the cell cycle have overlapping roles and compensate in each other's absence. ChIP-sequencing studies from our lab have shown that several of the CDK proteins are direct targets of PRC2 (Stanford lab

unpublished data). Some of the well documented PRC2 targets belonging to the CKI group of proteins are INK4 family. While the knockout of *p16*^{INK4a} (*Cdkn2a*) leads to HSC defects with aging (Serrano, Lee et al. 1996, Janzen, Hake et al. 2006), the knockout of *p18*^{INK4c} (*Cdkn2c*) increases HSC self-renewal (Yuan, Shen et al. 2004, Yu, Alder et al. 2006). Furthermore, inhibition of classical PRC2 target CKIs from the CIP/KIP family such as *p21*^{CIP} (*Cdkn1a*) (Cheng, Rodrigues et al. 2000) and *p57*^{KIP2} (*Cdkn1c*), leads to reduction in HSC quiescence (Matsumoto, Takeishi et al. 2011). These findings taken together show that the PRC2 plays an important role in HSCs by enforcing a balance between cycling and quiescence.

PRC2 hematopoietic mouse model phenotypes

As mentioned previously, core PRC2 members are essential for early embryonic development. Studies show that *Suz12*, *Ezh2* and *Eed* knockouts are lethal early post-implantation (e7.5-e8.5) (Faust, Schumacher et al. 1995, O'Carroll, Erhardt et al. 2001, Pasini, Bracken et al. 2004). PRC2 has also been shown to play critical roles in hematopoiesis. Mice with an ENU-induced hypomorphic mutation in *Suz12* had enhanced hematopoietic stem cell (HSC) activity (Majewski, Blewitt et al. 2008). Conditional ablation in the hematopoietic system using Cre drivers has shown a critical role for *Ezh2* in early B cell development (Su, Basavaraj et al. 2003) and fetal HSCs, although Ezh2 is dispensable in adult HSCs through compensatory Ezh1 (Mochizuki-Kashio, Mishima et al. 2011). Additionally, both over- and under-expression of PRC2 members *Ezh2* and *Suz12* have been associated with various types of cancers (Sauvegeau and Sauvegeau 2010). Ectopic expression of *Ezh2* also leads to myeloproliferative disorder in mice (Herrera-Merchan, Arranz et al. 2012). Down-regulation of *Ezh2* can attenuate *MLL-AF9* driven Acute Myeloid Leukemia (AML) (Tanaka, Miyagi et al. 2012), although ablation of *Ezh2* promotes

lymphoid transformation (Beguelin, Popovic et al. 2013). In contrast to the role of core proteins, PRC2 accessory proteins, such as Jarid2 required for early differentiation, but are critical for later embryonic development. *Jarid2* knockout mice die at e11.5-e15.5 and display neural, cardiac, liver and hematopoietic defects including anemia (Takeuchi, Yamazaki et al. 1995, Motoyama, Kitajima et al. 1997, Jung, Mysliwiec et al. 2005) although strain-specific defects are observed.

PRC2 and leukemia

Genome-wide DNA hypomethylation and regionalized promoter hypermethylation leads to genomic instability (Chen, Pettersson et al. 1998, Tuck-Muller, Narayan et al. 2000) and repression of tumor-suppressor genes, respectively (Luczak and Jagodzinski 2006). Methylation- and histone-modifying drugs have the capacity to inhibit malignancy in a number of cancer types as well as myelodysplastic syndromes (MDS) (Ptak and Petronis 2008). EZH2 inhibitors have shown promise in treating MLL rearranged leukemia. H3K27me3 is associated with DNA hypermethylated promoters that are transcriptionally repressed in adult cancers (McGarvey, Fahrner et al. 2006, Schlesinger, Straussman et al. 2007). Recent evidence shows that PRC2 expression level is required within a specific window in the hematopoietic system, as over-expression and loss-of-expression both result in leukemogenesis. For example, missense mutations and deletions in *EZH2* are associated with AML (Ernst, Chase et al. 2010, Morin, Johnson et al. 2010, Nikoloski, Langemeijer et al. 2010), while *EZH2* over-expression has been reported in MDS patients, including MDS patients that progress to AML (Xu, Li et al. 2011).

Acute Myeloid Leukemia

AML is a heterogeneous group of myeloid lineage malignancies that is characterized by

the accumulation of immature blast cells in the bone marrow. AML is one of the most common adult blood neoplasm and is one of the most lethal cancers. The frontline treatment for AML in patients under the age of 65 years is induction therapy (Cytarabine and either Idarubicin or Daunorubicin), which has not changed over the past 30 years. While treatment for AML has largely been the same, an area that has dramatically advanced is the identification of biomarkers. The advancements of sequencing technologies over the past decade have increased our understanding of AML genetics. Next-generation, whole-genome sequencing has uncovered several recurrent somatic mutations that better define the landscape of AML genomics and predict patient survival. Interestingly, these studies have revealed that the epigenetic modifiers (TET2, DNMT3A, IDH1/2) are the most commonly mutated genes within AML and that mutations within these genes predict poor over-all survival (Walter, Shen et al. 2012, Cancer Genome Atlas Research, Ley et al. 2013). This enhanced understanding of AML genomics has allowed us to establish prognostic relevance for recurrent cytogenetics, which enables AML patients to be stratified into 4 European Leukemia Net (ELN) (ELN) risk profiles (Favorable, Intermediate-I, Intermediate-II and Adverse) (Dohner, Estey et al. 2017). Despite these advances, 20% of AML patients do not respond to standard induction therapy and therefore are classified as refractory. Within the patients that do respond, 40% of AML patients relapse within 5 years and are often refractory to induction therapy. Patients with refractory AML have very poor survival rates and often die within the first year. Surprisingly, many of these patients fall into the intermediate or favorable categories, thus indicating that the AML risk categories have limited ability to predict which patients will or will not respond to induction chemotherapy. Thus, there is an urgent need to discover new molecular biomarkers that can predict refractory AML with better accuracy and identify drug targets that can used to identify novel therapeutics.

Differences between mouse and human hematopoietic cell fate decisions

While the mouse provides a powerful, invaluable model to understand the complex molecular mechanisms that govern human hematopoiesis, important differences exist between murine and human hematopoietic systems (Doulatov, Notta et al. 2010). For example, the mouse and human HSCs present different set of cell surface antigens. While the murine HSCs can be enriched to a frequency of 1 in 5 using Lineage-negative (Lin^-) $Sca\text{-}1^+Kit^+$ $CD150^+CD48^-$ surface antigens (Kiel, Yilmaz et al. 2005), the human HSCs are enriched 1 in 10 based on $Rho^{lo}CD34^+CD38^-CD45RA^-CD49f^+CD90^+$ cell surface antigens (Notta, Doulatov et al. 2011). Furthermore, a common lymphocyte progenitor subpopulation exists in the mouse hematopoietic hierarchy with restricted lymphoid differentiation potential whereas a multi-lymphoid progenitor exists in humans with lymphoid and also limited myeloid differentiation potential (Kondo, Weissman et al. 1997, Akashi, Traver et al. 2000, Doulatov, Notta et al. 2010) (Figure 1.5).

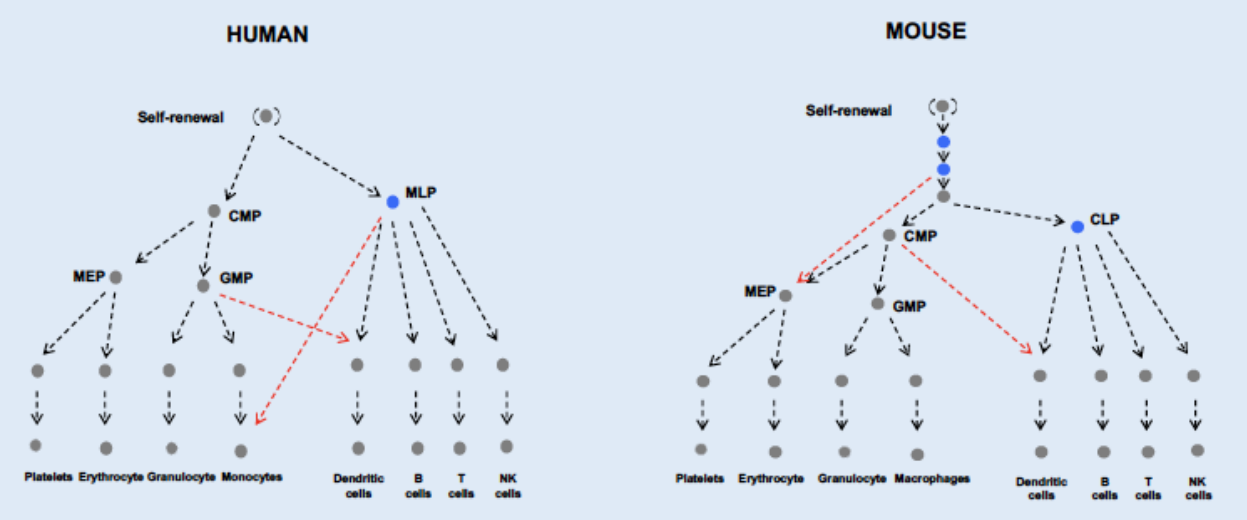

Figure 1.5. Hematopoietic lineage determination in mice is different to the one observed in the human hematopoietic system. *The differences in lineage determination between mouse and human, are represented in represented in blue and red.*

In addition, murine and human HSCs appear to have different self-renewal properties; for example, overexpressing HoxB4 causes a 40-fold expansion of murine HSC, but only a modest 2.5-fold expansion of human HSC (Antonchuk, Sauvageau et al. 2002, Amsellem, Pflumio et al. 2003). Furthermore, while the loss of *Pcl2/Mtf2* expression within murine HSPCs affects erythroid differentiation, increased lymphoid differentiation and HSC self-renewal (discussed in detail in chapter 2), PCL2/MTF2 deficient HSPCs give rise to increased number of myeloid progenitor cells in *in vitro* clonogenic assays (Figure 1.6 A,B). Furthermore, competitive transplant *in vivo* assays revealed that PCL2/MTF2 deficient HSPCs out compete the wild type HSPCs (Figure 1.6 D), have a higher proliferative index (Figure 1.6 E) and give rise to more myeloid cells (Figure 1.6 F) (Stanford lab unpublished data).

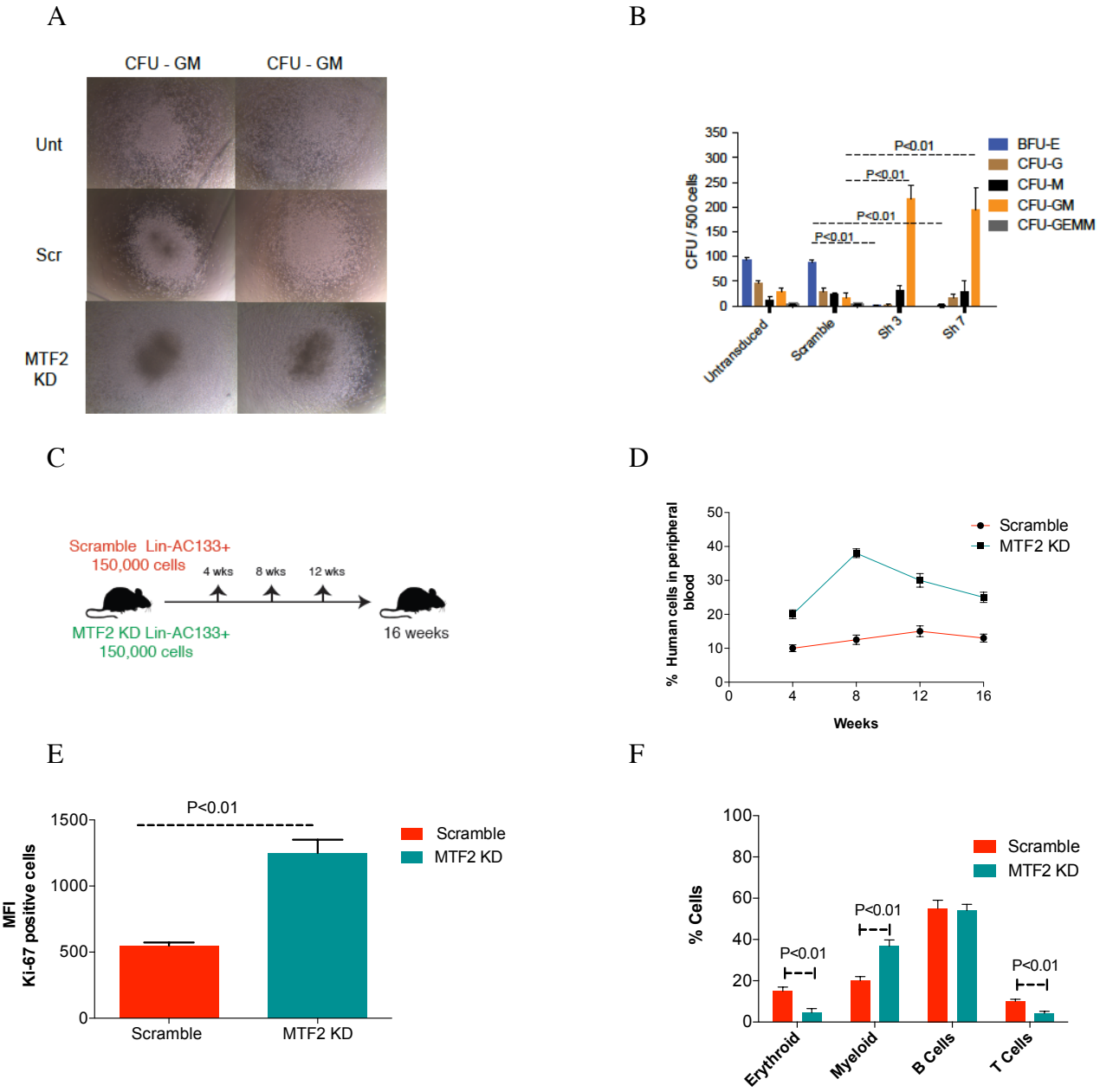

Figure 1.6. MTF2 loss within umbilical cord blood isolated human HSPCs causes a myeloproliferative phenotype. *(A,B) Clonogenic assays showed that loss of MTF2 led to increased number of proliferative Granulocyte-Macrophage progenitor (CFU-GM) colonies and fewer erythroid, granulocyte colonies, macrophage colonies (BFU-E, CFU-G, CFU-M, respectively) and more CFU-GM colonies. (C) Schematic showing repopulation experiment using scramble transduced (RFP) and MTF2 KD (GFP) Hematopoietic stem and progenitor cells (HSPCs). (D) Percentage of MTF2 KD HSPC derived cells in the peripheral blood of recipient animals were found to be significantly more compared to the scramble transduced HSPC derived*

cells. (E) MTF2 KD HSPC derived cells in the peripheral blood had higher proliferative index compared to scramble transduced HSPC derived cells. (F) MTF2 deficient HSPCs give rise to more myeloid, fewer erythroid and lymphoid cells 16 weeks post-transplantation into NOD scid gamma (NSG) mice.

Rationale and overview

The Stanford lab previously identified *Pcl2*/*Mtf2* as a critical regulator of mouse ESC fate (Walker, Chang et al. 2010). Loss of *Mtf2* in mESCs led to enhanced self-renewal and increased proliferation. Using *Mtf2* knockdown (KD) transcriptomic and ChIP-seq data, we drafted the Mtf2-PRC2 Gene Regulatory Network (GRN) in ESCs (Walker, Chang et al. 2010). Gene Ontology (GO) analysis of this transcriptome data showed that *Mtf2* represses the expression of a number of oncogenes involved in AML.

Although, Mtf2 is well-studied in the ESC model system, it role in homeostasis and disease states is not well understood. Analysis of tissue array datasets revealed that during development, in mice *Mtf2* was highly expressed in the YS and FL both of which are sites of hematopoiesis. These findings taken together suggested that Mtf2 may play an important role in hematopoiesis. Therefore, using a gene-targeting approach we assessed the role of Mtf2 in embryonic hematopoietic development using a *Mtf2*$^{-/-}$ mouse model. Using an unbiased systems biology approach, we identified a hematopoietic-specific Mtf2-PRC2 GRN containing multiple modules that explain the functional hematopoietic phenotypes observed. Through work described in chapter 2 we uncovered novel pathways regulated by Mtf2 in the murine hematopoietic system.

Deep sequencing has revealed that epigenetic modifiers are the most mutated genes in Acute Myeloid Leukemia (AML) (Cancer Genome Atlas Research, Ley et al. 2013, Papaemmanuil, Gerstung et al. 2016). Furthermore, our data from *in vitro* clonogenic and *in vivo* competitive transplant assays showed that loss of MTF2 within human HSPCs caused a myelo-

proliferative phenotype (discussed above) and provide a competitive advantage (> 2 fold) over wild type cells, a phenotype commonly observed in pre-leukemic clones isolated from AML patients (Shlush, Zandi et al. 2014). Therefore, to test whether MTF2 plays a role in AML for my PhD thesis project, I pursued the following:

Overarching hypothesis

Loss of MTF2 changes the behaviour of human hematopoietic stem and progenitor cells (HSPCs) such that they are highly susceptible to leukemogenesis

Specific Aims:

Aim1: Determine the effect of manipulating *MTF2* expression in human HSPCs.

Aim2: Using a systems biology approach, dissect the molecular function of MTF2-PRC2 in human HSPCs.

Aim3: Determine the mechanisms by which MTF2 expression is altered in AML patients.

Chapter 2

Janet L. Manias Rothberg*, Harinad B. Maganti*, Hani Jrade, Christopher J. Porter, Gareth A. Palidwor, Christopher Cafariello, Theodore J. Perkins, Robert F. Paulson,Caryn Y. Ito, William L. Stanford. **Mtf2 dynamically regulates Wnt and Hippo signaling to control hematopoiesis**

*Equal contributions

Author contributions: JMR, HBM, along with CI and WLS, conceptualized experiments. JMR conducted all *in vivo* experiments. HBM assisted in conducting the *in vivo* experiments. HBM conducted all the in vitro experiments, including the *in vitro* functional validation experiments. HJ independently analyzed and interpreted the *in vitro* functional validation results. JMR and HBM analyzed data and prepared figures. Original gene targeted chimeras were generated by the Centre for Phenogenomics (Toronto). JMR maintained all mouse colonies and performed breeding and genotyping. HBM developed the low cell number ChIP-seq protocol. RMT, HBM, CJP, GAP and TJP performed initial bioinformatics analyses. HBM in collaboration with CI and WLS, wrote and prepared the manuscript. All authors assisted in editing the manuscript.

Mtf2 dynamically regulates Wnt and Hippo signaling to control hematopoiesis

Janet L. Manias Rothberg[1,2,3,*], Harinad B. Maganti[1,2,4,*], Hani Jrade[1,2,3], Christopher J. Porter[5], Gareth A. Palidwor[5], Christopher Cafariello[1,2,3], Theodore J. Perkins[1,4,5], Robert F. Paulson[6],Caryn Y. Ito[1,3], William L. Stanford[1,2,3,4]

[1]The Sprott Center for Stem Cell Research, Regenerative Medicine Program, Ottawa Hospital Research Institute, Ottawa, ON, Canada K1H 8L6;

[2]Ottawa Institute of Systems Biology, Ottawa, Ontario, Canada;

[3]Department of Cellular and Molecular Medicine, University of Ottawa, Ottawa, Ontario, Canada;

[4]Department of Biochemistry, Microbiology and Immunology, University of Ottawa, Ottawa, Ontario, Canada;

[5]Ottawa Bioinformatics Core Facility, The Sprott Center for Stem Cell Research, Ottawa Hospital Research Institute, Ottawa, ON, Canada K1H 8L6

[6]Department of Veterinary and Biomedical Sciences, Pennsylvania State University, University Park, Pennsylvania 16802, USA

Correspondence: cito@ohri.ca (C.Y.I.); wstanford@ohri.ca (W.L.S.)

[*]These authors contributed equally to this work.

Running Title: Mtf2 regulates Wnt and Hippo signaling to control hematopoiesis

Keywords: Polycomb, erythropoiesis, hematopoietic stem cell, Wnt signaling, Hippo signaling

Abstract

Polycomb repressive complex 2 (PRC2) accessory proteins play substoichiometric, tissue-specific roles to recruit PRC2 to specific genomic loci or increase enzymatic activity, while PRC2 core proteins are required for complex stability and global levels of trimethylation of Histone 3 lysine 27 (H3K27me3). Here, we demonstrate a role for the classical PRC2 accessory protein Mtf2/Pcl2 more akin to that of a core PRC2 protein in the hematopoietic system. *Mtf2*$^{-/-}$ hematopoietic progenitors demonstrate markedly decreased core PRC2 protein levels and a global loss of H3K27me3 at promoter-proximal regions. The resulting derepression of transcriptional and signaling networks blocks definitive erythroid development culminating in *Mtf2*$^{-/-}$ embryos dying by e15.5 due to severe anemia. Gene regulatory network (GRN) analysis identified Wnt signaling as derepressed in erythroblasts, while chemical inhibition of canonical Wnt signaling rescued Mtf2 deficient erythroblast differentiation *in vitro*. Similarly, GRN analysis of hematopoietic stem and progenitor cells (HSPCs) to explain the loss of the *Mtf2*$^{-/-}$ HSC pool in bone marrow transplants identified an epigenetic network in which Mtf2-PRC2 represses DMNT1. Mtf2-PRC2 deficiency leads to increased Dnmt1 levels which repress Mst1 and Mst2 expression, resulting in Taz nuclear translocation and increased expression of cell cycle genes that regulate the HSC pool. Using a combination of *in vitro*, *in vivo* and systems analyses, we report for the first time PRC2-mediated regulation of Dnmt1, demonstrate that Mtf2 is a critical epigenetic regulator of Wnt and Hippo signaling in hematopoiesis, and recast the role of Polycomb accessory proteins in a tissue specific context.

Introduction

Epigenetic regulation of cell signaling profoundly affects stem cell functions, such as proliferation, pluripotency and self-renewal(Sato, Meijer et al. 2004, Beerman and Rossi 2015). The Polycomb Repressive Complex 2 (PRC2), made up of core and accessory proteins, represses gene transcription by catalyzing the trimethylation of lysine 27 of histone 3 (H3K27me3).

PRC2 accessory proteins, such as Metal Regulatory Transcription Factor 2 (Mtf2; a.k.a., *Polycomb-like 2* [*Pcl2*]), contain DNA-binding domains which confer its role in PRC2 targeting and stability at particular genomic loci within embryonic stem cells (ESCs)(Peng, Valouev et al. 2009, Shen, Kim et al. 2009, Landeira, Sauer et al. 2010, Li, Margueron et al. 2010, Pasini, Cloos et al. 2010, Walker, Chang et al. 2010, Casanova, Preissner et al. 2011, Walker, Manias et al. 2011). Mtf2 knockdown in ESCs led to reduced H3K27me3 levels at Mtf2 target loci but did not affect global H3K27me3 levels(Walker, Chang et al. 2010, Casanova, Preissner et al. 2011). Moreover, manipulating the expression of Mtf2 did not affect the expression of core PRC2 complex members(Casanova, Preissner et al. 2011, Walker, Manias et al. 2011), supporting its role as a PRC2 accessory protein in ESCs. While the function of Mtf2 has been characterized in ESCs, the role of Mtf2 *in vivo* is poorly understood.

Epigenetic regulation of signaling pathways is critical for stem cell self-renewal and differentiation. The Wnt/ß-catenin signaling pathway is highly conserved and has been previously shown to regulate stem cell fate and pluripotency across multiple lineages during development(Shtutman, Zhurinsky et al. 1999, Reya, Duncan et al. 2003, Wang, Gao et al. 2015). It has recently been shown that repression of Wnt signaling by PRC2 controls cell growth in chondrocytes(Kobayashi, Uehara et al. 2016) and homeostasis in intestinal cells(Oittinen, Popp et al. 2016). The canonical Wnt signaling pathway is also critical in the self-renewal and

differentiation of hematopoietic stem cells (HSCs); overexpression of activated ß-catenin leads to loss of HSC multipotency(Kirstetter, Anderson et al. 2006). Additionally, regulation of the Hippo signaling pathway is also critical for cell proliferation, tissue homeostasis and organ size. Epigenetic silencing of Hippo pathway components, including hypermethylation of Mst1/2 and Lats1/2, has been implicated in cancer progression(Takahashi, Miyoshi et al. 2005, Jiang, Li et al. 2006, Seidel, Schagdarsurengin et al. 2007). Yet it is not clear how the Hippo and Wnt signaling pathways are epigenetically regulated and little is known about the role of PRC2 in regulating these pathways.

Here we show the PRC2 accessory protein, Mtf2, is required for embryonic and erythroid development and for maintenance of the hematopoietic stem and progenitor cell (HSPC) pool by epigenetically repressing multiple transcriptional and signaling pathways during hematopoiesis leading to diverse cell fate decisions. In HSPCs, Mtf2 deficiency results in a global loss of promoter-proximal H3K27me3, thus Mtf2 functions similarly to core PRC2 proteins. We further demonstrate that Mtf2-PRC2 represses canonical Wnt signaling, which regulates erythroid maturation by controlling critical differentiation genes, including Gata2 and Myb. Additionally, in HSPCs, Mtf2-PRC2 modulates Hippo signaling by regulating Dnmt1 and DNA methylation of *Mst1* and *Mst2*, thereby controlling nuclear Taz levels and cell cycle gene expression to regulate HSPC activity. Together, these findings demonstrate that Mtf2 is required for PRC2-mediated epigenetic regulation of crucial signaling pathways during hematopoiesis and establish core-like properties of PRC2-associated proteins.

Results

Mtf2 null mice die *in utero* from impaired definitive erythropoiesis

Mtf2 is highly expressed in ESCs however our *in silico* analysis of mouse tissue microarrays (Zhang, Morris et al. 2004) determined that *Mtf2* has a more restricted pattern in adults, with higher expression in sites of hematopoiesis. Using intracellular flow cytometry, we analyzed Mtf2 protein abundance in various hematopoietic lineages isolated from bone marrow (BM) and observed that Mtf2 expression is high in long- and short-term HSCs (LT-HSCs and ST-HSCs, respectively), progenitors (LSK cells) and various stages of erythroblast development (indicated by CD71 and/or Ter119 expression; Fig. S2.1A-C). In erythroblasts, Mtf2 expression is modulated during the cell cycle with highest expression observed during the S and G2/M phases (Fig. S2.1D).

Previous work addressing the role of Mtf2 *in vivo* has been limited to gene trap mutants that display variable phenotypes (Wang, He et al. 2007, Li, Isono et al. 2011). Since gene trap mutations are often hypomorphic (Stanford, Cohn et al. 2001) and to maintain strain fidelity, which has also led to variable phenotypes with other Polycomb mutants (Motoyama, Kitajima et al. 1997, Kitajima, Kojima et al. 1999), we chose to generate Mtf2 null (*Mtf2*$^{-/-}$) mice in the *C57BL/6* background using gene-targeted ESCs (Fig. 2.1A,B).

In contrast to the gene trap mutants, no homozygous gene-targeted mice were present at parturition; thus, embryos were analyzed at different developmental stages. *Mtf2*$^{-/-}$ mice die at e15.5, displaying growth defects, hemorrhage, and severe anemia (Fig. 2.1C-E). Embryos also display skeletal alterations, including fusion of vertebrae and ectopic ribs, as observed in the gene trap mutants (data not shown). Based both on the gross pathology of the *Mtf2*$^{-/-}$ embryos and the expression pattern of Mtf2 in adult erythroblasts (Fig. S2.1C), we further investigated erythroid

development in viable *Mtf2*$^{-/-}$ e14.5 embryos. At this embryonic stage, the fetal liver is the central site of hematopoietic development and fetal liver (FL) cellularity was significantly reduced in *Mtf2*$^{-/-}$ embryos (30.9±1.88 x10^{6} cells per embryo compared to 64.7±8.95 x10^{6} cells in wild-type (WT) embryos, p=0.013), albeit FL size as a percentage of body weight was not affected (Fig. 2.1F). Moreover, peripheral blood smears from *Mtf2*$^{-/-}$ embryos showed fewer enucleated mature red blood cells and more nucleated, large primitive erythroblasts compared to *Mtf2*$^{+/+}$ controls (Fig. 2.1G). Hematocrits were also dramatically reduced in *Mtf2*$^{-/-}$ embryos (Fig. 2.1H). In addition, the mRNA levels of adult □1 hemoglobin, which is normally expressed by maturing red blood cells at this stage of development, was reduced in *Mtf2*$^{-/-}$ embryos while embryonic globin (□Y) expression was elevated (Fig. 2.1I).

To discern which stage of erythroid development was blocked in *Mtf2*$^{-/-}$ cells, we used the cell surface markers CD71 and Ter119 to track erythroid maturation in the FL (Koulnis, Pop et al. 2011). We identified a delay in erythroblast differentiation, with an increased frequency of Ter119^{lo} *Mtf2*$^{-/-}$ cells (erythroid stages S0-S2) and reduced frequency of Ter119^{+} (stage S3) *Mtf2*$^{-/-}$ cells (Fig. 2.2A-B). Despite alterations in cell number between genotypes within FL erythroid sub-populations S2 and S3, cell morphology between genotypes was unaltered, as assessed by imaging flow cytometry (Fig. S2.2A,B). Similar to our observations in the FL, we observed increased numbers of proerythroblasts (Ter119^{lo}, Thiazole Orange^{hi}) in the peripheral blood of e14.5 *Mtf2*$^{-/-}$ embryos. However, *Mtf2*$^{-/-}$ Ter119^{hi} Thiazole Orange^{hi} cells that remained in the peripheral blood are more immature than their WT counterparts, as indicated by more centrally located nuclei (Delta XY centroid values of *Mtf2*$^{-/-}$ versus WT: 0.69±0.01 vs. 0.83±0.01, respectively; Fig. 2.2C). There is also a reduction in the number of reticulocytes and mature red blood cells in *Mtf2*$^{-/-}$ e14.5 peripheral blood (0.7% Ter119^{-} DNA^{-} cells versus 1.89% in WT), corroborating our qualitative

observations in blood smears (Fig 2.1G). Together, these observations demonstrate that Mtf2 plays a critical role in erythroid maturation.

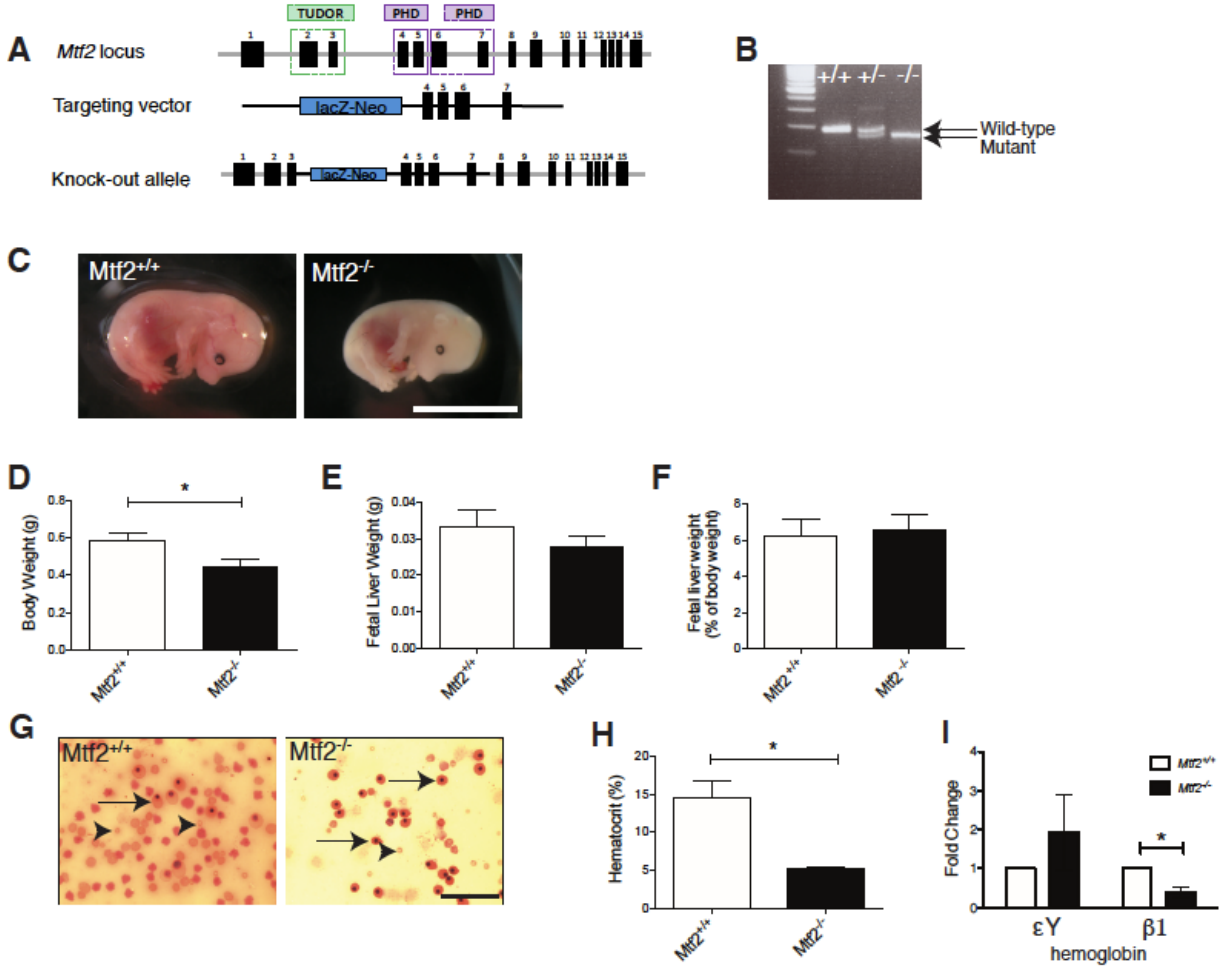

Figure 2.1. *Mtf2*$^{-/-}$ mice die at e15.5 due to severe anemia. A, Schematic of the gene targeted ESCs used to create Mtf2 knockout mice. Mtf2 protein domains (Tudor, PHD) are indicated. **B,** A PCR-based genotyping strategy was used to identify homozygous mutants. **C,** *Mtf2*$^{-/-}$ embryos readily display anemia and growth defects, dying by e15.5. **D,** e15.5 *Mtf2*$^{-/-}$ embryos are significantly smaller than their wild-type littermates but have **(E-F)** normal fetal liver (FL) weight as a measure of body size. **G,** Peripheral blood taken from e15.5 *Mtf2*$^{-/-}$ embryos has fewer cells than wild-type littermates and very few enucleated red blood cells (arrowheads). The cells that do remain are large nucleated erythroid precursors (arrows). **H,** Null embryos have a lower hematocrit

and **(I)** fail to express adult β1 hemoglobin transcript at the appropriate level. All data are shown as mean ± SEM, n=3, *p<0.05. **See also Figure S2.1.**

Mtf2 is required for erythroid maturation in a cell-intrinsic manner

Since Mtf2 is expressed in various hematopoietic progenitors (Fig. S2.1A,B), we assessed the impact of Mtf2 deficiency on the differentiation potential of progenitors using *in vitro* colony forming unit (CFU) assays. *Mtf2*$^{-/-}$ embryos contained fewer erythroid progenitors (CFU-E) but more multipotent clonogenic progenitors (CFU-granulocyte, erythrocyte, monocyte, megakaryocyte; or CFU-GEMM) than WT embryos, further demonstrating a block in erythroid differentiation potential (Fig. 2.2D,E). To address the mechanism underlying the observed erythroblast maturation defect, we first determined whether cell cycle and apoptosis was normal in *Mtf2*$^{-/-}$ erythroblasts. No increase in Annexin V staining was detected in either *Mtf2*$^{-/-}$ Ter119^{lo} or Ter119^{+} cells (Fig S2.2C,D). Thus, the reduction in *Mtf2*$^{-/-}$ mature erythroblasts seen in the FL is not due to enhanced apoptosis. *Mtf2*$^{-/-}$ Ter119^{lo} erythroblasts displayed increased cycling with a higher percentage of cells in S phase and a reduced number of cells in G_0/G_1 phase compared to WT erythroblasts (Fig S2.2E,F). The increased proliferation in these erythroblast progenitors may contribute to their differentiation defect, as erythroid maturation is linked to cell cycle exit (Clark, Doyle et al. 2004). Collectively, these data illustrate that Mtf2 is required for definitive erythropoiesis.

In our constitutive Mtf2 knockout mouse model, Mtf2 is deleted both in developing hematopoietic cells as well as the supporting stromal cells of the fetal liver. Therefore, we tested whether the role of Mtf2 in erythroid development could be due to the hematopoietic cell microenvironment, as has been previously attributed to the role of Jarid2 in erythroid maturation (Takeuchi, Yamazaki et al. 1995, Motoyama, Kitajima et al. 1997). Using competitive

repopulation (Fig.2.2F), we observed that *Mtf2*$^{-/-}$ and WT FL cells were equally capable of homing to the BM 17 hours after injection (Fig.2.2G). Additionally, the contribution of donor-derived (CD45.2^{+}) cells in the peripheral blood up to 16 weeks following primary transplant was comparable between genotypes (Fig.2.2H). Strikingly, analysis of erythroid progenitors demonstrated that *Mtf2*$^{-/-}$ donor-derived cells were also defective in erythroid maturation with an accumulation of proerythroblasts (ProE) and late basophilic (EryB) erythroblasts (Fig.2.2I). This erythroid maturation delay is similar to that observed in the Mtf2 null embryos and therefore not due to a defect in the FL microenvironment. These data demonstrate that Mtf2, unlike Jarid2, plays a cell-intrinsic role in erythroblast maturation that is not limited to fetal development.

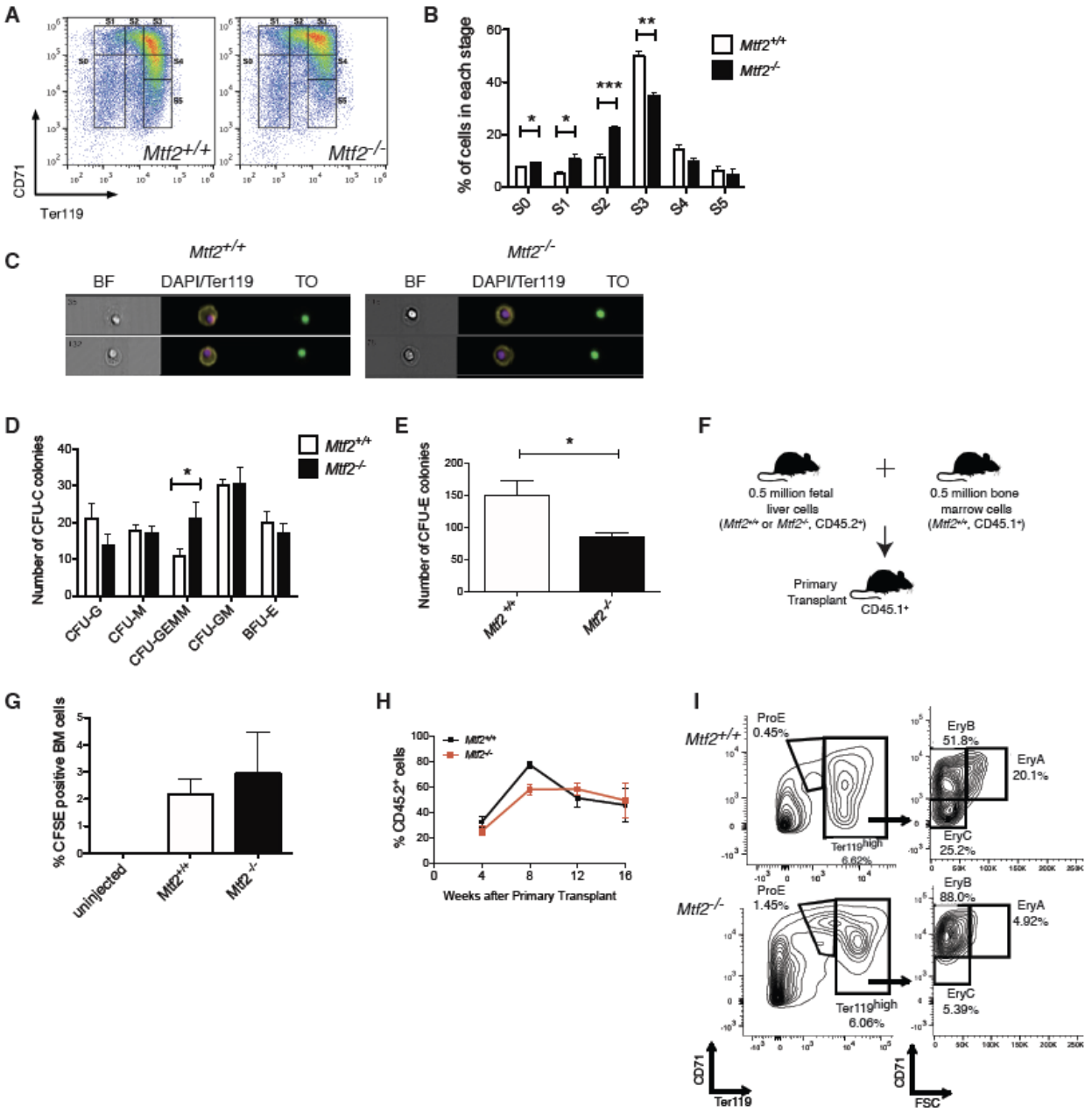

Figure 2.2. Mtf2 is required for normal erythroid differentiation. **A-B,** *Mtf2*$^{-/-}$ FL cells have increased frequency of pro-erythroblasts (stages S0-S2) and fewer CD71^{+}Ter119^{+} erythroblasts (stage S3). **C,** Representative pictures from imaging flow cytometry on *Mtf2*$^{-/-}$ e14.5 peripheral blood. *Mtf2*$^{-/-}$ Ter119^{+} cells have more centrally located nuclei than their wild-type counterparts (Delta XY centroid values 0.69± 0.01 vs. 0.83± 0.01,p<0.01). BF, brightfield; TO, thiazole orange. **D-E,** FL cells from *Mtf2*$^{-/-}$ embryos contain fewer erythroid progenitors (colony forming unit-erythroid, CFU-E) but have higher numbers of multipotent clonogenic progenitors (colony

forming unit-granulocyte, erythrocyte, macrophage, megakaryocyte, CFU-GEMM). CFU-G, colony forming unit-granulocyte; CFU-M, colony forming unit-macrophage; CFU-GM, colony forming unit-granulocyte, macrophage; BFU-E, burst forming-unit, erythroid. Data are shown as number of colonies per $2x10^5$ FL cells plated, mean ± SEM for n=4 mice, in triplicate. **F,** Schematic showing primary repopulation experiments using donor wild-type and *Mtf2*$^{-/-}$ e14.5 FL cells. **G,** *Mtf2*$^{-/-}$ FL cells are able to home to the bone marrow 17 hours after injection as well as wild-type cells. **H,** The percentage of CD45.2^{+} donor derived cells in the peripheral blood of recipient animals is similar when either wild-type or *Mtf2*$^{-/-}$ FL donor cells are injected. **I,** Erythroid defects observed in *Mtf2*$^{-/-}$ FL are cell-intrinsic and recapitulated in recipient mice. A higher frequency of *Mtf2*$^{-/-}$ FL donor-derived pro-erythroblasts (ProE), and fewer mature erythroblasts (EryC) were observed compared to WT FL donor cells. *p<0.05, **p<0.01, ***p<0.001. **See also Figure S2.2.**

Mtf2 is required for maintenance of the HSC pool

Although, there were similar engraftment levels of *Mtf2*$^{+/+}$ and *Mft2*$^{-/-}$ donor cells in primary recipients (Fig.2.2H), we tested whether Mtf2 deficiency would affect HSPC self-renewal and differentiation since Mtf2 is also highly expressed in stem and progenitor cells (Fig.S2.1A-B). Therefore, we performed secondary bone marrow transplants to assess the role of Mtf2 in the maintenance of the HSC pool (Fig.2.3A). Surprisingly, unlike primary transplants, total *Mtf2*$^{-/-}$ donor derived cells, especially Ter119+ erythroblasts, in the peripheral blood were drastically decreased at 8 and 16 weeks post-secondary transplantation (Fig.2.3B,C). This marked difference in repopulation potential demonstrates that Mtf2 regulates the size of the HSC pool. Indeed, *Mtf2*$^{-/-}$ donor-derived short term (ST)- and long term (LT)-HSCs were decreased in secondary transplants but not in primary transplants (Fig.2.3D,E). Within the significantly decreased *Mtf2*$^{-/-}$ donor cell population in bone marrow of secondary recipients, the proportion of common myeloid progenitors (CMPs), megakaryocyte-erythroid progenitors (MEPs) and granulocyte-monocyte progenitors

(GMPs) derived from *Mtf2*$^{-/-}$ cells was similar to BM of recipients engrafted with *Mtf2*$^{+/+}$ cells 16 weeks post-secondary transplantation (Fig.2.3F). In contrast, the frequency of common lymphoid progenitors (CLPs) derived from *Mtf2*$^{-/-}$ cells was significantly increased in the BM following secondary transplant, indicating a role for Mtf2 in the regulation of both myeloid and lymphoid commitment (Fig.2.3F).

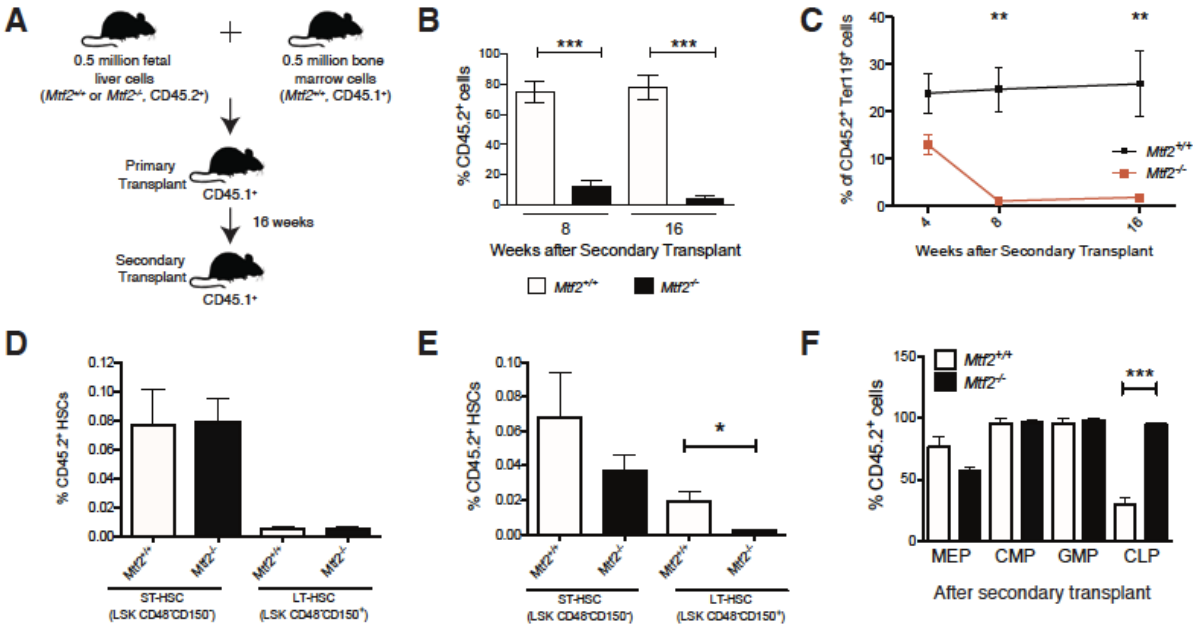

Figure 2.3. Mtf2 is required for HSC self-renewal. **A,** Schematic of secondary reconstitution experiments. **B,** In secondary transplants, *Mtf2*$^{-/-}$ cells have significantly decreased repopulation potential, demonstrating a requirement of Mtf2 in HSC maintenance. At 8 and 16 weeks post-secondary transplantation, the numbers of *Mtf2*$^{-/-}$ donor cells are significantly reduced in peripheral blood. **C,** *Mtf2*$^{-/-}$ donor-derived Ter119^{+} erythroblasts are greatly reduced in peripheral blood of secondary recipients. **D,** The number of *Mtf2*$^{-/-}$-derived short-term and long-term HSCs (LSK CD48^{-} CD150^{-} and LSK CD48^{-}CD150^{+}, respectively) was similar to wild-type derived ST- and LT-HSCs 16 weeks after the primary transplant but **(E)** was markedly decreased in recipient bone marrow at 16 weeks post-secondary transplant. **F,** Analysis of various progenitor types in BM of secondary

transplant recipients after 16 weeks indicates the fraction of donor-derived MEPs and GMPs is similar to wild-type but a large increase in the fraction of donor-derived common lymphoid progenitors (CLPs) is observed with *Mtf2*$^{-/-}$ donors.

Mtf2 regulates core PRC2 member protein abundance in the hematopoietic system

In ESCs, Mtf2 has been identified as a PRC2 accessory protein as it associates with PRC2 core proteins but does not modulate their expression (Walker, Chang et al. 2010, Casanova, Preissner et al. 2011, Li, Isono et al. 2011). Thus, we analyzed the effects of Mtf2 loss on PRC2 expression to determine whether Mtf2 plays a similar role in hematopoietic cells. In *Mtf2*$^{-/-}$ erythroblasts, we observed no significant differences in the transcript levels of core PRC2 members, such as Suz12 and Ezh2, although we observed an approximately 50% decrease in Jarid2 mRNA ($p=0.028$, Fig.2.4A). Surprisingly, Ezh2 and Jarid2 protein levels were significantly decreased in *Mtf2*$^{-/-}$ sorted e14.5 primary hematopoietic cells (Fig.2.4B), when assessed using capillary electrophoresis immunodetection, which enables protein analysis in very low cell numbers (O'Neill, Bhamidipati et al. 2006, Fan, Deb-Basu et al. 2009). To confirm this analysis and gain insight into the role of Mtf2 in the adult hematopoietic system, lentiviral-mediated knockdown of Mtf2 in adult BM HSPCs was performed, which resulted in a concomitant decrease in Suz12, Ezh2, and Ezh1 abundance ($p<0.001$, Fig.S2.3A-D). The reduction in PRC2 core proteins indicates that Mtf2 is required for the function of the PRC2 complex in hematopoietic cells, a role more akin to a PRC2 core protein than an accessory protein.

While the reduction of Mtf2 in ESCs affected H3K27me3 levels at particular loci, it did not result in changes in global levels of H3K27me3 (Walker, Chang et al. 2010). Therefore, we were surprised to find a global decrease in total H3K27me3 levels upon knockdown of Mtf2 in

bone marrow cells ($p<0.001$, Fig.S2.3E), suggesting that Mtf2 deficiency, in part through its control of PRC2 core protein levels, results in the loss of PRC2-mediated epigenetic repression.

Mtf2 regulates promoter-proximal H3K27me3 in erythroblasts

To understand the effect of reduced global levels of H3K27me3 at the genomic resolution, we examined the functional consequences of Mtf2 deficiency by ChIP-seq. We performed H3K27me3 ChIP in FL-derived (e14.5) cells from two distinct stages of erythropoiesis: $CD71^{+}Ter119^{-/lo}$ (stage S1 & S2) proerythroblasts and $CD71^{+}Ter119^{+}$ (stage S3) erythroblasts. We chose these two fractions of cells since they flank the block in erythroid development we observe in Mtf2 deficient mice (Fig.2A,B).

Using unsupervised *k-means* clustering to characterize groups of genes with distinct binding patterns of H3K27me3 within WT and knockout erythroblasts, we observed that Mtf2-null cells display a genome-wide loss of H3K27me3, specifically around the TSS (Fig.2.4C). This is even more evident by choosing one cluster (Cluster 5) and plotting read density within 5kb of the TSS (Fig.2.4D), clearly demonstrating a specific loss of H3K27me3 at promoter-proximal regions. Over multiple iterations of clustering, we identified 2404 genes that have strong H3K27me3 binding at the promoter region of WT erythroblasts, which is virtually eliminated in erythroblasts lacking Mtf2 (Table S1). This group of 2404 genes is highly enriched for master regulators of many key biological processes including members of the Hox, Wnt, Gata and Lhx families.

Since Mtf2 recruits PRC2 to chromatin, we examined Mtf2-chromatin interactions by performing Mtf2 ChIP-seq in our two erythroid subgroups. Over 72% of genes harboring H3K27me3 marks in WT cells had reduced H3K27me3 in *Mtf2*$^{-/-}$ proerythroblasts and half of these

genes were bound by Mtf2 at this stage of development (Fig.2.4E). Interestingly, genes associated with Mtf2 binding peaks in $CD71^{+}Ter119^{-/lo}$ proerythroblasts or $CD71^{+}Ter119^{+}$ erythroblasts show very little overlap with Mtf2 or other PRC2 binding profiles in ESCs (Peng, Valouev et al. 2009, Walker, Chang et al. 2010, Hunkapiller, Shen et al. 2012) (Fig.S2.4), demonstrating cell type specific interactions of Mtf2 with chromatin. Recognizing that ChIP-seq only provides a snapshot of transcription factor binding, genes that lost H3K27me3 in Mtf2 null cells were classified as "Mtf2-PRC2 targets", although not necessarily direct Mtf2 targets, and the data was used as a first step in mapping the molecular mechanisms behind the hematopoietic defects observed in Mtf2 null mice.

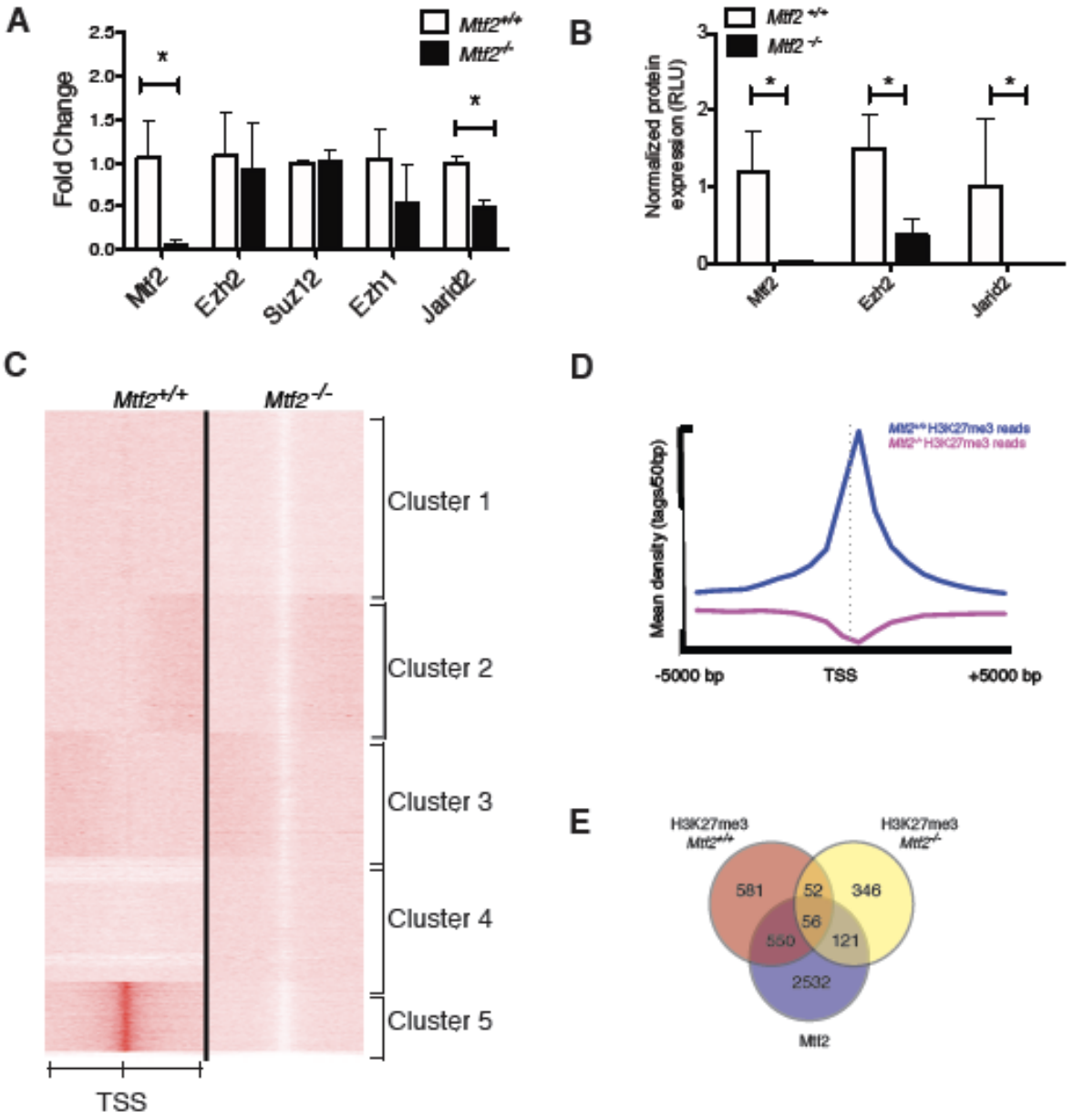

Figure 2.4. Mtf2 is required for promoter-proximal histone trimethylation of lysine 27. A, Transcript levels of PRC2 complex members, Suz12 and Ezh2, are unchanged in *Mtf2*$^{-/-}$ proerythroblasts as determined by RT-qPCR, although mRNA of the accessory protein Jarid2 is reduced. **B,** Protein abundance analysis by capillary electrophoresis in CD45^{+} FL cells shows down-regulation of Ezh2 and Jarid2 in *Mtf2*$^{-/-}$ mice (n=3-7 mice, shown as mean area under the curve ± SEM, normalized to expression in WT animals). *p<0.05. **C,** *k*-mean clustering identifies

patterns of H3K27me3 enrichment in primary erythroblasts. Globally, a loss of enrichment centered around transcriptional start sites (TSS) is seen in cells lacking Mtf2. **D,** H3K27me3 ChIP-seq reads density is plotted within 5kb of the TSS within one cluster of approximately 2400 genes (Cluster 5). In these genes, H3K27me3 binding is specifically reduced immediately around the TSS in Mtf2-null erythroblasts. **E,** Overlap of genes associated with binding sites identified by ChIP-seq. 1131 genes have lost H3K27me3 marks upon misregulation of Mtf2/PRC2 and 550 of those targets also show Mtf2 binding. **See also Figure S2.3, S2.4.**

Mtf2 regulates Wnt-dependent erythroid maturation

To investigate the role of Mtf2 in the transcriptional regulation of erythropoiesis, we used RNA-seq profiling of fetal liver erythroid progenitors from the same stages outlined for our ChIP-seq studies. Differential gene expression analysis revealed that 751 genes were significantly misregulated ($p<0.05$) in *Mtf2*$^{-/-}$ proerythroblasts, while 2999 genes were misregulated ($p<0.05$) in *Mtf2*$^{-/-}$ CD71^{+}Ter119^{+} erythroblasts compared to WT. Within the sets of differentially expressed genes, 92.9% and 98% of them were upregulated in the *Mtf2*$^{-/-}$ proerythroblasts and erythroblasts, respectively. These results are consistent with the role of Mtf2 as a transcriptional repressor.

To model the effects of Mtf2 on erythroblast maturation, RNA-seq, Mtf2 ChIP-seq and H3K27me3 ChIP-seq data were integrated to draft an erythroid-specific gene regulatory network (GRN) of 461 genes controlled by Mtf2-PRC2 (Table S2). Gene ontology enrichment analysis revealed this network consists of genes important in regulation of transcription, hematopoietic development, migration, cell cycle, TGF-ß signaling and Wnt signaling (Fig.2.5A).

To determine the role of Wnt signaling on differentiation potential of progenitor cells deficient in Mtf2, we performed functional colony-forming assays in the presence of two different small molecule inhibitors of activated ß-catenin (Fig.2.5B). Adult mouse BM HSPCs with reduced levels of Mtf2 form significantly fewer BFU-E colonies than their scramble control counterparts

(Fig.2.5C). Blocking Wnt signaling during colony growth significantly increased BFU-E colony frequency in Mtf2-knockdown (Mtf2 KD) HSPCs (Fig.2.5C). Although the numbers of BFU-E colonies arising from inhibitor-treated Mtf2 KD HSPCs was still lower than that observed from control cells, the rescue of erythroid differentiation to the BFU-E stage was observed using two different inhibitors specific to the canonical Wnt signaling pathway (ICG001 or JW74) and two different Mtf2 knockdown clones (Sh3 and Sh7) (Fig.2.5C). These data suggest that Mtf2-PRC2 functions in a feed-forward circuit to repress Wnt signaling and allow erythroid differentiation.

To further demonstrate the impact of Wnt signaling on erythroid maturation, we used an *ex-vivo* erythroid maturation assay, in which $CD71^{+}Ter119^{-/lo}$ pre-erythroblasts are exposed to differentiation signals, including Epo, and allowed to mature to $CD71^{+}Ter119^{+}$ polychromatophilic erythroblasts over 2 days (Fig.2.5D). Mtf2 KD proerythroblasts are deficient in their differentiation capacity, as only 1/3 as many cells differentiated to $CD71^{+}Ter119^{+}$ erythroblasts, compared with scramble controls (Fig.2.5E,F; S2.5A,B). Inhibiting Wnt signaling, using ICG001 or JW74, during *ex-vivo* differentiation leads to rescue of the Mtf2-deficient erythroid phenotype demonstrated by a significant increase in the frequency of $CD71^{+}Ter119^{+}$ arising from Mtf2 KD proerythroblasts following Wnt inhibition (Fig.2.5E,F; S2.5A,B).

Wnt inhibitor-treated Mtf2 KD erythroblasts were also analyzed for changes in gene expression after differentiation. Genes such as *Gata2, Myb, Stat5b, Fli1, Gata1, Tal1,* and *Crebbp* are all significantly increased in Mtf2-deficient $CD71^{+}Ter119^{+}$ cells, but are decreased upon Wnt inhibition (Fig.2.5G, S2.5C). The critical regulators of erythroid differentiation such as Gata2 are found in our Mtf2-PRC2 erythroid specific GRN and lose H3K27me3 upon loss of Mtf2 (Fig. S2.6). Overexpression of these master regulators *via* loss of PRC2-mediated repression can result in uncoordinated and stalled erythroid maturation, as seen in our Mtf2-deficient mice. Inhibition

of these de-repressed genes by blocking Wnt signaling largely rescues the erythroid maturation defect and further suggests a mechanism whereby Mtf2 maintains erythroid differentiation and maturation by repressing the Wnt pathway (Fig.2.5H).

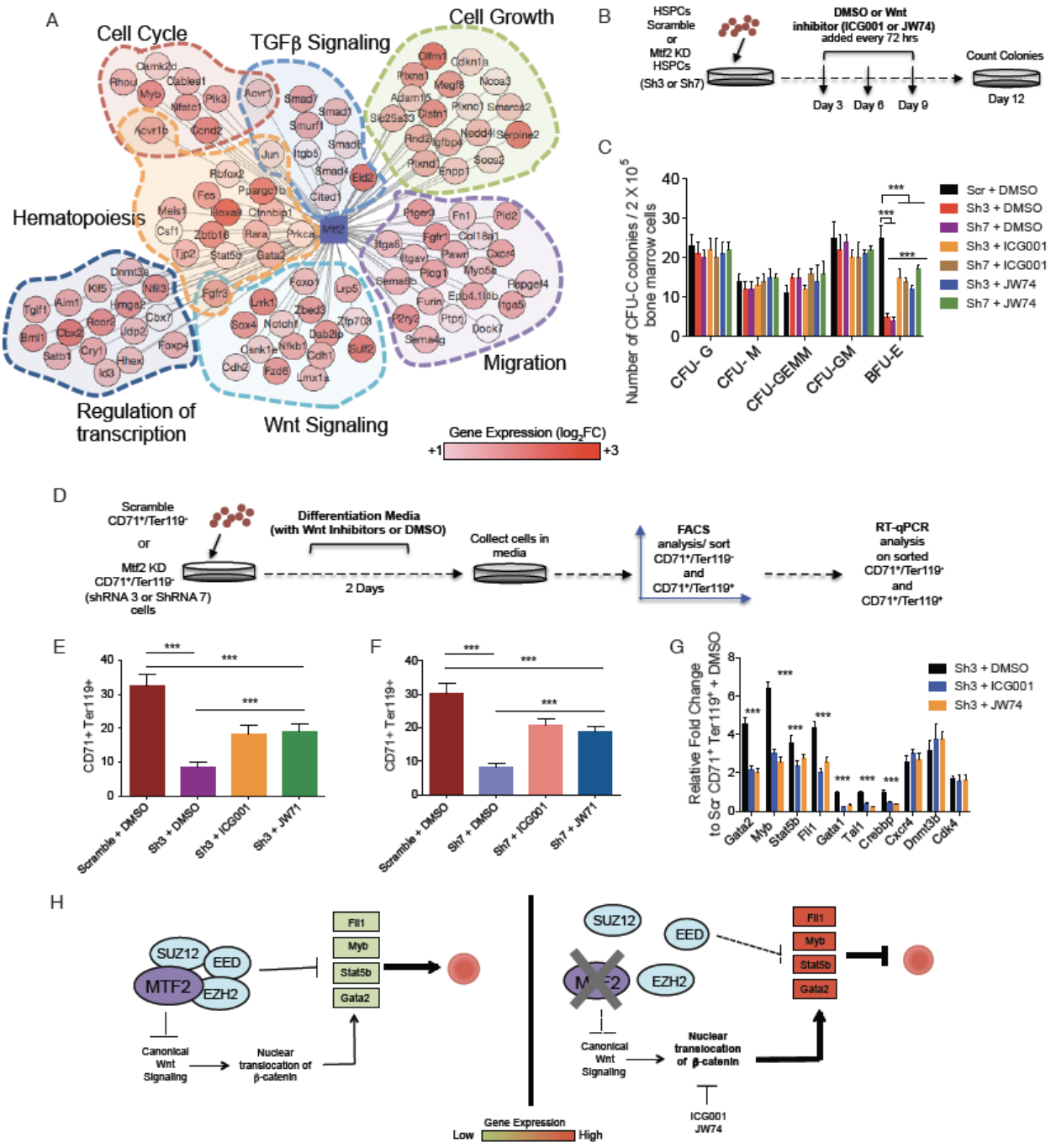

Figure 2.5. Mtf2 regulates Wnt-dependent erythroid maturation. **A,** An erythroid-specific GRN was drafted using RNA-seq from WT and Mtf2-null mouse erythroblasts and integrating genes that have lost H3K27me3 upon loss of Mtf2. Important regulatory pathways are highlighted. Node color represents change in gene expression. **B,** Experimental schematic of CFU-C assay, where scramble transduced HSPCs and Mtf2-deficient HSPCs (transduced with two independent

shRNAs against Mtf2) were treated with DMSO or Wnt inhibitors (either ICG001 or JW74), respectively. **C,** Wnt inhibition via ICG001 or JW74 small molecule treatment in Mtf2-deficient HSPCs gives rise to significantly more BFU-E colonies. **D,** Experimental schematic of *ex vivo* erythroid differentiation assay using FACS sorted Mtf2-deficient or scramble transduced $CD71^{+}Ter119^{-}$ cells. **E-F,** FACS sorted Mtf2-deficient proerythroblasts ($CD71^{+}Ter119^{-}$ cells) treated with Wnt inhibitors (ICG001 or JW71) for 2 days in erythroid differentiation culture media, show an increased capacity to differentiate into $CD71^{+}Ter119^{+}$ cells. **G,** Mtf2-knockdown $CD71^{+}Ter119^{+}$ cells treated with Wnt inhibitors show inhibition of derepressed erythroid genes. **H,** In a normal erythroblast (left), Mtf2-PRC2 repression of important erythroid maturation genes and repression canonical Wnt signaling results in proper erythroid maturation. In the absence of Mtf2 (right), derepression of erythroid regulators and Wnt signaling results in a block in erythroid differentiation, which can be largely rescued by chemical inhibition of ß-catenin. **See also Figure S2.5, S2.6.**

Wnt inhibition does not affect HSC activity in Mtf2-deficient cells

We also observed increased nuclear localization of β-catenin in Mtf2-knock down HSPCs using imaging flow cytometry (Fig.S2.7A). To test whether epigenetic regulation of the Wnt pathway by Mtf2-PRC2 is critical for HSPC maintenance, activated ß-catenin within Mtf2-deficient HSPCs was blocked using small molecule inhibitors and the effects assessed by long-term culture-initiating cell (LT-CIC) assays. Mtf2 KD HSPCs formed significantly fewer LT-CICs compared to scrambled control HSPCs. Chemical inhibition of the canonical Wnt pathway, however, did not rescue the number of LT-CIC colonies formed from Mtf2-deficient HSPCs (Fig. S2.7B,C), indicating Wnt does not play a role in Mtf2-mediated loss of HSC activity. To interrogate the mechanisms by which Mtf2 regulates HSC maintenance, transcriptomic changes due to loss of Mtf2 were analyzed by performing RNA-seq on lineage-negative HSPCs from WT and Mtf2-null FL cells from e14.5 embryos. Postulating that epigenetic changes observed in proerythroblasts may be a result of changes at the level of HSPCs, the RNA-seq data was integrated

with our H3K27me3 ChIP-seq data from *Mtf2*$^{-/-}$ CD71^{+}Ter119$^{-/lo}$ proerythroblasts to generate a 936 gene Mtf2-PRC2 HSPC GRN (Table S3). Many of the 434 upregulated genes within this network function in cell cycle and pathways involved in cancer (Fig.2.6A). The other 55% of the network includes downregulated genes that play a role in cell-cell interactions and the Hippo signaling pathway (Fig.2.6A).

Mtf2 regulates primitive progenitor cell self-renewal *via* Hippo signaling

YAP/TAZ play important roles in the regulation of the Hippo signaling pathway. As overexpression of YAP within HSPCs does not affect their differentiation or proliferation (Jansson and Larsson 2012), we focused on its paralog, Taz, and observed increased nuclear Taz levels in Mtf2 KD HSPCs (Fig.2.6B,C). While Taz transcript levels are unchanged in Mtf2 KD HSPCs, increased nuclear Taz protein suggests dysregulated Hippo signaling in Mtf2-deficient cells. Hippo orthologs Mst1 and Mst2, are serine/threonine kinases upstream of Taz are down-regulated (Fig.2.6D) and CpG islands in their promoters are hypermethylated (Fig.2.6E) in Mtf2 KD HSPCs. This hypermethylation is consistent with overexpression of DNA methylases Dnmt1 and Dnmt3b in Mtf2 KD HSPCs (Fig.2.6F). Therefore, we analyzed the epistatic relationship between Mst1/2, Dnmt1/3b and Mtf2 in HSPCs. Overexpression of Mst1/2 in Mtf2 KD HSPCs increases the number of LTC-ICs, consistent with a role downstream of Mtf2 to regulate HSC activity (Fig. S2.7D). Overexpression of Dmnt1, but not Dmnt3b, phenocopies Mtf2 loss, resulting in hypermethylation of the Mst1/Mst2 sites (Fig.2.6G) and reduced Mst1/2 expression (Fig.2.6H), implicating Dnmt1 as an upstream regulator of Mst1/2 in HSPCs. Furthermore, when Dmnt1 is depleted in Mtf2 KD HSPCS, this result is reversed; Mst1/2 expression is upregulated and promoter regions are hypomethylated (Fig.2.6I). Knockdown of Dnmt1 also restores the numbers

of LTC-ICs in Mtf2 KD HSPCs (Fig.2.6J). Therefore, in the absence of Mtf2, derepression of Dmnt1 decreases Mst1 and Mst2 expression via hypermethylation of their promoters, which ultimately leads to reduced phosphorylation and increased nuclear translocation of Taz.

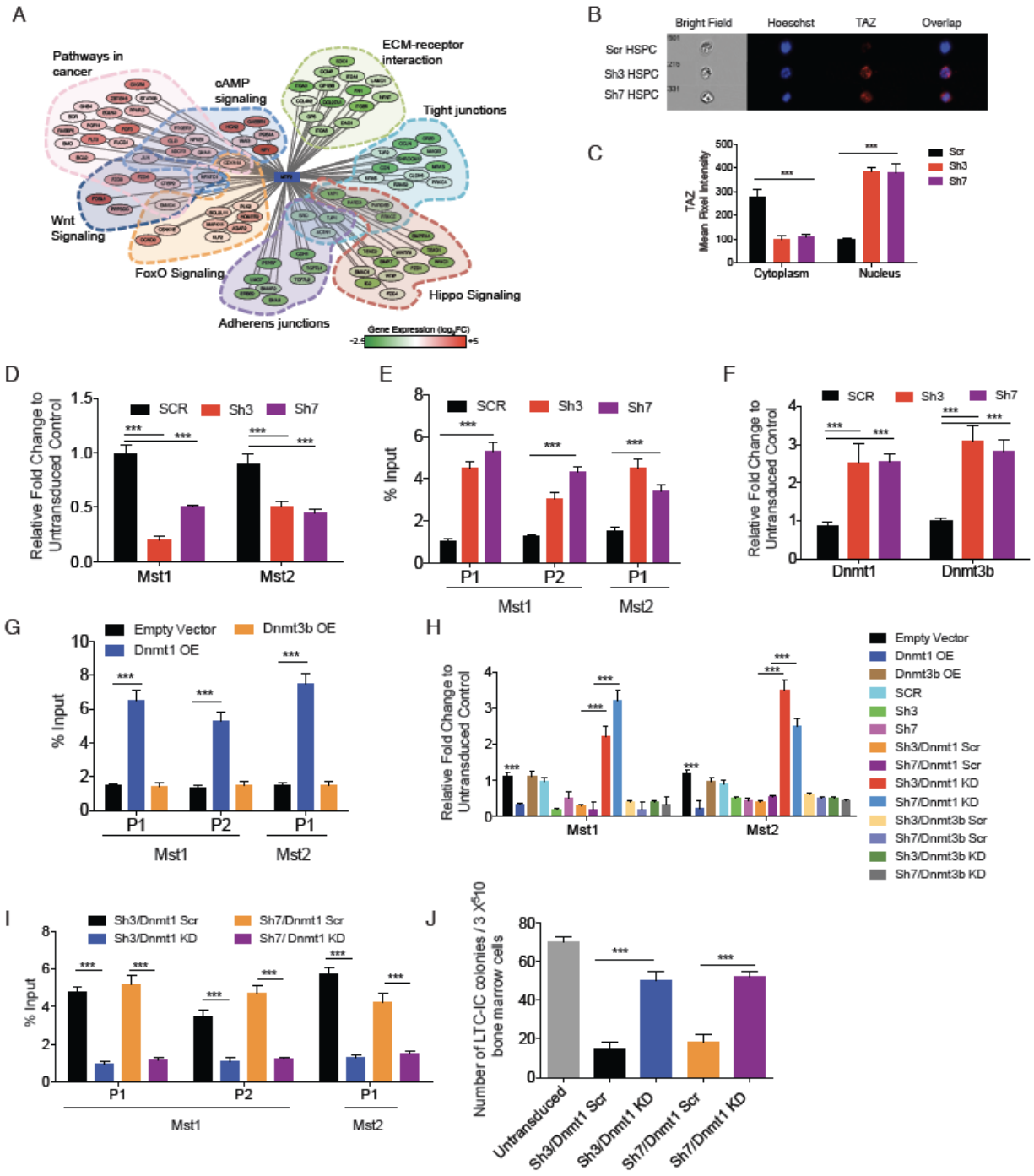

Figure 2.6. Mtf2 regulates multiple signaling nodes in HSPCs. **A,** An Mtf2-PRC2 GRN was drafted using RNA-seq analysis from Mtf2 knockout lineage-negative HSPCs and genes which lost H3K27me3 in *Mtf2*$^{-/-}$ erythroid cells. Multiple regulatory pathways, including Wnt and Hippo signaling are misregulated in cells lacking Mtf2. **B-C,** Imaging flow cytometric quantification of nuclear Taz indicates increased nuclear translocation in Mtf2-deficient HSPCs. **D,** In Mtf2-knockdown HSPCs, Mst1 and Mst2, upstream regulators of Taz, are downregulated at the transcript level and **(E)** CpG islands of Mst1 and Mst2 promoters are hypermethylated. **F,** Dnmt1 and Dnmt3b are upregulated in Mtf2-knockdown HSPCs. **G,** Overexpression of Dnmt1, but not Dnmt3b, in wild-type HSPCs leads to hypermethylation of the Mst1/2 promoters and **(H)** reduced Mst1/2 expression. Furthermore, knockdown of Dnmt1 **(I)** rescues Mst1/2 expression in Mtf2-deficient HSPCs and **(J)** results in Mst1/2 promoter hypomethylation. **K,** Functionally, knockdown of Dnmt1 rescues the reduction in stem cell activity in Mtf2-deficient HSPCs, as seen by the increase number of LT-CIC colonies. *** $p<0.01$. **See also Figure S2.6.**

Blocking nuclear translocation of Taz within Mtf2-deficient HSPCs, using small molecule inhibitors (Dasatinib and Pazopanib), rescued the deficiency in primitive progenitor formation, as observed by an increase in the number of LT-CIC colonies (Fig.2.7A, B). More specifically, knocking down Taz in Mtf2 KD HSPCs rescued HSPC activity and increased the number of LT-CIC colonies (Fig.2.7C), indicating that strict regulation of Taz and the Hippo pathway is critical in regulating the HSPC pool.

We observed overexpression of many master regulators of cell cycle and differentiation in Mtf2 KD HPSCs, including *Cdk4/6, E2F1, E2F2, Cdkn1a, Cdkn1b*, and *Gata2 and PU.1* (Fig.2. 7D). The overexpression of these cell cycle proteins promotes decreased HSC quiescence or increased progression through the cell cycle(Saito, Helin et al. 1995, Gala, Marreiros et al. 2001, Matushansky, Radparvar et al. 2003, Laurenti, Frelin et al. 2015, Mende, Kuchen et al. 2015). Blocking the accumulation of nuclear Taz in Mtf2 KD HSPCs by treatment with Dasatinib or Pazopanib prevents the elevated expression of cell cycle genes Cdk4/6, E2F1 and E2F2 (Fig.2.7D).

Additionally, knockdown of Taz in Mtf2 deficient HSPCs also decreases Cdk4/6 and E2F1/2 expression (Fig.2.7E, S2.7E), revealing the first identified link between Hippo signaling and cell cycle control in HSPCs. Taken together, our data suggest that regulation of the Hippo signaling pathway via Mtf2-PRC2 mediated Dnmt1 repression of Mst1/2 moderates HSPC maintenance *via* activation of master cell cycle genes (Fig.2.7F).

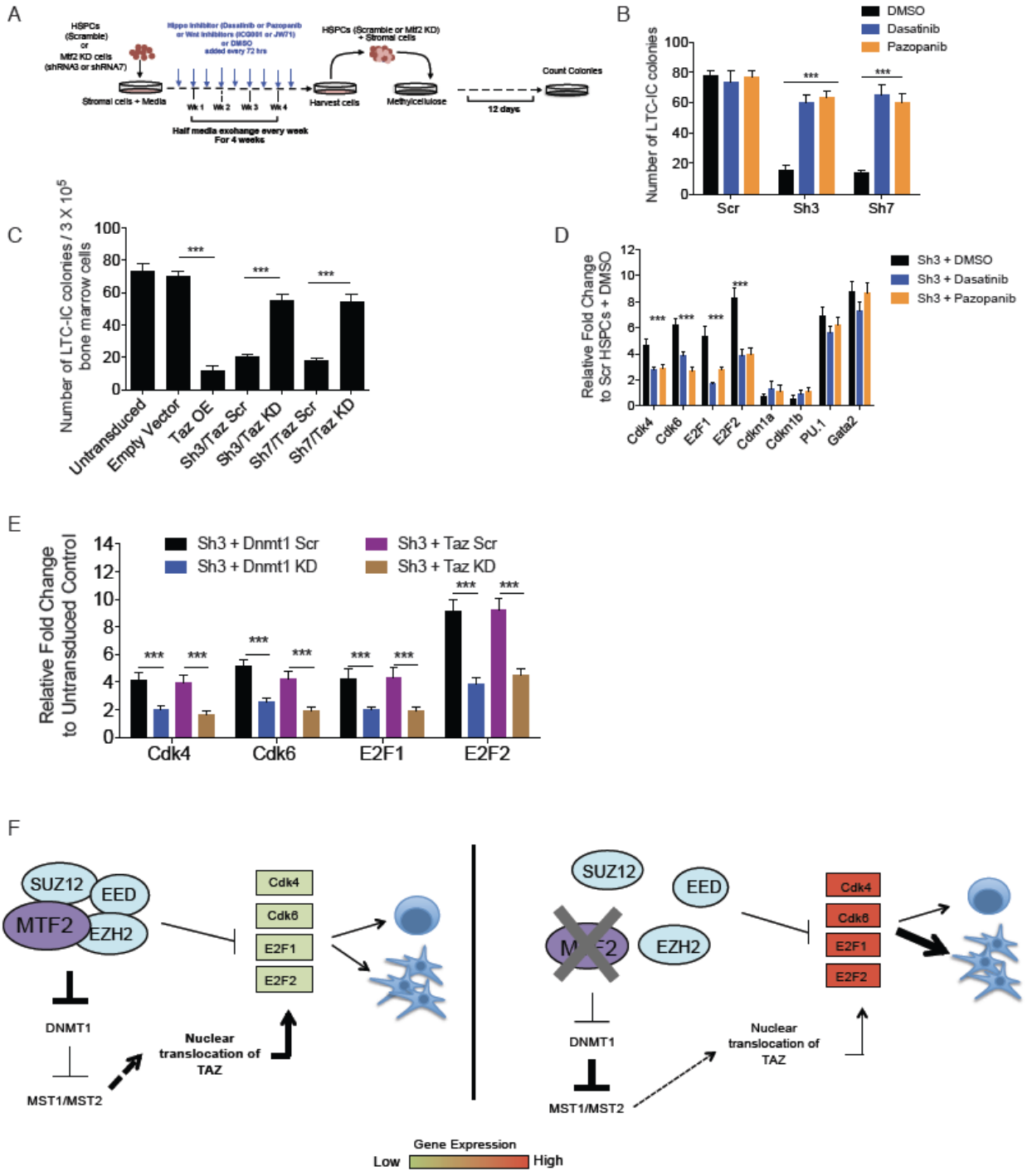

Figure 2.7. Hippo pathway regulation by Taz inhibitors Dasatinib and Pazopanib rescues primitive progenitor cell exhaustion caused by loss of Mtf2. A, Experimental schematic of LT-CIC assay, where scramble transduced HSPCs and Mtf2-deficient HSPCs (transduced with two independent shRNAs against Mtf2, Sh3 or Sh7) were treated with either DMSO, or a Yap/Taz

inhibitor (either Dasatinib or Pazopanib). Data is shown as LT-CIC colonies per $3x10^5$ bone marrow cells. **B,** Mtf2-deficient HSPCs treated with Dasatinib or Pazopanib give rise to significantly more primitive progenitor colonies (LT-CIC). **C,** Overexpression of Taz in wild-type HSPCs reduced stem cell activity, phenocopying a loss of Mtf2. Knockdown of Taz in Mtf2-deficient cells rescues stem cell activity and leads to an increase in the number of LT-CIC. **D,** RT-qPCR analysis of Mtf2-deficient HSPCs treated with Dasatinib or Pazopanib for 3 days show reduced expression of cell cycle regulator genes. Data are shown as mean +/- SD, n=3, *** $p<0.01$. **E,** Knockdown of either Dnmt1 or Taz in Mtf2-deficient HSPCs reduces the expression of critical cell cycle genes, such as Cdk4/6 and E2F1/2. **F,** In a normal HSPC (left), Mtf2-PRC2 repression of critical cell cycle genes and repression of DNA methylases leads to expression of Mst1/2, inhibiting phosphorylation of Taz resulting in balanced HSPC self-renewal and differentiation. Absence of Mtf2 (right) causes derepression of cell cycle genes and Dnmt1. Hypermethylation and subsequent loss of Mst1/2 indirectly leads to nuclear translocation of Taz, resulting in primitive progenitor cell exhaustion, which can be partially rescued by chemical inhibition of the Yap/Taz pathway or knockdown of Taz or Dnmt1. **See also Figure S2.7.**

Discussion

Using a systems approach, we uncovered a unique and fundamental role for Mtf2 in erythrocyte differentiation and HSPC maintenance, which occurs in part through PRC2-mediated epigenetic regulation of Wnt and Hippo signaling, respectively. The cell-intrinsic role of Mtf2 in hematopoiesis and its regulation of core PRC2 complex members re-defines its traditional role as a Polycomb accessory protein to an essential core-like PRC2 protein within the hematopoietic system. This novel discovery is in contrast to its role in ESCs(Walker, Chang et al. 2010, Casanova, Preissner et al. 2011) and to the role of other PRC2 accessory proteins within the hematopoietic system, such as Jarid2(Motoyama, Kitajima et al. 1997, Kitajima, Kojima et al. 1999). The dynamic epigenetic regulation of key genes by Mtf2, including PRC2 members, makes it a critical transcriptional repressor within the hematopoietic system.

To elucidate the molecular mechanisms underlying defective erythroid differentiation and HSPC maintenance in Mtf2 deficient mice, we drafted Mtf2 GRNs in erythroblasts and HSPCs and tested the epistatic relationships between Mtf2 and canonical Wnt and Hippo signaling pathways, respectively. Precise regulation of the canonical Wnt/ß-catenin pathway is essential for the development and function of HSCs and defects in the signalling pathway are associated with hematological malignancies (Kirstetter, Anderson et al. 2006, Malhotra and Kincade 2009, Wang, Krivtsov et al. 2010). Not surprisingly, multiple epigenetic modulators can regulate expression of Wnt pathway constituents (Wang, Diao et al. 2016). Our analysis reveals a specific role for Mtf2-PRC2 in regulating canonical Wnt signaling during erythropoiesis. Inhibition of activated ß-catenin by small molecules decreases canonical Wnt signaling which extensively rescued the erythroid maturation defect seen in Mtf2 KD HSPCs, as demonstrated by both colony forming and *ex vivo* maturation assays. Attenuating Wnt signaling *via* ß-catenin inhibition reduced the expression of critical erythroid genes, such as Gata2, Myb, Stat5b and Fli1, which were derepressed upon loss of Mtf2. Thus, we have elucidated for the first time a role for PRC2-mediated epigenetic regulation of canonical Wnt signaling in erythroblasts and its downstream effect on genes critical for cell fate decisions.

Little is known regarding how epigenetic regulation of the Hippo pathway may affect cell differentiation. While overexpression of the Hippo protein Yap does not affect HSPC self-renewal or proliferation (Jansson and Larsson 2012), Yap and its paralog Taz have distinct functions within other organ systems (Varelas, Sakuma et al. 2008, Van Hateren, Das et al. 2011) and the role of Taz within the hematopoietic system has been largely overlooked. Within cancer cells, unphosphorylated Yap/Taz localizes to the nucleus and regulates cell proliferation and stem/progenitor cell self-renewal (Zhao, Lei et al. 2008, Pan 2010);(Zhao, Li et al. 2010). In Mtf2

KD HSPCs, we observed high levels of nuclear Taz and an HSPC exhaustion phenotype suggesting Mtf2-PRC2 indirectly regulates Hippo signaling, affecting HSPC maintenance. We show that derepression of DNA methylase Dnmt1 by Mtf2-PRC2 reduces the expression of Hippo proteins Mst1 and Mst2 via hypermethylation at CpG islands within the Mst1/2 promoters. The reduced expression of Mst1/2 indirectly leads to increased nuclear localization of Taz (Grusche, Richardson et al. 2010, Halder and Johnson 2011, Yu and Guan 2013), which we observed in our Mtf2 KD HSPCs. Derepression of Hippo inhibition by Mtf2-PRC2 results in higher levels of key cell cycle regulators, such as Cdk4/6 and E2F family members, which require precise control in HSCs for both maintenance of quiescence during homeostasis and periods of rapid expansion after stress. For instance, altered expression of *Cdk4*, *Cdk6* or *p53* has significant effects on HSC activity (Malumbres, Sotillo et al. 2004, Dumble, Moore et al. 2007). Overexpression of CDK6 in human HSCs was shown to control exit from quiescence (Laurenti, Frelin et al. 2015). Misregulation of multiple regulators of the cell cycle pathway, including Hippo signaling, may underlie an enhanced exit from quiescence or increase cycling in our *Mtf2*$^{-/-}$ HSCs and contribute to the observed loss of the HSC pool.

Tightly regulated epigenetic control of gene expression is critical to coordinate multiple signaling pathways during development. Here, using an unbiased systems biology approach we report for the first time PRC2-mediated H3K27me3 regulation of Dnmts. Although, Dnmts have been previously shown to modulate distinct polycomb-mediated histone modifications (Jin, Yao et al. 2009), the reverse has not been previously reported to our knowledge. Furthermore, we demonstrate a unique role for Mtf2 in erythroid development and HSPC self-renewal *via* epigenetic regulation of canonical Wnt/ß-catenin and Hippo signaling pathways. Collectively, our data illustrate how Mtf2 functions as an essential PRC2 component in the hematopoietic system,

regulating core PRC2 components and modulating PRC2-mediated promoter-proximal H3K27me3 methylation and repression of multiple gene networks that are essential for hematopoietic development and function.

Materials and Methods

Generation of Mice and Embryonic Analysis

Gene-targeted mouse C57Bl/6 ESCs were obtained through EUCOMM and were aggregated with CD1 blastocysts to form chimeras. Germline transmission was confirmed using PCR-based genotyping (primers listed in Table S4) and all future breeding was done on the C57Bl6/J strain to maintain this background. Peripheral blood analysis on embryos was completed as described(Masuoka and Townes 2002). Blood smears were stained with Wright-Giemsa. For Mtf2 expression in developing tissues, WT and Mtf2-null mice at various embryonic stages of development were fixed in 4% paraformaldehyde (PFA) and paraffin-embedded. Immunofluorescence was performed on 4 μm sections of paraffin-embedded embryos *via* overnight incubation with antibody against Mtf2 (also known as M96, Genway). Confocal microscopy was performed using a Zeiss Inverted LSM510 microscope. For CFU analysis on fetal liver cells, 2 x 10^5 cells were isolated and plated in methylcellulose media containing growth factors (Stem Cell Technologies), and colonies were enumerated after 12 days of growth.

Flow Cytometry

For flow cytometric analyses, samples were first subjected to red blood cell lysis and stained with antibodies directed against lineage markers. Mouse peripheral blood, fetal liver or bone marrow was stained with antibodies (from eBiosciences) directed against CD4 (Clone

GK1.5), CD8 (53-6.7), CD11b (M1/70), CD71 (R17217), Ter119 (TER119), B220 (RA3-6B2), and Gr1 (RB6-8C5) for lineage analysis. To distinguish donor-derived cells during transplantation, samples were also stained with anti-CD45.2 (104). For mouse stem and progenitor cell analysis, mouse BM and FL cells were first incubated with rat antibodies against CD3 (17A2), CD4, CD5 (53-7.3), CD8, CD11b, Ter119, and B220 then depleted using Sheep Anti-Rat Dynabeads (LifeTech) (CD11b was excluded in FL analysis). Lineage-depleted samples were then stained with antibodies (from eBiosciences) against cKit (2B8), Sca1 (D7), CD34 (RAM34), CD16/CD32 (93), CD127 (A7R34), CD48 (HM48-1) and CD150 (mShad150). For cell cycle analysis, pregnant dams (e14.5) were injected with BrdU (1 mg, i.p) and embryos were harvested 2 hr later. Cells were fixed in ice-cold ethanol, treated with 1.5 M HCl for 30 min then stained with an antibody against BrdU (Millipore) and a fluorescence-conjugated secondary antibody. Cells were stained with propidium iodide (Sigma) to assess cell cycle state. For erythroblast morphology analysis, cells were stained with antibodies against Ter119 and CD71 as above, and with Hoechst (LifeTech) and Thiazole Orange (Sigma) for nucleic acid detection. Cells were analyzed using the ImageStream imaging flow cytometer (Amnis) and classified based on the parameters outlined in(McGrath, Bushnell et al. 2008). Size measurements were based on area of brightfield images and cells with centrally located nuclei were determined based on delta XY centroid measurements(Konstantinidis, Pushkaran et al. 2014). HSPCs were fixed with 4% PFA, permeabilized with 0.3% Triton, and stained for either TAZ (Cell Signaling) or active ß-catenin (Millipore), and DRAQ5. The nuclear and cytoplasmic contents of TAZ and active ß-catenin were determined using the “Nuclear Localization” algorithm in the ImageStream software.

Capillary Electrophoresis Immunodetection

Hematopoietic cells were isolated from e14.5 mouse FL and enriched by $CD45^+$ selection using immunomagnetic selection with anti-CD45 (eBioscience) and Sheep Anti-Rat Dynabeads (Life Tech). Cells were lysed in Bicine/CHAPS buffer with DMSO and protease inhibitors (Protein Simple). Lysates were prepared according to instructions for the NanoPro 1000 and protein was quantified using the Bradford assay. Lysates containing 0.1 mg protein were combined with a G2 ampholyte mixture (pH 3-10, Protein Simple) containing fluorescence standards and charge-based separation was performed within glass capillaries using the NanoPro 1000 system (Protein Simple). After UV cross-linking, samples were probed with antibodies against Mtf2 (Genway, 1:50), Jarid2 (Aviva, 1:50), Ezh2 (Active Motif 1:50), Ezh1 (Abcam, 1:50), followed by secondary, HRP-conjugated antibodies (Protein Simple, 1:100), and detection by chemiluminescence. Peaks associated with specific protein expression were manually identified and the areas under the curves were calculated and normalized to a loading control (Hsp70). Duplicate technical replicates were performed for each biological sample (n=3 to 7 mice).

Lentiviral production of Mtf2 shRNA

293T cells were co-transfected with lentiviral plasmids pMD2G, pPAX2 and pGIPZ containing the shRNA (ThermoScientific) of interest using polyethylenimine (see table below). The supernatant containing the virus was collected 48 and 72 hrs post transfection. The virus was concentrated through ultracentrifugation and was stored at -80°C.

shRNA	**Sequence**
Mtf2 shRNA Clone 3	TAATGTATGTCATAAGC
Mtf2 shRNA Clone 7	TTGGCTTTATGTCCATCC
Scrambled shRNA	GTTACACGATATGTTATC

Lentivirus-mediated Mtf2 knockdown of mouse bone marrow cells

Adult mouse bone marrow was isolated and lineage-depleted to enrich for stem and progenitor cells (Stem Cell Technologies). Cells were maintained in IMDM media containing bovine serum albumin, insulin, and transferrin (Stem Cell Technologies), 100 U/ml penicillin-streptomycin (ThermoFisher), SCF (50 ng/mL), TPO (10 ng/mL), Flt3 (10 ng/mL), IL6 (10 ng/mL). Growth factors were purchased from Peprotech. On day 1 of infection, cells were incubated with polybrene (6 mg/ml) for 2 hr at 37°C, then combined with viral supernatants containing either a GFP-tagged Mtf2 shRNA clone or a scrambled shRNA control (ThermoFisher). Cells were pelleted at 400*x g* for 20 min, then maintained at 37°C. On day 2, infection was repeated. Cells were grown for 3 days using a fed-batch culture system then sorted according to GFP-expression. High GFP cells were fixed in 4% PFA, permeabilized with 0.3% Triton and labeled with antibodies against Mtf2 (Genway), Ezh2 (Cell Signaling), Suz12 (Millipore), or H3K27me3 (Millipore) and stained with the appropriate secondary antibodies. Protein expression was determined by flow cytometry compared with an isotype-only control. Data analysis compared mean fluorescent intensity values using a ratio paired t-test.

Colony Forming Assays and LT-CIC analysis

For CFU assays, $2x10^5$ GFP^+ lentivirus-transduced HSPCs were isolated and plated in MethoCult GF M3434 media containing growth factors (Stem Cell Technologies), and colonies were enumerated after 12 days. For LT-CIC assays, 300,000 GFP^+ lentivirus-transduced HSPCs were cultured on MS5 cells in a 24-well plate, containing MyeloCult 5300 supplemented with 10^{-6} M hydrocortisone. Cultures were incubated at 33°C in 5% CO_2 for 4 weeks with half media exchanges performed weekly. At the end of 4 weeks, all cells (both adherent and non-adherent)

were harvested and seeded on MethoCult GF M3434 and incubated at 37°C in 5% CO_2. Colonies were enumerated after 14 days of culture.

RNA-seq and ChIP-seq

FL cells from e14.5 *Mtf2*$^{+/+}$ and *Mtf2*$^{-/-}$ embryos were isolated and CD71^{+}Ter119^{Mid} and CD71^{+}Ter119^{+} fractions were sorted directly into lysis buffer by FACS. Lineage-negative HSPCs were isolated from FLs of e14.5 *Mtf2*$^{+/+}$ and *Mtf2*$^{-/-}$ mice using antibodies against lineage markers, as described above. For RNA-seq, RNA was isolated (Arcturus PicoPure Kit, LifeTech) and DNase treated (Qiagen). The quality of RNA was determined using an Agilent 2100 Bioanalyzer. Library preparation was performed using 150 ng high-quality RNA (TruSeq Library Prep Kit, Illumina), and sequenced on a HiSeq 2000 (Illumina). Replicate data was analyzed using TopHat v1.4.1 and Cuffdiff v1.3.0(Trapnell, Roberts et al. 2012) to map reads to a reference mouse genome assembly (mm9) and expression differences against the Ensembl release 67 gene model were determined. Significant fold changes were determined using the Benjamini-Hochberg corrected *p*-value of 0.05. Raw RNA-seq data is available in GEO (Accession # - to be completed upon acceptance). Data was analyzed using the DAVID bioinformatics tool for functional annotation(Reimand, Kull et al. 2007, Reimand, Arak et al. 2011) and Cytoscape with the Enrichment Map plugin for visualization(Merico, Isserlin et al. 2010, Merico, Isserlin et al. 2011). RNA-seq targets were validated by qPCR after RNA was converted to cDNA using Superscript II (LifeTech). Raw RNA-seq data is available in GEO (Accession # - to be completed upon acceptance).

For ChIP-seq, sorted cells were crosslinked with 1% formaldehyde for 10 min at room temperature. Samples were sheared using a Covaris sonicator until the DNA reached a final size

of 75-700bp. 10 μg antibody (anti-Mtf2, Genway; anti-H3K27me3, Millipore) was bound to pre-blocked Protein A magnetic beads (Millipore), combined with the sonicated DNA and incubated overnight. After incubation, the beads were collected and the DNA-antibody complexes were eluted at 65°C. The crosslinks were reversed overnight at 65°C. Samples were treated with Proteinase K and RNase A and the DNA was purified using phenol-chloroform. 500,000 cells per sample were used for both immunoprecipitation and control (IgG, SantaCruz). For sequencing, 10 μg DNA was used for amplification and library preparation (Diagenode Microplex Library Preparation Kit). DNA was analyzed for quality, quantity and size using an Agilent 2100 Bioanalyzer and digital PCR. Libraries were used for sequencing on a HiSeq 2000 (Illumina). Bowtie v2.2.3(Langmead and Salzberg 2012) and MACS 1.3.7(Zhang, Liu et al. 2008) were used for alignments and peak calling, respectively. Gene annotations and peak profile analysis were completed using PAVIS(Huang, Loganantharaj et al. 2013) and GREAT(McLean, Bristor et al. 2010). The DAVID bioinformatics tool was used for functional annotation with a Benjamini-Hochberg FDR correction test, unless otherwise indicated(Reimand, Kull et al. 2007, Reimand, Arak et al. 2011). Repeated *k*-means clustering analysis of methylation occupancy was completed using seqMINER(Ye, Krebs et al. 2011). ChIP-seq targets were validated by ChIP-qPCR. All qPCR analysis was completed on a Roche Light Cycler 480 using Sybr Green MasterMix (Roche) and 0.1 mM primers. Primer sequences are listed in Table S4.

Bone marrow transplants and analysis

For homing experiments, 5 x 10^6 FL cells from *Mtf2*$^{-/-}$ or WT e14.5 embryos were isolated and labeled with carboxyfluorescein diacetate succinimidyl ester (CFSE) (5 **µ**M/mL, Molecular Probes) and 5 x 10^6 washed cells were injected *via* tail vein into lethally irradiated *B6.SJL-Ptprca*

Pep3b/BoyJ (CD45.1$^+$) mice (Jackson Labs). BM was harvested 17 hr later and assessed for CFSE fluorescence. For primary competitive transplants, 0.5 x 10^6 million FL cells from either *Mtf2*$^{-/-}$ or WT e14.5 embryos (CD45.2$^+$) were combined with 0.5 x 10^6 BM cells from adult CD45.1$^+$ mice and injected *via* tail vein into lethally irradiated CD45.1$^+$ mice. Peripheral blood was assessed by flow cytometry at various time points up to 4 months post-transplantation. For secondary transplants, 5 x 10^6 cells were isolated from BM of primary transplant recipients and injected *via* tail vein into lethally irradiated CD45.1$^+$ mice.

Dual knock down experiments

Adult mouse bone marrow HSPCs were isolated as mentioned previously. The cells were maintained in IMDM media containing bovine serum albumin, insulin, and transferrin (Stem Cell Technologies), 100 U/ml penicillin-streptomycin (ThermoFisher), SCF (50 ng/mL), TPO (10 ng/mL), Flt3 (10 ng/mL), IL6 (10 ng/mL). On day 1 of infection, cells were transduced with lentivirus expressing either a GFP or RFP-tag that targeted the first gene. Transduced cells were sorted 48 hours post transduction using the fluorescence tag and were subjected to a second round of transduction using different set of virus expressing either a GFP or RFP-tag that targeted the second gene. The lentivirus targeting one gene always expressed a different fluorescence protein compared to the lentivirus targeting the other gene. Dual transduced cells expressed both GFP and RGP fluorescence proteins and were sorted 48 hours post secondary transduction using the GFP and RFP markers and were subjected to various functional experiments. The cells were grown using a fed-batch culture system throughout the duration of the experiment. The MOI used for these experiments was 50.

Wnt and Hippo inhibition

The Wnt and Hippo inhibitors, ICG001, JW74, Dasatinib and Pazopanib, were dissolved in DMSO. For the CFU and the LT-CIC assays, the drugs were added every 72 hr directly to the MethoCult GF M3434 media and MyeloCult 5300 respectively. The Wnt pathway inhibitors, ICG001 and JW74, were added at concentrations of 2 μM and 1.5 μM, respectively. The Hippo pathway inhibitors, Dasatinib (Sigma-Aldrich) and Pazopanib (Sigma-Aldrich) were added at concentrations of 1 μM and 1.5 μM, respectively. Enumeration of colonies was compared with WT HSPCs transduced with scrambled shRNA and treated with vehicle (DMSO).

Methyl-ChIP-qPCR

Methyl ChIP-qPCR analyses were performed using the EpiMark Methylated DNA Enrichment Kit (New England Biosciences), according to manufacturer's instructions. Briefly, DNA was isolated from adult mouse HSPCs transduced with shRNA against Mtf2 or a scrambled control. DNA was fragmented and combined with methyl-CpG-binding domain protein 2 (MBD2) bound to magnetic beads to capture methylated DNA. Methylated CpG DNA was eluted from beads. Enriched DNA was used for RT-qPCR using primers listed in Table S4.

Ex-vivo differentiation of erythroblasts

GFP^+ lentivirus-transduced erythroblasts ($CD71^+/Ter119^-$) were seeded at a density of 1 x 10^6 cells/mL in StemPro-34 SFM (ThermoFisher) supplemented with L-glutamine (1%; ThermoFisher), Epo (Peprotech; 10 U/mL) and transferrin (Sigma-Aldrich; 1 mg/mL). The GFP^+ cells were cultured for 48 hr in the presence and absence of ICG001 (Tocris) and JW74 (Tocris).

Half media exchange was performed after 24 hr and after 48 hr the cells were collected, stained with CD71 and Ter119 antibodies and analyzed using flow cytometry.

Statistics

All data are presented as mean ± SEM. Data was analyzed using Prism 5.0 (GraphPad Software). Statistical significance of differences was measured by 2-tailed Student's t test. A *p*-value < 0.05 was used as a cut-off to indicate statistical significance.

Study Approval

All animal experiments were conducted with the approval of the University of Ottawa Animal Care Committee, in accordance with the Canadian Council on Animal Care Standards and the Province of Ontario's Animals for Research Act.

Acknowledgments

We thank the OHRI Stem Core Facility for their assistance with FACS and sequencing and M Brand, J Dilworth, and D Picketts for critical reading, and A Sheftel for assistance in editing. Chimeras were generated by the Toronto Centre for Phenogenomics. This work was supported by operating grants from the Canadian Cancer Society Research Institute, the Cancer Research Society, and the Canadian Institutes of Health Research to WLS and CI. JMR was supported by an Ontario Graduate Scholarship and a CIHR Banting and Best CGS Doctoral Research Award, RFP is supported by a USDA-NIFA Hatch project number 4581 and NIH grant DK080040, and WLS was supported by a Tier 1 Canada Research Chair in Integrative Stem Cell Biology. The authors have declared that no conflict of interest exists.

Supplementary Figures

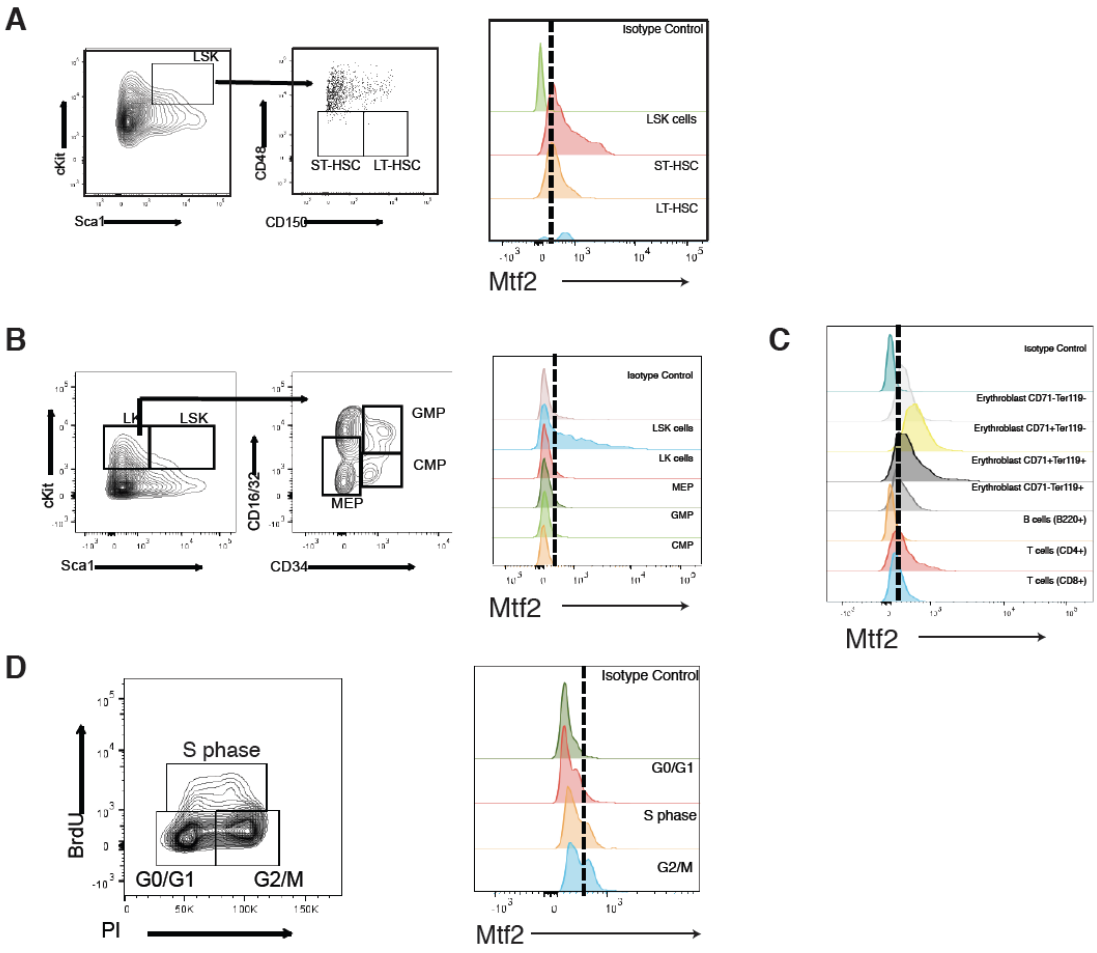

Figure S2.1. Mtf2 expression in the mouse hematopoietic system. Related to Figure 2.1. A, Mtf2 protein expression is high in Lineage$^-$Sca1$^+$cKit$^+$ (LSK) stem and progenitor cells, including LSK CD48$^-$CD150$^-$ short term HSCs (ST-HSC) and LSK CD48$^-$CD150$^+$ long term HSCs (LT-HSCs). Dotted lines indicate level of isotype control expression. **B-C,** Mtf2 protein expression was analyzed in progenitor and mature hematopoietic lineages by flow cytometry. A representative gating strategy is shown for progenitor analysis. Mtf2 is highly expressed in LSK progenitors, but expression is decreased in more restricted MEP, GMP and CMP progenitors. In mature cells, Mtf2 is highly expressed in erythroid progenitors and its expression is relatively lower in T and B cells (n=3). **D,** In CD71$^+$ Ter119$^+$ erythroid progenitors, Mtf2 expression is also regulated during the cell cycle, with highest expression seen in during S and G2/M phase, based on BrdU/PI staining.

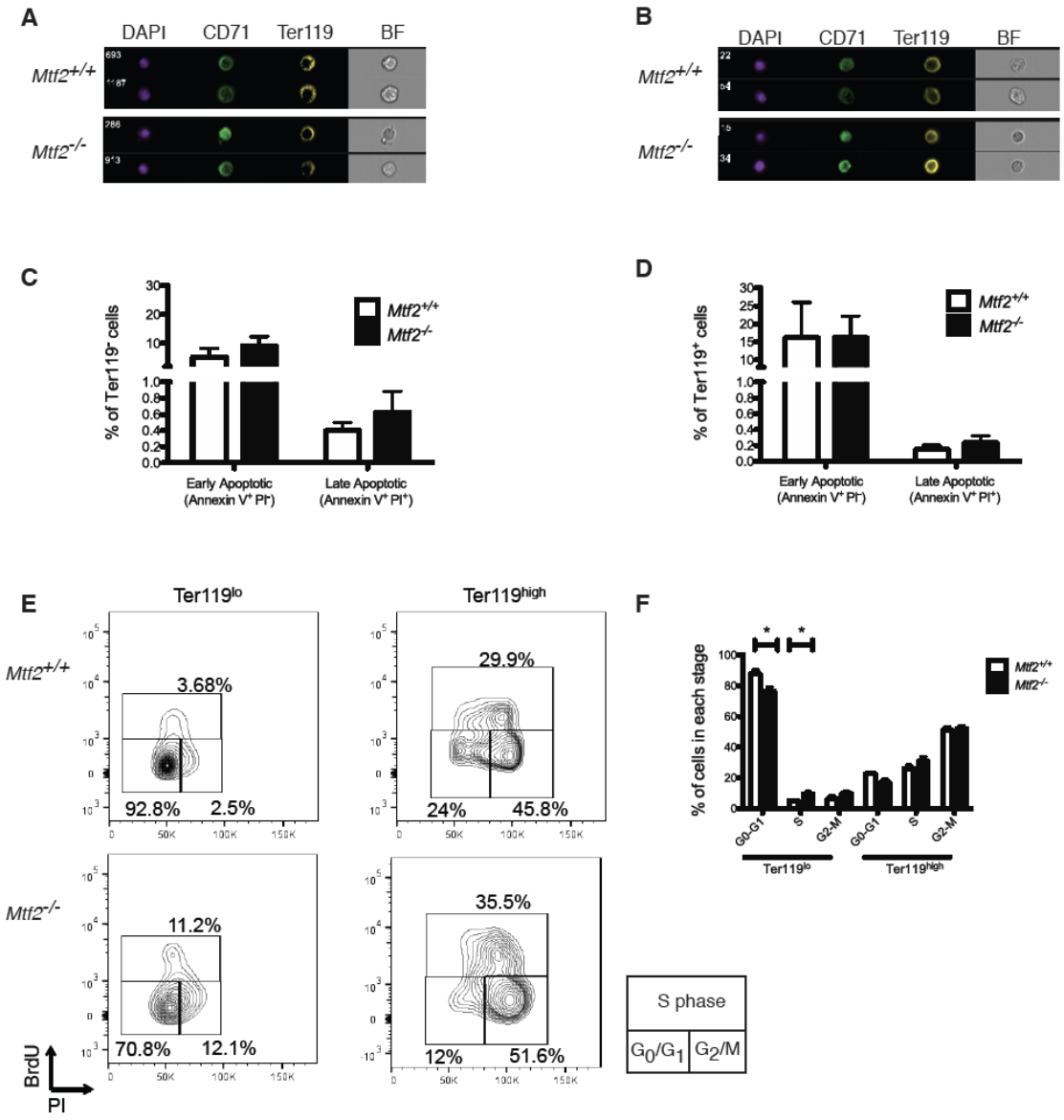

Figure S2.2. Morphology of wild-type and *Mtf2-/-* fetal liver and peripheral blood erythroblasts. Related to Figure 2.2. A-B, Fetal liver from e14.5 WT and *Mtf2*$^{-/-}$ embryos were isolated and stained for markers of erythroblast development (CD71, Ter119). Using imaging flow cytometry, cells from either genotype within the S2 and S3 populations of erythroblasts (**A** and **B**, respectively) have similar morphology. BF, brightfield. **C,** Ter119^{-} FL cell or **(D)** Ter119^{+} from *Mtf2*$^{-/-}$ embryos do not show increased early or late-stage apoptosis, based on Annexin V staining. **E,** Representative cell cycle profiles of WT and *Mtf2*$^{-/-}$ Ter119^{lo} and Ter119^{hi} fetal liver erythroblasts were assessed using BrdU and PI staining. In the Ter119^{lo} fraction, there are fewer *Mtf2*$^{-/-}$ cells in G0/G1 and more in S phase. **F,** A higher frequency of *Mtf2*$^{-/-}$ Ter119^{lo} pro-erythroblasts are found

in S-phase and fewer in G0/G1 phase, indicating a defect in cell cycling. Data are shown as mean ± SEM, n=3, *p<0.05, **p<0.01, ***p<0.001.

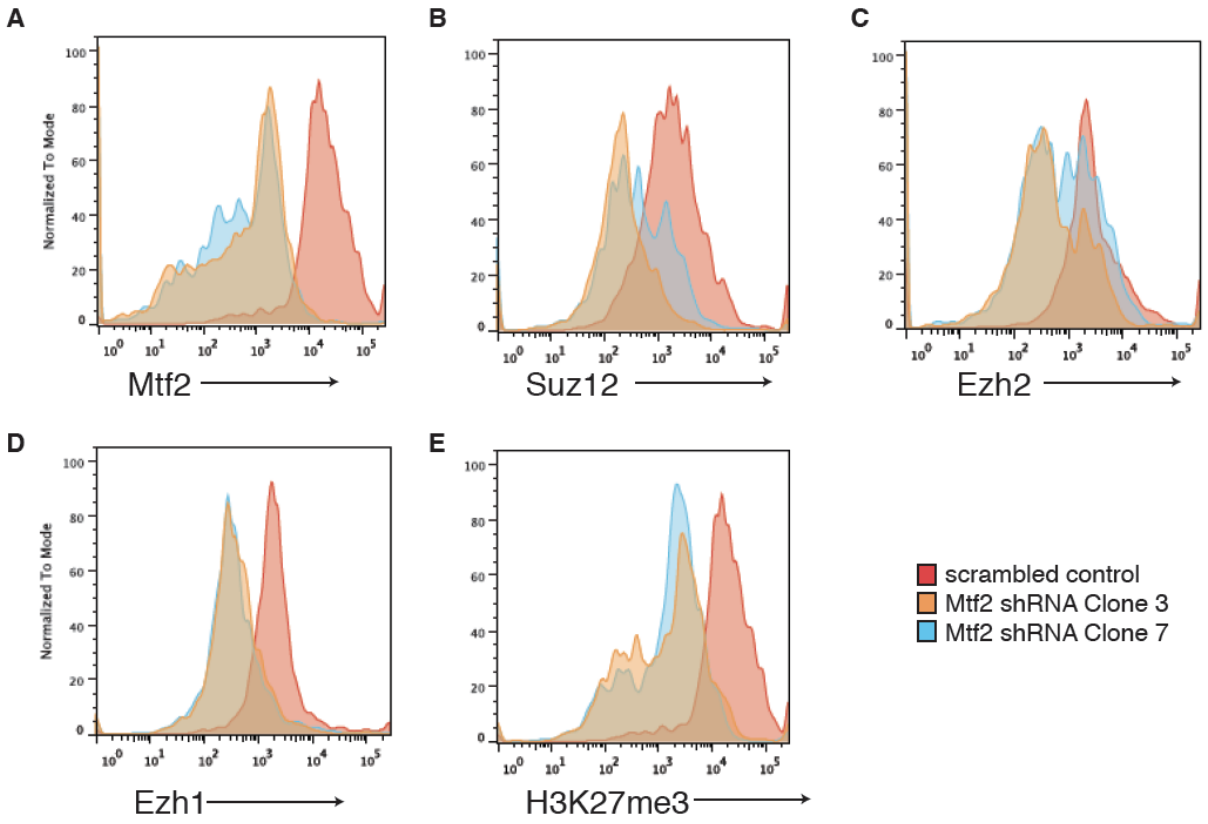

Figure S2.3. Mtf2 regulates core PRC2 protein levels and H3K27me3 in erythroblasts. Related to Figure 2.3. A, Mtf2 levels are reduced after lentiviral-mediated knockdown in BM HSPCs using two different shRNA clones. Mtf2 levels cells transduced with a scrambled shRNA control vector are shown for comparison. **B-E,** Upon knockdown of Mtf2, levels of Suz12, Ezh2, Ezh1, and H3K27me3 are also reduced ($p<0.001$).

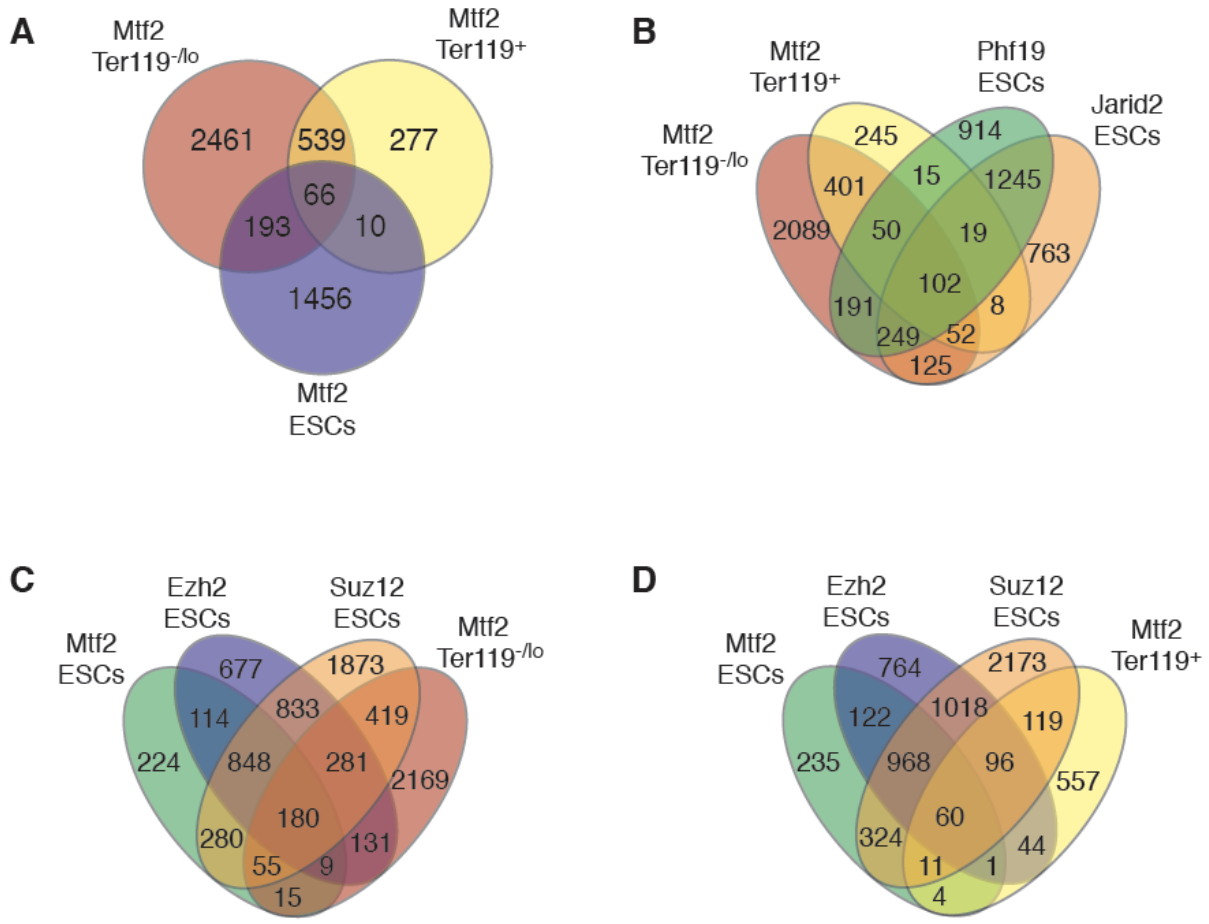

Figure S2.4. Genes associated with Mtf2 binding in erythroid cells show little overlap with Mtf2 and PRC2 targets in ESCs. Related to Figure 2.3. A, Mtf2 targets determined by ChIP-seq are distinct from Mtf2 targets identified in ESCs. **B-D,** Targets of PRC2 members identified in ESCs show little overlap with Mtf2 targets identified in primary erythroid cells (Mtf2 data (Walker, 2010), Ezh2 & Jarid2 data (Peng,2009), Suz12 & Phf19 data (Hunkapiller, 2013)).

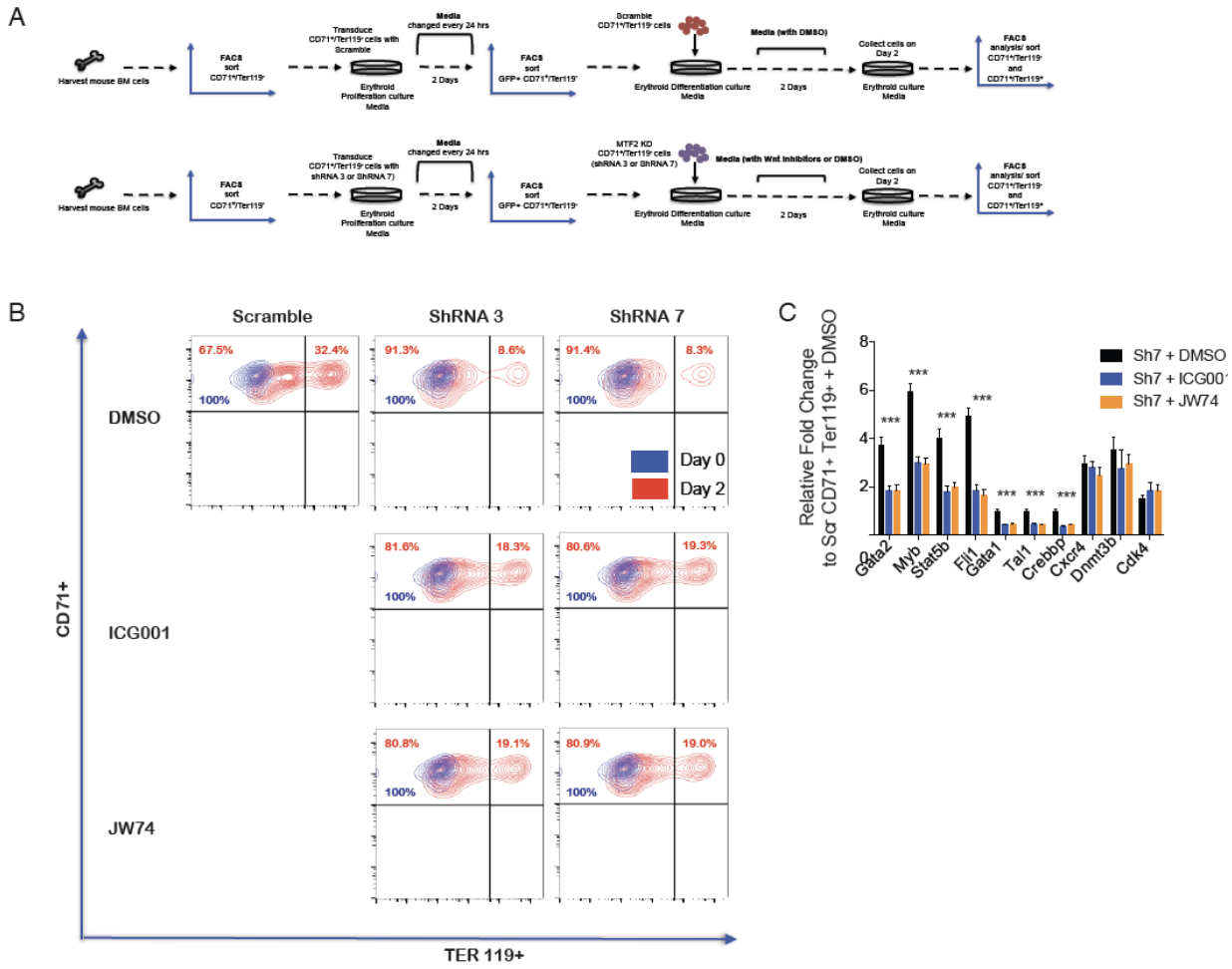

Figure S2.5. Wnt pathway inhibition in Mtf2-deficient erythroblasts increases their ability to differentiate. Related to Figure 5. A, Schematic of *ex vivo* erythroid differentiation assay with Mtf2-deficient (transduced with two independent shRNAs against Mtf2) and scramble transduced proerythroblasts ($CD71^{+}Ter119^{-}$) cells. **B,** Flow cytometry reveals Mtf2 deficient proerythroblasts show an increased capacity to differentiate when treated with small molecule inhibitors of Wnt (ICG001 or JW74). **C,** Mtf2-knockdown $CD71^{+}Ter119^{+}$ cells treated with Wnt inhibitors show inhibition of de-repressed erythroid genes. ***$p<0.001$.

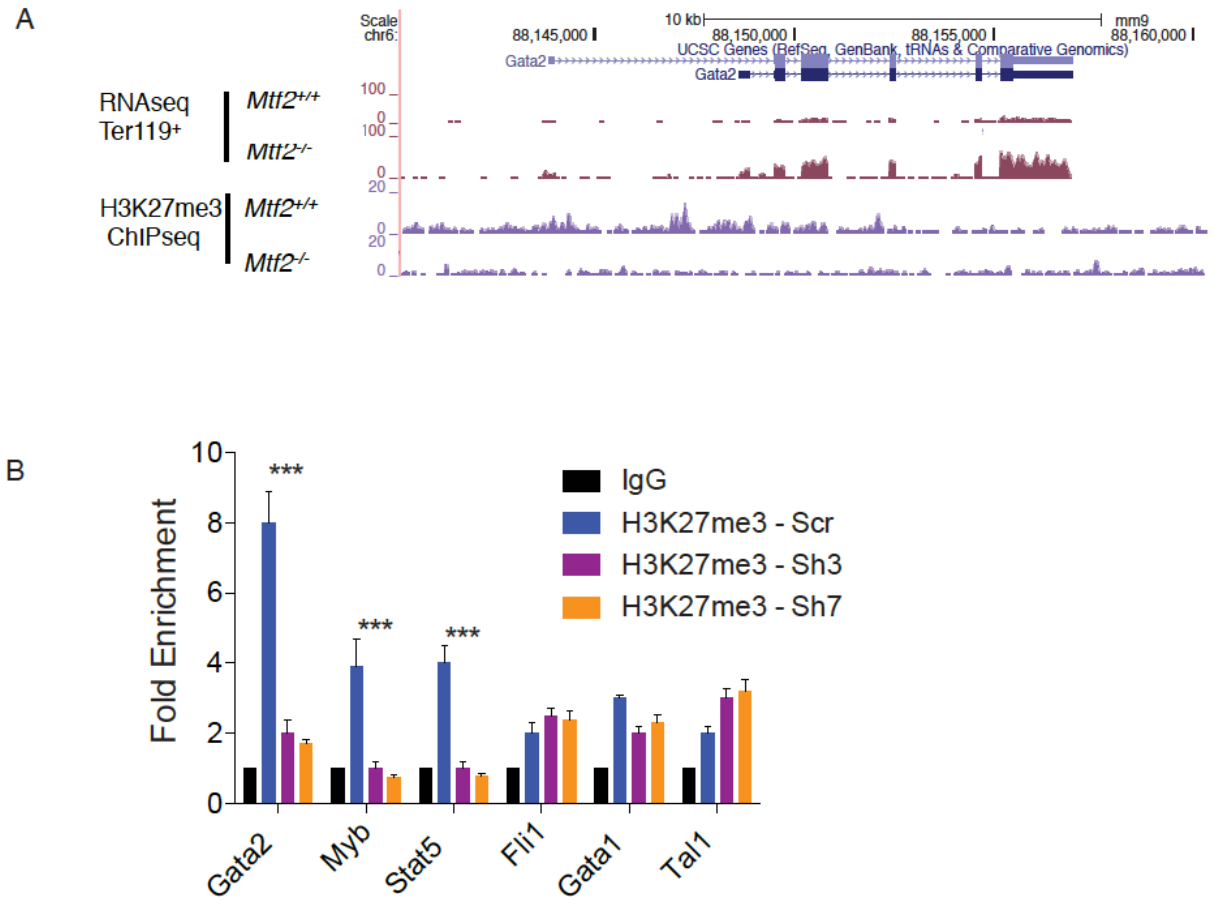

Figure S2.6. Some erythroid master regulators are targets of Mtf2-PRC2 as seen through loss of H3K27me3. Related to Figure 2.5. A, RNA-sequencing and ChIP-seq traces showing overexpression of Gata2 and loss of H3K27me3 at promoter-promimal regions in Mtf2-null erythroblasts. **B,** Validation of ChIP-seq results by ChIP-qPCR shows binding of H3K27me3 to Gata2, Myb and Stat5 promoters in HSPCs treated with scrambled shRNA. H3K27me3 marks are lost when Mtf2 is knocked down using shRNAs (Sh3, Sh7). Other genes, like Fli1, Gata1 and Tal1, do not show a loss of H3K27me3 upon loss of Mtf2. ***p<0.001.

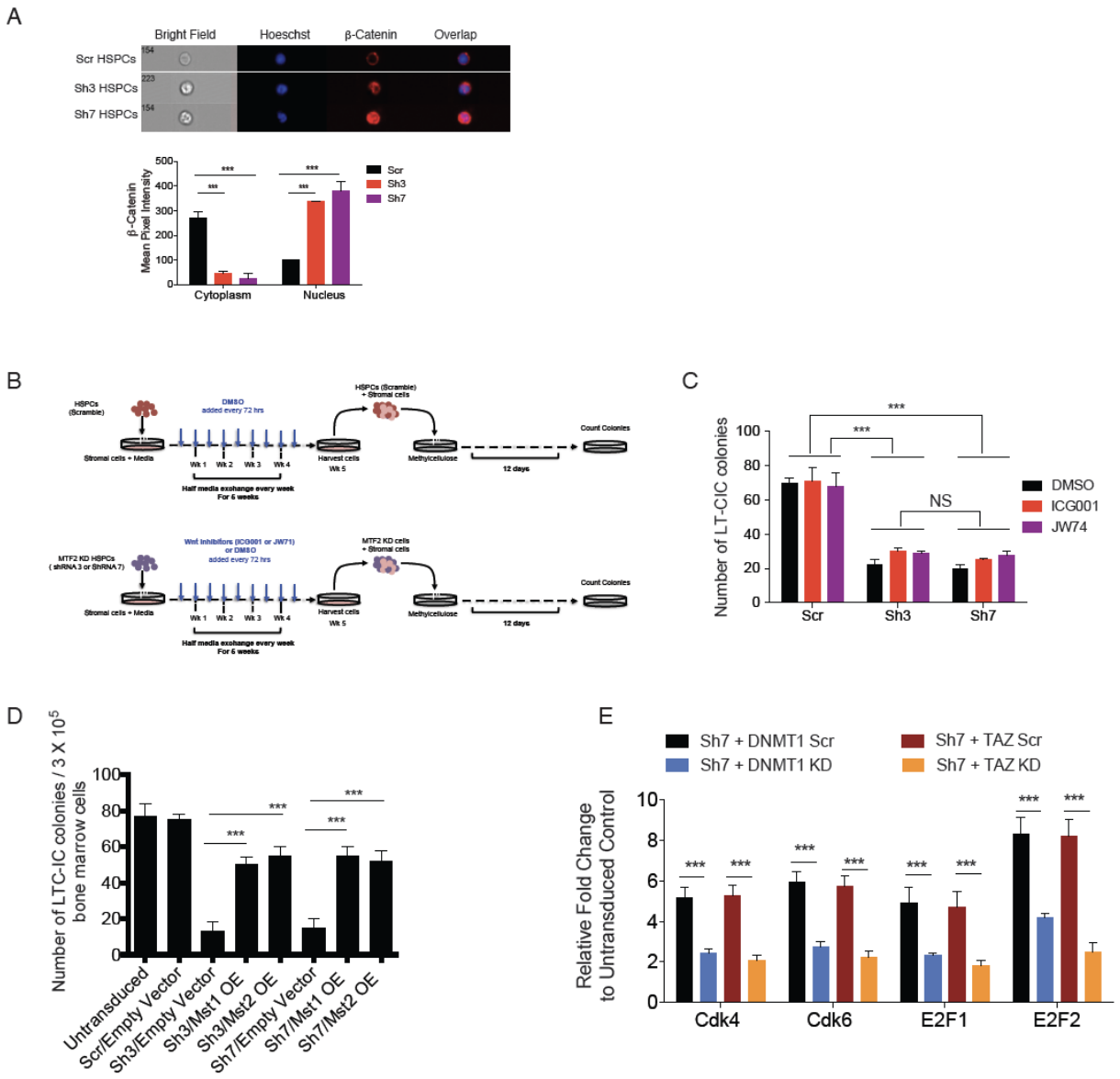

Figure S2.7. Wnt pathway inhibition in Mtf2-deficient HSPCs does not affect the number of LT-CIC colonies observed. Related to Figure 2.6 and Figure 2.7. A, Mtf2-deficient HSPCs express higher levels of activated β-catenin within their nuclei, compared to control cells infected with scrambled constructs, indicating activation of the Wnt signaling pathway. Protein levels were quantified in single cells using imaging flow cytometry. **B,** Experimental schematic for LT-CIC assay, where scramble transduced HSPCs and Mtf2 deficient HSPCs (transduced with two independent shRNAs against Mtf2) were treated with either DMSO or a Wnt inhibitor (either ICG001 or JW74). **C,** No significant difference is observed in the number of LT-CIC colonies under Wnt signaling inhibition. Data is shown as number of LT-CIC colonies per 3x105 bone

marrow cells. **D,** Overexpression of MST1/2 in Mtf2-deficient HSPCs increases the number of LT-CIC colonies, compared to empty vector controls. **E,** Knockdown of either Dnmt1 or Taz reduces expression of cell cycle genes such as Cdk4, Cdk6, E2F1 and E2F2 that were overexpressed in Mtf2-deficient HSPCs.

Chapter 3

Harinad B. Maganti*, Hani Jrade*, Christopher Cafariello, Janet L. Manias Rothberg Christopher J. Porter, Julien Yockell-Lelièvre, Hannah L. Battaion, Safwat T. Khan, Theodore J. Perkins, Mitchell Sabloff, Caryn Y. Ito & William L. Stanford. T**argeting the Epigenetic Program Underlying Refractory Acute Myeloid Leukemia.**

*Equal contributions

Author contributions

HBM, MS, CYI and WLS designed the study, interpreted the results, and wrote the manuscript. JMR, CC, HJ and STK assisted HBM in the establishment of the AML biobank. HBM conducted the *in vivo* and *in vitro* functional assays. HJ analyzed the results in a blinded manner. HJ conducted the commet assay experiments. HM and JYL analyzed the results in a blinded manner. STK assisted in the immunohistochemistry experiments. MS performed the clinical care, analysis and data interpretation. HBM, CJP and TJP performed all bioinformatic analyses. All authors assisted in editing the manuscript.

Targeting the Epigenetic Program Underlying Refractory Acute Myeloid Leukemia

Harinad B. Maganti[1,2,3†], Hani Jrade[1,2,4†], Christopher Cafariello[1,2,4], Janet L. Manias Rothberg[1,2,4]

Christopher J. Porter[5], Julien Yockell-Lelièvre[1,2], Hannah L. Battaion[1,2,4], Safwat T. Khan[1],

Theodore J. Perkins[1,3,5], Mitchell Sabloff[6,7], Caryn Y. Ito[1,3*] & William L. Stanford[1,2,3,4*]

[1]The Sprott Center for Stem Cell Research, Regenerative Medicine Program, Ottawa Hospital Research Institute, Ottawa, ON, Canada K1H 8L6;

[2]Ottawa Institute of Systems Biology, Ottawa, Ontario, Canada;

[3]Department of Biochemistry, Microbiology and Immunology, University of Ottawa, Ottawa, Ontario, Canada;

[4]Department of Cellular and Molecular Medicine, University of Ottawa, Ottawa, Ontario, Canada;

[5]Ottawa Bioinformatics Core Facility, The Sprott Center for Stem Cell Research, Ottawa Hospital Research Institute, Ottawa, ON, Canada K1H 8L6

[6]Division of Hematology, Department of Medicine, University of Ottawa, Ottawa, Canada

[7]Ottawa Hospital Research Institute, Ottawa, ON, Canada Canada K1H 8L6

[†]These authors contributed equally to this work.

Abstract

Deep sequencing has revealed that epigenetic modifiers are the most mutated genes in acute myeloid leukemia (AML). Thus, elucidating epigenetic dysregulation in AML is crucial in understanding disease mechanisms. Here, we demonstrate that Polycomblike2 (PCL2/MTF2) plays a fundamental role in the Polycomb repressive complex 2 (PRC2) and that its loss elicits an altered epigenetic state underlying refractory AML. Unbiased systems analyses identified MTF2-PRC2 repression of MDM2 as central to and therefore a biomarker for refractory AML. Thus, MTF2-deficient leukemic stem cell (LSC) enriched populations overexpress MDM2, thereby inhibiting p53 and leading to chemoresistance due to defects in cell cycle regulation and apoptosis. Targeting this dysregulated signaling pathway by MTF2 overexpression or MDM2 inhibitors sensitized refractory patient LSC-enriched populations to induction chemotherapeutics and prevented relapse in AML patient-derived xenograft (PDX) mice. Therefore, we have uncovered a direct mechanism by which MTF2 functions as a tumor suppressor required for AML chemotherapeutic sensitivity.

Introduction

Standard induction chemotherapy has been the frontline therapeutic to treat AML for the past 30 years. Although standard induction chemotherapy can induce remission in most AML patients, 30-40% of patients are unresponsive to treatment. Unfortunately, as many as 60-90% of refractory AML patients will not survive their disease regardless of additional therapies (Thol, Schlenk et al. 2015). To move beyond generalized treatments, targeted therapeutics and biomarkers are actively being pursued to customize treatment regimens to attain complete remission and improve overall survival rates. Despite recent advances in genetic markers that stratify AML patients into favorable, intermediate and adverse risk categories, refractory AML patients are found across all risk groups (Döhner, Estey et al. 2017). This suggests that a non-mutational mechanism plays an important role in refractory AML. This hypothesis is further supported by insightful deep sequencing studies which have revealed that epigenetic modifiers are predominantly mutated in AML (Glass, Hassane et al. 2017). While these studies have relied heavily on DNA sequencing to identify key mutations, RNA expression levels and the epigenetic regulation within refractory AML cells have largely been overlooked. Recent studies have shown that H3K27me3-mediated epigenetic regulation can predict disease outcome in many cancers (Cai, Hou et al. 2011, Wassef, Rodilla et al. 2015). However, the mechanisms of H3K27me3-mediated epigenetic regulation of refractory disease have not been elucidated. Understanding the mechanism is further complicated by the fact that studies are largely performed using heterogeneous populations containing both mature and immature cells. To reduce heterogeneity, we utilized LSC-enriched immature primary AML patient-derived $CD34^{+}CD38^{-}$ cells to investigate the role of PRC2 and H3K27me3 in refractory AML and employed an unbiased system approach to dissect the underlying molecular networks that drive refractory AML. Using this strategy, we discovered that

the MDM2-p53 axis is directly regulated by MTF2 and targeting this pathway reverses MTF2-PRC2 mediated chemoresistance associated with refractory AML.

Results

Patients with MTF2 deficiency respond poorly to induction chemotherapy

To determine whether H3K27me3 levels within LSC-enriched cells are altered in AML, we analyzed the global levels of this repressive histone mark within $CD34^{+}CD38^{-}$ cells isolated from 32 blinded diagnostic AML BM aspirates isolated from patients who underwent induction therapy (Tables S5-S7). Strikingly, we identified two patient groups based on total H3K27me3 levels; one with levels similar to control normal BM cells and another with markedly reduced levels. Independent clinical patient follow-up revealed that the H3K27me3-reduced LSC-enriched cohort was primarily comprised of patients failing to achieve complete remission, otherwise referred to as non-responders or refractory AML patients (Fig.3.1A,B). Furthermore, reduced H3K27me3 levels within patient $CD34^{+}CD38^{-}$ cells predicted poor patient survival. In fact, the mean survival time of patients with normal levels of H3K27me3 was three times longer than patients with reduced H3K27me3 levels (Fig.3.1C and Tables S5-S7). Next, we used RT-qPCR to test whether there is a correlation between H3K27me3 levels and PRC2 member expression. Linear regression analysis revealed a highly significant correlation between H3K27me3 levels and *MTF2* mRNA expression (R^2=0.9416) within the patient cohort $CD34^{+}CD38^{-}$ cells (Fig.3.1D). However, the correlation for other PRC2 members was much weaker (Fig.3.1E,F). Reduced *MTF2* mRNA expression within the patient $CD34^{+}CD38^{-}$ cells also was associated with poor response to standard induction chemotherapy (Fig.3.1G,H) and poor survival (Fig.S3.1A,B). Cytogenetics analysis revealed that our cohort consisted of patients belonging to all the three European

LeukemiaNet (ELN) risk categories (Fig.S3.1C). Interestingly, within the favorable cytogenetics category, *MTF2* levels were able to further stratify patients based on overall survival (Fig.S3.1D); although, this was not found to be the case in the intermediate cytogenetics category (Fig.S3.1E). These results were further validated using the TCGA dataset (Cancer Genome Atlas Research, Ley et al. 2013), where AML patients received an induction therapy regimen identical to the treatment given to our cohort (Extended Methods). Kaplan-Meier analysis of the TCGA dataset revealed that patients with reduced levels of *MTF2* within bulk BM cells had reduced overall survival and disease free survival, while altered expression of other PRC2 members did not affect either parameter (Fig.S3.1F-M and Table S8).

Considering *MTF2* is rarely mutated in AML, we analyzed the *MTF2* promoter for evidence of hypermethylation and discovered that at least one of the two CpG islands in the *MTF2* promoter was hypermethylated in all MTF2-deficient AML samples, while neither CpG island is methylated in healthy BM (H-BM) or AML samples with normal (basal) MTF2 levels (B-AML) (Fig.S3.2A). The close correlation between MTF2 expression and H3K27me3 levels (Walker, Chang et al. 2010) led us to test whether downregulation of MTF2 is sufficient to reduce H3K27me3 levels. Thus, umbilical cord-derived $CD34^{+}CD38^{-}$ cells were transduced with two different MTF2 shRNA GFP-encoded lentiviruses. Flow cytometry analysis of H3K37me3 levels in GFP^{+} cells revealed markedly reduced H3K27me3 within 96 hours of MTF2 knockdown (Fig.3.1I-J). Further investigation demonstrated that MTF2 knockdown results in reduced abundance of PRC2 core proteins EZH1, EZH2, and SUZ12 (Fig.S3.2B), suggesting that reduced MTF2 impacts PRC2 levels resulting in decreased H3K27me3. In contrast, ectopic expression of MTF2 in MTF2-deficient $CD34^{+}CD38^{-}$ leukemic cells rescued MTF2 expression and re-

established global H3K27me3 levels (Fig.S3.3A-D), further demonstrating that MTF2 proportionately dictates H3K27me3 levels in hematopoietic progenitors.

We next used chromatin immunoprecipitation-sequencing (ChIP-seq) to investigate the changes in H3K27me3 levels triggered by MTF2 deficiency. To aid in relative H3K27me3 quantification across samples, *Drosophila* chromatin spike-in controls were added to the samples and H3K27me3 signal was normalized to total H3 ChIP-seq signal that was performed in parallel. Principal component analysis (PCA) of H3K27me3 revealed that MTF2-knockdown $CD34^{+}CD38^{-}$ BM cells cluster close to refractory patient LSC-enriched $CD34^{+}CD38^{-}$ BM cells, while scramble shRNA control $CD34^{+}CD38^{-}$ BM cells cluster with LSC-enriched $CD34^{+}CD38^{-}$ BM cells from induction therapy-responsive patients (Fig.3.1K-L). Taken together, these results demonstrate that MTF2 deficiency and reduced H3K27me3 levels within LSC-enriched $CD34^{+}CD38^{-}$ cells correlate with refractory AML. Moreover, MTF2 deficiency within healthy $CD34^{+}CD38^{-}$ cells triggers an H3K27me3 landscape that is similar to that found within refractory LSCs.

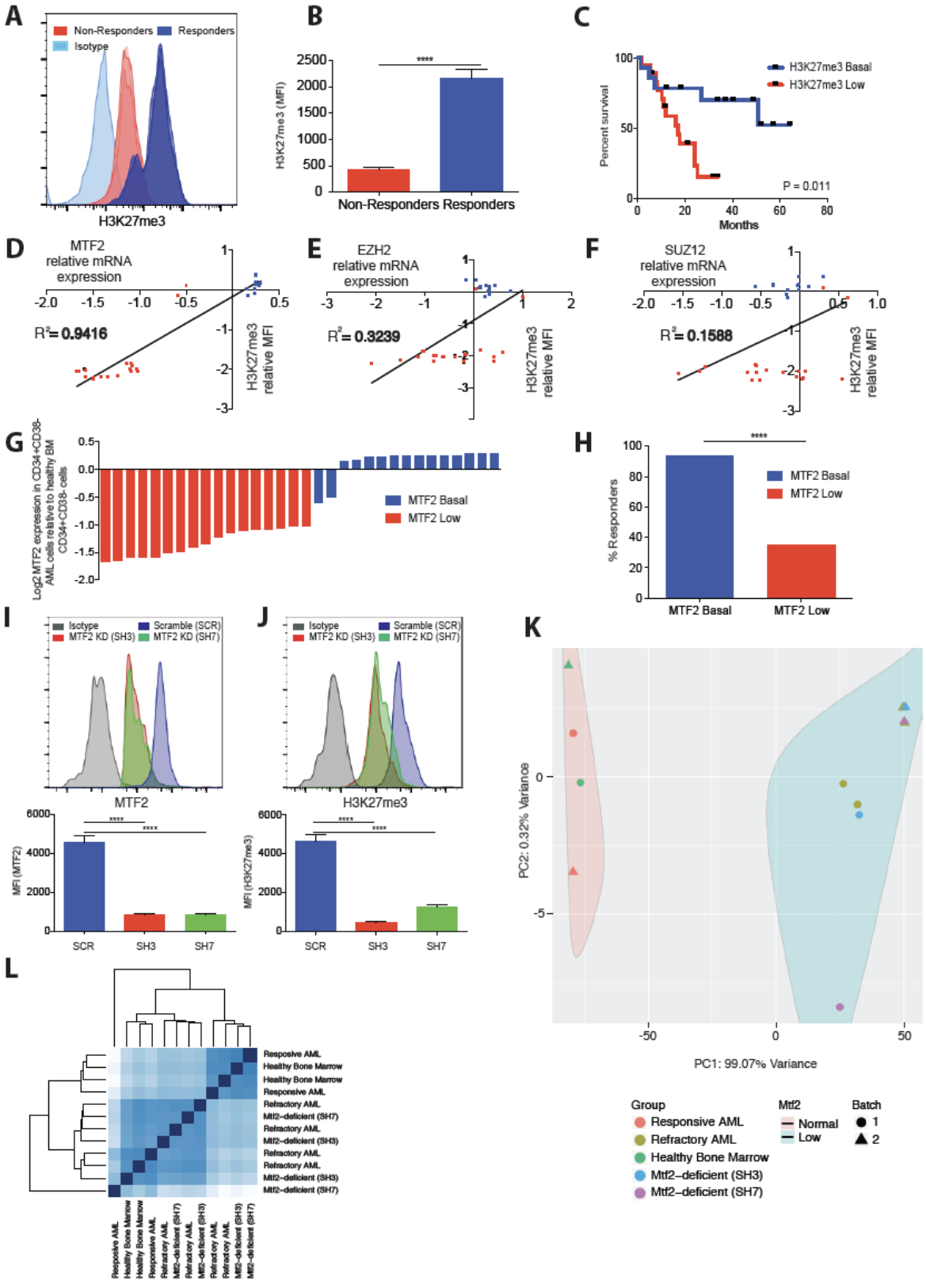
A
Non-Responders
Responders
Isotype
H3K27me3
B
H3K27me3 (MFI)
****
Non-Responders
Responders
C
H3K27me3 Basal
H3K27me3 Low
Percent survival
P = 0.011
Months
D
MTF2 relative mRNA expression
R²= 0.9416
H3K27me3 relative MFI
E
EZH2 relative mRNA expression
R²= 0.3239
H3K27me3 relative MFI
F
SUZ12 relative mRNA expression
R²= 0.1588
H3K27me3 relative MFI
G
Log2 MTF2 expression in CD34+CD38- AML cells relative to healthy BM CD34+CD38- cells
MTF2 Basal
MTF2 Low
H
% Responders
****
MTF2 Basal
MTF2 Low
I
Isotype
Scramble (SCR)
MTF2 KD (SH3)
MTF2 KD (SH7)
MTF2
MFI (MTF2)
SCR
SH3
SH7
J
Isotype
Scramble (SCR)
MTF2 KD (SH3)
MTF2 KD (SH7)
H3K27me3
MFI (H3K27me3)
SCR
SH3
SH7
K
PC2: 0.32% Variance
PC1: 99.07% Variance
Group
Responsive AML
Refractory AML
Healthy Bone Marrow
Mtf2–deficient (SH3)
Mtf2–deficient (SH7)
Mtf2
Normal
Low
Batch
1
2
L
Responsive AML
Healthy Bone Marrow
Healthy Bone Marrow
Responsive AML
Refractory AML
Mtf2–deficient (SH7)
Refractory AML
Mtf2–deficient (SH3)
Refractory AML
Refractory AML
Mtf2–deficient (SH3)
Mtf2–deficient (SH7)

Figure 3.1. MTF2 deficiency correlates with poor response to standard treatment of care. A, Representative flow cytometry histogram comparing H3K27me3 levels within the $CD34^+CD38^-$ LSC-enriched population isolated from several AML patient bone marrow (BM) samples. **B,** The H3K27me3 mean fluorescence intensity (MFI) obtained from flow cytometry analysis of 32 diagnostic BM samples demonstrates that reduced levels of H3K27me3 correlates with poor response to induction therapy. **C,** Survival analysis of the 32 AML patients treated by induction therapy shows H3K27me3 levels within patient $CD34^+CD38^-$ cells correlated with patient outcome; P value was calculated using Log-rank (Mantel-Cox) test. **D-F,** Linear regression analysis of PRC2 complex members (**D**) *MTF2*, (**E**) *EZH2*, and (**F**) *SUZ12*, revealed only *MTF2* mRNA expression correlates strongly with H3K27me3 levels within our patient cohort. **G,** *MTF2* expression within $CD34^+CD38^-$ cells isolated from 32 diagnostic AML BM aspirates compared to $CD34^+CD38^-$ HSPCs from 7 healthy BM aspirates assessed by RT-qPCR. 17 aspirates were determined to have low levels of *MTF2* expression (<-1) and 15 aspirates were determined to have basal levels of *MTF2* expression (-1 to +1). **H,** A double blinded drug response analysis determined that patients within our cohort with low *MTF2* expression responded poorly to standard induction chemotherapy. **I-J,** Knockdown of (**I**) MTF2, within $CD34^+CD38^-$ HSPCs decreases (**J**) H3K27me3 levels, assessed by flow cytometry. **K,** Principal component analysis of spike-in normalized H3K27me3 ChIP-seq data from $CD34^+CD38^-$ BM cells isolated from refractory AML patients (n=4 samples) responsive AML patients (n=2 samples) or healthy BM transduced with MTF2 (n=4 samples) or scramble (n=2 samples) lentivirus shRNA. The H3K27me3 ChIP sequencing was performed in 2 independent batches (batch 1 = •, batch 2 = ▲). **L,** Hierarchical clustering analysis demonstrated that the MTF2-deficient $CD34^+CD38^-$ BM population clusters closely to the $CD34^+CD38^-$ population isolated from refractory AML BM aspirates. All data represent mean ± standard deviation; *P<0.05, **P<0.005, ***P<0005, ****P<0.00005 by Student's T-test.

MTF2 loss within hematopoietic stem and progenitor cells (HSPCs) and $CD34^+$ leukemic cells drives resistance to standard induction therapy drugs

To test whether MTF2 deficiency confers resistance to standard induction therapy, HSPCs and Lin^-CD34^+ leukemic cells with normal (basal) levels of MTF2 (B-AML) were transduced with

MTF2 shRNA GFP-tagged lentiviruses. GFP^+ viable cells were sorted 72-hours post-transduction, then treated with the induction therapy drugs Daunorubicin or Cytarabine. 48 hours later, less than 6% of the scramble shRNA control cells survived, while more than 60% of MTF2-deficient cells were viable (Fig.3.2A,B, and Fig.S3.4A,B). Similarly, more than 25% of MTF2 knockdown B-AML cells were viable, while only less than 1% of the scramble control B-AML cells survived (Fig.3.2C,D, S3.5A,B). Furthermore, nearly two-thirds of the viable MTF2-deficient HSPCs and over 50% of the leukemic cells were $PCNA^+$, demonstrating that MTF2-deficient cells continue to proliferate despite chemotherapy treatment (Fig.3.2E,H, and Fig.S3.5C,D). Considering both Daunorubicin and Cytarabine target proliferating cells by inducing DNA damage (Come, Skladanowski et al. 1999, Xie, Edwards et al. 2010), we examined DNA damage accumulation in scramble and MTF2 shRNA transduced HSPCs and Lin^-CD34^+ leukemic cells over a 48-hour period during which the samples were treated with either Daunorubicin or Cytarabine. DNA damage accumulation was assessed using the alkaline comet assay, where the Olive moment was measured in a blinded fashion. Across all time points, the highest levels of DNA damage were found in the scramble control HSPCs (Fig.3.2I,J and Fig.S3.4C,D) and scramble control B-AML leukemic cells (Fig.3.2K,L). Conversely, rescuing MTF2 expression in $CD34^+CD38^-$ cells from refractory, MTF2-deficient AML cells (MD-AML) by lentivirus-induced MTF2 expression sensitized refractory AML cells to Daunorubicin and Cytarabine (Fig.3.2M,N). Thus, MTF2 deficiency confers a refractory phenotype since inducing MTF2 loss in HSPCs or chemoresponsive leukemic cells renders them chemoresistant and able to proliferate despite DNA damage.

Dual inhibition of EZH1 and EZH2 methyltransferase activity confers resistance to standard induction therapy drugs

EZH1 and EZH2 are the two PRC2 methyltransferases responsible for the maintenance of the H3K27me3 levels and are both lost in the absence of MTF2 (Fig.S3.2B); thus, we investigated whether inhibition of the methyltransferase activity of these enzymes would confer resistance to standard induction therapy drugs. Both HSPCs and Lin^-CD34^+ leukemic cells from 2 different AML patients with normal (basal) levels of MTF2 (B-AML) and H3K27me3 levels were pre-treated with EZH1/2 inhibitor (UNC1999) (Xu, On et al. 2015) or EZH2 inhibitor (EPZ005687) (Knutson, Wigle et al. 2012) for 3 days followed by treatment with Daunorubicin or Cytarabine for 48 hours. Interestingly, while less than 2% of the EZH2 inhibitor treated cells were viable 48 hours post treatment with Daunorubicin or Cytarabine, over 65% and 25% of HSPCs and B-AML cells, respectively, treated with the dual EZH1/2 UNC1999 were viable (Fig.3.2O-R, and Fig.S3.6A-F). Furthermore, over 50% of the UNC1999 treated viable cells were $PCNA^+$ (Fig.3.2S-V) and showed the lowest amount of DNA damage accumulation across all time points (Fig.3.2W-Z). Taken together these results show that dual loss of EZH1 and EZH2, but not EZH2 alone, is required to confer resistance to standard induction therapy within HSPCs and Lin^-CD34^+ B-AML leukemic cells.

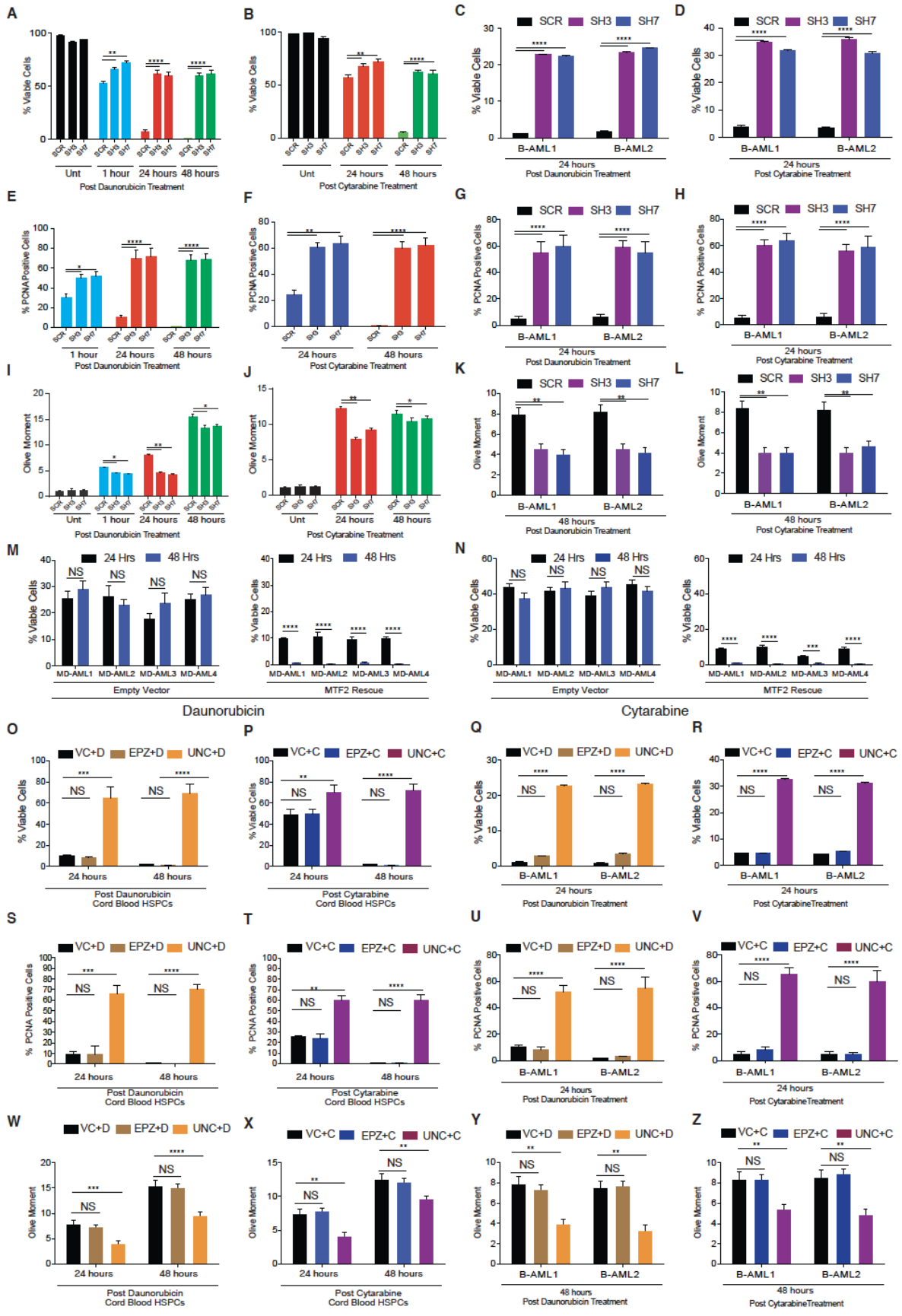
A
% Viable Cells
SCR SH3 SH7
Unt 1 hour 24 hours 48 hours
Post Daunorubicin Treatment
B
% Viable Cells
Unt 24 hours 48 hours
Post Cytarabine Treatment
C
SCR SH3 SH7
% Viable Cells
B-AML1 B-AML2
24 hours
Post Daunorubicin Treatment
D
SCR SH3 SH7
% Viable Cells
B-AML1 B-AML2
24 hours
Post Cytarabine Treatment
E
% PCNA Positive Cells
1 hour 24 hours 48 hours
Post Daunorubicin Treatment
F
% PCNA Positive Cells
24 hours 48 hours
Post Cytarabine Treatment
G
SCR SH3 SH7
% PCNA Positive Cells
B-AML1 B-AML2
24 hours
Post Daunorubicin Treatment
H
SCR SH3 SH7
% PCNA Positive Cells
B-AML1 B-AML2
24 hours
Post Cytarabine Treatment
I
Olive Moment
Unt 1 hour 24 hours 48 hours
Post Daunorubicin Treatment
J
Olive Moment
Unt 24 hours 48 hours
Post Cytarabine Treatment
K
SCR SH3 SH7
Olive Moment
B-AML1 B-AML2
48 hours
Post Daunorubicin Treatment
L
SCR SH3 SH7
Olive Moment
B-AML1 B-AML2
48 hours
Post Cytarabine Treatment
M
24 Hrs 48 Hrs
% Viable Cells
MD-AML1 MD-AML2 MD-AML3 MD-AML4
Empty Vector
MTF2 Rescue
Daunorubicin
N
24 Hrs 48 Hrs
% Viable Cells
MD-AML1 MD-AML2 MD-AML3 MD-AML4
Empty Vector
MTF2 Rescue
Cytarabine
O
VC+D EPZ+D UNC+D
% Viable Cells
24 hours 48 hours
Post Daunorubicin
Cord Blood HSPCs
P
VC+C EPZ+C UNC+C
% Viable Cells
24 hours 48 hours
Post Cytarabine
Cord Blood HSPCs
Q
VC+D EPZ+D UNC+D
% Viable Cells
B-AML1 B-AML2
24 hours
Post Daunorubicin Treatment
R
VC+C EPZ+C UNC+C
% Viable Cells
B-AML1 B-AML2
24 hours
Post CytarabineTreatment
S
VC+D EPZ+D UNC+D
% PCNA Positive Cells
24 hours 48 hours
Post Daunorubicin
Cord Blood HSPCs
T
VC+C EPZ+C UNC+C
% PCNA Positive Cells
24 hours 48 hours
Post Cytarabine
Cord Blood HSPCs
U
VC+D EPZ+D UNC+D
% PCNA Positive Cells
B-AML1 B-AML2
24 hours
Post Daunorubicin Treatment
V
VC+C EPZ+C UNC+C
% PCNA Positive Cells
B-AML1 B-AML2
24 hours
Post CytarabineTreatment
W
VC+D EPZ+D UNC+D
Olive Moment
24 hours 48 hours
Post Daunorubicin
Cord Blood HSPCs
X
VC+C EPZ+C UNC+C
Olive Moment
24 hours 48 hours
Post Cytarabine
Cord Blood HSPCs
Y
VC+D EPZ+D UNC+D
Olive Moment
B-AML1 B-AML2
48 hours
Post Daunorubicin Treatment
Z
VC+C EPZ+C UNC+C
Olive Moment
B-AML1 B-AML2
48 hours
Post CytarabineTreatment

Figure 3.2. MTF2 knockdown in Lin$^-$CD34$^+$ HSPCs or chemoresponsive leukemic cells, but not EZH2 inhibition alone confers resistance to standard treatment of care.

A-B, Viability and apoptosis of scramble control (SCR) and MTF2 (SH3 or SH7) shRNA knockdown (KD) HSPCs were assessed over a 48-hour time period post-treatment with (**A**) Daunorubicin or (**B)** Cytarabine. **C-D,** Viability and apoptosis of scramble control (SCR) and MTF2 (SH3 or SH7) shRNA KD Lin$^-$CD34$^+$ chemoresponsive leukemic cells isolated from MTF2-basal AML samples [B-AML] were assessed post-treatment with (**C**) Daunorubicin or (**D)** Cytarabine. By 24 hours post-treatment, over 25%, but less than 2% of KD B-AML and scramble control cells, respectively, remain viable. **E-F,** PCNA proliferation marker analysis of scramble control (SCR) and MTF2-deficient (SH3, SH7) shRNA KD HSPCs 48 hours (**E**) post-Daunorubicin or (**F**) Cytarabine treatment. Viable cells from **(A-B**) were stained for PCNA, to assess cell proliferation. **G-H,** Proliferation analysis of scramble control (SCR) and MTF2 (SH3, SH7) shRNA KD B-AML cells 24 hours (**G**) post-Daunorubicin or (**H**) post-Cytarabine treatment. Viable cells from **(C-D**) were stained for PCNA, to assess cell proliferation. Both MTF2-deficient HSPCs and B-AML cells continue to proliferate significantly more than control cells post-treatment. **I-J,** Overall DNA damage accumulation post-induction treatment with (**I**) Daunorubicin or (**J**) Cytarabine was assessed over 48 hours via the alkaline comet assay. Blinded, ImageJ OpenComet analysis of the Olive moment was used to quantify DNA damage at the single cell level and while both the scramble (SCR) and MTF2 (SH3 or SH7) KD HSPCs accumulated DNA damage over time, the MTF2 KD HSPCs accumulated significantly less damage at each individual time point. **K-L,** Overall DNA damage accumulation in B-AML cells post-induction treatment with (**K**) Daunorubicin or (**L**) Cytarabine was assessed over 48 hours via the alkaline comet assay. MTF2 KD leukemic B-AML cells accumulated significantly less DNA damage. **M,** (**Left**) The CD34$^+$CD38$^-$ BM subpopulation from AML patients with MTF2 deficiency [MD-AML] treated with 0.5μM Daunorubicin remain viable over 48 hours. (**Right**) Restoration of MTF2 via lentiviral-induced expression sensitized the MD-AML cells to Daunorubicin. **N,** (**Left**) Similar results were observed when CD34$^+$CD38$^-$ cells isolated from MD-AML patient BM were treated with 1μM Cytarabine. (**Right**) MTF2 restoration abolished the chemoresistance observed within 48 hours. **O-P**, Apoptosis analysis of HSPCs treated with either 2 μM EZH2 inhibitor EPZ005687 [EPZ] or 2 μM of the EZH1/2 inhibitor UNC1999 [UNC] for 72hours, followed by co-treatment with one of two induction drugs (**O**) Daunorubicin [D] or (**P**) Cytarabine [C] over 48hours. **Q-R,**

Apoptosis analysis of Lin$^-$ CD34$^+$ B-AML cells that underwent the same treatment regimen as in (**Fig. 2O-P**). **S-V**, PCNA proliferation marker analysis of (**S-T**) HSPCs or (**U-V**) Lin$^-$ CD34$^+$ B-AML cells that underwent the same treatment regimen as in (**Fig. 2O-P**). PCNA expression in UNC1999 plus either induction drug treated cells showed significantly increased proliferation over 48hours. **W-Z**, DNA damage accumulation was assessed by Comet assay analysis of (**W-X**) HSPCs or (**Y-Z**) Lin$^-$ CD34$^+$ B-AML cells that underwent the same treatment regimen as in (**Fig. 2O-P**). Co-treatment of UNC1999 plus either induction drug showed the lowest Olive moment representative DNA damage accumulation over 48hours. Taken together these results show that dual loss of EZH1 and EZH2 is required to confer resistance to standard induction therapy within HSPCs and Lin$^-$CD34$^+$ leukemic cells. Viable cells were determined by the percent of Annexin V-negative/7-AAD-negative cells. Representative dot plots are shown in **(Supplementary Fig. S3.4A,B)**. Representative comets of each condition are shown in **(Supplementary Fig. S3.4C,D)**. All data represent mean ± standard deviation; *P<0.05, **P<0.005, ***P<0005 by Two-Way ANOVA.

MTF2 gene regulatory network (GRN) controls multiple signalling pathways implicated in DNA damage, chemoresistance and cancer

To identify potential molecular mechanisms underlying altered DNA damage response (DDR) and poor therapeutic response in MTF2-deficient cells, we knocked down MTF2 in HSPCs by shRNA lentiviral transduction and performed RNA-seq. Enrichment map analysis of the transcriptomic data revealed DDR, anti-apoptosis and cell cycle pathways were affected (Fig.3.3A). Further dissection of the affected DDR transcripts showed numerous genes belonging to various DNA repair pathways were upregulated within the MTF2-deficient HSPCs compared to the scramble control, consistent with the reduced DNA damage observed in the MTF2-deficient HSPCs following induction treatment (Fig.S3.7A,B). To identify targets of the MTF2-PRC2 complex, we integrated the H3K27me3 ChIP-seq (Fig.3.1K,L) with the *MTF2* knockdown RNA-seq data. The resultant MTF2-PRC2 gene regulatory network (GRN) in human HSPCs revealed

the oncogenic pathways repressed by MTF2 included the PI3 kinase and p53 pathways that regulate cell cycle, apoptosis, DDR and chemoresistance (Fig.3.3B).

While p53 is not a direct target of MTF2-PRC2, the E3-ubiquitin ligase MDM2 that targets p53 for degradation (Marine and Lozano 2010) is a direct target. Thus, the p53 module within the MTF2 GRN predicts that MTF2 deficiency leads to MDM2 overexpression, resulting in p53 degradation (Fig.3.3C). Indeed, ChIP-seq analysis demonstrated that MTF2 deficiency leads to loss of H3K27me3 at the *MDM2* locus, while total H3 levels were unaltered (Fig.3.3D), concomitant with increased *MDM2* mRNA levels observed by RNA-seq (Fig.3.3E). The MTF2-PRC2 GRN was validated via RT-qPCR and ChIP-qPCR (Fig.3.3F,G, Fig.S3.7C,D and Table S9). Functional validation using imaging flow cytometry showed that MTF2-deficient HSPCs had high MDM2 and low p53 levels (Fig.3.3H). Therefore, we hypothesized that MDM2 inhibitors would restore p53 levels in MTF2-deficient cells. Strikingly, p53 levels within MTF2-deficient HSPCs and Lin$^-$CD34$^+$ leukemic cells from refractory patient BM aspirates (MD-AML) were rescued by treatment with Nutlin3A or MI-773, which block MDM2-p53 interaction (McCormack, Haaland et al. 2012, Wang, Sun et al. 2014) (Fig.3.3H and Fig.S3.8A-E). Furthermore, cell cycle and PCNA analyses revealed that rescuing p53 levels within MTF2-deficient HSPCs using MDM2 inhibitors decreased their proliferation rate and arrested the cells in the G0/G1 cell cycle stage (Fig.S3.9A,B). To test whether MTF2 regulates the MDM2-p53 axis in refractory AML patient BM cells, MTF2 expression was rescued within the MTF2-deficient Lin$^-$CD34$^+$ refractory patient BM aspirates (MD-AML) by lentivirus-mediated MTF2 expression; this resulted in MDM2 repression and elevated p53 protein levels (Fig.S3.10A,B). Taken together, these results indicate that MTF2 regulates p53 levels via transcriptional repression of MDM2 and that MDM2 inhibitors rescue p53 levels in MTF2-deficient cells.

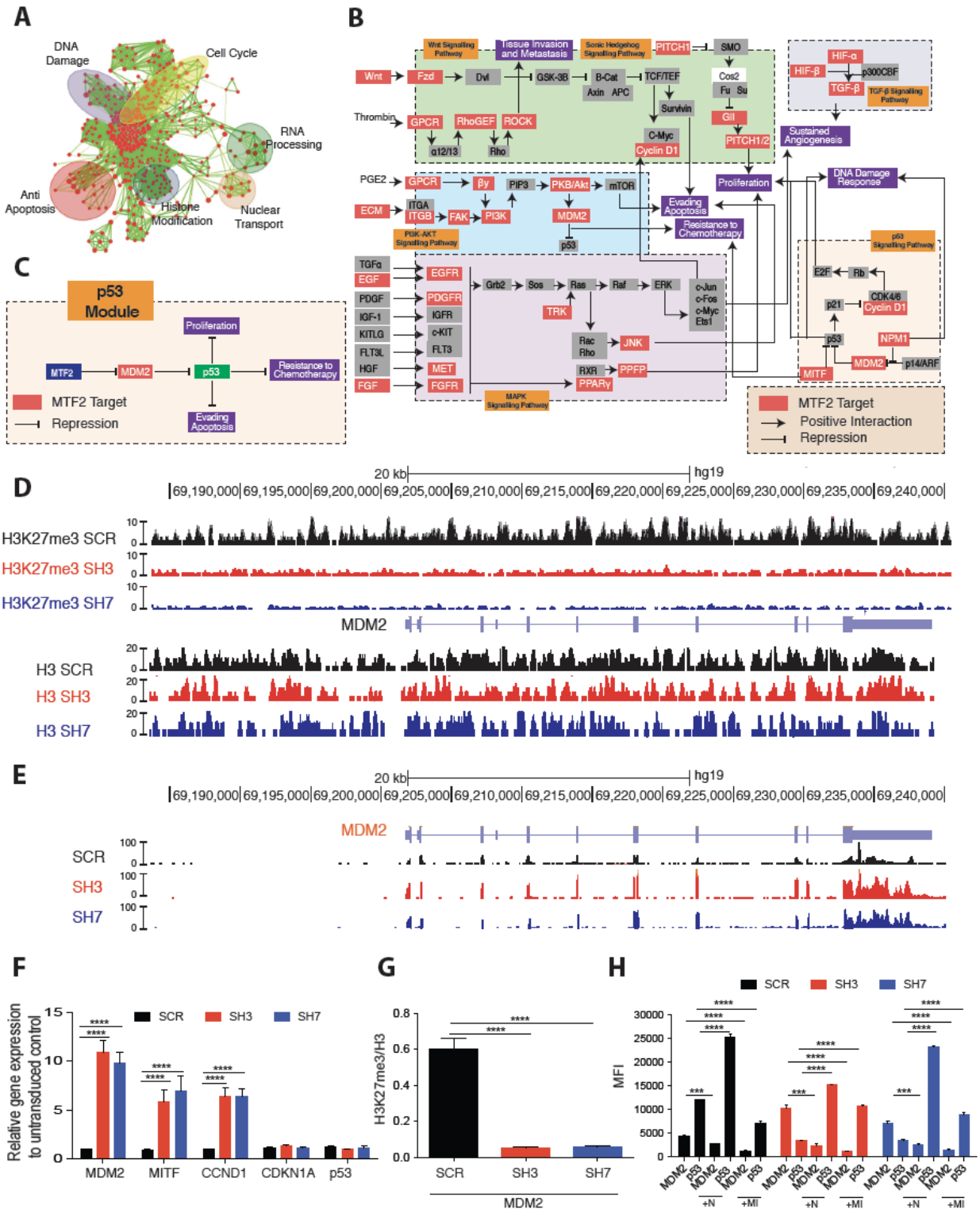

Figure 3.3. MTF2 gene regulatory network (GRN) modulates refractory AML via the MDM2/p53 signaling pathway. **A,** Gene ontology enrichment analysis of MTF2-deficient

HSPCs identified genes misregulated in processes such as cell cycle, RNA processing, nuclear transport, anti-apoptosis, histone modifications and DNA damage response (DDR). **B,** KEGG-pathway analysis of the MTF2-PRC2 GRN from integrated RNA-seq and H3K27me3 ChIP-seq data in human HSPCs uncovered oncogenic pathways that are directly regulated by MTF2-PRC2. **C,** Oncogenic module within the MTF2-PRC2 GRN revealed that MTF2 directly represses MDM2, a direct inhibitor of the p53 pathway. **D,** Drosophila chromatin spike-in normalized ChIP-seq traces show loss of the repressive H3K27me3 marks at the MDM2 genomic locus in MTF2 knockdown HSPCs relative to total Histone 3. **E,** RNA-seq traces display increased MDM2 mRNA levels in MTF2 knockdown HSPCs. **F-G,** (**F**) RT-qPCR and (**G**) ChIP-qPCR performed on target genes validated the MTF2 GRN. **H,** Imaging flow cytometry analysis of MDM2 and p53 revealed increased MDM2 and decreased p53 levels within MTF2 (SH3 or SH7) shRNA knockdown HSPCs. Decreased p53 levels within MTF2-deficient HSPCs were rescued by treatment with MDM2 inhibitors Nutlin3a [N] or MI-773 [MI]. All analyses compared MTF2 knockdown (SH3 or SH7) with scramble control (SCR) HSPCs. All data represent mean ± standard deviation; ***P<0005, ****P<0.00005 by Two-way ANOVA.

Targeting the MDM2/p53 network module sensitizes MTF2-deficient refractory AML to standard induction chemotherapy drugs

Under normal circumstances, activation of the p53 pathway inhibits the propagation of cells that carry damaged DNA. In AML, inactivation of p53 is associated with chemoresistance, refractory disease, adverse risk group, and poor survival (Cancer Genome Atlas Research, Ley et al. 2013). We therefore hypothesized that rescuing p53 levels in MTF2-deficient HSPCs with MDM2 inhibitors would sensitize them to standard induction therapy drugs. To test this hypothesis, we transduced and sorted viable GFP^+ MTF2 knockdown HSPCs as above and treated them with Cytarabine or Daunorubicin in combination with the MDM2 inhibitors Nutlin3A or MI-773, then assayed DNA damage accumulation and cell viability. Importantly, MTF2-deficient HSPCs exposed to the dual treatment of an MDM2 inhibitor with an induction chemotherapeutic

exhibited the same amount of DNA damage accumulation as that found within scramble controls and were sensitized to induction therapy drugs (Fig.3.4A-C). Moreover, MTF2-deficient refractory AML cells (MD-AML) underwent apoptosis when treated with Cytarabine or Daunorubicin in combination with Nutlin3A or MI-773 (Fig.3.4D,E and Fig.S3.11A-D). These *in vitro* results led us to further test this combination therapy regimen (standard induction drugs plus MDM2 inhibition) *in vivo*.

Mindful of the disparity between pre-clinical and clinical trial results (Zuber, Radtke et al. 2009, Francia, Cruz-Munoz et al. 2011), we designed a pre-clinical study that would closely mirror a clinical trial. Thus, we incorporated the following principles: AML patient derived xenograft (PDX) mice would be treated only after the mice presented with a substantial leukemic burden, the efficacy of combination therapy would be compared against standard induction chemotherapy and the study would be blinded. Irradiated NSG mice were injected with either chemoresponsive MTF2-basal AML (B-AML) or refractory MTF2-deficient AML (MD-AML) patient-derived xenograft (PDX) cells. Once the transplanted mice presented with ≥20% $CD45^{+}CD33^{+}$ blast cells in their peripheral blood, the mice were randomized into 4 groups, which were treated with either vehicle control, Nutlin3A, induction therapy or combination therapy that included induction therapy plus Nutlin3A. While mice belonging to the chemoresponsive B-AML PDX cohort did not respond to vehicle control or Nutlin 3A alone, the B-AML PDX mice treated with induction therapy or combination therapy survived until the experiment was terminated at 16-weeks post-treatment (Fig.S3.12A-G). However, within the cohort of mice engrafted with refractory MD-AML PDX cells, only the mice treated with combination therapy survived until the experiment was terminated at 16-weeks post-treatment (Fig.3.4F). The weights of mice belonging to the

refractory AML cohort were monitored throughout the study and reflected their survival with weights plummeting during the 5-day treatment; only combination therapy-treated mice regained their weight and recovered (Fig.3.4G). Wright-Giemsa staining of BM cells harvested at endpoint from the refractory cohort showed a stark contrast between the immature blast cells isolated from induction therapy-treated mice and the differentiated BM cells isolated from the combination therapy treated mice (Fig.3.4H). Flow cytometry analysis also confirmed a dramatic loss in the blast-containing $CD45^{+}CD33^{+}$ and LSC-rich populations in the combination therapy cohort (Fig.S3.13A-F).

To test whether the remaining PDX cells in the combination treated mice within the MD-AML refractory cohort retained residual disease, we performed secondary transplants without additional treatment. The secondary transplants showed no evidence of AML during the 16-week post-transplantation observation period, after which the experiment was terminated. Flow cytometry analysis of BM cells from secondary transplants revealed that the transplanted cells were capable of multi-lineage engraftment, suggesting that the combination therapy spared normal HSPCs (Fig.S3.14A-G). Finally, flow cytometric analysis showed the combination therapy treated mice and their secondary transplant recipients had reduced bone marrow cellularity, compared to DMSO, Nutlin3A alone or induction treated mice cohorts (Fig.3.4I).

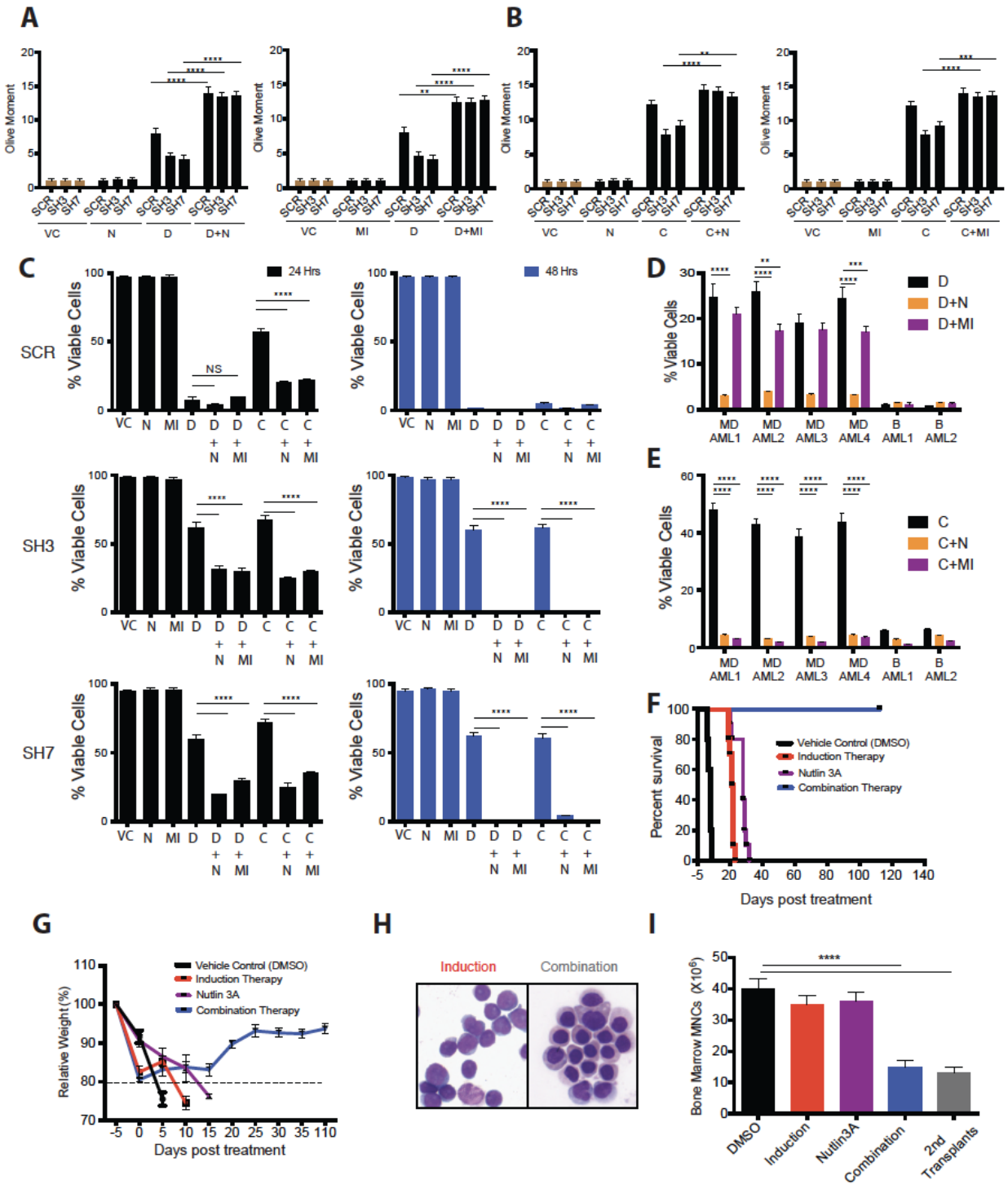

Figure 3.4. MDM2 inhibitors sensitize MTF2-deficient HSPCs and primary refractory AML samples to standard treatment of care. **A-B,** Alkaline comet analysis of control (SCR) and

MTF2-deficient (SH3, SH7) HSPCs treated with vehicle control [VC], (**A**) Daunorubicin [D], or (**B**) Cytarabine [C] in combination with one of two MDM2 inhibitors, Nutlin3A [N] or MI-773 [MI]. **C-E,** Viability and apoptosis analysis to assess chemoresistance post-treatment with induction drugs, MDM2 inhibitors or both. (**C)** MTF2-deficient HSPCs undergo apoptosis post-combination treatment with induction drug plus MDM2 inhibitor, over 48 hours. MTF2-deficient refractory AML cells [MD-AML] showed increased sensitivity to (**D**) Daunorubicin and (**E**) Cytarabine, when treated in combination with MI-773 [MI] or Nutlin3A [N] within 24 hours comparable to MTF2-basal AML samples [B-AML]. Analysis 48 hours post-treatment is shown in (**Supplementary Fig. S3.11A,B**). **F,** Kaplan-Meier curve of MD-AML patient-derived xenograft (PDX) NSG mice treated with either vehicle control, Nutlin3A alone, induction therapy or combination therapy (n=4 refractory AML samples; n = 8 mice per treatment group). **G,** Mouse weight was monitored up to16 weeks post-treatment. Initial weight loss was observed in all conditions, but weight recovery was only observed in mice that underwent combination treatment. **H,** Wright-Giemsa stained cytospins of BM samples from MD-AML PDX mice treated with induction therapy and combination therapy demonstrate a loss of immature blast cells following combination treatment only. **I,** BM mononuclear cell (MNC) counts from MD-AML PDX moribund mice following treatment with either vehicle control [VC], Nutlin3A or induction therapy and from surviving mice administered combination therapy 16-weeks post-treatment. A profound decrease in MNCs was observed in the BM of primary mice that received combination therapy and their secondary transplant recipients. Engraftment of secondary transplants is shown in **(Supplementary Fig. S3.14)**. All data represent mean ± standard deviation; All data represent mean ± standard deviation; *P<0.05, **P<0.005, ***P<0005, P<0.00005 by Two-Way ANOVA.

Discussion

Altered epigenetic states such as H3K27me3 deficiency are observed in different types of cancer and have been correlated with poor outcome (Torchia, Golbourn et al. 2016). However, the mechanism underlying H3K27me3 deficiency and how it contributes to a poor prognosis has been unclear, although a recent report suggested that EZH2 deficiency is associated with AML relapse (Gollner, Oellerich et al. 2017). Here, we establish using HSPCs and Lin$^-$CD34$^+$ leukemic cells that

loss of EZH2 methyltransferase alone is not sufficient to confer chemoresistance and in fact the refractory phenotype is only manifested when the methyltransferase activities of EZH1 and EZH2 are both inhibited (Fig.3.2, Fig.S3.5, Fig.S3.6). This is consistent with the fact that EZH1 can compensate for EZH2 within adult bone marrow (Xie, Xu et al. 2014) and our finding that MTF2 is required for EZH1 and EZH2 expression in HSPCs. Furthermore, for the first time we demonstrate that reduced expression of MTF2, a member of the PRC2, and low H3K27me3 levels within enriched LSC populations prospectively identify refractory AML at diagnosis and provide a direct mechanism for MTF2- and PRC2-mediated chemoresistance. As relapse and poor survival have also been associated with LSCs and to limit sample heterogeneity (Ding, Ley et al. 2012), we performed blinded analyses of primary $CD34^{+}CD38^{-}$ populations of diagnostic AML samples, revealing H3K27me3 deficiency co-segregates with reduced expression of MTF2 along with failure to respond to induction therapy. In both our local patient cohort and reported TCGA survival data, MTF2 deficiency correlated with poor survival much better than EZH2 loss (Fig.3.1 and Fig.S3.1), consistent with low survival rates among refractory AML patients. In fact, as a prognostic marker, MTF2 is capable of further stratifying patients with favourable cytogenetics (Fig.S3.1). Mechanistically, we demonstrated that MTF2 repression is due to hypermethylation of its promoter, thus leading to de-repression of *MDM2*, p53 degradation and ensuing aberrant apoptosis, cell cycling and DDR. Furthermore, rescuing MTF2 expression in primary MTF2-low LSC-enriched populations reversed chemoresistance, while knockdown of MTF2 in HSPCs and $Lin^{-}CD34^{+}$ leukemic cells with normal levels of MTF2 induced resistance to induction chemotherapy drugs. Because MTF2 plays a fundamental role in chemoresistance, MTF2 deficiency is not only correlative, but predictive of refractory AML.

Recent deep sequencing studies have suggested that epigenetic alterations and changes in the epigenome, which are commonly observed across all cancers, are often associated with genetic mutations or transcriptional alterations of many genes related to cancer progression (Li, Garrett-Bakelman et al. 2016). Hence, targeting the epigenome is currently an area of intense research to improve upon standard of care chemotherapies (Kuhn, Song et al. 2016, Shih, Meydan et al. 2017). By targeting the dysregulated epigenetic pathway associated with refractory AML, we demonstrate that MDM2 inhibitors in combination with standard induction chemotherapy provide a promising strategy to treat chemoresistant AML. While p53 mutations are typically associated with aggressive refractory disease (Kruiswijk, Labuschagne et al. 2015), large-scale deep sequencing datasets show that 2-8% of AML patients have p53 mutations (Patel , Gönen et al. 2012, Cancer Genome Atlas Research, Ley et al. 2013). In fact, multivariate analysis on p53 wild type AML patient samples from TCGA revealed *MTF2* levels as an independent risk factor, capable of predicting both OS (Supplementary Table S9) and DFS (Supplementary Table S10). Therefore, our proposed combination therapy could effectively treat the vast majority of refractory AML patients. In fact, our data predict that in the absence of MDM2 inhibitors, MTF2-deficient AML cells will cycle through induction therapy and accumulate additional mutations, potentially including p53 therapy-induced mutations, which would render the cells resistant to MDM2 inhibitors. Since MDM2 inhibitors are now in clinical trials for a number of indications including treatment of AML, it would be prudent to screen AML patients at diagnosis for MTF2 and H3K27me3 levels to prospectively identify chemoresistant AML prior to treatment to identify candidates who will benefit the most from this targeted combination therapy.

Materials and Methods

Reproducibility and Double-Blinded acquisition of data

In vitro and *in vivo* functional assays in this study were performed in a double-blinded manner to remove investigator bias whenever possible as described in more detail below. Analysis of MTF2 and H3K27me3 expression in diagnostic AML patient bone marrow samples was performed without knowledge of the clinical outcome. Likewise, the Kaplan-Meier analysis of our AML cohort was also performed without knowledge of the molecular analysis of patient samples. Data analysis was performed in an unbiased manner by use of preset algorithms to analyze data with the FlowJo, IDEAS and ImageJ OpenComet software.

Patient treatment and response analysis

Diagnostic bone marrow samples from patients with AML were obtained after informed consent. Patients were treated as per the protocols at The Ottawa General Hospital, Ontario, Canada. In addition to the usual supportive care, they received induction chemotherapy with Idarubicin (12mg/m^2 daily for 3 days) and Cytarabine (200mg/m^2/day by continuous infusion for 7 days). A bone marrow sampling was repeated upon recovery of blood counts and/or between days 25-40. Responsive disease was defined as <5% blasts in the bone marrow. Patients who had ≥5% blast in the marrow were designated as failing or resistant to induction, for the purposes of this study. These patients were then treated with a salvage chemotherapy and considered for an allogeneic hematopoietic stem? cell transplant. Patients who did achieve a complete remission proceeded to receive consolidation and were considered for an allogeneic hematopoietic stem cell transplant.

Umbilical cord blood and bone marrow samples

Human umbilical cord blood samples were obtained from the Canadian Blood Services (Ottawa, Canada) and the Mount Sinai Hospital Research Centre for Women's and Infants' Health BioBank, (Toronto, Canada). Informed consent, collection and research use of the cord blood samples were approved by respective Research Ethics Boards and the Ottawa Hospital Research Ethics Board. AML patient bone marrow samples were collected after informed consent at The Ottawa Hospital. Procurement and use of patient samples for research was approved by The Ottawa Hospital Research Ethics Board.

Isolation of mononuclear cells from umbilical cord blood

Hespan (B.Braun Medical Inc) was used for mononuclear cell isolation from umbilical cord blood. Cord blood was mixed with Hespan at a final ration of 5:1 and centrifuged at 50 RCF for 10 minutes at room temperature. Post-centrifugation the serum supernatant containing the mononuclear cells was collected and centrifuged at 400RCF for 10 minutes. Red blood cells were then lysed with Red Blood Cell lysis buffer (1g/L $KHCO_3$, 8.2g/L NH_4Cl, 0.37g/L EDTA) to eliminate residual red blood cells before being frozen down in 10% DMSO using an ethanol-based control rate freezer (Kinetic), allowing high viability after thawing.

Isolation of mononuclear cells from bone marrow aspirates

Ficoll (GE Healthcare Life Sciences) was used for mononuclear cell isolation from bone marrow aspirates. Density centrifugation to isolate mononuclear cells using Ficoll was done at 400 RCF for 20 minutes. All density centrifugations were done at room temperature, without brakes. Red blood cells were lysed and cells frozen as described above.

Enrichment of stem and progenitor populations

Lineage-negative (Lin^-) umbilical cord blood or bone marrow cells were obtained using the EasySep™ Human Progenitor Cell Enrichment Kit with Platelet Depletion to enrich for stem and progenitor cells (HSPCs). $CD34^+$ positive selection was performed on Lin^- cells, using the EasySep™ Human $CD34^+$ selection kit (Stem Cell Technologies).

For the experiments using $CD34^+CD38^-$ cells, Lin^- cells were directly stained for $CD34^+$ (Clone 4H11) and $CD38^+$ (HIT2) cell surface markers and sorted for $CD34^+CD38^-$ cells using the Beckman Coulter MoFlo sorter.

Lentivirus production of MTF2 shRNA

293T cells were co-transfected with lentiviral plasmids pMD2G, pPAX2 and pGIPZ encoding scramble or MTF2 shRNAs (ThermoScientific) using polyethylenimine (see table below). Supernatant containing the virus was collected 48 and 72 hours post-transfection. Virus was concentrated through ultracentrifugation and cells were infected at a MOI of 100.

	shRNA Sequence
MTF2 shRNA Clone 3	TAATGTATGTCATAAGC
MTF2 shRNA Clone 7	TTGGCTTTATGTCCATCC
Scrambled shRNA	GTTACACGATATGTTATC

Lentiviral-mediated MTF2 knockdown of HSPCs from umbilical cord blood cells

HSPCs (Lin^-CD34^+) were maintained in IMDM media containing bovine serum albumin, insulin, and transferrin (Stem Cell Technologies), 1% PenStrep (ThermoFisher), SCF (100ng/mL), TPO (50ng/mL), FLT3 (100ng/mL), 1% Glutamax (Invitrogen), and LDL (1μg/ml) (Calbiochem).

Growth factors were purchased from Peprotech. On Day 1 of infection, cells were incubated with polybrene (Sigma) (6mg/ml) for 2 hours at 37°C, then combined with viral supernatants containing either a GFP-tagged MTF2 shRNA clone or a scrambled shRNA control (ThermoFisher) at a MOI of 100. Cells were centrifuged at 400g for 20 minutes, then maintained at 37°C. On Day 2, the infection was repeated. Cells were grown for 3 days using a fed-batch culture system, then sorted for high GFP-expression and viability by negative selection of Propidium Iodide using the Beckman Coulter MoFlo sorter.

Lentiviral-mediated rescue of MTF2 expression within patient Leukemic Cells

Lin$^-$CD34$^+$ primary AML bone marrow cells were maintained in IMDM media containing SCF (100ng/mL), FLT3 (50ng/mL), IL-3 (20ng/mL), G-CSF (20ng/mL) and 10^{-4}M Beta-mercaptoethanol. Growth factors were purchased from Peprotech. On Day 1 of infection, cells were incubated with polybrene (6mg/ml) for 2 hours at 37°C, then combined with viral supernatants containing either a GFP-tagged MTF2 overexpression vector clone or an empty vector control (abm plasmids) at a MOI of 30.

In vitro EZH1 and EZH2 inhibition

HSPCs isolated from cord bood and Lin$^-$CD34$^+$ primary AML bone marrow cells were maintained in IMDM media containing SCF (100ng/mL), FLT3 (50ng/mL), IL-3 (20ng/mL), G-CSF (20ng/mL) and 10^{-4}M Beta-mercaptoethanol. Growth factors were purchased from Peprotech. Cells were treated with UNC1999 (2uM) or EPZ005687 (2uM) for 3 days. Both the inhibitors were purchased through Cedarlane.

Intracellular staining

Cells were sorted using cell surface markers, then fixed in 4% PFA, permeabilized with 0.3% Triton and stained for MTF2 (Genway, clone M96), EZH2 (Millipore, clone AC22), SUZ12 (Millipore, clone 2AO9), H3K27me3 (Cell Signaling, clone C36B11), PCNA (Santa Cruz, clone C10), p53 (Cell Signaling, clone 1C12), or MDM2 (Santa Cruz, clone C18) and appropriate secondary antibodies. Protein expression was determined by flow cytometry compared with an isotype only control and ran on the LSRFortessa™ Cell Analyzer (BD Biosciences). Data analysis was performed using FlowJo v10.2 to compare mean fluorescent intensity values.

Imaging Flow Cytometry – Amnis

For cell cycle analysis, cells were fixed and stained with DRAQ5 (BD Biosciences). For assessing p53 expression in MTF2 rescue experiments, cells were stained with antibodies against p53, MDM2 or H3K27me3 as above and with DRAQ5 for nucleic acid detection. Cells were analyzed using the ImageStream imaging flow cytometer (Amnis). The nuclear contents of each protein were determined using the preset wizard tool "Nuclear Localization", within the Amnis IDEAS analysis software.

Apoptosis assay

Apoptosis was assessed by the dual staining of AnnexinV and 7-AAD (eBiosciences). Flow cytometric analyses of treated samples were performed consistently, using the same gating strategy throughout. Viable cells were categorized as being AnnexinV and 7-AAD negative, late apoptotic/dead cells were categorized as being AnnexinV and 7-AAD positive.

Comet assay

Alkaline comet assays were performed using GelBond Films and buffers were prepared as described (Olive and Banath 2006, Al-Khalaf, Blake et al. 2016). Slides were stained with SYBR Gold and imaged using Zeiss Axio2 Imaging inverted microscope equipped with a 5× Plan-NEOFLUAR 0.3NA objective and an AxioCam MRm camera through a FITC-compatible filter. At least 10 random fields containing a minimum of 20 non-overlapping comets in each group total were photographed. Blinded imaging acquisition and analysis was performed using ImageJ software (NIH) and the OpenComet comet assay plugin calculating Olive moment (arbitrary units) on the basis of comet head and tail sizes (measured in pixels) and their integral intensity. The magnitude of these parameters depends on time of electrophoresis, staining brightness and image magnification, which were constant within each assay and between experiments. Comet assays were independently repeated using HSPCs isolated from 3 different UCB samples. Statistical significance was determined by two-way ANOVA using GraphPad Prism software version 6.

RNA-seq and ChIP-seq

HSPCs (Lin^-CD34^+) were transduced either with the GFP-tagged MTF2 shRNAs or a scrambled shRNA control. Transduced GFP^+ cells were sorted 72 hours post-transduction using a MoFlo sorter. RNA was extracted from 150,000 cells per condition for RNA-seq analysis. RNA was isolated (Arcturus PicoPure Kit, LifeTech) and DNase treated (Qiagen). Quality of RNA was determined using a Bioanalyzer. Library preparation was performed using (TruSeq Library Prep Kit, Illumina), and sequenced on a HiSeq 2000 (Illumina). Replicate data was analyzed using TopHat v1.4.1 and Cuffdiff v1.3.0 (Trapnell, Roberts et al. 2012) to map reads to a reference human genome assembly (hg19) and determine expression differences against the Ensembl release

67 gene model. Significant fold changes were determined using Benjamini-Hochberg corrected *p* value of 0.05. Raw RNA-seq data is available in GEO (Accession # - to be completed upon acceptance). Data was analyzed using DAVID bioinformatics tool for functional annotation (Reimand, Kull et al. 2007, Reimand, Arak et al. 2011) and Cytoscape with Enrichment Map plugin for visualization (Merico, Isserlin et al. 2010, Merico, Isserlin et al. 2011). RNA-seq targets were validated by RT-qPCR after RNA was converted to cDNA using Superscript II (LifeTech). The qPCR experiments were performed on LightCycler 480 (Roche). Raw RNA-seq data is available in GEO (Accession # - to be completed upon acceptance).

For ChIP-seq, $CD34^{+}CD38^{-}$ sorted cells were crosslinked with 1% formaldehyde for 10 minutes at room temperature. Samples were sheared using a Covaris sonicator until DNA reached a final size of 100-300bp. 750ng of drosophila spike in chromatin (Active Motif) was added to each sonicated sample. 4ug of anti-H3K27me3 antibody (Cell Signaling, c36B11) or H3 (Abcam, ab1791) was bound to pre-blocked Protein A magnetic beads (Millipore) in combination with 2ug of Spike-in antibody (Active Motif) for 12 hours. The beads were then combined with sonicated sample containing *Drosophila* spike in chromatin and incubated overnight. After incubation, beads were collected and DNA-antibody complexes were eluted at 65°C. Crosslinks were reversed overnight at 65°C. Samples were treated with Proteinase K (Fisher Scientific) and RNase A (Fisher Scientific) and DNA was purified using phenol-chloroform. All ChIP-seq experiments were cell number normalized and 150,000 cells per biological sample were used for each H3 and H3K27me3 ChIP experiment.

DNA was analyzed for quality, quantity and size using Fragment Analyzer (AAT1) and Qubit (ThermoFisher). For sequencing total ChIP DNA was used for library preparation (NextFlex Illumina Chip-seq kit). All samples underwent 1X75 cycles of single-end sequencing on NextSeq 500 (Illumina). Reads were mapped separately to the reference human (hg19) and *Drosophila melanogaster* (BDGP6.0) genome assemblies using Bowtie 2.2.6 (Langmead and Salzberg 2012). For each sample, the number of *Drosophila* spike-in reads was used to calculate normalization factor, with a greater number of *Drosophila* reads indicating a smaller amount of ChIP human DNA.

Principal component analysis (PCA)

A BED file of non-overlapping 20kb windows was generated to cover the human (hg19) genome using the BEDTools 'makewindow' command (Quinlan and Hall 2010). The BEDTools 'multicov' command was used to count the number of reads overlapping each window (calculated separately for H3 and H3K27me3 ChIP-seq data), and the data were loaded into DESeq2 (Love, Huber et al. 2014). For each sample, the ratio of *Drosophila* spike-in reads to the number of spike-in reads in the 'Basal-1' sample was used in lieu of '*estimateSizeFactors'*, and the DESeq2 '*estimateDispersions'* and '*nbinomWaldTest'* functions were applied to the data set. The normalized count matrix was then transformed using the '*rlog*' regularized log transformation, and PCA was performed on the rlog-transformed normalized count matrix using the DESeq2 '*plotPCA*' function on the most variable 5000 20kb windows (*ntop=5000* parameter for *plotPCA*).

Differential H3K27me3 coverage

Regions of differential H3K27me3 coverage were detected in the ChIP-seq data using diffReps (Shen, Shao et al. 2013) to compare coverage in refractory MTF2 patient $CD34^+CD38^-$ cells against coverage in responsive patient $CD34^+CD38^-$ bone marrow cells with normal MTF2 levels, and in MTF2 deficient $CD34^+CD38^-$ cells (transduced with SH3 & SH7) against healthy $CD34^+CD38^-$ bone marrow cells. For each comparison, H3K27me3 ChIP-seq reads were first filtered to remove reads mapping to ENCODE ChIP-seq blacklist regions, and diffReps was run using normalization factors calculated as described above for PCA analysis. Association between regions of reduced H3K27me3 and genes was taken directly from the diffReps output files.

Hierarchical clustering

The matrix of rlog-transformed count values was used to generate a matrix of pairwise Euclidian distances between samples. These distances were hierarchically clustered using complete linkage clustering, and a heatmap plotted to illustrate the distance relationships between samples.

Genome coverage calculations

BEDTools was used to convert BAM files of mapped reads into BED files, extend reads to 200bp length, and to calculate coverage depth across the human genome. The coverage depth was scaled by the ratio of *Drosophila* spike-in reads in the 'Basal-1' sample to the number of spike-in reads in the sample in question (*i.e.* the inverse of the size factor estimates used for DESeq2 analysis), and converted to bigWig format using the UCSC 'bedGraphToBigWig' tool (Kent, Zweig et al. 2010).

Validation of ChIP-seq targets was completed by ChIP-qPCR. All qPCR analysis was completed on a Roche Light Cycler 480 using Sybr Green MasterMix (Roche) and 0.1mM primers. Primer sequences are listed in Supplementary Table 9.

Methyl-ChIP-qPCR

Methyl ChIP-qPCR analyses were performed using the EpiMark Methylated DNA Enrichment Kit (New England Biosciences), according to manufacturer's instructions. Briefly, DNA was isolated from Lin$^-$CD34$^+$ cells isolated from the bone marrow aspirates of healthy individuals and patients with AML. DNA was fragmented and combined with methyl-CpG-binding domain protein 2 (MBD2) bound to magnetic beads to capture methylated DNA. Methylated CpG DNA was eluted from beads. Enriched DNA was used for RT-qPCR using primers listed in Supplementary Table 9.

Animal Study Approval

All animal experiments were conducted with the approval from the University of Ottawa Animal Care Committee, in accordance with the Canadian Council on Animal Care Standards and the Province of Ontario's Animals for Research Act. NOD-*scid* IL2Rgamma^{null} (NSG) mice were purchased from Jackson Labs. Mice were maintained in sterile housing conditions and given autoclaved chow and water ad libitum.

AML Xenograft mouse model

Anonymized, coded primary diagnostic AML bone marrow (BM) samples were obtained from patients as described above. Researchers were blinded to the clinical diagnosis and outcome

of the AML patients until the MTF2 and H3K27me3 analysis was complete. AML patient BM cells were expanded in NSG mice to obtain large numbers of patient derived xenograft (PDX) cells for the animal studies (Wunderlich, Mizukawa et al. 2013). Briefly, NSG mice were sub lethally irradiated with 300 Rads (Gammacell 3000) and transplanted via tail vein with 1 million BM cells. After 6-8 weeks, BM cells from the tibiae and femurs of the NSG mice were harvested and frozen in 10% DMSO using a controlled rate freezer (Kinetic) and stored at -150°C for future studies.

In vivo Treatment

Female NSG >7 week old mice were sublethally irradiated with 300 Rads and transplanted via tail vein with 1 million PDX cells; n=8 mice were transplanted per AML PDX sample. The peripheral blood of the transplanted mice was collected from the saphenous vein 3-4 weeks post-transplantation and analyzed for $CD45^+CD33^+$ cells. Upon the presence of >20% $CD45^+CD33^+$ cells in the peripheral blood, mice were randomized into 4 treatment groups (n=4 PDX samples; n=2 mice per group; n=8 mice total per group) and treated with i) DMSO, ii) nutlin3A, iii) induction therapy or iv) combination therapy (see below for details). To conceal the identity of the treatment received, syringes containing the vehicle control or drugs were prepared and coded by one person, while another person administered the treatment intravenously via tail vein. Coded treatments were assigned to the corresponding mouse.

Mice belonging to the induction therapy cohort, were treated using the previously published 5+3 treatment regimen. The mice were treated for the first three days with both Cytarabine (50 mg/kg) and Daunorubicin (1.5mg/kg), while during the last 2 days the mice were treated with Cytarabine (50 mg/kg) alone. Mice belonging to the combination therapy cohort, were

given the 5+3 treatment regimen in combination with Nutlin3A (12mg/kg). Nutlin3a was given for the entire duration of the 5 days. Weights were taken daily during treatment, and doses were recalculated by the researcher preparing the syringes to ensure that the mice received a consistent dose.

Post-treatment, the weights of the mice were monitored every 5 days. Moribund endpoint was determined as >20% loss in body weight, loss of mobility, loss of appetite and hunched posture. Otherwise if mice survived, endpoint was at 16 weeks post-treatment, when the experiment was terminated. Upon reaching endpoint, the BM of the mice was harvested and human cell engraftment was analyzed by flow cytometry (described below).

Lineage determination of PDX in vivo samples

To analyze PDX cells post-treatment, cells were harvested from the peripheral blood or bone marrow of NSG mice. To assess human cell engraftment in the mice, red blood cells were lysed and mononuclear cells were stained with antibodies directed against human specific lineage markers CD34 (Clone 4H11), CD38 (HIT2), CD45 (HI130), CD33 (P67.6), CD19 (HIB19), CD15 (HI98), CD3 (OKT30), CD4 (OKT4), CD8 (OKT8), CD14 (61D3) (eBioscience). Cells were then analyzed by flow cytometry using the BD LSR Fortessa II.

Immunohistochemistry

Blinded analysis of bone marrow cytospins of patient derived xenograft (PDX) mice, were performed using a total of 500,000 cells per slide. The slides were stained with Wright-Giemsa stain for 5 minutes and de-stained in water (PH 7.2) for 2 minutes. This process was repeated twice

for each slide and photomicrographs were obtained using a Zeiss Inverted LSM510 microscope. The pictures were taken at a magnification of 40X.

Cell viability assays

Lin$^-$CD34$^+$ cells isolated from either umbilical cord blood or primary AML patient bone marrow aspirates were transduced as above, sorted for GFP$^+$ and cultured in 96-well plates at 100,000 cells/100uL/well in duplicates. Daunorubicin, Cytarabine, Nutlin3a and MI773 were dissolved in DMSO. Cytarabine and Daunorubicin were added at concentrations of 1μM and 0.5μM, respectively. After 1 hour of incubation with Daunorubicin, cells were collected and transferred into fresh media to remove Daunorubicin from the media. The MDM2 pathway inhibitors, Nutlin3a and MI773 were added at concentrations of 1 μM.

Statistics

All data were expressed as mean ± SEM or SD. Data was analyzed using Prism 6.0 (GraphPad Software). Two-way Anova measured statistical significance between the conditions. A P value < 0.05 was used as a cut-off to indicate statistical significance.

Acknowledgments

We thank the OHRI Stem Core Facility for their assistance with FACS and sequencing and the University of Ottawa/ Ottawa Heart Institute Animal Care Facility for their invaluable assistance with the mouse experiments. HBM, HJ, MS, CYI and WLS designed the study, interpreted the results, and wrote the manuscript. HBM, HJ, CF, JMR, JYL, HB and STK conducted experiments and analyzed data. MS performed the clinical care, analysis and data interpretation. HBM, CJP and TJP performed all bioinformatic analyses. All authors assisted in editing the manuscript. This work was supported by operating grants from the Canadian Cancer

Society Research Institute, Canadian Institutes of Health Research, and the Cancer Research Society to WLS and CYI. WLS was supported by a Tier 1 Canada Research Chair in Integrative Stem Cell Biology. Sequencing data can be found in GEO (Accession # provided upon acceptance).

Supplementary Figures

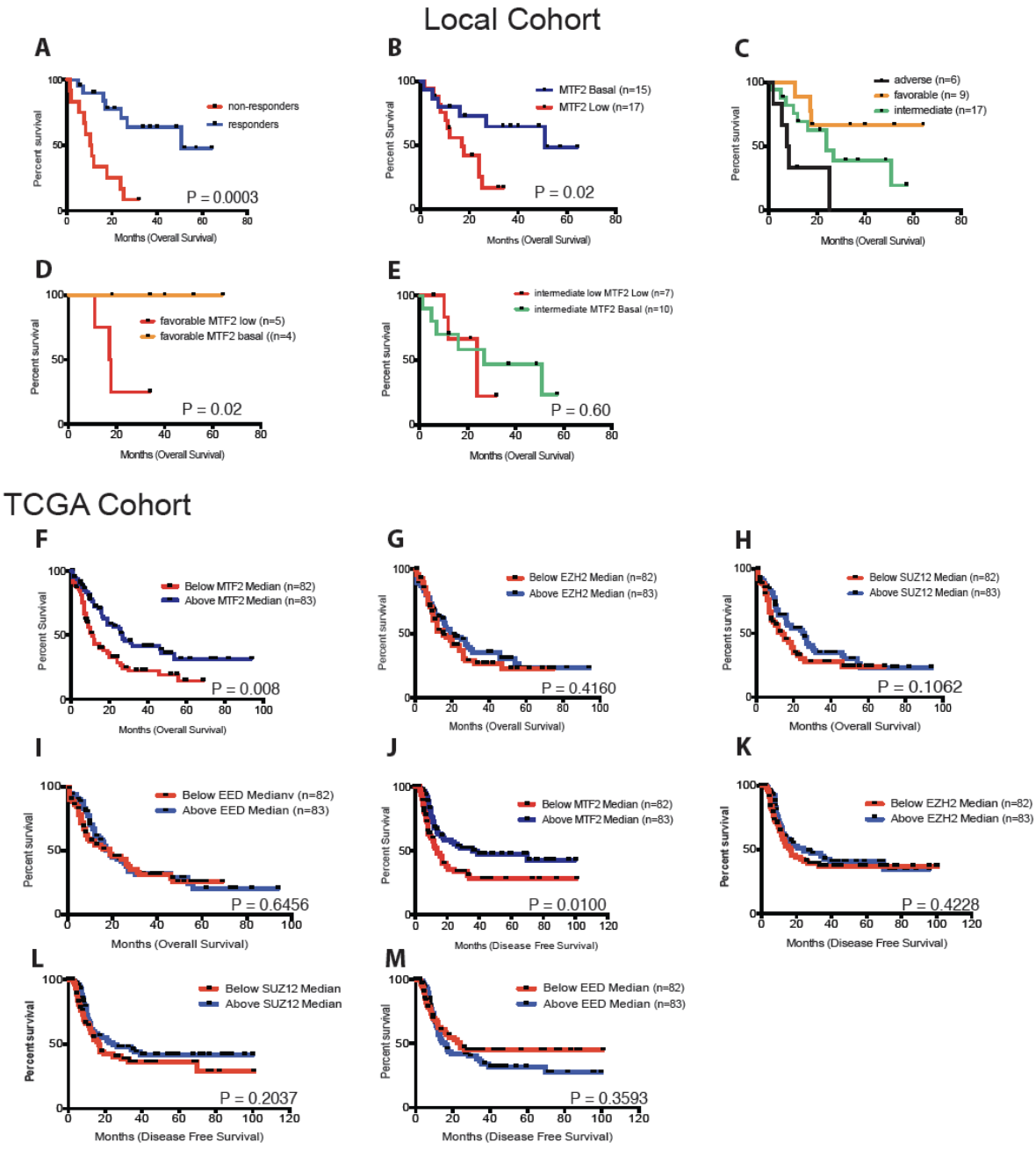

Figure S3.1. MTF2 deficiency correlates with poor prognosis. *MTF2* mRNA expression was analyzed within CD34$^+$CD38$^-$ LSC enriched cells from the local patient cohort (n=32) at diagnosis and normalized to *MTF2* mRNA expression within CD34$^+$CD38$^-$ cells isolated from healthy bone marrow aspirates (n=7). A, Kaplan-Meier analysis of local patient cohort (n=32)

shows that patients who do not respond to traditional induction chemotherapy regimen (extended methods) have significantly reduced overall survival compared to patients who respond to treatment. **B,** Kaplan-Meier analysis of local patient cohort (n=32) treated with traditional induction chemotherapy regimen showed that patients expressing low MTF2 (n=17) at diagnosis have poor survival times, P=0.02. **C,** Stratification of the local patient cohort using ELN cytogenetic metrics divides the patients into 3 risk groups that predict survival. **D**-**E,** Within the ELN favorable risk group based on cytogenetics, Kaplan-Meier analysis unveiled poor survival of patients with **(D)** low MTF2 expression, P=0.02, however no significant difference was observed within the **(E)** intermediate risk group, P=0.60. **F-M,** Analysis of TCGA AML patient dataset. mRNA expression of PRC2 members within bulk AML bone marrow aspirates at diagnosis show that deficiency (n=82) in MTF2 but not in SUZ12 or EZH2 or EED predicts survival. Patients expressing **(F)** low MTF2 have poor overall survival, P=0.008, while this is not true for patients with low **(G)** EZH2, P=0.4160, **(H)** SUZ12, P=0.1602, or **(I)** EED, P=0.6456. Analysis of disease free survival shows a similar trend, where **(J)** MTF2-deficient patients, P=0.01 fare poorly, while this is not true for patients with low **(K)** EZH2, P=0.4228, **(L)** SUZ12, P=0.2037, or **(M)** EED, P=0.3593. Kaplan-Meier analysis of (**F-M**) was performed in patients belonging to the TCGA AML cohort (n=165) who underwent traditional 7+3 induction therapy. P value was calculated using Log-rank (Mantel-Cox) test.

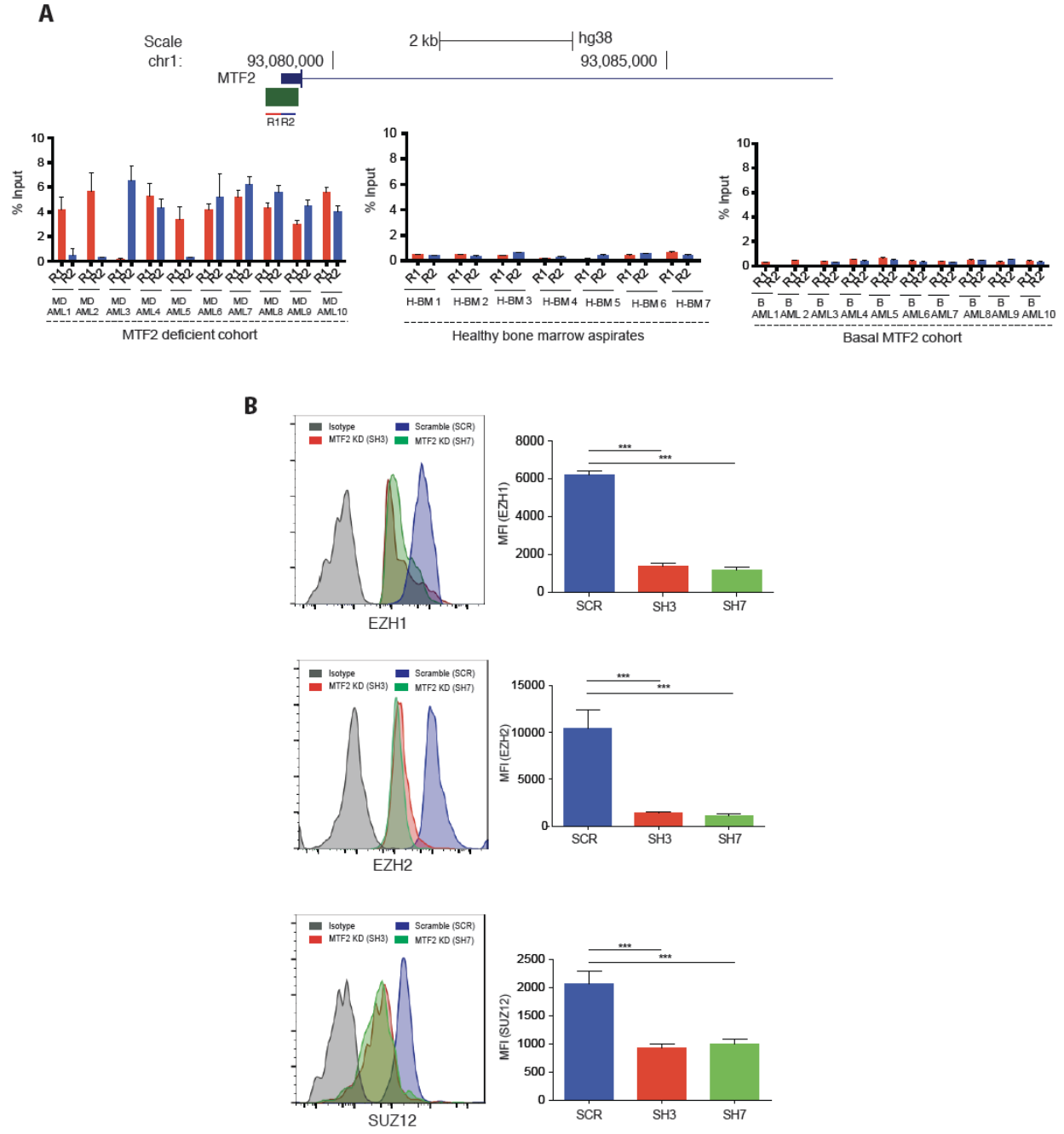

Figure S3.2. MTF2 deficiency correlates with poor response to standard treatment of care. **A,** (**Top**) *MTF2* gene locus, depicting the two CpG islands [R1 and R2] found within its promoter region. (**Bottom**), Hypermethylation of at least one of the CpG islands is observed in MTF2-deficient AML [MD-AML] (left) whereas methylation of these islands is normal in healthy BM [H-BM] (center) and MTF2-basal AML samples [B -AML] (right). **B,** Knockdown of MTF2 with two independent shRNA clones (SH3 or SH7) within CD34^{+}CD38^{-} cells results in decreased core

PRC2 members EZH1, EZH2 and SUZ12 measured by flow cytometric analysis. All data represent mean ± standard deviation; All data represent mean ± standard deviation; *P<0.05, **P<0.005, ***P<0005, P<0.00005 by Two-Way ANOVA.

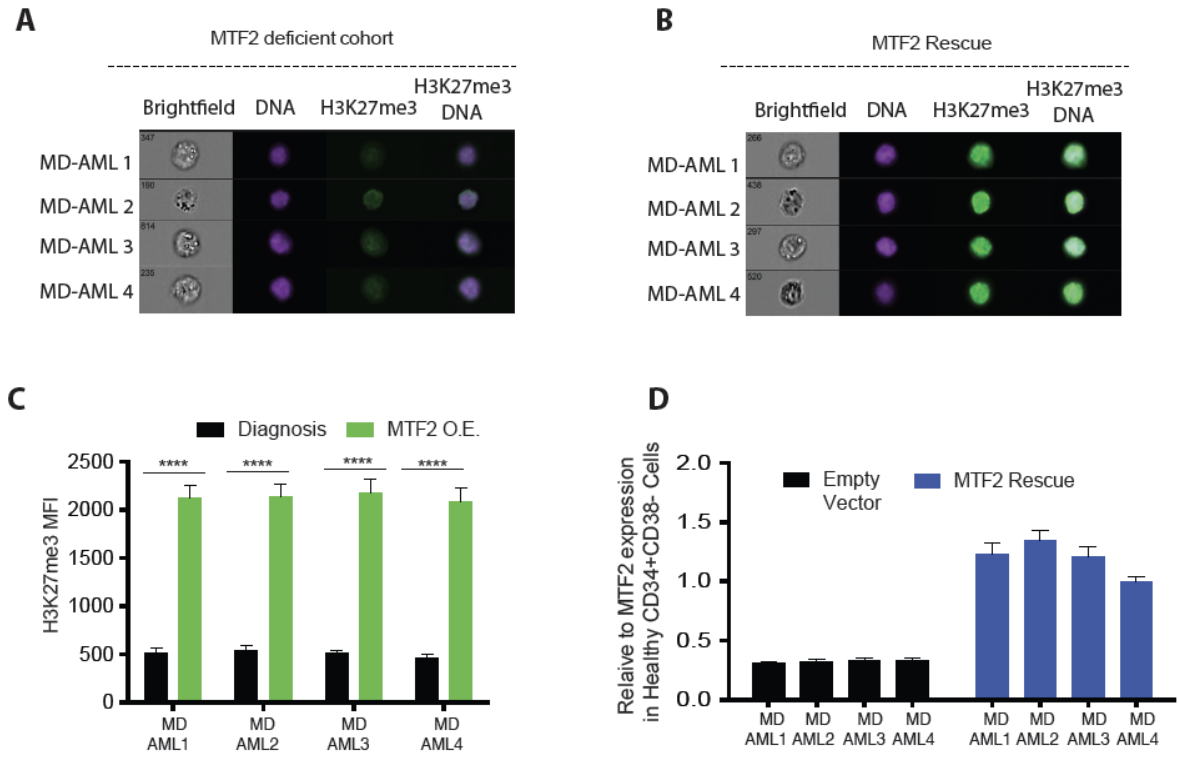

Figure S3.3. Restoring MTF2 levels re-establishes H3K27me3 levels within patient AML CD34^{+}CD38^{-} cells. **A-C,** 4 AML patients with MTF2 deficiency [MD-AML] analyzed by imaging flow cytometry show **(A)** low levels of H3K27me3 at diagnosis that is re-established when **(B-C)** MTF2 levels are rescued by lentivirus-mediated overexpression. **D,** RT-qPCR validation of MTF2 expression in rescued MD-AML samples. Expression levels of H3K27me3 were assessed by measuring the mean fluorescence intensity (MFI) within the nucleus by a preset algorithm in the IDEAS software. All data represent mean ± standard deviation; *P<0.05, **P<0.005, ***P<0005, P<0.00005 by Two-Way ANOVA.

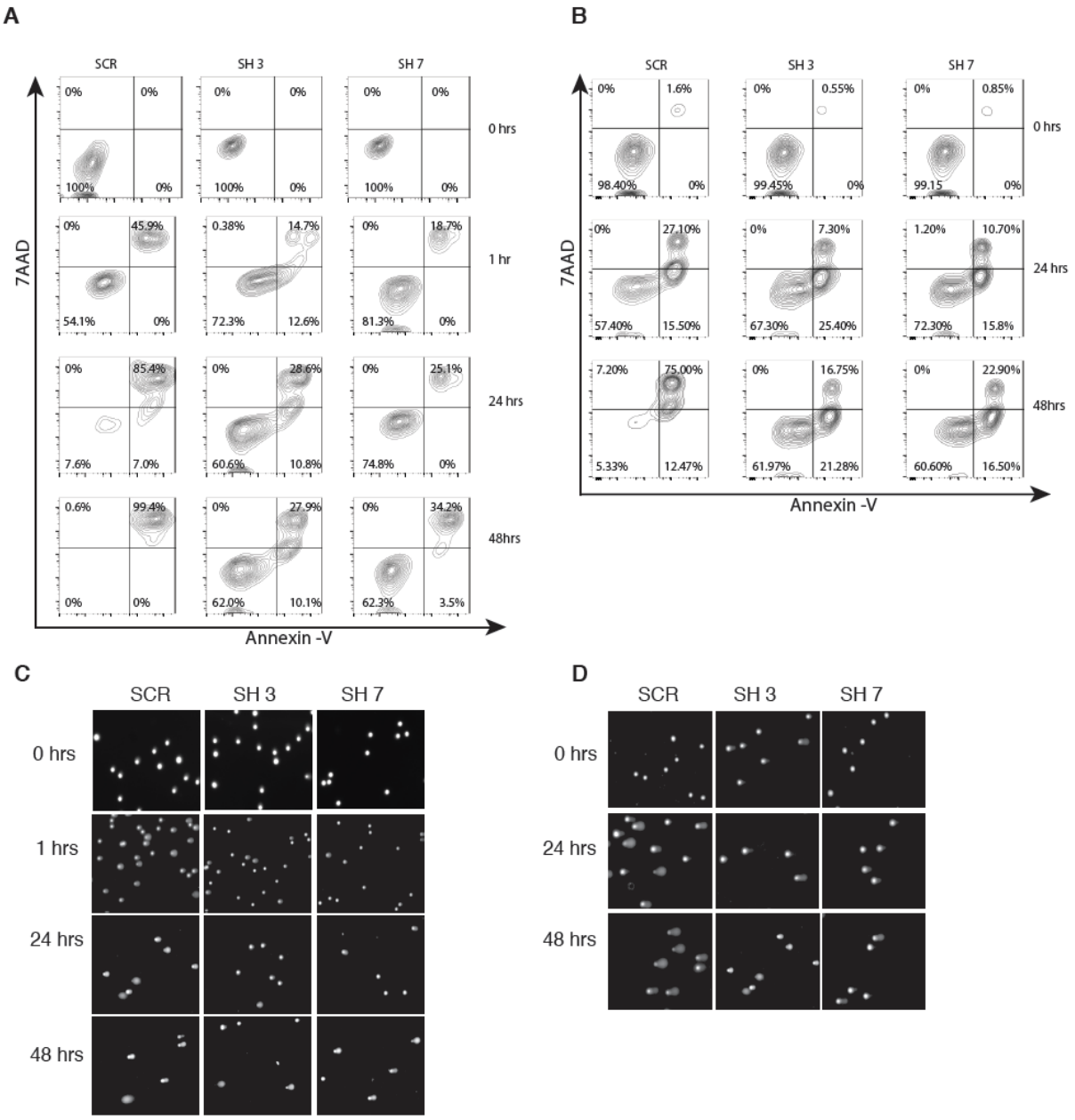

Figure S3.4. MTF2 deficiency promotes an anti-apoptotic effect and resistance to DNA damage post induction treatment. Cord blood Lin$^-$CD34$^+$ cells were transduced with GFP-tagged lentivirus encoding Scramble (SCR) or MTF2 (SH3, SH7) shRNA. Viable GFP$^+$ transduced cells were sorted and treated with induction drugs. **A-B,** Flow cytometry plots measuring apoptotic cells treated with either **(A)** 0.5μM Daunorubicin or **(B)** 1μM Cytarabine. Viable cells were determined at different time points by the percent of Annexin V-negative/7-AAD-negative cells, while early-apoptotic cells were measured by the percentage of the Annexin V-positive/7-AAD-negative cells.

Percentage of late apoptotic, dead cells was obtained by the positive dual staining of Annexin V-positive/7-AAD-positive. **C-D,** Representative comet images depicting DNA damage accumulation within $CD34^{+}CD38^{-}$ cells post-treatment with either (**C**) 0.5μM Daunorubicin or (**D**) 1μM Cytarabine. With time, an increase in comet-like nuclei indicating an accumulation of damaged DNA is observed over 48 hours. Blinded analysis of >200 comets were scored per condition and time point using a comet assay ImageJ OpenComet application (n=3).

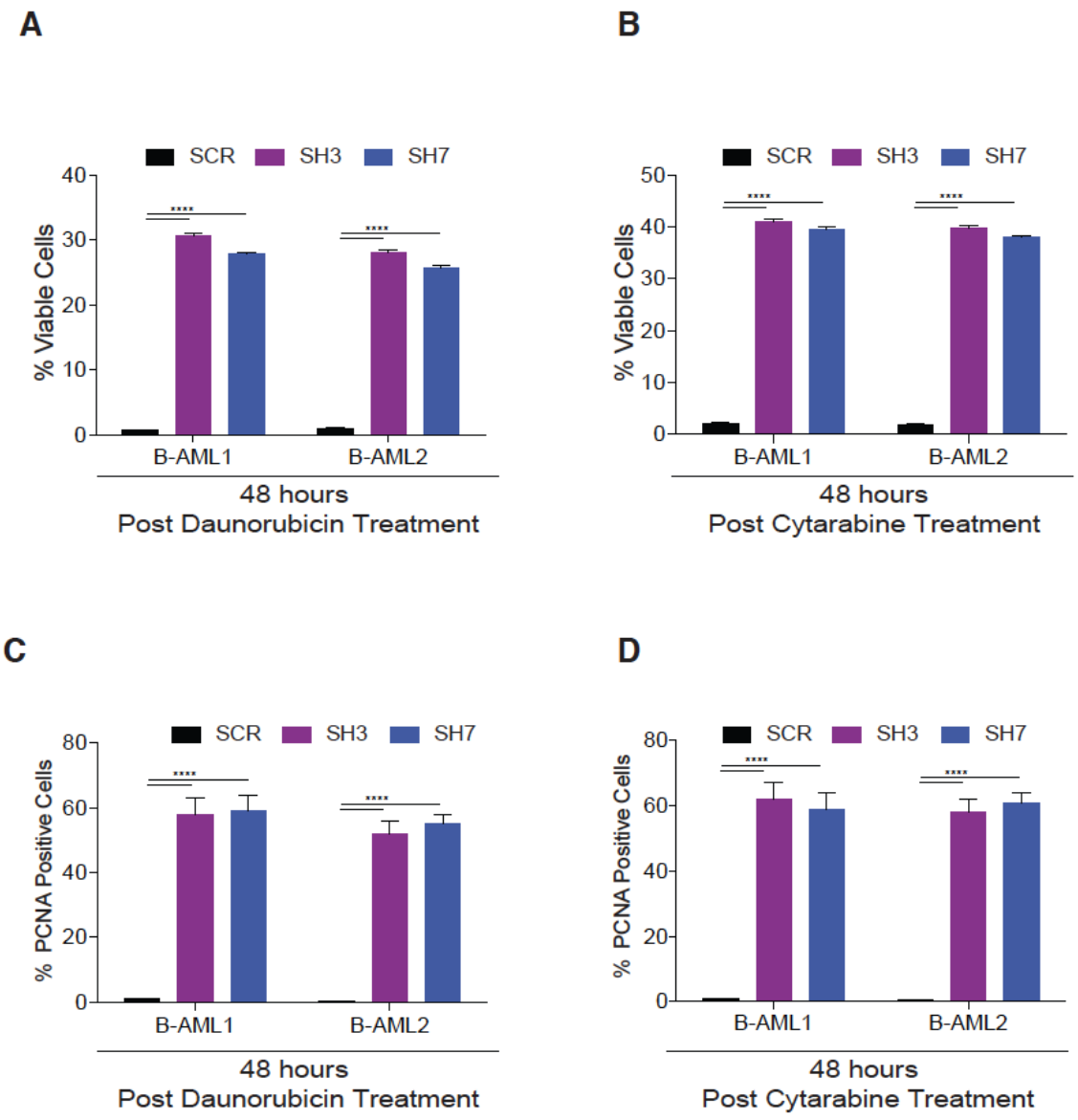

Figure S3.5. Knocking down MTF2 levels in leukemic Lin$^-$CD34$^+$cells with basal levels of MTF2 [B-AML] alters their chemoresponsivenes. A-B, Viability and apoptosis of scramble control (SCR) and MTF2 (SH3 or SH7) shRNA knockdown cells were analyzed over a 48-hour time period post-treatment with (**A**) Daunorubicin or (**B**) Cytarabine. Viable cells were determined by the percent of Annexin V-negative/7-AAD-negative cells. By 48 hours post-treatment, over 25% of MTF2-deficient cells remain viable, while nearly all of the scramble control cells have undergone apoptosis. **C-D,** PCNA proliferation marker analysis of scramble control (SCR) and MTF2-deficient (SH3 or SH7) shRNA knockdown cells 48 hours (**C**) post-Daunorubicin or (**D**) Cytarabine treatment. Viable cells from (**A-B**) were stained for PCNA, to

assess cell proliferation. MTF2-deficient cells continue to proliferate significantly more than control cells post-treatment. All data represent mean ± standard deviation; *P<0.05, **P<0.005, ***P<0005, P<0.00005 by Two-Way ANOVA.

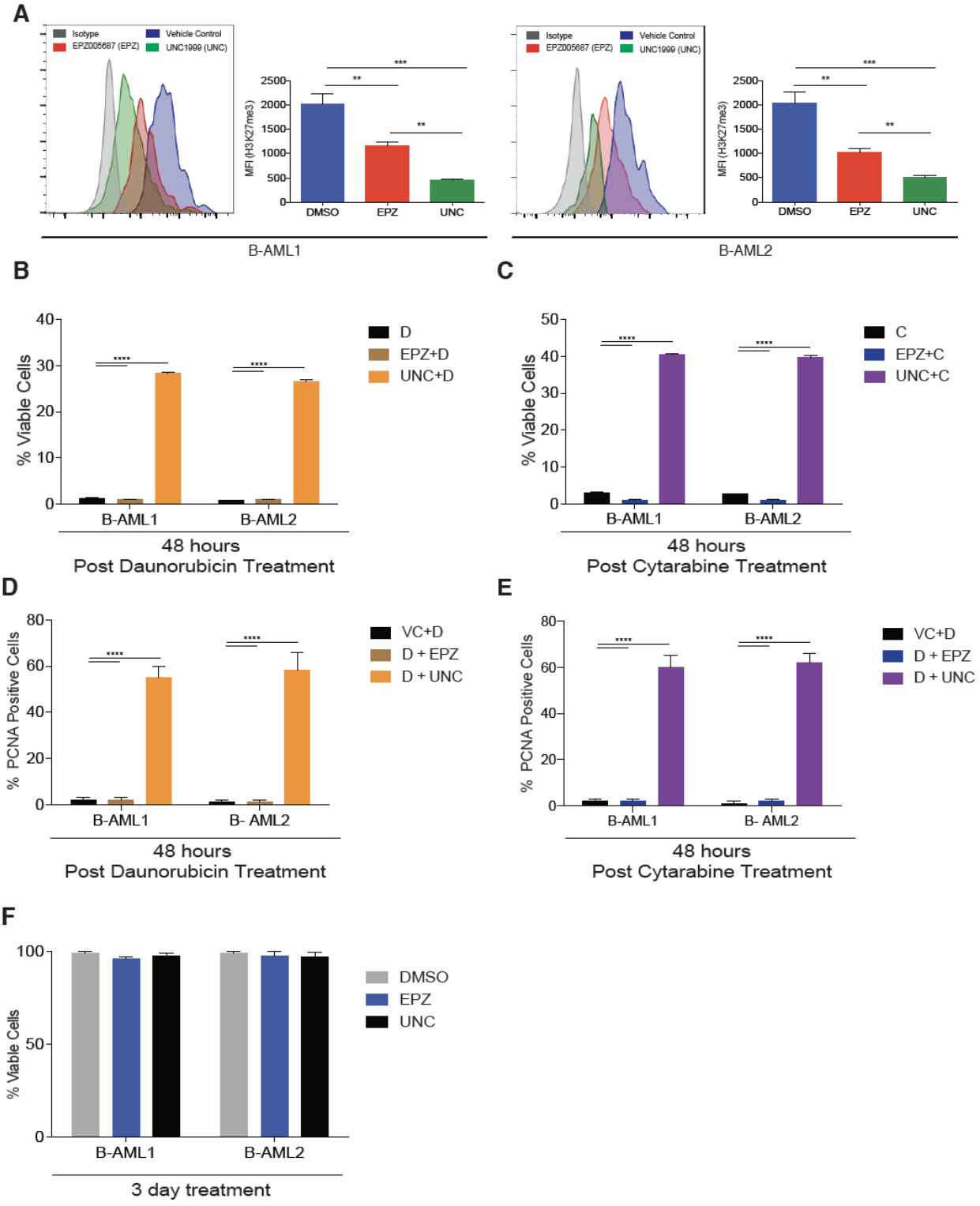

Figure S3.6. Dual inhibition of EZH1 and EZH2 methyltransferase activity confers chemoresistance in responsive primary AML cells. Chemoresponsive AML patient cells with basal levels of MTF2 [B-AML] were pre-treated with EZH2 inhibitor [EPZ] or EZH1/2 inhibitor

[UNC] for 3 days followed by co-treatment with Daunorubicin or Cytarabine for 48 hours. **A,** Chemoresponsive B-AML cells showed loss of global H3K27me3 levels when treated with both the small molecule inhibitors. Only pre-treatment of B-AML cells with the EZH1/2 inhibitor confers chemoresistance to (**B**) Daunorubicin and (**C**) Cytarabine at 48 hours that is comparable to MTF2-basal AML patient cells transduced with MTF2 shRNA knockdown virus (**Supplementary Fig. S3.5A,B**). **D-E,** PCNA proliferation marker analysis of EZH2 inhibitor [EPZ] or EZH1/2 inhibitor [UNC] pre-treated MTF2-basal AML patient cells 48 hours (**D**) post-Daunorubicin or (**E**) post-Cytarabine treatment. Viable cells from **(B-C**) were stained for PCNA, to assess cell proliferation. The EZH1/2 inhibitor [UNC] treated cells continue to proliferate significantly more than vehicle control [VC] and EZH2 inhibitor [EPZ] treated cells. **F**. Pre-treatment of B-AML cells with vehicle control [VC], EZH2 inhibitor [EPZ] or EZH1/2 inhibitor [UNC] alone did not affect cell viability. Cells analyzed by flow cytometry using viability and apoptosis markers 7AAD and Annexin V. *P<0.05, **P<0.005, ***P<0.0005, ****P<0.00005 by Two-Way ANOVA.

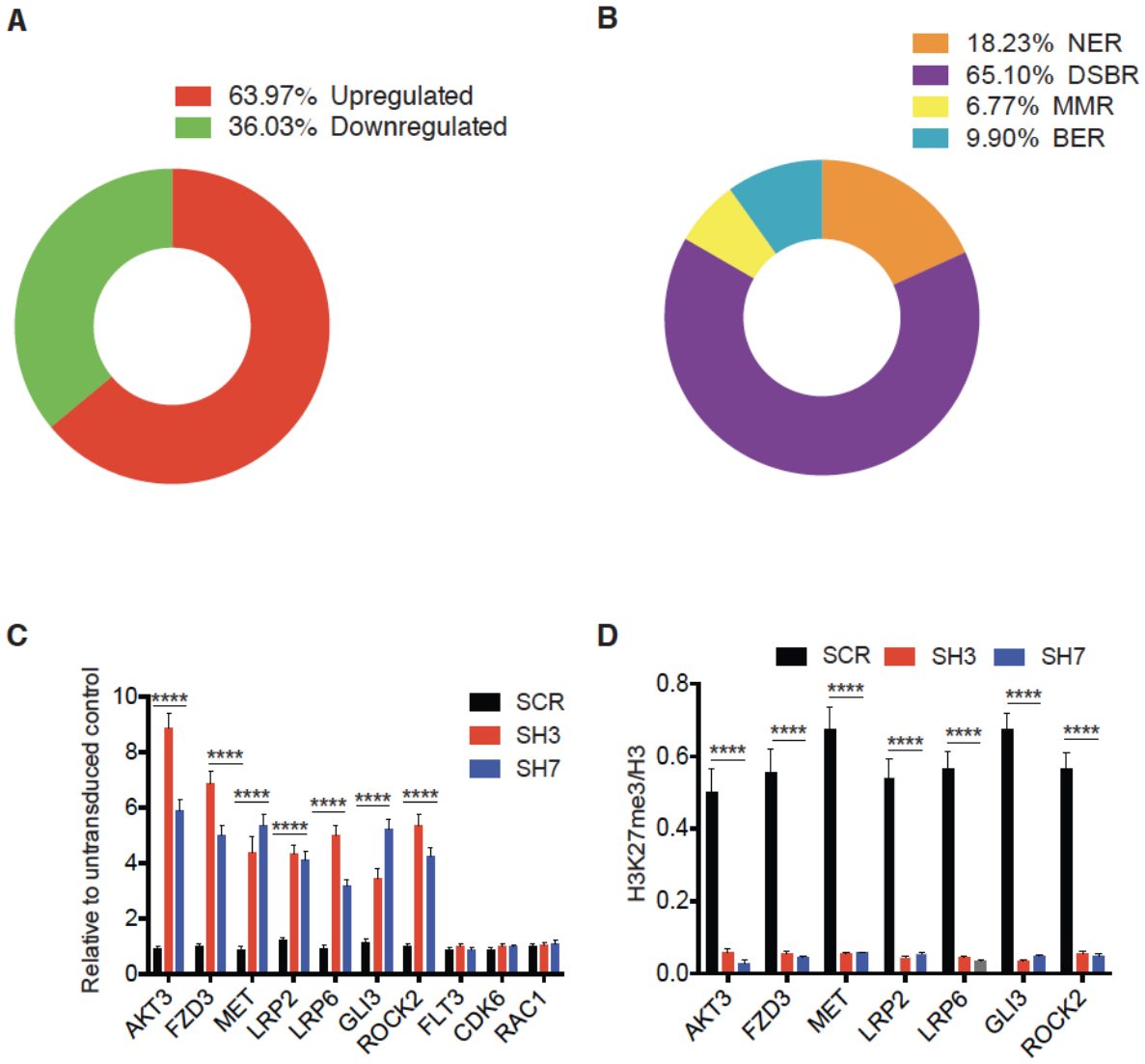

Figure S3.7. DNA damage response (DDR) is hyperactivated in MTF2-deficient HSPCs. A, Dissection of the DDR enrichment term from (**Fig. 3.3A)** revealed an upregulation in 63.97% (190 out of 297) of the genes associated with this GO term. **B,** Further analysis of the upregulated DDR genes revealed their role in Nucleotide Excision repair [NER] (35 genes) Double stranded break repair [DSBR] (123 genes) Mismatch Repair [MMR] (13 genes) and Base Excision Repair [BER] (19 genes). **C-D,** (**C**) RT-qPCR and (**D**) ChIP-qPCR validation of the MTF2 GRN, including DDR genes, in scramble or MTF2 (SH3 or SH7) knockdown HSPCs. Experiments were performed in triplicate (n=3). All data represent mean ± standard deviation; *P<0.05, **P<0.005, ***P<0.0005, ****P<0.00005 by Two-Way ANOVA.

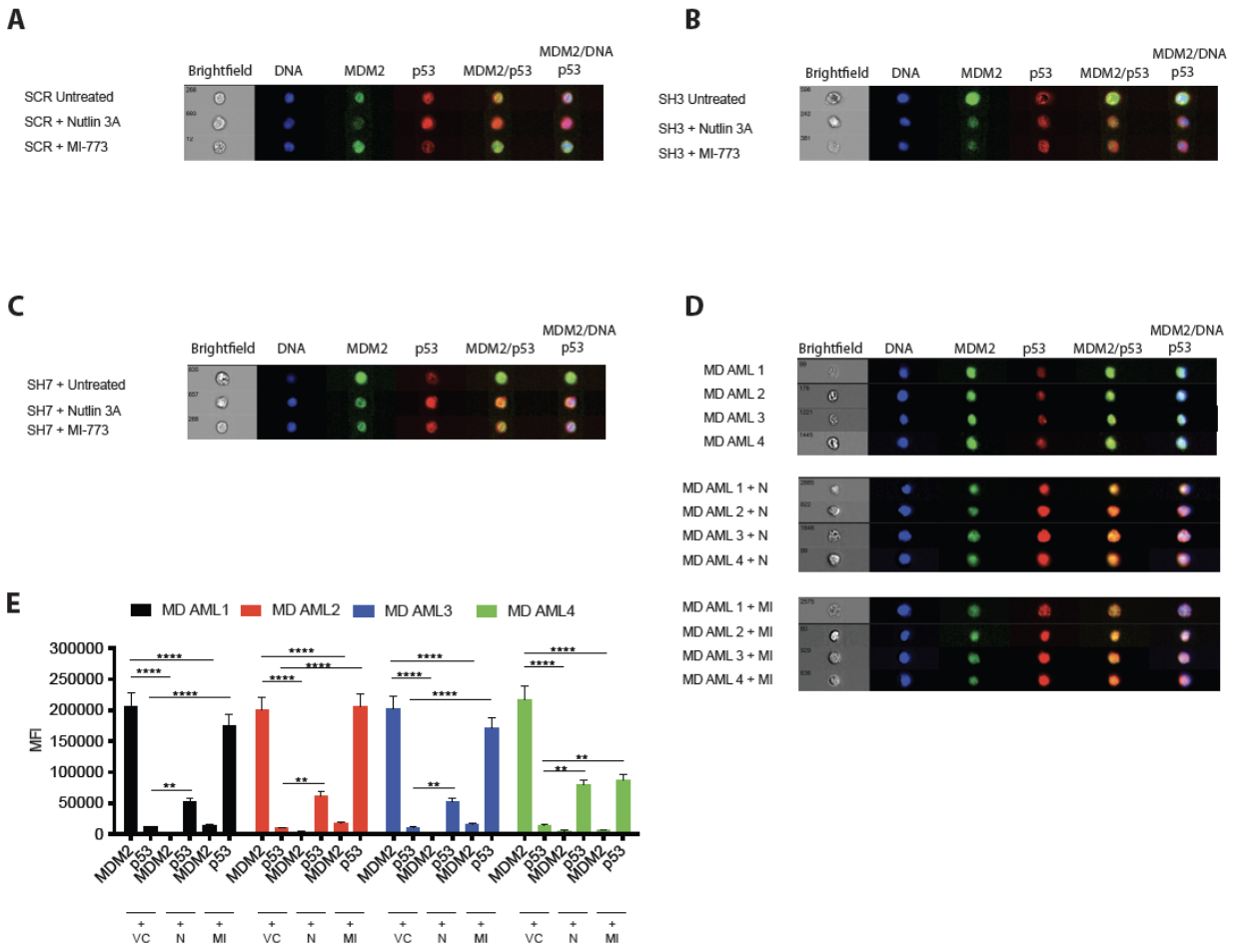

Figure S3.8. MDM2 inhibitors restore p53 levels within MTF2-deficient cells. A-C, Imaging flow cytometry analysis of MTF2 (SH3 or SH7) shRNA knockdown HSPCs demonstrate that these cells exhibit low levels of p53 and high MDM2 levels within the nucleus compared to the scramble (SCR) control cells. The use of two individual MDM2 inhibitors with different chemical backbones, either 1μM of Nutlin3a or 1μM of MI-773, reestablished MDM2 and p53 levels to those observed in the scramble untreated control. **D,** Much like MTF2 knockdown HSPCs (**Fig. 3.3H**), Lin$^-$CD34$^+$ leukemic cells from refractory AML patient bone marrow aspirates [MD-AML] in the top panel showed increased MDM2 and decreased p53 expression. p53 levels were also restored post-treatment with MDM2 inhibitors, represented in the panels below. **E,** Expression levels of p53 and MDM2 were determined by measuring the MFI within the nucleus using a preset algorithm in the IDEAS software (Amnis). An overlay of p53 and MDM2 is shown in the right column representing the overlap within the nucleus used for analysis. (MD AML, MTF2-deficient AML; VC, Vehicle control; N, Nutlin3A; MI, MI-773.)

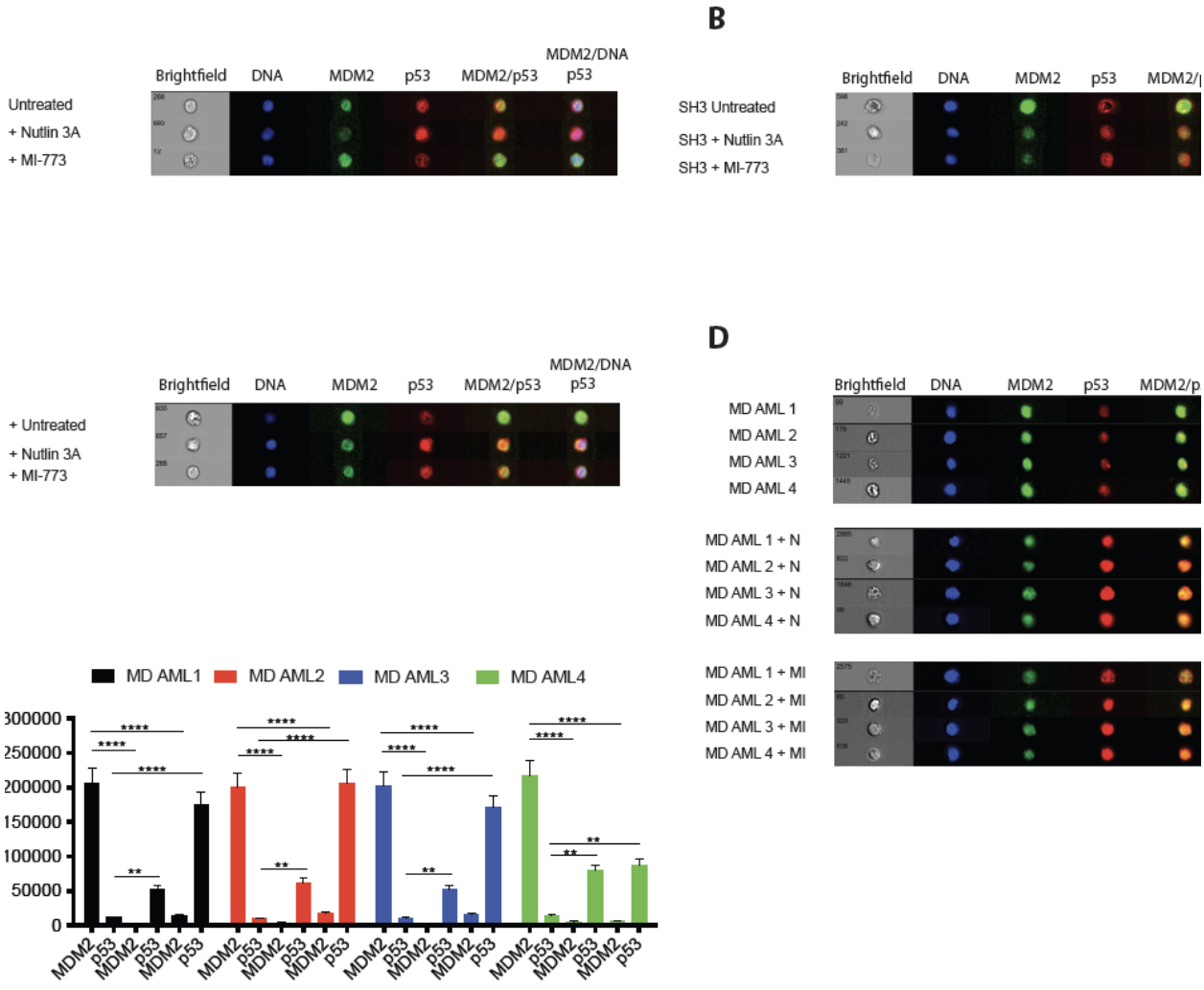

Figure S3.9. Cell cycle progression and proliferation is normalized when p53 levels are restored. A, Left, flow cytometric analysis of cell cycle profiles of vehicle control [VC], Nutlin3a [N], or MI-773 [MI] treated scramble (SCR) control or MTF2 (SH3 or SH7) knockdown shRNA cells. Gating the individual cell cycle stages was performed by modeling the profile to the preset algorithm "Dean Jett Fox". Right, quantification of the population distribution within the cell cycle stages demonstrates cells arresting in G0/G1 when treated with either 1μM Nutlin3a or MI-773 for 24hours. **B,** Proliferation was also assessed 24 hours post-treatment with either 1μM Nutlin3a or MI-773 where a decrease in overall PCNA levels are observed in MTF2-deficient HSPCs.

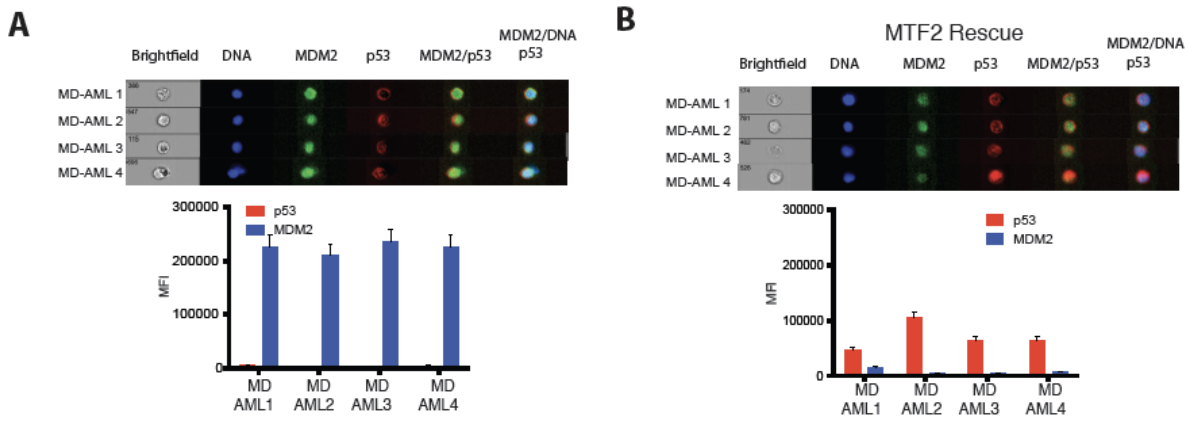

Figure S3.10. Rescue of MTF2 within MTF2-deficient refractory patient BM aspirates decreases MDM2 and restores p53 levels. **A-B,** MDM2 and p53 levels were analyzed in Lin$^-$ CD34$^+$ leukemic cells from MTF2-deficient refractory AML patient BM aspirates [MD-AML] by imaging flow cytometric analysis. Data indicated (**A**) an overexpression of MDM2 and low p53 levels in MD-AML cells, which is reversed when MTF2 is overexpressed in these patient cells via lentiviral transduction, resulting in (**B**) decreased MDM2 and increased p53 levels.

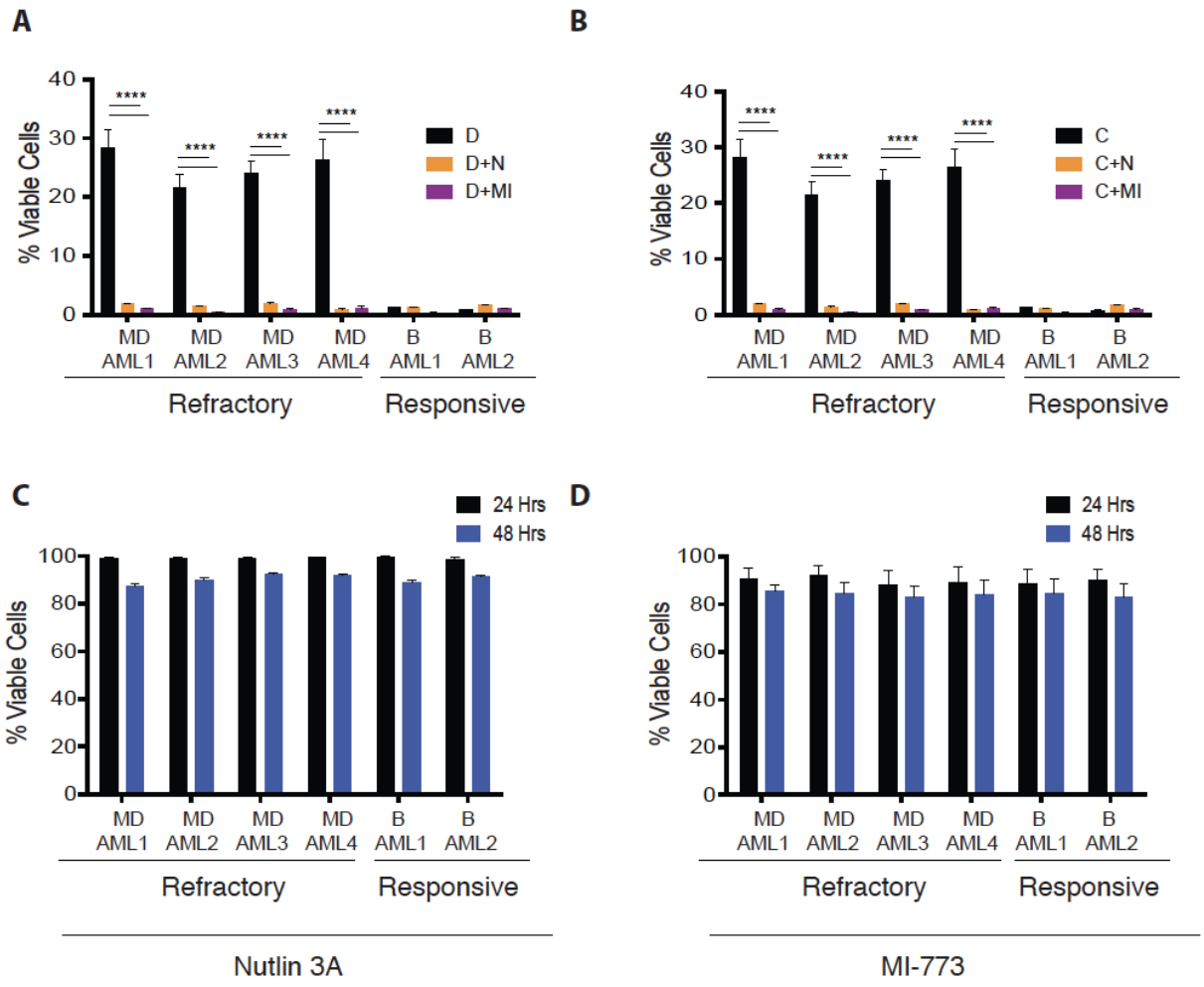

Figure S3.11. Combinatory treatment regimen comprised of an MDM2 inhibitor and induction drugs reverses chemoresistance in MTF2-deficient cells. A-B, MTF2-deficient refractory AML patient cells [MD-AML] showed increased sensitivity to (**A**) Daunorubicin and (**B**) Cytarabine when treated in combination with MDM2 inhibitor MI-773 [MI] or Nutlin3A [N] for 48 hours that is comparable to MTF2-basal AML patient cells [B-AML]. **C-D,** Treatment with (**C**) Nutlin3a or (**D**) MI-773 alone elicited a very low apoptotic effect over the course of 48hours, suggesting a low cytotoxic effect individually. Flow cytometry analysis was used to detect viable cells, which were determined by the percent of Annexin V-negative/7-AAD-negative cells. All data represent mean ± standard deviation; *P<0.05, **P<0.005, ***P<0.0005, ****P<0.00005 by Two-Way ANOVA.

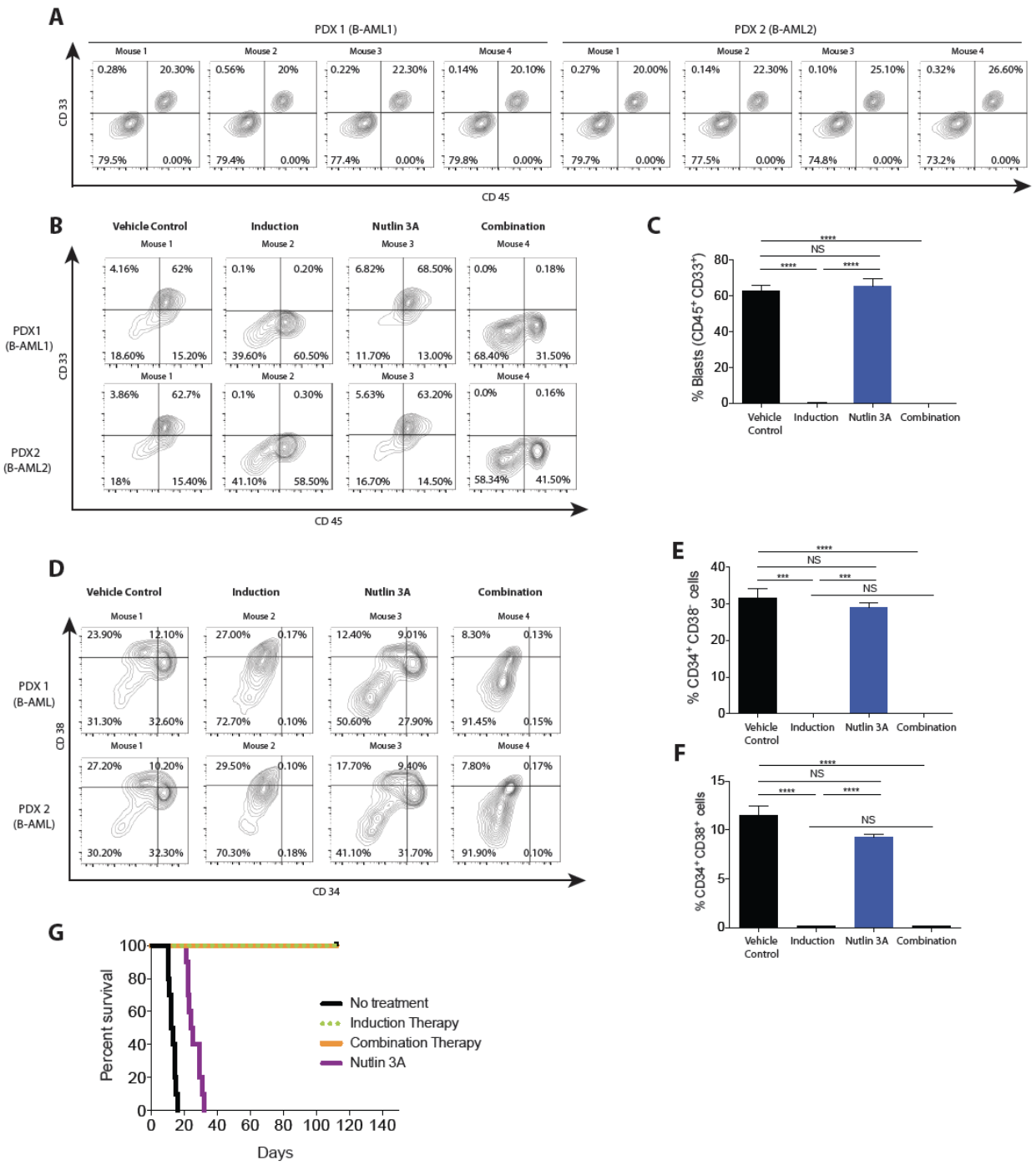

Figure S3.12. Induction therapy and combination therapy kills chemoresponsive AML cells with basal MTF2 levels *in vivo*. A, Representative flow cytometry plots demonstrating ≥20% engraftment of patient derived xenograft (PDX) $CD45^{+}CD33^{+}$ cells in the peripheral blood of NSG mice that were transplanted with normal (basal) levels of MTF2 [B-AML] via tail vein (n=4 chemoresponsive B-AML samples). **B-C,** Upon ≥20% engraftment of B-AML PDX $CD45^{+}CD33^{+}$

cells, mice were treated with either vehicle control [VC], induction therapy, Nutlin3A alone, or combination therapy (Nutlin3a + induction therapy). Representative flow cytometry plots analyzing (**B**) $CD45^{+}CD33^{+}$ cells in the BM of treated mice at time of sacrifice. Quantification of flow cytometry analysis demonstrates (**C**) a significant decrease of $CD33^{+}$ cells within the bone marrow of the induction and combination drug cohort compared with the other treatment cohorts. **D-F,** Representative flow cytometry plots of bone marrow analyses assessing (**D**) the percent $CD34^{+}CD38^{-}$ LSC-enriched and $CD34^{+}CD38^{+}$ populations of mice in each treatment group at time of sacrifice. 16-weeks event-free post-treatment, the induction and combination treatment dramatically reduced the **(E)** $CD34^{+}CD38^{-}$ and **(F)** $CD34^{+}CD38^{+}$ populations within the bone marrow. Vehicle control and Nutlin 3A cohorts were moribund and sacrificed < 6 weeks post-treatment, but the induction and combination treatment cohorst were sacrificed 16 weeks post-treatment when the experiment was terminated. (n=4 B-AML samples, n=2 mice per treatment group and n=8 mice total per treatment group). **F,** Kaplan-Meier curve of chemoresponsive B-AML patient-derived xenograft (PDX) NSG mice treated with either vehicle control, Nutlin3A alone, induction therapy or combination therapy (n=4 refractory AML samples; n = 8 mice per treatment group). All data represent mean ± standard deviation; *P<0.05, **P<0.005, ***P<0.0005, ****P< 0.00005 by Two-Way ANOVA.

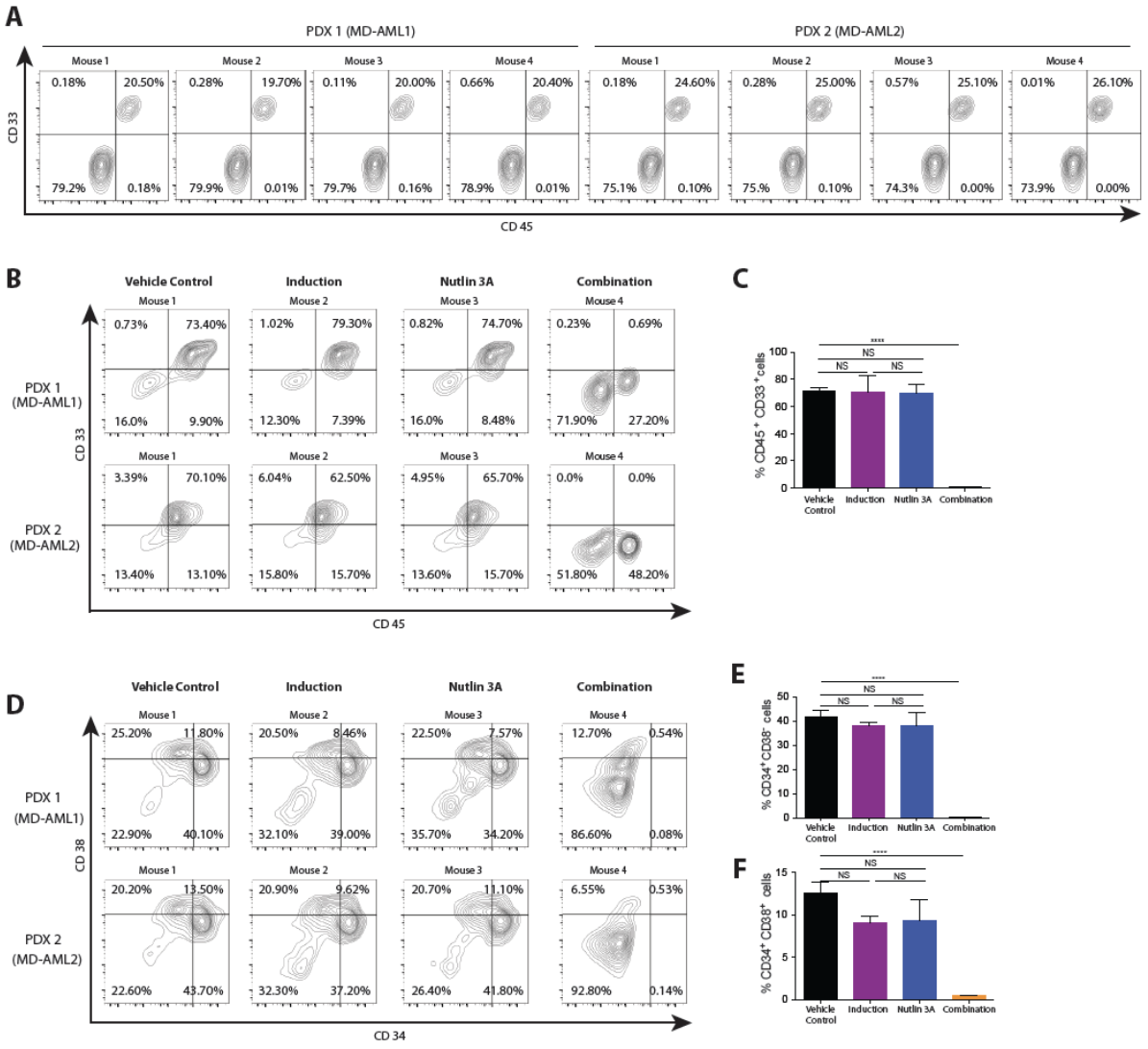

Figure S3.13. Combination therapy kills MTF2-deficient refractory AML cells *in vivo*. **A,** Representative flow cytometry plots demonstrating ≥20% engraftment of patient derived xenograft (PDX) $CD45^{+}CD33^{+}$ cells in the peripheral blood of NSG mice that were transplanted with MTF2-deficient AML BM patient cells [MD-AML] via tail vein (n=4 refractory AML samples). **B-C,** Upon ≥20% engraftment of PDX $CD45^{+}CD33^{+}$ cells, mice were treated with either vehicle control [VC], induction therapy, Nutlin3A alone, or combination therapy (Nutlin3a + induction therapy). Representative flow cytometry plots analyzing (**B**) $CD45^{+}CD33^{+}$ cells in the BM of treated mice at time of sacrifice. Quantification of flow cytometry analysis demonstrates (**C**) a significant decrease of $CD33^{+}$ cells within the bone marrow of the combination drug cohort compared with the other treatment cohorts. **D-F,** Representative flow cytometry plots of bone marrow analyses assessing

(**D**) the percent $CD34^{+}CD38^{-}$ LSC-enriched and $CD34^{+}CD38^{+}$ populations of mice in each treatment group at time of sacrifice. 16-weeks event-free post-treatment, the combination treatment dramatically reduced the **(E)** $CD34^{+}CD38^{-}$ and **(F)** $CD34^{+}CD38^{+}$ populations within the bone marrow. Vehicle control, Nutlin 3A and induction therapy cohorts were moribund and sacrificed < 6 weeks post-treatment, but the combination treatment cohort was sacrificed 16 weeks post-treatment when the experiment was terminated. (n=4 MD-AML samples, n=2 mice per treatment group and n=8 mice total per treatment group). All data represent mean ± standard deviation; *P<0.05, **P<0.005, ***P<0.0005, ****P<0.00005 by Two-Way ANOVA.

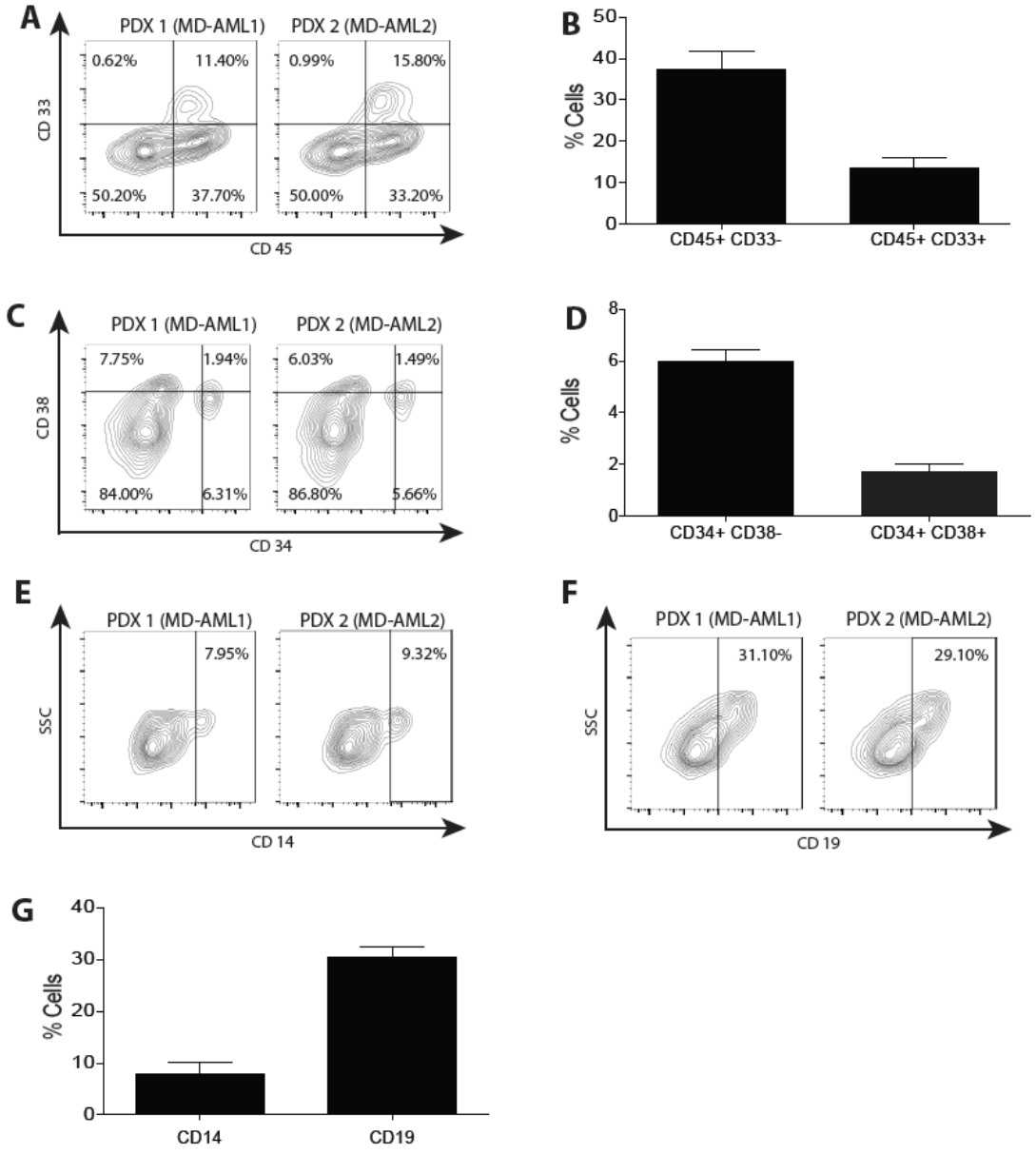

Figure S3.14. Combination therapy treated PDX cells demonstrate multi-lineage engraftment potential and contribute to event free survival in secondary transplants. BM from primary NSG mice transplanted with patient derived xenograft (PDX) MTF2-deficient AML [MD-AML] and treated with combination therapy was harvested 16 weeks post-treatment and transplanted into secondary recipients. Event-free multi-lineage engraftment potential of HSPCs, myeloid and lymphoid lineages was assessed at 16 weeks post-secondary transplant. **A**-**B,** Representative flow cytometry plots of BM analysis of (**A**) $CD45^{+}CD33^{+}$ myeloid cells in

secondary recipients and (**B**) mean $CD45^{+}CD33^{+}$ percentage shows robust myeloid engraftment. **C-D,** Representative flow cytometry analysis of BM assessing (**C**) HSPC populations and quantitative assessment of the HSPC populations based on (**D**) CD34 and CD38 expression within the BM of the secondary recipients. **E-G,** Representative flow cytometry BM analyses assessing the percent (**E**) $CD14^{+}$ monocyte and (**F**) $CD19^{+}$ B-lymphocyte engraftment in secondary transplants. (**G**) Mean $CD14^{+}$ and $CD19^{+}$ engraftment in secondary recipients. (n=4 AML refractory samples; n = 8 secondary mice in total).

Chapter 4

Discussion and Future Directions

4.1 Summary of major findings and significance

The Stanford lab discovered *Mtf2* to be an epigenetic repressor that regulates mouse embryonic stem cell (ESC) fate by controlling self-renewal, proliferation and differentiation gene regulatory networks (GRNs) (Walker, Chang et al. 2010). Gene Ontology (GO) analysis of this transcriptome data showed that *Mtf2* represses the expression of a number of oncogenes, including some that are involved in hematopoiesis and leukemia. While *Mtf2* has been well studied within the ESC model system, its role within somatic stem cells and tissues has not been explored. Therefore, to understand the role of Mtf2 during development, we took a reductionist approach and implemented gene targeting and systems biology to uncover a unique and fundamental role of *Mtf2* in erythrocyte differentiation and HSC self-renewal. By integrating RNA-seq and ChIP-seq data, we show for the first time that both Wnt and Hippo signaling are epigenetically regulated by Mtf2 in a cell intrinsic manner. Remarkably, the loss of Mtf2 within hematopoietic cells results in global loss of H3K27me3 levels at promoter proximal sites that results in de-repression of multiple signaling networks and pathways. Surprisingly, our GRN analysis identified a novel epigenetic network that directly links the PRC2 proteins with DNA methyltransferase proteins.

These major findings presented in the second chapter, place Mtf2 as a critical regulator of hematopoiesis and expand its role beyond that of a canonical accessory PcG protein. Furthermore, these findings also recast the role of Polycomb accessory proteins in a tissue specific context.

While our murine studies revealed that the loss of Mtf2 did not cause leukemia in mice, our studies of MTF2 in human cells demonstrated that MTF2 deficiency within human HSPCs

causes a myelo-proliferative phenotype that is reminiscent of pre-leukemia. In humans, 40% of AML patients do not respond to standard induction therapy; these refractory AML patients have exceptionally poor survival rates, often dying within a year of diagnosis. Unfortunately, there are no biomarkers and limited treatment options currently available that identify and treat patients with refractory AML. The major findings outlined in the third chapter identify MTF2 and H3K27me3 levels as functional biomarkers that identify and drive refractory AML.

We show using both local and public AML datasets (Cancer Genome Atlas Research, Ley et al. 2013) that patients with low levels of MTF2 have significantly poor overall survival. Furthermore, our response to standard induction therapy analysis within our local cohort demonstrated that 80% of the patients belonging to the MTF2 low cohort do not respond to standard induction therapy and the 20% that did respond, relapsed within 6 months. Using imaging flow cytometry, standard flow cytometry and ChIP-sequencing, we show that MTF2 dictates the H3K27me3 landscape within LSC-enriched populations and its loss drives the refractory phenotype. Implemeting an unbiased systems biology approach, we identified MTF2-PRC2 repression of MDM2 as central to driving chemoresistance. Targeting this dysregulated signaling pathway by MTF2 overexpression or MDM2 inhibitors showed that it sensitized refractory patient LSC-enriched populations to induction chemotherapeutics and prevented relapse in AML patient-derived xenograft mice. This work now allows us to identify patients with refractory AML at diagnosis and allows us to provide them with a therapeutic option.

4.2 Expanding the role of PRC2 accessory proteins

Accessory proteins were originally defined based on their co-immunoprecipitation association with core complex members (Kim, Kraus et al. 2003, Cao and Zhang 2004, Nekrasov, Klymenko et al. 2007, Peng, Valouev et al. 2009, Pasini, Cloos et al. 2010, Walker, Chang et al. 2010). Since then, accessory proteins have been shown within ESCs to have minor roles in PRC2 targeting, complex stability, and enhancement of H3K27me3 levels (Peng, Valouev et al. 2009, Hunkapiller, Shen et al. 2012). However, the role of accessory PcG proteins within somatic stem cells and adult tissues have not been well studied. This is important considering accessory proteins have often been found to have a tissue-restricted expression pattern. Indeed, we demonstrated that *Mtf2* is highly expressed within the hematopoietic system (described in Chapter 1) and that it is critical in hematopoiesis (described in Chapters 1, 2). One of the interesting findings from this study was that loss of Mtf2 led to post-transcriptional loss of the core PRC2 complex members and global loss of promoter proximal H3K27me3 levels. We therefore propose that Mtf2 in hematopoietic cells functions as a core complex member. Interestingly, this proposed tissue-specific role of accessory PRC2 complex proteins may not be limited to Mtf2. A previous study has shown that shRNA mediated knock down of *Jarid2* within HSPCs gives rise to a phenotype similar to *Suz12* knock out (Kinkel, Galeev et al. 2015). While the reduction of Jarid2 did not affect the transcript levels of *Suz12* and *Ezh2*, the changes in the protein levels were not analyzed. It will therefore be important to study the role of PRC2 accessory proteins and their role in complex stabilization in a tissue/cell type specific manner. It also raises an important question on how the accessory proteins compete among each other for binding PRC2 and what defines their tissue specific role. Furthermore, it would be important to understand whether the accessory proteins can compensate for each other even when overexpressed.

4.3 Mtf2 regulates cell type specific gene regulatory networks

While Mtf2 deficiency within ESCs leads to enhanced self-renewal (Walker, Chang et al. 2010), the loss of Mtf2 within HSC leads to loss of HSC self-renewal and exhaustion. These differences in the functional phenotypes between HSCs and ESCs prompted us to draft cell-specific GRNs to gain insight on the molecular programs driving these functional phenotypes. We therefore performed transcriptional factor (TF) ChIP-seq and RNA-seq in low numbers of sorted primary hematopoietic cells. Comparison of the *Mtf2*-PRC2 network from ESCs with hematopoietic cells revealed that *Mtf2* regulates a distinct gene regulatory network (less then 10% overlap with the ESC network). While in ESCs, loss of *Mtf2* results in overexpression of self-renewal and pluripotency factors (Walker, Chang et al. 2010); in HSCs, loss of *Mtf2* leads to de-repression of cell cycle genes and therefore leads to increased cycling. Interestingly, our GRN analysis also identified several lineage specific GRNs regulated by Mtf2 within the hematopoietic system. For example, we noticed that the Mtf2-PRC2 complex direct controls that expression of several histone deacetylases (HDACs) and PRC1 proteins within the erythroid cells that are not observed within the Mtf2 null HSPCs. Some factors that contribute to these cell type specific GRNs include chromatin confirmation and accessibility by histone modifications (Heintzman, Hon et al. 2009, Ernst and Kellis 2013). However, it is important to note that this phenomenon is not common among all TFs and some TFs such as CTCF, may have a more consistent binding profile across multiple cell types (Shen, Yue et al. 2012, Griffon, Barbier et al. 2015). It will therefore be important to perform ATAC-seq and chromatin confirmation studies and integrate these data with our H3K27me3 and RNA-seq datasets from *Mtf2*$^{-/-}$ and *Mtf2*$^{+/+}$ cells to reveal the lineage specific reinforcement of the open chromatin landscape.

4.4 Mtf2 facilitates H3K27me3 mediated repression of DNA methyltransferases

DNA methylation and H3K27me3 are both responsible for the establishment and maintenance of epigenetic memory. Previously, some studies have shown a cooperative relationship between Ezh2 and DNA methyltransferases (Dnmts), where Ezh2, independent of the PRC2 complex, was responsible for recruiting Dnmts to its target gene promoters and facilitating DNA methylation (Vire, Brenner et al. 2006). Furthermore, the knockdown of *Ezh2* within cancer cell lines (Osteosarcoma and colorectal cancer cells) leads to loss of DNA methylation (McGarvey, Van Neste et al. 2008). Alternatively, several other studies have shown that the relationship between PRC2 complex and Dnmts can be antagonistic. For example, proteomic analysis show that the PRC2 core components such as Suz12 and Eed are excluded from methylated DNA (Bartke, Vermeulen et al. 2010). Moreover, in neural stem cells Dnmt3a deficiency leads to increased global levels of H3K27me3 levels (Wu, Coskun et al. 2010). While the relationship between Dnmts and PRC2 appear to be contradicting and tissue dependent, it is clear that the relationship between these marks is important in both normal and neoplastic cells. In this work, our unbiased systems biology analyses demonstrate for the first time Mtf2/H3K27me3 mediated repression of Dnmts within the hematopoietic system. We show that Mtf2-PRC2 directly repress Dnmts and the loss of Mtf2 within HSPCs leads to de-repression of Dnmts, which then ultimately leads to the inactivation of the Hippo tumor suppressor pathways.

4.5 Exploring the *in vivo* role of Mtf2 using a constitutive gene-targeted mouse model

The *in vivo* role of *Mtf2* was previously described using gene trap mouse strains. The interruption of *Mtf2* between 4th and 5th exon generated viable mice with skeletal abnormalities (Wang, He et al. 2007). A second mixed background strain generated from gene-trapped ESCs

phenocopied the skeletal defects previously observed; however, these mice also demonstrated early post-natal lethality (Li, Isono et al. 2011). The polyA trap *Mtf2* model developed by the Stanford lab showed developmental defects, including situs inversus and hair cycling defects (Stanford Lab unpublished data). Such variation in phenotypes have also been previously observed among other Polycomb mutants (Motoyama, Kitajima et al. 1997, Kitajima, Kojima et al. 1999). Since gene trap mutants can often be hypomorphic (Stanford, Cohn et al. 2001), they can often lead to variable phenotypes depending on the background strain. Therefore, to generate Mtf2 null mice, we chose to use a gene targeting strategy and used gene targeted ESCs to generate *Mtf2* null (*Mtf2*$^{-/-}$) mice in a *C57BL/6J* background.

Unlike the previous gene trap mutants, the knockout of *Mtf2* using gene targeting led to embryonic lethality. The *Mtf2*$^{-/-}$ embryos died at e15.5 and showed several hematopoietic phenotypes including anemia. Unfortunately, the early death of the *Mtf2* mutant embryos prevented us from exploring the role of *Mtf2* within non-hematopoietic tissues. Considering we were using a constitutive knock out mouse model, we wanted to make sure the hematopoietic phenotypes we observed were not being caused due to the fetal liver niche. Polycomb members have previously been shown to play a role in regulating the niche. For example, the niche of *Bmi1*$^{-/-}$ mice have been shown to not support HSC self-renewal (Iwama, Oguro et al. 2004). Furthermore, depending on the mouse strain, the role of Jarid2 in hematopoiesis has been attributed to microenvironment defects (Takeuchi, Yamazaki et al. 1995, Motoyama, Kitajima et al. 1997). Understanding and mapping the role of the niche and how it impacts hematopoiesis is important, considering several studies have reported a reciprocal relationship where alterations in the BM niche may influence disease development and malignant cells have been shown to alter the BM niche (Mendez-Ferrer, Michurina et al. 2010, Ding, Saunders et al. 2012, Ding and Morrison 2013,

Greenbaum, Hsu et al. 2013). In the context of diseases, such as myelodysplasia or leukemia, recent studies have shown that alterations in the BM niche can influence disease progression (Medyouf, Mossner et al. 2014). Therefore, to test whether *Mtf2* phenotypes are caused due to a cell intrinsic or extrinsic mechanism, we performed competitive transplant experiments and demonstrated that *Mtf2*$^{-/-}$ HSCs have defects in long term self-renewal and erythropoiesis. Taken together, these data demonstrate that the *Mtf2* phenotypes are due to cell intrinsic mechanisms.

4.6 Comparing human vs murine GRNs

While mouse models have been instrumental in our understanding of hematopoiesis, recent studies have demonstrated important differences between human and mouse hematopoiesis (discussed in chapter 1). Dissection and overlapping our Mtf2/MTF2 GRNs within the mouse/human HSPCs respectively, helped us identify pathways that may be unique to them. For example, pathway analysis of the RNA-seq data from *Mtf2*$^{-/-}$ FL-HSPCs identified Hippo and Wnt signaling, similar analysis using our human RNA-seq data identified RNA-splicing, p53 signaling pathways and DNA damage response as our top hits. Interestingly, while *Mtf2*$^{-/-}$ HSPCs showed no differences in p53 levels, MTF2 KD human HSPCs showed loss of p53 and increased levels of MDM2. Another important difference we noticed between our RNA-seq datasets from human and mice HSPCs is the enrichment of myeloid genes. We noticed that several important myeloid genes (C-Jun, PU.1, C/EBP-alpha) were only upregulated within the human dataset. These data taken together demonstrates that several important differences exist within the gene regulatory circuits controlled by Mtf2/MTF2 within the mouse/human HSPCs respectively. These findings can potentially hold true for other proteins that are part of epigenome modifying complexes. We do

however realize that some of these differences might be due to the fact that we are comparing a constitutive gene-targeted KO model to a shRNA mediated KD model.

4.7 MTF2 a novel predictor of H3K27me3 levels within AML

High EZH2 levels were shown previously to predict poor prognosis within solid tumors such as prostate and breast cancer (Varambally, Dhanasekaran et al. 2002, Kleer, Cao et al. 2003). Overexpression of EZH2 in cancer was proposed to be caused due to gene amplification (Bracken, Pasini et al. 2003) or down regulation of microRNA 101 (miRNA-101) (Varambally, Cao et al. 2008), and stimulation of its expression by the pRB-E2F (Bracken, Pasini et al. 2003) and MEK-ERK pathways. However, since then, several studies have reported a paradoxical relationship between EZH2 and H3K27me3 levels. While high levels of EZH2 predict poor prognosis, low levels of H3K27me3 predict poor prognosis in breast and prostate cancers (Wei, Xia et al. 2008, Holm, Grabau et al. 2012, Xu, Wu et al. 2012, Healey, Hu et al. 2014, Bae, Yoo et al. 2015). This has led many groups to propose that EZH2 might play PRC2-independent roles in cancer (Lee, Li et al. 2011, Xu, Wu et al. 2012). Recently, in leukemia EZH2 has been shown to play a role outside of the PRC2 complex, where it acts as a transcriptional activator and functions independent of its histone methyltransferase activity (Yan, Ng et al. 2013). These findings are consistent with the data presented in this thesis, where we demonstrate that the inhibition of the methyltransferase activity of EZH2 within healthy HSPCs does not trigger a refractory phenotype, however low levels of H3K27me3 levels do. Interestingly, the refractory phenotype only manifests upon the knock down of *MTF2* or dual inhibition of EZH1 and EZH2. These results are consistent with the fact that loss of MTF2 results in dual loss of EZH1/2 and that EZH1 has been previously reported to compensate for EZH2 (Xie, Xu et al. 2014) within the hematopoietic system. Importantly, we

show that the rescue of MTF2 restores the global H3K27me3 levels and sensitizes refractory AML cells to standard induction therapy drugs. This data highlights the first known incidence of an accessory member dictating the H3K27 landscape within healthy and neoplastic cells. The evidence provided in this thesis also suggests that focusing on the tissue specific role of PRC2 accessory proteins will enable a better understanding of H3K27me3 mediated mechanisms in healthy and disease states.

4.8 Future Directions

I have identified a novel prognostic marker, *MTF2* (low expression levels) that can predict refractory AML at diagnosis. *MTF2* is a tumor suppressor gene, that is epigenetically silenced in the bone marrow of approximately 40% of the AML patients. These AML patients with deficient levels of MTF2 do not respond to standard induction therapy and are therefore classified to have refractory AML. Consistent with basal levels of MTF2 necessary for successful induction therapy response, MTF2 deficient cells generated by lentiviral knockdown are resistant to standard induction therapy drugs such as Cytarabine and Daunorubicin. Furthermore, we show that the MTF2 deficient cells continue to proliferate despite the accumulation of DNA damage. Therefore, as future work, it would be important to validate the role of MTF2 as a biomarker and test the therapeutic potential of 'combination therapy' via a clinical trial. Furthermore, considering some AML patients (especially the elderly) are not treated with induction therapy but instead receive hypo-methylating drugs (Azacytidine, Decitabine), it would important to investigate whether *MTF2* mRNA levels can predict response to the hypo-methylating drugs. Outside of the clinical trial, we should explore the role of MTF2-PRC2 in DNA damage response as well as identify genes that are required for the viability of MTF2 deficient cells.

4.8.1 Elucidate the role of MTF2-PRC2 within DNA damage response

DNA damage that occurs within a cell, can be of many different types and there are a variety of pathways that are involved. For example, in the presence of single-stranded DNA (ssDNA) breaks which occur due to the stalling of the replication fork, ataxia telangiectasia mutated and Rad3-related (ATR) kinase and poly[ADP-ribose] polymerase 1 (PARP1) are the principal proteins that get activated to initiate the DDR (Nam and Cortez 2011) (Ciccia and Elledge 2010, Polo and Jackson 2011, Luo and Kraus 2012). However, when endogenous or exogenous DNA double stranded breaks occur, the site of DNA is marked by the phosphorylation on histone H2A.X by members of the phosphatidylinositol-3-kinase (PI-3K) family (ataxia telangiectasia mutated (ATM), ATR or DNA-dependent protein kinase (DNA-PK)), which in turn initiate the DDR (Kuo and Yang 2008, Derheimer and Kastan 2010).

PcG proteins have recently been shown to directly and indirectly regulate the various aspects of the DDR. For example, Bmi1 was found to maintain cellular redox homeostasis and the KD or KO of Bmi1 in mice has been shown to lead to accumulation of ROS that cause DNA damage and DDR activation (Liu, Cao et al. 2009). Furthermore, Ezh2 has been reported to indirectly affect DSB repair by repressing Rad51, an enzyme involved in homologous recombination (Chang, Yang et al. 2011). Ezh2 has also been shown to regulate BRCA1, a tumour suppressor that regulates DNA repair, cell-cycle checkpoints, and chromosomal stability (Gonzalez, DuPrie et al. 2011). While PRC2 core components have been shown to localize to sites of DSBs in U2OS and human fibroblasts, however the role of H3K27me3 in DDR, still remains unclear. Moreover, the role of MTF2-PRC2 in the hematopoietic DDR is still unknown and is yet to be elucidated.

4.8.2 Screening for new drug targets in MTF2 deficient refractory AML cells

It will be important to identify proteins that are required for the viability of MTF2 deficient cells. This knowledge can then be used to identify drugs that inhibit these target proteins and enable the treatment of MTF2 deficient patients, without affecting the cells with basal levels of MTF2. One strategy that this goal can be achieved is to perform a genome wide CRISPR/cas9 synthetic lethal screen. The hits obtained from this screen can be ranked and then functionally validated using primary refractory AML patient cells. Known inhibitors of the target genes and pathways can be tested using cytotoxicity assays.

4.8.3 Dissecting the *Mtf2*$^{-/-}$ phenotype using a conditional knock out model

While our gene-targeted Mtf2 knockout mouse model provides an excellent model to study the role of Mtf2 during development *in vivo*, it is not without drawbacks. Because Mtf2 loss leads to embryonic lethality, it prevents us from further dissecting the molecular pathways that are part of the Mtf2-PRC2 GRN. Considering Mtf2 deficiency results in abnormal expression of multiple pathways and triggers cross talk between multiple epigenetic regulators (PRC2, HDACs, Dnmts) it will therefore be important to perform epistasis experiments. Performing epistasis experiments will allow us to decipher the extent to which the altered pathways and epigenetic cross-talk contribute to the HSC and erythroid phenotypes. An alternative approach that will allow us to perform these experiments is the conditional knock out strategy. Furthermore, the conditional knockout strategy will also allow us to study the role of Mtf2 within other non-hematopoietic tissues within which it is highly expressed.

4.9 Conclusions

In this thesis, I have combined systems biology and reductionist approaches to build a comprehensive story on the role of Mtf2/MTF2 within mouse and human hematopoiesis and leukemia, respectively. We used the functional and molecular outcomes to drive our research and show that Mtf2/MTF2 is a critical regulator of murine and human hematopoiesis. While the loss of Mtf2 within murine HSPCs causes an erythroid blockage, the loss of MTF2 within human HSPCs triggers both an increase in myeloid differentiation, proliferation in addition to a block in erythropoiesis. Taken together, these results show that while the murine system is a powerful, invaluable model to understand complex molecular mechanisms that govern human hematopoiesis, important differences exist between the mouse and human hematopoietic systems.

The work presented in this thesis further builds on recent findings from whole genome sequencing studies that identify epigenetic modifiers as the most commonly mutated genes in AML. We screened *MTF2* expression within LSC enriched cells isolated from primary AML patient samples and uncovered that *MTF2* is mis-regulated in AML and its loss predicts refractory AML. We drafted a MTF2 specific GRN within LSC enriched cells and uncovered a direct mechanism by which MTF2 regulates chemoresistance in AML and show that targeting this mechanism sensitizes refractory AML to standard induction therapy. In summary, the work presented in this thesis, lays the foundation for the development of diagnostic kits that would help identify refractory AML at diagnosis and demonstrates a targeted therapeutic strategy for patients with MTF2 low refractory AML.

Akashi, K., D. Traver, T. Miyamoto and I. L. Weissman (2000). "A clonogenic common myeloid progenitor that gives rise to all myeloid lineages." Nature **404**(6774): 193-197.

Al-Khalaf, M. H., L. E. Blake, B. D. Larsen, R. A. Bell, S. Brunette, R. J. Parks, M. A. Rudnicki, P. J. McKinnon, F. Jeffrey Dilworth and L. A. Megeney (2016). "Temporal activation of XRCC1-mediated DNA repair is essential for muscle differentiation." Cell Discov **2**: 15041.

Amsellem, S., F. Pflumio, D. Bardinet, B. Izac, P. Charneau, P. H. Romeo, A. Dubart-Kupperschmitt and S. Fichelson (2003). "Ex vivo expansion of human hematopoietic stem cells by direct delivery of the HOXB4 homeoprotein." Nat Med **9**(11): 1423-1427.

Antonchuk, J., G. Sauvageau and R. K. Humphries (2002). "HOXB4-induced expansion of adult hematopoietic stem cells ex vivo." Cell **109**(1): 39-45.

Bae, W. K., K. H. Yoo, J. S. Lee, Y. Kim, I. J. Chung, M. H. Park, J. H. Yoon, P. A. Furth and L. Hennighausen (2015). "The methyltransferase EZH2 is not required for mammary cancer development, although high EZH2 and low H3K27me3 correlate with poor prognosis of ER-positive breast cancers." Mol Carcinog **54**(10): 1172-1180.

Ballare, C., M. Lange, A. Lapinaite, G. M. Martin, L. Morey, G. Pascual, R. Liefke, B. Simon, Y. Shi, O. Gozani, T. Carlomagno, S. A. Benitah and L. Di Croce (2012). "Phf19 links methylated Lys36 of histone H3 to regulation of Polycomb activity." Nat Struct Mol Biol **19**(12): 1257-1265.

Bartke, T., M. Vermeulen, B. Xhemalce, S. C. Robson, M. Mann and T. Kouzarides (2010). "Nucleosome-interacting proteins regulated by DNA and histone methylation." Cell **143**(3): 470-484.

Beerman, I. and D. J. Rossi (2015). "Epigenetic Control of Stem Cell Potential during Homeostasis, Aging, and Disease." Cell Stem Cell **16**(6): 613-625.

Beguelin, W., R. Popovic, M. Teater, Y. Jiang, K. L. Bunting, M. Rosen, H. Shen, S. N. Yang, L. Wang, T. Ezponda, E. Martinez-Garcia, H. Zhang, Y. Zheng, S. K. Verma, M. T. McCabe, H. M. Ott, G. S. Van Aller, R. G. Kruger, Y. Liu, C. F. McHugh, D. W. Scott, Y. R. Chung, N. Kelleher, R. Shaknovich, C. L. Creasy, R. D. Gascoyne, K. K. Wong, L. Cerchietti, R. L. Levine, O. Abdel-Wahab, J. D. Licht, O. Elemento and A. M. Melnick (2013). "EZH2 is required for germinal center formation and somatic EZH2 mutations promote lymphoid transformation." Cancer Cell **23**(5): 677-692.

Benveniste, P., C. Frelin, S. Janmohamed, M. Barbara, R. Herrington, D. Hyam and N. N. Iscove (2010). "Intermediate-term hematopoietic stem cells with extended but time-limited reconstitution potential." Cell Stem Cell **6**(1): 48-58.

Blackledge, N. P., A. M. Farcas, T. Kondo, H. W. King, J. F. McGouran, L. L. Hanssen, S. Ito, S. Cooper, K. Kondo, Y. Koseki, T. Ishikura, H. K. Long, T. W. Sheahan, N. Brockdorff, B. M. Kessler, H. Koseki and R. J. Klose (2014). "Variant PRC1 complex-dependent H2A

ubiquitylation drives PRC2 recruitment and polycomb domain formation." Cell **157**(6): 1445-1459.

Boisset, J. C., W. van Cappellen, C. Andrieu-Soler, N. Galjart, E. Dzierzak and C. Robin (2010). "In vivo imaging of haematopoietic cells emerging from the mouse aortic endothelium." Nature **464**(7285): 116-120.

Bowie, M. B., K. D. McKnight, D. G. Kent, L. McCaffrey, P. A. Hoodless and C. J. Eaves (2006). "Hematopoietic stem cells proliferate until after birth and show a reversible phase-specific engraftment defect." J Clin Invest **116**(10): 2808-2816.

Bracken, A. P., D. Pasini, M. Capra, E. Prosperini, E. Colli and K. Helin (2003). "EZH2 is downstream of the pRB-E2F pathway, essential for proliferation and amplified in cancer." EMBO J **22**(20): 5323-5335.

Brien, G. L., G. Gambero, D. J. O'Connell, E. Jerman, S. A. Turner, C. M. Egan, E. J. Dunne, M. C. Jurgens, K. Wynne, L. Piao, A. J. Lohan, N. Ferguson, X. Shi, K. M. Sinha, B. J. Loftus, G. Cagney and A. P. Bracken (2012). "Polycomb PHF19 binds H3K36me3 and recruits PRC2 and demethylase NO66 to embryonic stem cell genes during differentiation." Nat Struct Mol Biol **19**(12): 1273-1281.

Brien, G. L., E. Healy, E. Jerman, E. Conway, E. Fadda, D. O'Donovan, A. V. Krivtsov, A. M. Rice, C. J. Kearney, A. Flaus, S. S. McDade, S. J. Martin, A. McLysaght, D. J. O'Connell, S. A. Armstrong and A. P. Bracken (2015). "A chromatin-independent role of Polycomb-like 1 to stabilize p53 and promote cellular quiescence." Genes Dev **29**(21): 2231-2243.

Cabezas-Wallscheid, N., D. Klimmeck, J. Hansson, D. B. Lipka, A. Reyes, Q. Wang, D. Weichenhan, A. Lier, L. von Paleske, S. Renders, P. Wunsche, P. Zeisberger, D. Brocks, L. Gu, C. Herrmann, S. Haas, M. A. Essers, B. Brors, R. Eils, W. Huber, M. D. Milsom, C. Plass, J. Krijgsveld and A. Trumpp (2014). "Identification of regulatory networks in HSCs and their immediate progeny via integrated proteome, transcriptome, and DNA methylome analysis." Cell Stem Cell **15**(4): 507-522.

Cai, L., S. B. Rothbart, R. Lu, B. Xu, W. Y. Chen, A. Tripathy, S. Rockowitz, D. Zheng, D. J. Patel, C. D. Allis, B. D. Strahl, J. Song and G. G. Wang (2013). "An H3K36 methylation-engaging Tudor motif of polycomb-like proteins mediates PRC2 complex targeting." Mol Cell **49**(3): 571-582.

Cai, M. Y., J. H. Hou, H. L. Rao, R. Z. Luo, M. Li, X. Q. Pei, M. C. Lin, X. Y. Guan, H. F. Kung, Y. X. Zeng and D. Xie (2011). "High expression of H3K27me3 in human hepatocellular carcinomas correlates closely with vascular invasion and predicts worse prognosis in patients." Mol Med **17**(1-2): 12-20.

Cancer Genome Atlas Research, N., T. J. Ley, C. Miller, L. Ding, B. J. Raphael, A. J. Mungall, A. Robertson, K. Hoadley, T. J. Triche, Jr., P. W. Laird, J. D. Baty, L. L. Fulton, R. Fulton, S. E. Heath, J. Kalicki-Veizer, C. Kandoth, J. M. Klco, D. C. Koboldt, K. L. Kanchi, S. Kulkarni, T.

L. Lamprecht, D. E. Larson, L. Lin, C. Lu, M. D. McLellan, J. F. McMichael, J. Payton, H. Schmidt, D. H. Spencer, M. H. Tomasson, J. W. Wallis, L. D. Wartman, M. A. Watson, J. Welch, M. C. Wendl, A. Ally, M. Balasundaram, I. Birol, Y. Butterfield, R. Chiu, A. Chu, E. Chuah, H. J. Chun, R. Corbett, N. Dhalla, R. Guin, A. He, C. Hirst, M. Hirst, R. A. Holt, S. Jones, A. Karsan, D. Lee, H. I. Li, M. A. Marra, M. Mayo, R. A. Moore, K. Mungall, J. Parker, E. Pleasance, P. Plettner, J. Schein, D. Stoll, L. Swanson, A. Tam, N. Thiessen, R. Varhol, N. Wye, Y. Zhao, S. Gabriel, G. Getz, C. Sougnez, L. Zou, M. D. Leiserson, F. Vandin, H. T. Wu, F. Applebaum, S. B. Baylin, R. Akbani, B. M. Broom, K. Chen, T. C. Motter, K. Nguyen, J. N. Weinstein, N. Zhang, M. L. Ferguson, C. Adams, A. Black, J. Bowen, J. Gastier-Foster, T. Grossman, T. Lichtenberg, L. Wise, T. Davidsen, J. A. Demchok, K. R. Shaw, M. Sheth, H. J. Sofia, L. Yang, J. R. Downing and G. Eley (2013). "Genomic and epigenomic landscapes of adult de novo acute myeloid leukemia." N Engl J Med **368**(22): 2059-2074.

Cao, R., H. Wang, J. He, H. Erdjument-Bromage, P. Tempst and Y. Zhang (2008). "Role of hPHF1 in H3K27 methylation and Hox gene silencing." Mol Cell Biol **28**(5): 1862-1872.

Cao, R. and Y. Zhang (2004). "SUZ12 is required for both the histone methyltransferase activity and the silencing function of the EED-EZH2 complex." Mol Cell **15**(1): 57-67.

Casanova, M., T. Preissner, A. Cerase, R. Poot, D. Yamada, X. Li, R. Appanah, K. Bezstarosti, J. Demmers, H. Koseki and N. Brockdorff (2011). "Polycomblike 2 facilitates the recruitment of PRC2 Polycomb group complexes to the inactive X chromosome and to target loci in embryonic stem cells." Development **138**(8): 1471-1482.

Challen, G. A., N. C. Boles, S. M. Chambers and M. A. Goodell (2010). "Distinct hematopoietic stem cell subtypes are differentially regulated by TGF-beta1." Cell Stem Cell **6**(3): 265-278.

Chang, C. J., J. Y. Yang, W. Xia, C. T. Chen, X. Xie, C. H. Chao, W. A. Woodward, J. M. Hsu, G. N. Hortobagyi and M. C. Hung (2011). "EZH2 promotes expansion of breast tumor initiating cells through activation of RAF1-beta-catenin signaling." Cancer Cell **19**(1): 86-100.

Chen, R. Z., U. Pettersson, C. Beard, L. Jackson-Grusby and R. Jaenisch (1998). "DNA hypomethylation leads to elevated mutation rates." Nature **395**(6697): 89-93.

Cheng, T., N. Rodrigues, H. Shen, Y. Yang, D. Dombkowski, M. Sykes and D. T. Scadden (2000). "Hematopoietic stem cell quiescence maintained by p21cip1/waf1." Science **287**(5459): 1804-1808.

Cheshier, S. H., S. J. Morrison, X. Liao and I. L. Weissman (1999). "In vivo proliferation and cell cycle kinetics of long-term self-renewing hematopoietic stem cells." Proc Natl Acad Sci U S A **96**(6): 3120-3125.

Chronis, C., P. Fiziev, B. Papp, S. Butz, G. Bonora, S. Sabri, J. Ernst and K. Plath (2017). "Cooperative Binding of Transcription Factors Orchestrates Reprogramming." Cell **168**(3): 442-459 e420.

Ciccia, A. and S. J. Elledge (2010). "The DNA damage response: making it safe to play with knives." Mol Cell **40**(2): 179-204.

Clark, A. J., K. M. Doyle and P. O. Humbert (2004). "Cell-intrinsic requirement for pRb in erythropoiesis." Blood **104**(5): 1324-1326.

Come, M. G., A. Skladanowski, A. K. Larsen and G. Laurent (1999). "Dual mechanism of daunorubicin-induced cell death in both sensitive and MDR-resistant HL-60 cells." Br J Cancer **79**(7-8): 1090-1097.

Coulson, M., S. Robert, H. J. Eyre and R. Saint (1998). "The identification and localization of a human gene with sequence similarity to Polycomblike of Drosophila melanogaster." Genomics **48**(3): 381-383.

de Napoles, M., J. E. Mermoud, R. Wakao, Y. A. Tang, M. Endoh, R. Appanah, T. B. Nesterova, J. Silva, A. P. Otte, M. Vidal, H. Koseki and N. Brockdorff (2004). "Polycomb group proteins Ring1A/B link ubiquitylation of histone H2A to heritable gene silencing and X inactivation." Dev Cell **7**(5): 663-676.

Derheimer, F. A. and M. B. Kastan (2010). "Multiple roles of ATM in monitoring and maintaining DNA integrity." FEBS Lett **584**(17): 3675-3681.

Ding, L., T. J. Ley, D. E. Larson, C. A. Miller, D. C. Koboldt, J. S. Welch, J. K. Ritchey, M. A. Young, T. Lamprecht, M. D. McLellan, J. F. McMichael, J. W. Wallis, C. Lu, D. Shen, C. C. Harris, D. J. Dooling, R. S. Fulton, L. L. Fulton, K. Chen, H. Schmidt, J. Kalicki-Veizer, V. J. Magrini, L. Cook, S. D. McGrath, T. L. Vickery, M. C. Wendl, S. Heath, M. A. Watson, D. C. Link, M. H. Tomasson, W. D. Shannon, J. E. Payton, S. Kulkarni, P. Westervelt, M. J. Walter, T. A. Graubert, E. R. Mardis, R. K. Wilson and J. F. DiPersio (2012). "Clonal evolution in relapsed acute myeloid leukaemia revealed by whole-genome sequencing." Nature **481**(7382): 506-510.

Ding, L. and S. J. Morrison (2013). "Haematopoietic stem cells and early lymphoid progenitors occupy distinct bone marrow niches." Nature **495**(7440): 231-235.

Ding, L., T. L. Saunders, G. Enikolopov and S. J. Morrison (2012). "Endothelial and perivascular cells maintain haematopoietic stem cells." Nature **481**(7382): 457-462.

Döhner, H., E. Estey, D. Grimwade, S. Amadori, F. R. Appelbaum, T. Büchner, H. Dombret, B. L. Ebert, P. Fenaux, R. A. Larson, R. L. Levine, F. Lo-Coco, T. Naoe, D. Niederwieser, G. J. Ossenkoppele, M. Sanz, J. Sierra, M. S. Tallman, H.-F. Tien, A. H. Wei, B. Löwenberg and C. D. Bloomfield (2017). "Diagnosis and management of AML in adults: 2017 ELN recommendations from an international expert panel." Blood **129**(4): 424-447.

Dohner, H., E. Estey, D. Grimwade, S. Amadori, F. R. Appelbaum, T. Buchner, H. Dombret, B. L. Ebert, P. Fenaux, R. A. Larson, R. L. Levine, F. Lo-Coco, T. Naoe, D. Niederwieser, G. J.

Ossenkoppele, M. Sanz, J. Sierra, M. S. Tallman, H. F. Tien, A. H. Wei, B. Lowenberg and C. D. Bloomfield (2017). "Diagnosis and management of AML in adults: 2017 ELN recommendations from an international expert panel." Blood **129**(4): 424-447.

Doulatov, S., F. Notta, K. Eppert, L. T. Nguyen, P. S. Ohashi and J. E. Dick (2010). "Revised map of the human progenitor hierarchy shows the origin of macrophages and dendritic cells in early lymphoid development." Nat Immunol **11**(7): 585-593.

Drummond-Barbosa, D. (2008). "Stem cells, their niches and the systemic environment: an aging network." Genetics **180**(4): 1787-1797.

Dumble, M., L. Moore, S. M. Chambers, H. Geiger, G. Van Zant, M. A. Goodell and L. A. Donehower (2007). "The impact of altered p53 dosage on hematopoietic stem cell dynamics during aging." Blood **109**(4): 1736-1742.

Duncan, I. M. (1982). "Polycomblike: a gene that appears to be required for the normal expression of the bithorax and antennapedia gene complexes of Drosophila melanogaster." Genetics **102**(1): 49-70.

Dykstra, B., D. Kent, M. Bowie, L. McCaffrey, M. Hamilton, K. Lyons, S. J. Lee, R. Brinkman and C. Eaves (2007). "Long-term propagation of distinct hematopoietic differentiation programs in vivo." Cell Stem Cell **1**(2): 218-229.

Ernst, J. and M. Kellis (2013). "Interplay between chromatin state, regulator binding, and regulatory motifs in six human cell types." Genome Res **23**(7): 1142-1154.

Ernst, T., A. J. Chase, J. Score, C. E. Hidalgo-Curtis, C. Bryant, A. V. Jones, K. Waghorn, K. Zoi, F. M. Ross, A. Reiter, A. Hochhaus, H. G. Drexler, A. Duncombe, F. Cervantes, D. Oscier, J. Boultwood, F. H. Grand and N. C. Cross (2010). "Inactivating mutations of the histone methyltransferase gene EZH2 in myeloid disorders." Nat Genet **42**(8): 722-726.

Fan, A. C., D. Deb-Basu, M. W. Orban, J. R. Gotlib, Y. Natkunam, R. O'Neill, R. A. Padua, L. Xu, D. Taketa, A. E. Shirer, S. Beer, A. X. Yee, D. W. Voehringer and D. W. Felsher (2009). "Nanofluidic proteomic assay for serial analysis of oncoprotein activation in clinical specimens." Nat Med **15**(5): 566-571.

Faust, C., A. Schumacher, B. Holdener and T. Magnuson (1995). "The eed mutation disrupts anterior mesoderm production in mice." Development **121**(2): 273-285.
Francia, G., W. Cruz-Munoz, S. Man, P. Xu and R. S. Kerbel (2011). "Mouse models of advanced spontaneous metastasis for experimental therapeutics." Nat Rev Cancer **11**(2): 135-141.

Gala, S., A. Marreiros, G. J. Stewart and P. Williamson (2001). "Overexpression of E2F-1 leads to cytokine-independent proliferation and survival in the hematopoietic cell line BaF-B03." Blood **97**(1): 227-234.

Galloway, J. L. and L. I. Zon (2003). "Ontogeny of hematopoiesis: examining the emergence of hematopoietic cells in the vertebrate embryo." Curr Top Dev Biol **53**: 139-158.

Glass, J., D. C. Hassane, B. Wouters, H. Kunimoto, R. Avellino, F. E. Garrett-Bakelman, O. A. Guryanova, R. Bowman, S. Redlich, A. Intlekofer, C. Meydan, T. Qin, M. P. Fall, A. Alonso, M. L. Guzman, P. J. Valk, C. B. Thompson, R. L. Levine, O. Elemento, R. Delwel, A. Melnick and M. E. Figueroa (2017). "Epigenetic Identity in AML Depends on Disruption of Non-promoter Regulatory Elements and is Affected by Antagonistic Effects of Mutations in Epigenetic Modifiers." Cancer Discov.

Gollner, S., T. Oellerich, S. Agrawal-Singh, T. Schenk, H. U. Klein, C. Rohde, C. Pabst, T. Sauer, M. Lerdrup, S. Tavor, F. Stolzel, S. Herold, G. Ehninger, G. Kohler, K. T. Pan, H. Urlaub, H. Serve, M. Dugas, K. Spiekermann, B. Vick, I. Jeremias, W. E. Berdel, K. Hansen, A. Zelent, C. Wickenhauser, L. P. Muller, C. Thiede and C. Muller-Tidow (2017). "Loss of the histone methyltransferase EZH2 induces resistance to multiple drugs in acute myeloid leukemia." Nat Med **23**(1): 69-78.

Gonzalez, M. E., M. L. DuPrie, H. Krueger, S. D. Merajver, A. C. Ventura, K. A. Toy and C. G. Kleer (2011). "Histone methyltransferase EZH2 induces Akt-dependent genomic instability and BRCA1 inhibition in breast cancer." Cancer Res **71**(6): 2360-2370.

Greenbaum, A., Y. M. Hsu, R. B. Day, L. G. Schuettpelz, M. J. Christopher, J. N. Borgerding, T. Nagasawa and D. C. Link (2013). "CXCL12 in early mesenchymal progenitors is required for haematopoietic stem-cell maintenance." Nature **495**(7440): 227-230.

Griffon, A., Q. Barbier, J. Dalino, J. van Helden, S. Spicuglia and B. Ballester (2015). "Integrative analysis of public ChIP-seq experiments reveals a complex multi-cell regulatory landscape." Nucleic Acids Res **43**(4): e27.

Grijzenhout, A., J. Godwin, H. Koseki, M. R. Gdula, D. Szumska, J. F. McGouran, S. Bhattacharya, B. M. Kessler, N. Brockdorff and S. Cooper (2016). "Functional analysis of AEBP2, a PRC2 Polycomb protein, reveals a Trithorax phenotype in embryonic development and in ESCs." Development **143**(15): 2716-2723.

Grusche, F. A., H. E. Richardson and K. F. Harvey (2010). "Upstream regulation of the hippo size control pathway." Curr Biol **20**(13): R574-582.

Halder, G. and R. L. Johnson (2011). "Hippo signaling: growth control and beyond." Development **138**(1): 9-22.

Healey, M. A., R. Hu, A. H. Beck, L. C. Collins, S. J. Schnitt, R. M. Tamimi and A. Hazra (2014). "Association of H3K9me3 and H3K27me3 repressive histone marks with breast cancer subtypes in the Nurses' Health Study." Breast Cancer Res Treat **147**(3): 639-651.

Heintzman, N. D., G. C. Hon, R. D. Hawkins, P. Kheradpour, A. Stark, L. F. Harp, Z. Ye, L. K. Lee, R. K. Stuart, C. W. Ching, K. A. Ching, J. E. Antosiewicz-Bourget, H. Liu, X. Zhang, R. D. Green, V. V. Lobanenkov, R. Stewart, J. A. Thomson, G. E. Crawford, M. Kellis and B. Ren

(2009). "Histone modifications at human enhancers reflect global cell-type-specific gene expression." Nature **459**(7243): 108-112.

Herrera-Merchan, A., L. Arranz, J. M. Ligos, A. de Molina, O. Dominguez and S. Gonzalez (2012). "Ectopic expression of the histone methyltransferase Ezh2 in haematopoietic stem cells causes myeloproliferative disease." Nat Commun **3**: 623.

Holm, K., D. Grabau, K. Lovgren, S. Aradottir, S. Gruvberger-Saal, J. Howlin, L. H. Saal, S. P. Ethier, P. O. Bendahl, O. Stal, P. Malmstrom, M. Ferno, L. Ryden, C. Hegardt, A. Borg and M. Ringner (2012). "Global H3K27 trimethylation and EZH2 abundance in breast tumor subtypes." Mol Oncol **6**(5): 494-506.

Hong, Z., J. Jiang, L. Lan, S. Nakajima, S. Kanno, H. Koseki and A. Yasui (2008). "A polycomb group protein, PHF1, is involved in the response to DNA double-strand breaks in human cell." Nucleic Acids Res **36**(9): 2939-2947.

Huang, W., R. Loganantharaj, B. Schroeder, D. Fargo and L. Li (2013). "PAVIS: a tool for Peak Annotation and Visualization." Bioinformatics **29**(23): 3097-3099.

Hunkapiller, J., Y. Shen, A. Diaz, G. Cagney, D. McCleary, M. Ramalho-Santos, N. Krogan, B. Ren, J. S. Song and J. F. Reiter (2012). "Polycomb-like 3 promotes polycomb repressive complex 2 binding to CpG islands and embryonic stem cell self-renewal." PLoS Genet **8**(3): e1002576.

Ingham, P. W., S. M. Pinchin, K. R. Howard and D. Ish-Horowicz (1985). "Genetic Analysis of the Hairy Locus in DROSOPHILA MELANOGASTER." Genetics **111**(3): 463-486.

Iwama, A., H. Oguro, M. Negishi, Y. Kato, Y. Morita, H. Tsukui, H. Ema, T. Kamijo, Y. Katoh-Fukui, H. Koseki, M. van Lohuizen and H. Nakauchi (2004). "Enhanced self-renewal of hematopoietic stem cells mediated by the polycomb gene product Bmi-1." Immunity **21**(6): 843-851.

Jansson, L. and J. Larsson (2012). "Normal hematopoietic stem cell function in mice with enforced expression of the Hippo signaling effector YAP1." PLoS One **7**(2): e32013.

Janzen, C. J., S. B. Hake, J. E. Lowell and G. A. Cross (2006). "Selective di- or trimethylation of histone H3 lysine 76 by two DOT1 homologs is important for cell cycle regulation in Trypanosoma brucei." Mol Cell **23**(4): 497-507.
Jiang, Z., X. Li, J. Hu, W. Zhou, Y. Jiang, G. Li and D. Lu (2006). "Promoter hypermethylation-mediated down-regulation of LATS1 and LATS2 in human astrocytoma." Neurosci Res **56**(4): 450-458.

Jin, B., B. Yao, J. L. Li, C. R. Fields, A. L. Delmas, C. Liu and K. D. Robertson (2009). "DNMT1 and DNMT3B modulate distinct polycomb-mediated histone modifications in colon cancer." Cancer Res **69**(18): 7412-7421.

Jung, J., M. R. Mysliwiec and Y. Lee (2005). "Roles of JUMONJI in mouse embryonic development." Dev Dyn **232**(1): 21-32.

Kawakami, S., K. Mitsunaga, Y. Y. Kikuti, A. Ando, H. Inoko, K. Yamamura and K. Abe (1998). "Tctex3, related to Drosophila polycomblike, is expressed in male germ cells and mapped to the mouse t-complex." Mamm Genome **9**(11): 874-880.

Kennison, J. A. and J. W. Tamkun (1988). "Dosage-dependent modifiers of polycomb and antennapedia mutations in Drosophila." Proc Natl Acad Sci U S A **85**(21): 8136-8140.

Kent, W. J., A. S. Zweig, G. Barber, A. S. Hinrichs and D. Karolchik (2010). "BigWig and BigBed: enabling browsing of large distributed datasets." Bioinformatics **26**(17): 2204-2207.

Kiel, M. J., G. L. Radice and S. J. Morrison (2007). "Lack of evidence that hematopoietic stem cells depend on N-cadherin-mediated adhesion to osteoblasts for their maintenance." Cell Stem Cell **1**(2): 204-217.

Kiel, M. J., O. H. Yilmaz, T. Iwashita, O. H. Yilmaz, C. Terhorst and S. J. Morrison (2005). "SLAM family receptors distinguish hematopoietic stem and progenitor cells and reveal endothelial niches for stem cells." Cell **121**(7): 1109-1121.

Kim, T. G., J. C. Kraus, J. Chen and Y. Lee (2003). "JUMONJI, a critical factor for cardiac development, functions as a transcriptional repressor." J Biol Chem **278**(43): 42247-42255.

Kinkel, S. A., R. Galeev, C. Flensburg, A. Keniry, K. Breslin, O. Gilan, S. Lee, J. Liu, K. Chen, L. J. Gearing, D. L. Moore, W. S. Alexander, M. Dawson, I. J. Majewski, A. Oshlack, J. Larsson and M. E. Blewitt (2015). "Jarid2 regulates hematopoietic stem cell function by acting with polycomb repressive complex 2." Blood **125**(12): 1890-1900.

Kirstetter, P., K. Anderson, B. T. Porse, S. E. Jacobsen and C. Nerlov (2006). "Activation of the canonical Wnt pathway leads to loss of hematopoietic stem cell repopulation and multilineage differentiation block." Nat Immunol **7**(10): 1048-1056.

Kitaguchi, T., K. Nakata, T. Nagai, J. Aruga and K. Mikoshiba (2001). "Xenopus Polycomblike 2 (XPcl2) controls anterior to posterior patterning of the neural tissue." Dev Genes Evol **211**(6): 309-314.

Kitajima, K., M. Kojima, K. Nakajima, H. Kondo, A. Miyajima and T. Takeuchi (1999). "Definitive But Not Primitive Hematopoiesis Is Impaired in jumonji Mutant Mice." Blood **1999**(93): 87-95.

Kitajima, K., M. Kojima, K. Nakajima, S. Kondo, T. Hara, A. Miyajima and T. Takeuchi (1999). "Definitive but not primitive hematopoiesis is impaired in jumonji mutant mice." Blood **93**(1): 87-95.

Kleer, C. G., Q. Cao, S. Varambally, R. Shen, I. Ota, S. A. Tomlins, D. Ghosh, R. G. Sewalt, A. P. Otte, D. F. Hayes, M. S. Sabel, D. Livant, S. J. Weiss, M. A. Rubin and A. M. Chinnaiyan

(2003). "EZH2 is a marker of aggressive breast cancer and promotes neoplastic transformation of breast epithelial cells." Proc Natl Acad Sci U S A **100**(20): 11606-11611.

Knutson, S. K., T. J. Wigle, N. M. Warholic, C. J. Sneeringer, C. J. Allain, C. R. Klaus, J. D. Sacks, A. Raimondi, C. R. Majer, J. Song, M. P. Scott, L. Jin, J. J. Smith, E. J. Olhava, R. Chesworth, M. P. Moyer, V. M. Richon, R. A. Copeland, H. Keilhack, R. M. Pollock and K. W. Kuntz (2012). "A selective inhibitor of EZH2 blocks H3K27 methylation and kills mutant lymphoma cells." Nat Chem Biol **8**(11): 890-896.

Kobayashi, Y., S. Uehara, N. Udagawa and N. Takahashi (2016). "Regulation of bone metabolism by Wnt signals." J Biochem **159**(4): 387-392.

Kondo, M., I. L. Weissman and K. Akashi (1997). "Identification of clonogenic common lymphoid progenitors in mouse bone marrow." Cell **91**(5): 661-672.

Konstantinidis, D. G., S. Pushkaran, K. Giger, S. Manganaris, Y. Zheng and T. A. Kalfa (2014). "Identification of a murine erythroblast subpopulation enriched in enucleating events by multi-spectral imaging flow cytometry." J Vis Exp(88).

Koulnis, M., R. Pop, E. Porpiglia, J. R. Shearstone, D. Hidalgo and M. Socolovsky (2011). "Identification and analysis of mouse erythroid progenitors using the CD71/TER119 flow-cytometric assay." J Vis Exp(54): 2809.

Kruiswijk, F., C. F. Labuschagne and K. H. Vousden (2015). "p53 in survival, death and metabolic health: a lifeguard with a licence to kill." Nat Rev Mol Cell Biol **16**(7): 393-405.

Kuhn, M. W., E. Song, Z. Feng, A. Sinha, C. W. Chen, A. J. Deshpande, M. Cusan, N. Farnoud, A. Mupo, C. Grove, R. Koche, J. E. Bradner, E. de Stanchina, G. S. Vassiliou, T. Hoshii and S. A. Armstrong (2016). "Targeting Chromatin Regulators Inhibits Leukemogenic Gene Expression in NPM1 Mutant Leukemia." Cancer Discov **6**(10): 1166-1181.

Kuo, L. J. and L.-X. Yang (2008). "γ-H2AX - A Novel Biomarker for DNA Double-strand Breaks." In Vivo **22**(3): 305-309.

Kuzmichev, A., K. Nishioka, H. Erdjument-Bromage, P. Tempst and D. Reinberg (2002). "Histone methyltransferase activity associated with a human multiprotein complex containing the Enhancer of Zeste protein." Genes Dev **16**(22): 2893-2905.

Landeira, D., S. Sauer, R. Poot, M. Dvorkina, L. Mazzarella, H. F. Jorgensen, C. F. Pereira, M. Leleu, F. M. Piccolo, M. Spivakov, E. Brookes, A. Pombo, C. Fisher, W. C. Skarnes, T. Snoek, K. Bezstarosti, J. Demmers, R. J. Klose, M. Casanova, L. Tavares, N. Brockdorff, M. Merkenschlager and A. G. Fisher (2010). "Jarid2 is a PRC2 component in embryonic stem cells required for multi-lineage differentiation and recruitment of PRC1 and RNA Polymerase II to developmental regulators." Nat Cell Biol **12**(6): 618-624.

Langmead, B. and S. L. Salzberg (2012). "Fast gapped-read alignment with Bowtie 2." Nat Methods **9**(4): 357-359.

Laurenti, E., C. Frelin, S. Xie, R. Ferrari, C. F. Dunant, S. Zandi, A. Neumann, I. Plumb, S. Doulatov, J. Chen, C. April, J. B. Fan, N. Iscove and J. E. Dick (2015). "CDK6 levels regulate quiescence exit in human hematopoietic stem cells." Cell Stem Cell **16**(3): 302-313.

Lee, S. T., Z. Li, Z. Wu, M. Aau, P. Guan, R. K. Karuturi, Y. C. Liou and Q. Yu (2011). "Context-specific regulation of NF-kappaB target gene expression by EZH2 in breast cancers." Mol Cell **43**(5): 798-810.

Levine, S. S., I. F. King and R. E. Kingston (2004). "Division of labor in polycomb group repression." Trends Biochem Sci **29**(9): 478-485.

Lewis, E. B. (1978). "A gene complex controlling segmentation in Drosophila." Nature **276**(5688): 565-570.

Li, G., R. Margueron, M. Ku, P. Chambon, B. E. Bernstein and D. Reinberg (2010). "Jarid2 and PRC2, partners in regulating gene expression." Genes Dev **24**(4): 368-380.

Li, S., F. E. Garrett-Bakelman, S. S. Chung, M. A. Sanders, T. Hricik, F. Rapaport, J. Patel, R. Dillon, P. Vijay, A. L. Brown, A. E. Perl, J. Cannon, L. Bullinger, S. Luger, M. Becker, I. D. Lewis, L. B. To, R. Delwel, B. Lowenberg, H. Dohner, K. Dohner, M. L. Guzman, D. C. Hassane, G. J. Roboz, D. Grimwade, P. J. Valk, R. J. D'Andrea, M. Carroll, C. Y. Park, D. Neuberg, R. Levine, A. M. Melnick and C. E. Mason (2016). "Distinct evolution and dynamics of epigenetic and genetic heterogeneity in acute myeloid leukemia." Nat Med **22**(7): 792-799.

Li, X., K. Isono, D. Yamada, T. A. Endo, M. Endoh, J. Shinga, Y. Mizutani-Koseki, A. P. Otte, M. Casanova, H. Kitamura, T. Kamijo, J. Sharif, O. Ohara, T. Toyada, B. E. Bernstein, N. Brockdorff and H. Koseki (2011). "Mammalian polycomb-like Pcl2/Mtf2 is a novel regulatory component of PRC2 that can differentially modulate polycomb activity both at the Hox gene cluster and at Cdkn2a genes." Mol Cell Biol **31**(2): 351-364.

Ling, K. W., K. Ottersbach, J. P. van Hamburg, A. Oziemlak, F. Y. Tsai, S. H. Orkin, R. Ploemacher, R. W. Hendriks and E. Dzierzak (2004). "GATA-2 plays two functionally distinct roles during the ontogeny of hematopoietic stem cells." J Exp Med **200**(7): 871-882.

Liu, J., L. Cao, J. Chen, S. Song, I. H. Lee, C. Quijano, H. Liu, K. Keyvanfar, H. Chen, L. Y. Cao, B. H. Ahn, N. G. Kumar, Rovira, II, X. L. Xu, M. van Lohuizen, N. Motoyama, C. X. Deng and T. Finkel (2009). "Bmi1 regulates mitochondrial function and the DNA damage response pathway." Nature **459**(7245): 387-392.

Liu, Y., G. Chen, N. Norton, W. Liu, H. Zhu, P. Zhou, M. Luan, S. Yang, X. Chen, L. Carroll, N. M. Williams, M. C. O'Donovan, G. Kirov and M. J. Owen (2009). "Whole genome association study in a homogenous population in Shandong peninsula of China reveals JARID2 as a susceptibility gene for schizophrenia." J Biomed Biotechnol **2009**: 536918.

Londhe, P. and J. K. Davie (2013). "Interferon-gamma resets muscle cell fate by stimulating the sequential recruitment of JARID2 and PRC2 to promoters to repress myogenesis." Sci Signal **6**(305): ra107.

Love, M. I., W. Huber and S. Anders (2014). "Moderated estimation of fold change and dispersion for RNA-seq data with DESeq2." Genome Biol **15**(12): 550.

Luczak, M. W. and P. P. Jagodzinski (2006). "The role of DNA methylation in cancer development." Folia Histochem Cytobiol **44**(3): 143-154.

Lund, A. H. and M. van Lohuizen (2004). "Polycomb complexes and silencing mechanisms." Curr Opin Cell Biol **16**(3): 239-246.

Luo, X. and W. L. Kraus (2012). "On PAR with PARP: cellular stress signaling through poly(ADP-ribose) and PARP-1." Genes Dev **26**(5): 417-432.

Majewski, I. J., M. E. Blewitt, C. A. de Graaf, E. J. McManus, M. Bahlo, A. A. Hilton, C. D. Hyland, G. K. Smyth, J. E. Corbin, D. Metcalf, W. S. Alexander and D. J. Hilton (2008). "Polycomb repressive complex 2 (PRC2) restricts hematopoietic stem cell activity." PLoS Biol **6**(4): e93.

Malhotra, S. and P. W. Kincade (2009). "Wnt-related molecules and signaling pathway equilibrium in hematopoiesis." Cell Stem Cell **4**(1): 27-36.

Malumbres, M., R. Sotillo, D. Santamaria, J. Galan, A. Cerezo, S. Ortega, P. Dubus and M. Barbacid (2004). "Mammalian cells cycle without the D-type cyclin-dependent kinases Cdk4 and Cdk6." Cell **118**(4): 493-504.

Marine, J. C. and G. Lozano (2010). "Mdm2-mediated ubiquitylation: p53 and beyond." Cell Death Differ **17**(1): 93-102.

Masuoka, H. C. and T. M. Townes (2002). "Targeted disruption of the activating transcription factor 4 gene results in severe fetal anemia in mice." Blood **99**(3): 736-745.

Matsumoto, A., S. Takeishi, T. Kanie, E. Susaki, I. Onoyama, Y. Tateishi, K. Nakayama and K. I. Nakayama (2011). "p57 is required for quiescence and maintenance of adult hematopoietic stem cells." Cell Stem Cell **9**(3): 262-271.

Matushansky, I., F. Radparvar and A. I. Skoultchi (2003). "CDK6 blocks differentiation: coupling cell proliferation to the block to differentiation in leukemic cells." Oncogene **22**(27): 4143-4149.

McCormack, E., I. Haaland, G. Venas, R. B. Forthun, S. Huseby, G. Gausdal, S. Knappskog, D. R. Micklem, J. B. Lorens, O. Bruserud and B. T. Gjertsen (2012). "Synergistic induction of p53 mediated apoptosis by valproic acid and nutlin-3 in acute myeloid leukemia." Leukemia **26**(5): 910-917.

McGarvey, K. M., J. A. Fahrner, E. Greene, J. Martens, T. Jenuwein and S. B. Baylin (2006). "Silenced tumor suppressor genes reactivated by DNA demethylation do not return to a fully euchromatic chromatin state." Cancer Res **66**(7): 3541-3549.

McGarvey, K. M., L. Van Neste, L. Cope, J. E. Ohm, J. G. Herman, W. Van Criekinge, K. E. Schuebel and S. B. Baylin (2008). "Defining a chromatin pattern that characterizes DNA-hypermethylated genes in colon cancer cells." Cancer Res **68**(14): 5753-5759.

McGrath, K. E., T. P. Bushnell and J. Palis (2008). "Multispectral imaging of hematopoietic cells: where flow meets morphology." J Immunol Methods **336**(2): 91-97.

McLean, C. Y., D. Bristor, M. Hiller, S. L. Clarke, B. T. Schaar, C. B. Lowe, A. M. Wenger and G. Bejerano (2010). "GREAT improves functional interpretation of cis-regulatory regions." Nat Biotechnol **28**(5): 495-501.

Medyouf, H., M. Mossner, J. C. Jann, F. Nolte, S. Raffel, C. Herrmann, A. Lier, C. Eisen, V. Nowak, B. Zens, K. Mudder, C. Klein, J. Oblander, S. Fey, J. Vogler, A. Fabarius, E. Riedl, H. Roehl, A. Kohlmann, M. Staller, C. Haferlach, N. Muller, T. John, U. Platzbecker, G. Metzgeroth, W. K. Hofmann, A. Trumpp and D. Nowak (2014). "Myelodysplastic cells in patients reprogram mesenchymal stromal cells to establish a transplantable stem cell niche disease unit." Cell Stem Cell **14**(6): 824-837.

Mejetta, S., L. Morey, G. Pascual, B. Kuebler, M. R. Mysliwiec, Y. Lee, R. Shiekhattar, L. Di Croce and S. A. Benitah (2011). "Jarid2 regulates mouse epidermal stem cell activation and differentiation." EMBO J **30**(17): 3635-3646.

Mende, N., E. E. Kuchen, M. Lesche, T. Grinenko, K. D. Kokkaliaris, H. Hanenberg, D. Lindemann, A. Dahl, A. Platz, T. Hofer, F. Calegari and C. Waskow (2015). "CCND1-CDK4-mediated cell cycle progression provides a competitive advantage for human hematopoietic stem cells in vivo." J Exp Med **212**(8): 1171-1183.
Mendez-Ferrer, S., T. V. Michurina, F. Ferraro, A. R. Mazloom, B. D. Macarthur, S. A. Lira, D. T. Scadden, A. Ma'ayan, G. N. Enikolopov and P. S. Frenette (2010). "Mesenchymal and haematopoietic stem cells form a unique bone marrow niche." Nature **466**(7308): 829-834.

Merico, D., R. Isserlin and G. D. Bader (2011). "Visualizing gene-set enrichment results using the Cytoscape plug-in enrichment map." Methods Mol Biol **781**: 257-277.

Merico, D., R. Isserlin, O. Stueker, A. Emili and G. D. Bader (2010). "Enrichment map: a network-based method for gene-set enrichment visualization and interpretation." PLoS One **5**(11): e13984.

Milo, R., S. Shen-Orr, S. Itzkovitz, N. Kashtan, D. Chklovskii and U. Alon (2002). "Network motifs: simple building blocks of complex networks." Science **298**(5594): 824-827.

Mochizuki-Kashio, M., Y. Mishima, S. Miyagi, M. Negishi, A. Saraya, T. Konuma, J. Shinga, H. Koseki and A. Iwama (2011). "Dependency on the polycomb gene Ezh2 distinguishes fetal from adult hematopoietic stem cells." Blood **118**(25): 6553-6561.

Morin, R. D., N. A. Johnson, T. M. Severson, A. J. Mungall, J. An, R. Goya, J. E. Paul, M. Boyle, B. W. Woolcock, F. Kuchenbauer, D. Yap, R. K. Humphries, O. L. Griffith, S. Shah, H. Zhu, M. Kimbara, P. Shashkin, J. F. Charlot, M. Tcherpakov, R. Corbett, A. Tam, R. Varhol, D. Smailus, M. Moksa, Y. Zhao, A. Delaney, H. Qian, I. Birol, J. Schein, R. Moore, R. Holt, D. E. Horsman, J. M. Connors, S. Jones, S. Aparicio, M. Hirst, R. D. Gascoyne and M. A. Marra (2010). "Somatic mutations altering EZH2 (Tyr641) in follicular and diffuse large B-cell lymphomas of germinal-center origin." Nat Genet **42**(2): 181-185.

Motoyama, J., K. Kitajima, M. Kojima, S. Kondo and T. Takeuchi (1997). "Organogenesis of the liver, thymus and spleen is affected in jumonji mutant mice." Mech Dev **66**(1-2): 27-37.

Motoyama, J., K. Kitajima, M. Kojima, S. Kondo and T. Takeuchi (1997). "Organogenesis of the liver, thymus and spleen is affected in jumonji mutant mice." Mechanisms of Development **66**: 27-37.

Muller, A. M., A. Medvinsky, J. Strouboulis, F. Grosveld and E. Dzierzak (1994). "Development of hematopoietic stem cell activity in the mouse embryo." Immunity **1**(4): 291-301.

Musselman, C. A., N. Avvakumov, R. Watanabe, C. G. Abraham, M. E. Lalonde, Z. Hong, C. Allen, S. Roy, J. K. Nunez, J. Nickoloff, C. A. Kulesza, A. Yasui, J. Cote and T. G. Kutateladze (2012). "Molecular basis for H3K36me3 recognition by the Tudor domain of PHF1." Nat Struct Mol Biol **19**(12): 1266-1272.

Nam, E. A. and D. Cortez (2011). "ATR signalling: more than meeting at the fork." Biochem J **436**(3): 527-536.
Nekrasov, M., T. Klymenko, S. Fraterman, B. Papp, K. Oktaba, T. Kocher, A. Cohen, H. G. Stunnenberg, M. Wilm and J. Muller (2007). "Pcl-PRC2 is needed to generate high levels of H3-K27 trimethylation at Polycomb target genes." EMBO J **26**(18): 4078-4088.

Nikoloski, G., S. M. Langemeijer, R. P. Kuiper, R. Knops, M. Massop, E. R. Tonnissen, A. van der Heijden, T. N. Scheele, P. Vandenberghe, T. de Witte, B. A. van der Reijden and J. H. Jansen (2010). "Somatic mutations of the histone methyltransferase gene EZH2 in myelodysplastic syndromes." Nat Genet **42**(8): 665-667.

North, T. E., M. F. de Bruijn, T. Stacy, L. Talebian, E. Lind, C. Robin, M. Binder, E. Dzierzak and N. A. Speck (2002). "Runx1 expression marks long-term repopulating hematopoietic stem cells in the midgestation mouse embryo." Immunity **16**(5): 661-672.

Notta, F., S. Doulatov, E. Laurenti, A. Poeppl, I. Jurisica and J. E. Dick (2011). "Isolation of single human hematopoietic stem cells capable of long-term multilineage engraftment." Science **333**(6039): 218-221.

Nygren, J. M., D. Bryder and S. E. Jacobsen (2006). "Prolonged cell cycle transit is a defining and developmentally conserved hemopoietic stem cell property." J Immunol **177**(1): 201-208.

O'Carroll, D., S. Erhardt, M. Pagani, S. C. Barton, M. A. Surani and T. Jenuwein (2001). "The polycomb-group gene Ezh2 is required for early mouse development." Mol Cell Biol **21**(13): 4330-4336.

O'Neill, R. A., A. Bhamidipati, X. Bi, D. Deb-Basu, L. Cahill, J. Ferrante, E. Gentalen, M. Glazer, J. Gossett, K. Hacker, C. Kirby, J. Knittle, R. Loder, C. Mastroieni, M. Maclaren, T. Mills, U. Nguyen, N. Parker, A. Rice, D. Roach, D. Suich, D. Voehringer, K. Voss, J. Yang, T. Yang and P. B. Vander Horn (2006). "Isoelectric focusing technology quantifies protein signaling in 25 cells." Proc Natl Acad Sci U S A **103**(44): 16153-16158.

Oittinen, M., A. Popp, K. Kurppa, K. Lindfors, M. Maki, M. U. Kaikkonen and K. Viiri (2016). "Polycomb Repressive Complex 2 Enacts Wnt Signaling in Intestinal Homeostasis and Contributes to the Instigation of Stemness in Diseases Entailing Epithelial Hyperplasia or Neoplasia." Stem Cells.

Olive, P. L. and J. P. Banath (2006). "The comet assay: a method to measure DNA damage in individual cells." Nat Protoc **1**(1): 23-29.

Orford, K. W. and D. T. Scadden (2008). "Deconstructing stem cell self-renewal: genetic insights into cell-cycle regulation." Nat Rev Genet **9**(2): 115-128.

Orkin, S. H. and L. I. Zon (2008). "Hematopoiesis: an evolving paradigm for stem cell biology." Cell **132**(4): 631-644.
Pan, D. (2010). "The hippo signaling pathway in development and cancer." Dev Cell **19**(4): 491-505.

Papaemmanuil, E., M. Gerstung, L. Bullinger, V. I. Gaidzik, P. Paschka, N. D. Roberts, N. E. Potter, M. Heuser, F. Thol, N. Bolli, G. Gundem, P. Van Loo, I. Martincorena, P. Ganly, L. Mudie, S. McLaren, S. O'Meara, K. Raine, D. R. Jones, J. W. Teague, A. P. Butler, M. F. Greaves, A. Ganser, K. Dohner, R. F. Schlenk, H. Dohner and P. J. Campbell (2016). "Genomic Classification and Prognosis in Acute Myeloid Leukemia." N Engl J Med **374**(23): 2209-2221.

Pasini, D., A. P. Bracken, M. R. Jensen, E. Lazzerini Denchi and K. Helin (2004). "Suz12 is essential for mouse development and for EZH2 histone methyltransferase activity." EMBO J **23**(20): 4061-4071.

Pasini, D., P. A. Cloos, J. Walfridsson, L. Olsson, J. P. Bukowski, J. V. Johansen, M. Bak, N. Tommerup, J. Rappsilber and K. Helin (2010). "JARID2 regulates binding of the Polycomb repressive complex 2 to target genes in ES cells." Nature **464**(7286): 306-310.

Patel , J. P., M. Gönen , M. E. Figueroa , H. Fernandez , Z. Sun , J. Racevskis , P. Van Vlierberghe , I. Dolgalev , S. Thomas , O. Aminova , K. Huberman , J. Cheng , A. Viale , N. D. Socci , A. Heguy , A. Cherry , G. Vance , R. R. Higgins , R. P. Ketterling , R. E. Gallagher , M.

Litzow , M. R. M. van den Brink , H. M. Lazarus , J. M. Rowe , S. Luger , A. Ferrando , E. Paietta , M. S. Tallman , A. Melnick , O. Abdel-Wahab and R. L. Levine (2012). "Prognostic Relevance of Integrated Genetic Profiling in Acute Myeloid Leukemia." New England Journal of Medicine **366**(12): 1079-1089.

Pedrosa, E., K. Ye, K. A. Nolan, L. Morrell, J. M. Okun, A. D. Persky, T. Saito and H. M. Lachman (2007). "Positive association of schizophrenia to JARID2 gene." Am J Med Genet B Neuropsychiatr Genet **144B**(1): 45-51.

Peng, J. C., A. Valouev, T. Swigut, J. Zhang, Y. Zhao, A. Sidow and J. Wysocka (2009). "Jarid2/Jumonji coordinates control of PRC2 enzymatic activity and target gene occupancy in pluripotent cells." Cell **139**(7): 1290-1302.

Pereira, C. F., F. M. Piccolo, T. Tsubouchi, S. Sauer, N. K. Ryan, L. Bruno, D. Landeira, J. Santos, A. Banito, J. Gil, H. Koseki, M. Merkenschlager and A. G. Fisher (2010). "ESCs require PRC2 to direct the successful reprogramming of differentiated cells toward pluripotency." Cell Stem Cell **6**(6): 547-556.

Polo, S. E. and S. P. Jackson (2011). "Dynamics of DNA damage response proteins at DNA breaks: a focus on protein modifications." Genes & Development **25**(5): 409-433.
Ptak, C. and A. Petronis (2008). "Epigenetics and complex disease: from etiology to new therapeutics." Annu Rev Pharmacol Toxicol **48**: 257-276.

Quinlan, A. R. and I. M. Hall (2010). "BEDTools: a flexible suite of utilities for comparing genomic features." Bioinformatics **26**(6): 841-842.
Radulovic, V., G. de Haan and K. Klauke (2013). "Polycomb-group proteins in hematopoietic stem cell regulation and hematopoietic neoplasms." Leukemia **27**(3): 523-533.

Reimand, J., T. Arak and J. Vilo (2011). "g:Profiler--a web server for functional interpretation of gene lists (2011 update)." Nucleic Acids Res **39**(Web Server issue): W307-315.

Reimand, J., M. Kull, H. Peterson, J. Hansen and J. Vilo (2007). "g:Profiler--a web-based toolset for functional profiling of gene lists from large-scale experiments." Nucleic Acids Res **35**(Web Server issue): W193-200.

Reya, T., A. W. Duncan, L. Ailles, J. Domen, D. C. Scherer, K. Willert, L. Hintz, R. Nusse and I. L. Weissman (2003). "A role for Wnt signalling in self-renewal of haematopoietic stem cells." Nature **423**(6938): 409-414.

Saito, M., K. Helin, M. B. Valentine, B. B. Griffith, C. L. Willman, E. Harlow and A. T. Look (1995). "Amplification of the E2F1 transcription factor gene in the HEL erythroleukemia cell line." Genomics **25**(1): 130-138.

Sanchez, M. J., E. O. Bockamp, J. Miller, L. Gambardella and A. R. Green (2001). "Selective rescue of early haematopoietic progenitors in Scl(-/-) mice by expressing Scl under the control of a stem cell enhancer." Development **128**(23): 4815-4827.

Sanchez, M. J., A. Holmes, C. Miles and E. Dzierzak (1996). "Characterization of the first definitive hematopoietic stem cells in the AGM and liver of the mouse embryo." Immunity **5**(6): 513-525.

Sarma, K., R. Margueron, A. Ivanov, V. Pirrotta and D. Reinberg (2008). "Ezh2 requires PHF1 to efficiently catalyze H3 lysine 27 trimethylation in vivo." Mol Cell Biol **28**(8): 2718-2731.

Sato, N., L. Meijer, L. Skaltsounis, P. Greengard and A. H. Brivanlou (2004). "Maintenance of pluripotency in human and mouse embryonic stem cells through activation of Wnt signaling by a pharmacological GSK-3-specific inhibitor." Nat Med **10**(1): 55-63.

Sauvegeau, M. and G. Sauvegeau (2010). "Polycomb Group Proteins: Multi-Faceted Regulators of Somatic Stem Cells and Cancer." Cell Stem Cell **7**(3): 299-313.

Savla, U., J. Benes, J. Zhang and R. S. Jones (2008). "Recruitment of Drosophila Polycomb-group proteins by Polycomblike, a component of a novel protein complex in larvae." Development **135**(5): 813-817.

Scapoli, L., M. Martinelli, F. Pezzetti, A. Palmieri, A. Girardi, A. Savoia, A. M. Bianco and F. Carinci (2010). "Expression and association data strongly support JARID2 involvement in nonsyndromic cleft lip with or without cleft palate." Hum Mutat **31**(7): 794-800.
Schlesinger, Y., R. Straussman, I. Keshet, S. Farkash, M. Hecht, J. Zimmerman, E. Eden, Z. Yakhini, E. Ben-Shushan, B. E. Reubinoff, Y. Bergman, I. Simon and H. Cedar (2007). "Polycomb-mediated methylation on Lys27 of histone H3 pre-marks genes for de novo methylation in cancer." Nat Genet **39**(2): 232-236.

Seidel, C., U. Schagdarsurengin, K. Blumke, P. Wurl, G. P. Pfeifer, S. Hauptmann, H. Taubert and R. Dammann (2007). "Frequent hypermethylation of MST1 and MST2 in soft tissue sarcoma." Mol Carcinog **46**(10): 865-871.

Serrano, M., H. Lee, L. Chin, C. Cordon-Cardo, D. Beach and R. A. DePinho (1996). "Role of the INK4a locus in tumor suppression and cell mortality." Cell **85**(1): 27-37.

Shen, L., N. Y. Shao, X. Liu, I. Maze, J. Feng and E. J. Nestler (2013). "diffReps: detecting differential chromatin modification sites from ChIP-seq data with biological replicates." PLoS One **8**(6): e65598.

Shen, X., W. Kim, Y. Fujiwara, M. D. Simon, Y. Liu, M. R. Mysliwiec, G. C. Yuan, Y. Lee and S. H. Orkin (2009). "Jumonji modulates polycomb activity and self-renewal versus differentiation of stem cells." Cell **139**(7): 1303-1314.

Shen, Y., F. Yue, D. F. McCleary, Z. Ye, L. Edsall, S. Kuan, U. Wagner, J. Dixon, L. Lee, V. V. Lobanenkov and B. Ren (2012). "A map of the cis-regulatory sequences in the mouse genome." Nature **488**(7409): 116-120.

Shih, A. H., C. Meydan, K. Shank, F. E. Garrett-Bakelman, P. S. Ward, A. M. Intlekofer, A. Nazir, E. M. Stein, K. Knapp, J. Glass, J. Travins, K. Straley, C. Gliser, C. E. Mason, K. Yen, C. B. Thompson, A. Melnick and R. L. Levine (2017). "Combination Targeted Therapy to Disrupt Aberrant Oncogenic Signaling and Reverse Epigenetic Dysfunction in IDH2- and TET2-Mutant Acute Myeloid Leukemia." Cancer Discov **7**(5): 494-505.

Shlush, L. I., S. Zandi, A. Mitchell, W. C. Chen, J. M. Brandwein, V. Gupta, J. A. Kennedy, A. D. Schimmer, A. C. Schuh, K. W. Yee, J. L. McLeod, M. Doedens, J. J. Medeiros, R. Marke, H. J. Kim, K. Lee, J. D. McPherson, T. J. Hudson, H. P.-L. G. P. Consortium, A. M. Brown, F. Yousif, Q. M. Trinh, L. D. Stein, M. D. Minden, J. C. Wang and J. E. Dick (2014). "Identification of pre-leukaemic haematopoietic stem cells in acute leukaemia." Nature **506**(7488): 328-333.

Shtutman, M., J. Zhurinsky, I. Simcha, C. Albanese, M. D'Amico, R. Pestell and A. Ben-Ze'ev (1999). "The cyclin D1 gene is a target of the beta-catenin/LEF-1 pathway." Proc Natl Acad Sci U S A **96**(10): 5522-5527.

Simon, J. A. and R. E. Kingston (2013). "Occupying chromatin: Polycomb mechanisms for getting to genomic targets, stopping transcriptional traffic, and staying put." Mol Cell **49**(5): 808-824.

Sing, A., D. Pannell, A. Karaiskakis, K. Sturgeon, M. Djabali, J. Ellis, H. D. Lipshitz and S. P. Cordes (2009). "A vertebrate Polycomb response element governs segmentation of the posterior hindbrain." Cell **138**(5): 885-897.

Smits, A. H., P. W. Jansen, I. Poser, A. A. Hyman and M. Vermeulen (2013). "Stoichiometry of chromatin-associated protein complexes revealed by label-free quantitative mass spectrometry-based proteomics." Nucleic Acids Res **41**(1): e28.

Stanford, W. L., J. B. Cohn and S. P. Cordes (2001). "Gene-trap mutagenesis: past, present and beyond." Nat Rev Genet **2**(10): 756-768.

Steffen, P. A. and L. Ringrose (2014). "What are memories made of? How Polycomb and Trithorax proteins mediate epigenetic memory." Nat Rev Mol Cell Biol **15**(5): 340-356.

Struhl, G. and M. Akam (1985). "Altered distributions of Ultrabithorax transcripts in extra sex combs mutant embryos of Drosophila." EMBO J **4**(12): 3259-3264.

Su, I. H., A. Basavaraj, A. N. Krutchinsky, O. Hobert, A. Ullrich, B. T. Chait and A. Tarakhovsky (2003). "Ezh2 controls B cell development through histone H3 methylation and Igh rearrangement." Nat Immunol **4**(2): 124-131.

Surface, L. E., S. R. Thornton and L. A. Boyer (2010). "Polycomb group proteins set the stage for early lineage commitment." Cell Stem Cell **7**(3): 288-298.

Takahashi, M., M. Kojima, K. Nakajima, R. Suzuki-Migishima, Y. Motegi, M. Yokoyama and T. Takeuchi (2004). "Cardiac abnormalities cause early lethality of jumonji mutant mice." Biochem Biophys Res Commun **324**(4): 1319-1323.

Takahashi, M., M. Kojima, K. Nakajima, R. Suzuki-Migishima and T. Takeuchi (2007). "Functions of a jumonji-cyclin D1 pathway in the coordination of cell cycle exit and migration during neurogenesis in the mouse hindbrain." Dev Biol **303**(2): 549-560.

Takahashi, Y., Y. Miyoshi, C. Takahata, N. Irahara, T. Taguchi, Y. Tamaki and S. Noguchi (2005). "Down-regulation of LATS1 and LATS2 mRNA expression by promoter hypermethylation and its association with biologically aggressive phenotype in human breast cancers." Clin Cancer Res **11**(4): 1380-1385.

Takeuchi, T., M. Kojima, K. Nakajima and S. Kondo (1999). "jumonji gene is essential for the neurulation and cardiac development of mouse embryos with a C3H/He background." Mech Dev **86**(1-2): 29-38.

Takeuchi, T., Y. Yamazaki, Y. Katoh-Fukui, R. Tsuchiya, S. Kondo, J. Motoyama and T. Higashinakagawa (1995). "Gene trap capture of a novel mouse gene, jumonji, required for neural tube formation." Genes Dev **9**(10): 1211-1222.

Tanaka, S., S. Miyagi, G. Sashida, T. Chiba, J. Yuan, M. Mochizuki-Kashio, Y. Suzuki, S. Sugano, C. Nakaseko, K. Yokote, H. Koseki and A. Iwama (2012). "Ezh2 augments leukemogenicity by reinforcing differentiation blockage in acute myeloid leukemia." Blood **120**(5): 1107-1117.

Tavares, L., E. Dimitrova, D. Oxley, J. Webster, R. Poot, J. Demmers, K. Bezstarosti, S. Taylor, H. Ura, H. Koide, A. Wutz, M. Vidal, S. Elderkin and N. Brockdorff (2012). "RYBP-PRC1 complexes mediate H2A ubiquitylation at polycomb target sites independently of PRC2 and H3K27me3." Cell **148**(4): 664-678.

Thol, F., R. F. Schlenk, M. Heuser and A. Ganser (2015). "How I treat refractory and early relapsed acute myeloid leukemia." Blood **126**(3): 319-327.

Torchia, J., B. Golbourn, S. Feng, K. C. Ho, P. Sin-Chan, A. Vasiljevic, J. D. Norman, P. Guilhamon, L. Garzia, N. R. Agamez, M. Lu, T. S. Chan, D. Picard, P. de Antonellis, D. A. Khuong-Quang, A. C. Planello, C. Zeller, D. Barsyte-Lovejoy, L. Lafay-Cousin, L. Letourneau, M. Bourgey, M. Yu, D. M. Gendoo, M. Dzamba, M. Barszczyk, T. Medina, A. N. Riemenschneider, A. S. Morrissy, Y. S. Ra, V. Ramaswamy, M. Remke, C. P. Dunham, S. Yip, H. K. Ng, J. Q. Lu, V. Mehta, S. Albrecht, J. Pimentel, J. A. Chan, G. R. Somers, C. C. Faria, L. Roque, M. Fouladi, L. M. Hoffman, A. S. Moore, Y. Wang, S. A. Choi, J. R. Hansford, D. Catchpoole, D. K. Birks, N. K. Foreman, D. Strother, A. Klekner, L. Bognar, M. Garami, P. Hauser, T. Hortobagyi, B. Wilson, J. Hukin, A. S. Carret, T. E. Van Meter, E. I. Hwang, A. Gajjar, S. H. Chiou, H. Nakamura, H. Toledano, I. Fried, D. Fults, T. Wataya, C. Fryer, D. D. Eisenstat, K. Scheinemann, A. J. Fleming, D. L. Johnston, J. Michaud, S. Zelcer, R. Hammond, S. Afzal, D. A. Ramsay, N. Sirachainan, S. Hongeng, N. Larbcharoensub, R. G. Grundy, R. R. Lulla, J. R. Fangusaro, H. Druker, U. Bartels, R. Grant, D. Malkin, C. J. McGlade, T. Nicolaides, T. Tihan, J. Phillips, J. Majewski, A. Montpetit, G. Bourque, G. D. Bader, A. T. Reddy, G. Y. Gillespie, M. Warmuth-Metz, S. Rutkowski, U. Tabori, M. Lupien, M. Brudno, U. Schuller, T. Pietsch, A. R. Judkins, C. E. Hawkins, E. Bouffet, S. K. Kim, P. B. Dirks, M. D. Taylor, A. Erdreich-Epstein, C. H. Arrowsmith, D. D. De Carvalho, J. T. Rutka, N. Jabado and A. Huang

(2016). "Integrated (epi)-Genomic Analyses Identify Subgroup-Specific Therapeutic Targets in CNS Rhabdoid Tumors." Cancer Cell **30**(6): 891-908.

Toyoda, M., H. Shirato, K. Nakajima, M. Kojima, M. Takahashi, M. Kubota, R. Suzuki-Migishima, Y. Motegi, M. Yokoyama and T. Takeuchi (2003). "jumonji downregulates cardiac cell proliferation by repressing cyclin D1 expression." Dev Cell **5**(1): 85-97.

Trapnell, C., A. Roberts, L. Goff, G. Pertea, D. Kim, D. R. Kelley, H. Pimentel, S. L. Salzberg, J. L. Rinn and L. Pachter (2012). "Differential gene and transcript expression analysis of RNA-seq experiments with TopHat and Cufflinks." Nat Protoc **7**(3): 562-578.

Tuck-Muller, C. M., A. Narayan, F. Tsien, D. F. Smeets, J. Sawyer, E. S. Fiala, O. S. Sohn and M. Ehrlich (2000). "DNA hypomethylation and unusual chromosome instability in cell lines from ICF syndrome patients." Cytogenet Cell Genet **89**(1-2): 121-128.

Van Hateren, N. J., R. M. Das, G. M. Hautbergue, A. G. Borycki, M. Placzek and S. A. Wilson (2011). "FatJ acts via the Hippo mediator Yap1 to restrict the size of neural progenitor cell pools." Development **138**(10): 1893-1902.

Varambally, S., Q. Cao, R. S. Mani, S. Shankar, X. Wang, B. Ateeq, B. Laxman, X. Cao, X. Jing, K. Ramnarayanan, J. C. Brenner, J. Yu, J. H. Kim, B. Han, P. Tan, C. Kumar-Sinha, R. J. Lonigro, N. Palanisamy, C. A. Maher and A. M. Chinnaiyan (2008). "Genomic loss of microRNA-101 leads to overexpression of histone methyltransferase EZH2 in cancer." Science **322**(5908): 1695-1699.

Varambally, S., S. M. Dhanasekaran, M. Zhou, T. R. Barrette, C. Kumar-Sinha, M. G. Sanda, D. Ghosh, K. J. Pienta, R. G. Sewalt, A. P. Otte, M. A. Rubin and A. M. Chinnaiyan (2002). "The polycomb group protein EZH2 is involved in progression of prostate cancer." Nature **419**(6907): 624-629.

Varelas, X., R. Sakuma, P. Samavarchi-Tehrani, R. Peerani, B. M. Rao, J. Dembowy, M. B. Yaffe, P. W. Zandstra and J. L. Wrana (2008). "TAZ controls Smad nucleocytoplasmic shuttling and regulates human embryonic stem-cell self-renewal." Nat Cell Biol **10**(7): 837-848.

Vire, E., C. Brenner, R. Deplus, L. Blanchon, M. Fraga, C. Didelot, L. Morey, A. Van Eynde, D. Bernard, J. M. Vanderwinden, M. Bollen, M. Esteller, L. Di Croce, Y. de Launoit and F. Fuks (2006). "The Polycomb group protein EZH2 directly controls DNA methylation." Nature **439**(7078): 871-874.

Walker, E., W. Y. Chang, J. Hunkapiller, G. Cagney, K. Garcha, J. Torchia, N. Krogan, J. Reiter and W. L. Stanford (2010). "Polycomb-like 2 associates with PRC2 and regulates transcriptional networks during mouse embryonic stem cell self-renewal and differentiation. ." Cell Stem Cell **6**: 153-166.

Walker, E., W. Y. Chang, J. Hunkapiller, G. Cagney, K. Garcha, J. Torchia, N. J. Krogan, J. F. Reiter and W. L. Stanford (2010). "Polycomb-like 2 associates with PRC2 and regulates

transcriptional networks during mouse embryonic stem cell self-renewal and differentiation." Cell Stem Cell **6**(2): 153-166.

Walker, E., J. Manias, W. Y. Chang and W. L. Stanford (2011). "PCL2 modulates gene regulatory networks controlling self-renewal and commitment in embryonic stem cells." Cell Cycle **10**: 45-51.

Walker, E., J. L. Manias, W. Y. Chang and W. L. Stanford (2011). "PCL2 modulates gene regulatory networks controlling self-renewal and commitment in embryonic stem cells." Cell Cycle **10**(1): 45-51.

Walker, E., M. Ohishi, R. E. Davey, W. Zhang, P. A. Cassar, T. S. Tanaka, S. D. Der, Q. Morris, T. R. Hughes, P. W. Zandstra and W. L. Stanford (2007). "Prediction and testing of novel transcriptional networks regulating embryonic stem cell self-renewal and commitment." Cell Stem Cell **1**(1): 71-86.

Walter, M. J., D. Shen, L. Ding, J. Shao, D. C. Koboldt, K. Chen, D. E. Larson, M. D. McLellan, D. Dooling, R. Abbott, R. Fulton, V. Magrini, H. Schmidt, J. Kalicki-Veizer, M. O'Laughlin, X. Fan, M. Grillot, S. Witowski, S. Heath, J. L. Frater, W. Eades, M. Tomasson, P. Westervelt, J. F. DiPersio, D. C. Link, E. R. Mardis, T. J. Ley, R. K. Wilson and T. A. Graubert (2012). "Clonal architecture of secondary acute myeloid leukemia." N Engl J Med **366**(12): 1090-1098.

Wang, H., D. Diao, Z. Shi, X. Zhu, Y. Gao, S. Gao, X. Liu, Y. Wu, K. L. Rudolph, G. Liu, T. Li and Z. Ju (2016). "SIRT6 Controls Hematopoietic Stem Cell Homeostasis through Epigenetic Regulation of Wnt Signaling." Cell Stem Cell **18**(4): 495-507.

Wang, H., L. Wang, H. Erdjument-Bromage, M. Vidal, P. Tempst, R. S. Jones and Y. Zhang (2004). "Role of histone H2A ubiquitination in Polycomb silencing." Nature **431**(7010): 873-878.

Wang, S., Y. Gao, X. Song, X. Ma, X. Zhu, Y. Mao, Z. Yang, J. Ni, H. Li, K. E. Malanowski, P. Anoja, J. Park, J. Haug and T. Xie (2015). "Wnt signaling-mediated redox regulation maintains the germ line stem cell differentiation niche." Elife **4**: e08174.

Wang, S., F. He, W. Xiong, S. Gu, H. Liu, T. Zhang, X. Yu and Y. Chen (2007). "Polycomblike-2-deficient mice exhibit normal left-right asymmetry." Dev Dyn **236**(3): 853-861.

Wang, S., W. Sun, Y. Zhao, D. McEachern, I. Meaux, C. Barriere, J. A. Stuckey, J. L. Meagher, L. Bai, L. Liu, C. G. Hoffman-Luca, J. Lu, S. Shangary, S. Yu, D. Bernard, A. Aguilar, O. Dos-Santos, L. Besret, S. Guerif, P. Pannier, D. Gorge-Bernat and L. Debussche (2014). "SAR405838: an optimized inhibitor of MDM2-p53 interaction that induces complete and durable tumor regression." Cancer Res **74**(20): 5855-5865.

Wang, S., X. Yu, T. Zhang, X. Zhang, Z. Zhang and Y. Chen (2004). "Chick Pcl2 regulates the left-right asymmetry by repressing Shh expression in Hensen's node." Development **131**(17): 4381-4391.

Wang, Y., A. V. Krivtsov, A. U. Sinha, T. E. North, W. Goessling, Z. Feng, L. I. Zon and S. A. Armstrong (2010). "The Wnt/beta-catenin pathway is required for the development of leukemia stem cells in AML." Science **327**(5973): 1650-1653.

Wassef, M., V. Rodilla, A. Teissandier, B. Zeitouni, N. Gruel, B. Sadacca, M. Irondelle, M. Charruel, B. Ducos, A. Michaud, M. Caron, E. Marangoni, P. Chavrier, C. Le Tourneau, M. Kamal, E. Pasmant, M. Vidaud, N. Servant, F. Reyal, D. Meseure, A. Vincent-Salomon, S. Fre and R. Margueron (2015). "Impaired PRC2 activity promotes transcriptional instability and favors breast tumorigenesis." Genes Dev **29**(24): 2547-2562.

Wei, Y., W. Xia, Z. Zhang, J. Liu, H. Wang, N. V. Adsay, C. Albarracin, D. Yu, J. L. Abbruzzese, G. B. Mills, R. C. Bast, Jr., G. N. Hortobagyi and M. C. Hung (2008). "Loss of trimethylation at lysine 27 of histone H3 is a predictor of poor outcome in breast, ovarian, and pancreatic cancers." Mol Carcinog **47**(9): 701-706.

Woo, C. J., P. V. Kharchenko, L. Daheron, P. J. Park and R. E. Kingston (2010). "A region of the human HOXD cluster that confers polycomb-group responsiveness." Cell **140**(1): 99-110.
Wu, H., V. Coskun, J. Tao, W. Xie, W. Ge, K. Yoshikawa, E. Li, Y. Zhang and Y. E. Sun (2010). "Dnmt3a-dependent nonpromoter DNA methylation facilitates transcription of neurogenic genes." Science **329**(5990): 444-448.

Wunderlich, M., B. Mizukawa, F.-S. Chou, C. Sexton, M. Shrestha, Y. Saunthararajah and J. C. Mulloy (2013). "AML cells are differentially sensitive to chemotherapy treatment in a human xenograft model." Blood **121**(12): e90-e97.

Xie, C., H. Edwards, X. Xu, H. Zhou, S. A. Buck, M. L. Stout, Q. Yu, J. E. Rubnitz, L. H. Matherly, J. W. Taub and Y. Ge (2010). "Mechanisms of synergistic antileukemic interactions between valproic acid and cytarabine in pediatric acute myeloid leukemia." Clin Cancer Res **16**(22): 5499-5510.

Xie, H., J. Xu, J. H. Hsu, M. Nguyen, Y. Fujiwara, C. Peng and S. H. Orkin (2014). "Polycomb repressive complex 2 regulates normal hematopoietic stem cell function in a developmental-stage-specific manner." Cell Stem Cell **14**(1): 68-80.

Xu, B., D. M. On, A. Ma, T. Parton, K. D. Konze, S. G. Pattenden, D. F. Allison, L. Cai, S. Rockowitz, S. Liu, Y. Liu, F. Li, M. Vedadi, S. V. Frye, B. A. Garcia, D. Zheng, J. Jin and G. G. Wang (2015). "Selective inhibition of EZH2 and EZH1 enzymatic activity by a small molecule suppresses MLL-rearranged leukemia." Blood **125**(2): 346-357.

Xu, F., X. Li, L. Wu, Q. Zhang, R. Yang, Y. Yang, Z. Zhang, Q. He and C. Chang (2011). "Overexpression of the EZH2, RING1 and BMI1 genes is common in myelodysplastic syndromes: relation to adverse epigenetic alteration and poor prognostic scoring." Ann Hematol **90**(6): 643-653.

Xu, K., Z. J. Wu, A. C. Groner, H. H. He, C. Cai, R. T. Lis, X. Wu, E. C. Stack, M. Loda, T. Liu, H. Xu, L. Cato, J. E. Thornton, R. I. Gregory, C. Morrissey, R. L. Vessella, R. Montironi, C. Magi-Galluzzi, P. W. Kantoff, S. P. Balk, X. S. Liu and M. Brown (2012). "EZH2 oncogenic activity in castration-resistant prostate cancer cells is Polycomb-independent." Science **338**(6113): 1465-1469.

Yan, J., S. B. Ng, J. L. Tay, B. Lin, T. L. Koh, J. Tan, V. Selvarajan, S. C. Liu, C. Bi, S. Wang, S. N. Choo, N. Shimizu, G. Huang, Q. Yu and W. J. Chng (2013). "EZH2 overexpression in natural killer/T-cell lymphoma confers growth advantage independently of histone methyltransferase activity." Blood **121**(22): 4512-4520.

Ye, T., A. R. Krebs, M. A. Choukrallah, C. Keime, F. Plewniak, I. Davidson and L. Tora (2011). "seqMINER: an integrated ChIP-seq data interpretation platform." Nucleic Acids Res **39**(6): e35.

Yoder, M. C. and K. Hiatt (1997). "Engraftment of embryonic hematopoietic cells in conditioned newborn recipients." Blood **89**(6): 2176-2183.

Yoder, M. C., K. Hiatt and P. Mukherjee (1997). "In vivo repopulating hematopoietic stem cells are present in the murine yolk sac at day 9.0 postcoitus." Proc Natl Acad Sci U S A **94**(13): 6776-6780.

Yu, F. X. and K. L. Guan (2013). "The Hippo pathway: regulators and regulations." Genes Dev **27**(4): 355-371.

Yu, X., J. K. Alder, J. H. Chun, A. D. Friedman, S. Heimfeld, L. Cheng and C. I. Civin (2006). "HES1 inhibits cycling of hematopoietic progenitor cells via DNA binding." Stem Cells **24**(4): 876-888.

Yuan, Y., H. Shen, D. S. Franklin, D. T. Scadden and T. Cheng (2004). "In vivo self-renewing divisions of haematopoietic stem cells are increased in the absence of the early G1-phase inhibitor, p18INK4C." Nat Cell Biol **6**(5): 436-442.

Zhang, W., Q. D. Morris, R. Chang, O. Shai, M. A. Bakowski, N. Mitsakakis, N. Mohammad, M. D. Robinson, R. Zirngibl, E. Somogyi, N. Laurin, E. Eftekharpour, E. Sat, J. Grigull, Q. Pan, W. T. Peng, N. Krogan, J. Greenblatt, M. Fehlings, D. van der Kooy, J. Aubin, B. G. Bruneau, J. Rossant, B. J. Blencowe, B. J. Frey and T. R. Hughes (2004). "The functional landscape of mouse gene expression." J Biol **3**(5): 21.

Zhang, Y., T. Liu, C. A. Meyer, J. Eeckhoute, D. S. Johnson, B. E. Bernstein, C. Nusbaum, R. M. Myers, M. Brown, W. Li and X. S. Liu (2008). "Model-based analysis of ChIP-Seq (MACS)." Genome Biol **9**(9): R137.

Zhao, B., Q. Y. Lei and K. L. Guan (2008). "The Hippo-YAP pathway: new connections between regulation of organ size and cancer." Curr Opin Cell Biol **20**(6): 638-646.

Zhao, B., L. Li, Q. Lei and K. L. Guan (2010). "The Hippo-YAP pathway in organ size control and tumorigenesis: an updated version." Genes Dev **24**(9): 862-874.

Zuber, J., I. Radtke, T. S. Pardee, Z. Zhao, A. R. Rappaport, W. Luo, M. E. McCurrach, M. M. Yang, M. E. Dolan, S. C. Kogan, J. R. Downing and S. W. Lowe (2009). "Mouse models of human AML accurately predict chemotherapy response." Genes Dev **23**(7): 877-889.

Appendix A

Harinad Maganti CV

EDUCATION

2011- Current **Faculty of Medicine**, **University of Ottawa,** Ottawa, Ontario, Canada
Ph.D. student: *Department of Biochemistry, Microbiology and Immunology and* Sprott Centre for Stem Cell Research, OHRI

2010-2011 **McMaster University,** Hamilton, Ontario, Canada
M.Sc.: Department of Biology

2006-2010 **McMaster University,** Hamilton, Ontario, Canada
B.Sc. Honours Biology (Microbiology Biology and Biotechnology specialization)

AWARDS

2017-2018 Till & McCulloch Meetings Travel Award

2016-2017 Till & McCulloch Meetings Award – Under the Microscope Talk Award

2016-2017 Till & McCulloch Meetings Travel Award

2015-2016 Ontario Institute of Regenerative Medicine Award

2015-2016 Till & McCulloch Meetings Award

2011-2015 Faculty of Graduate and Postdoctoral Studies, University of Ottawa: Admission Scholarship

2010-2011 NSERC – Alexander Graham Bell Graduate Scholarship

2010-2011 McMaster University Graduate Scholarship

2010-2011 McMaster University Research Scholarship

2009-2010 Institute of Infectious Disease Research (IIDR), McMaster University: Research fellowship

2006-2007 Queen Elizabeth Scholarship

2006-2007 McMaster Undergraduate Admission Scholarship

HONOURS

2015-2016 Invited to act as Junior Chair at the annual Till & McCulloch Meetings

2012-2013 Invited to attend Hydra XI: European Summer School on Stem Cell Biology, Hydra, Greece.
- **The top 10% of the applicants from around the world are invited to attend.**

2010-2011 Completed M.Sc. in Biology within a record time of 13 months.
- **First person to do so in 92 years from the department of Biology at McMaster University.**

2010-2011 Nominated Valedictorian Candidate for Graduating Class of 2010/11 by the chair of graduate studies, Department of Biology, McMaster University for exceptional research productivity.

2009-2010 McMaster Dean's Honor list
- **Recognized for maintaining A average in my B.Sc. (honours) degree.**

PUBLICATIONS

Maganti, H., Yamamura, D., & Xu, J. (2011). Prevalent nosocomial clusters among causative agents for candidemia in Hamilton, Canada. ***Med Mycol,*** *49*(5), 530-538. doi: 10.3109/13693786.2010.547880 **(1st Author)**

Maganti, H., Bartfai, D., & Xu, J. (2011). Ecological structuring of yeasts associated with trees around Hamilton, Ontario, Canada. ***FEMS Yeast Res***. doi: 10.1111/j.1567-1364.2011.00756.x **(1st Author)**

Schoch, CL., Seifert, KA., Huhndorf, S., Robert, V., Spouge, JL., Levesque, CA., Chen, W., **Maganti, H** et al. (2012). Nuclear ribosomal internal transcribed spacer (ITS) region as a universal DNA barcode marker for Fungi. ***Proc Natl Acad Sci USA***, 109(16), 6241-6246. Epub 2012.03.27. **(8th Author)**

Maganti H and Stanford W, Faculty of 1000 evaluations, dissents and comments for Tavares L et al. RYBP-PRC1 complexes mediate H2A ubiquitylation at polycomb target sites independently of PRC2 and H3K27me3. **Cell.** 2012 Feb 17; 148(4): 664-78; doi: 10.1016/j.cell.2011.12.029]. Faculty of 1000, F1000.com/14261958 **(1st Author)**

Kadhim-Saleh, **Maganti H**, Farrokhyar F. Determining the efficacy of low-level laser therapy (LLLT) for neck pain reduction. A systematic review and meta-analysis. ***Rheumatology International,*** 10.1007/s00296-013-2742-z **(2nd Author)**

Carvalho C, Jiaqi Y, Vogan A, **Maganti H**, Yamamura D and Xu J. Genotype relationships between clinical and environmental Candida parapsilosis populations in Hamilton Ontario. ***Mycoses***. 58(5), 271-83 **(4th Author)**

Manias-Rothberg JL, **Maganti H**, Porter C et al, Polycomb-like 2 (PCL2) is required for hematopoietic development. Experimental Hematology, 42(8), S47. **(2nd Author)**

Juliana Barrera-Ramirez*****, Jessie R. Lavoie*****, **Maganti H** et al, Micro-RNA profiling of exosomes from marrow-derived mesenchymal stromal cells in patients with Acute Myeloid Leukemia: implications in leukemogenesis. ***Stem Cell Reviews and Reports. *Co-first authors*** **(2nd Author)**

Accepted with minor revisions

Manias-Rothberg JL*, **Maganti H*** et al, Mtf2 dynamically regulates Wnt and Hippo signaling to control hematopoiesis, ***Cell Discovery*****. *Co-first authors.**

In revision

Maganti H*, Hani Jrade* et al, Targeting the epigenetic program underlying refractory Acute Myeloid Leukemia, ***Cancer Discovery, *Co-first authors***

Tanner MR, **Maganti H** et al. ExCluster: Hierarchical clustering of expressed exons robustly detects differentially spliced genes in RNA-seq data, ***Genome Research*** **(2nd Author)**

Siriwardena D*, Choey C, **Maganti H** et al, An improved cecal puncture and humanized mouse model of sepsis, ***PLOS Medicine*** **(3rd Author)**

PATENT (Provisional)

Title: Treatment of Acute Myeloid Leukemia,
United States Provisional Patent Application No. 62/533,942
Inventors: STANFORD, William; ITO, Caryn; SABLOFF, Mitchell; **MAGANTI, Harinad**; JRADE, Hani

PRESENTATIONS (selected only)

1) **Till & McCulloch Meetings** (1 st place) **2016**
   Poster presentation: Maganti H, Manias JL, Ito CY and Stanford WL. "Role of MTF2 in human hematopoiesis".

2) **Till & McCulloch Meetings** **2015**
   Poster presentation: Maganti H, Manias JL, Ito CY and Stanford WL. "Role of MTF2 in Acute Myeloid Leukemia".

3) **Biochemistry: Microbiology and Immunology (BMI) Symposium** **2013**

Faculty of Medicine, Ottawa University, Ottawa, ON
Oral presentation: Maganti H, Manias JL, Ito CY and Stanford WL. "Role of MTF2 in Acute Myeloid Leukemia".

4) **Ottawa Hospital Research Institute (OHRI) Research Day** **2012**
Ottawa General Hospital, Ottawa, ON
Poster presentation: Maganti H, Manias JL, Ito CY and Stanford WL. "Role of PCL2 in Acute Myeloid Leukemia".

5) **Biochemistry: Microbiology and Immunology (BMI) Poster Day** **2011**
Faculty of Medicine, Ottawa University, Ottawa, ON
Poster presentation: Maganti H, Manias JL, Ito CY and Stanford WL. "Role of PCL2 in Acute Myeloid Leukemia".

6) **Genetics Society of Canada Conference (1st place)** **2011**
McMaster University, Hamilton, ON
Podium Presentation: Maganti H, Xu J. "ITS fungal Barcoding: A meta-analysis".

SKILLS AND WORKSHOPS

1) **UBCFlow: Advanced Multi-colour Cell Sorting** **2016**
University of British Columbia, Vancouver, Canada.

2) **Grant Review Workshop** **2014**
Till & McCulloch Meetings, Banff, Alberta.

3) **UBCFlow: Advanced Multi-colour Flow Cytometry Workshop** **2013**
University of British Columbia, Vancouver, Canada.

4) **Reviewing Scientific Articles** **2010**
Trillium Research Day – Primary Health Care Research Day 2011**,** University of Toronto, Toronto, Canada.

5) **Teaching Genetics** **2010**
Genetics Society of Canada Conference, McMaster University, Hamilton, Canada.

TEACHING EXPERIENCE

BioChem 3346: Advanced Biochemistry **2016-2017**

BioChem 2333: Introduction to Biochemistry **2015-2016**

BioChem 2333: Introduction to Biochemistry **2014-2015**

Biology 1A03: Structure, molecular composition and function of sub-cellular and cellular systems. **2010-2011**

Molecular Biology 4P03: Medical Mycology **2010-2011**

Table S1. Genes identified as losing H3K27me3 in Mtf2-/- erythroblasts

	Mtf2+/+ vs Mtf2-/- Ter119-/lo Erythroblasts			Mtf2+/+ vs Mtf2-/- Ter119high Erythroblasts		
Gene Name	**log2FoldChange**	**Adj p value**	**p<0.05**	**log2FoldChange**	**Adj p value**	**p<0.05**
0610010O12Rik	2.6501	0.1643	no	2.3812	0.1211	no
1110012J17Rik	8.0000	1.0000	no	18.0000	1.0000	no
1110032F04Rik	1.6204	0.3129	no	2.2126	0.0269	yes
1110067D22Rik	0.2483	0.9997	no	1.8882	0.0119	yes
1190005I06Rik	0.6894	0.9802	no	-0.7435	1.0000	no
1300014I06Rik	2.8239	0.0042	yes	1.7044	0.0120	yes
1520402A15Rik	1.3637	0.5980	no	0.4942	0.7969	no
1600021P15Rik	1.4149	1.0000	no	1.0249	1.0000	no
1600029O15Rik	-6.0000	1.0000	no	18.0000	1.0000	no
1700001C19Rik	0.1104	1.0000	no	-1.1472	1.0000	no
1700001O22Rik	8.0000	1.0000	no	0.0000	1.0000	no
1700018A14Rik	0.0000	1.0000	no	0.0000	1.0000	no
1700019N12Rik	8.0000	1.0000	no	18.0000	1.0000	no
1700025G04Rik	2.4364	0.0554	no	0.9311	0.2099	no
1700054N08Rik	0.2353	0.9997	no	0.0622	0.9591	no
1700101E01Rik	0.4990	1.0000	no	-1.1444	1.0000	no
1810019J16Rik	1.4665	1.0000	no	18.0000	1.0000	no
1810027O10Rik	0.3497	0.5868	no	-1.1053	0.0155	yes
2010107G23Rik	2.0753	0.1591	no	3.6454	0.0599	no
2010300C02Rik	8.0000	1.0000	no	18.0000	1.0000	no
2210411K11Rik	-0.0166	0.9997	no	0.9281	0.1949	no
2310014H01Rik	NA	NA	NA	NA	NA	NA
2410017I17Rik	0.0000	1.0000	no	0.0000	1.0000	no
2410022L05Rik	0.1964	0.9997	no	2.1028	0.0223	yes
2510009E07Rik	1.5162	0.3510	no	1.2627	0.1836	no
2610017I09Rik	0.0000	1.0000	no	0.0000	1.0000	no
2610019F03Rik	-0.0283	0.9997	no	18.0000	0.0371	yes
2610109H07Rik	1.0174	1.0000	no	-12.0000	1.0000	no
2700046G09Rik	-0.5767	1.0000	no	18.0000	1.0000	no
2700086A05Rik	8.0000	1.0000	no	0.6097	1.0000	no
2810025M15Rik	0.0321	0.9997	no	1.3412	0.1249	no
2810030E01Rik	1.9018	1.0000	no	1.1522	1.0000	no
2810032G03Rik	0.0000	1.0000	no	18.0000	1.0000	no
2810055F11Rik	1.8035	0.1069	no	1.8165	0.0625	no
2810410L24Rik	8.0000	1.0000	no	1.5771	0.2475	no
2810459M11Rik	1.9963	0.0270	yes	0.6165	0.4678	no
2900092D14Rik	NA	NA	NA	NA	NA	NA
3830403N18Rik	0.6354	0.9871	no	0.1402	0.9173	no
3830431G21Rik	1.6378	0.2398	no	4.2527	1.0000	no
4430402I18Rik	-0.2461	1.0000	no	18.0000	1.0000	no
4732471D19Rik	0.1851	0.9997	no	2.3770	0.0000	yes
4833427G06Rik	0.0000	1.0000	no	0.0000	1.0000	no
4921515J06Rik	-6.0000	1.0000	no	0.0112	1.0000	no

4930412O13Rik	8.0000	1.0000	no	18.0000	1.0000	no
4930420K17Rik	1.6353	0.2730	no	1.2071	0.2149	no
4930429B21Rik	0.0000	1.0000	no	0.0000	1.0000	no
4931408A02Rik	0.9708	1.0000	no	0.0006	0.9995	no
4931429I11Rik	0.0000	1.0000	no	-12.0000	1.0000	no
4932441J04Rik	0.0221	1.0000	no	0.0000	1.0000	no
4933406I18Rik	0.0000	1.0000	no	0.0000	1.0000	no
4933421O10Rik	0.7414	0.9414	no	0.2719	1.0000	no
4933439C10Rik	0.3894	0.9765	no	2.3368	0.0087	yes
5430405G05Rik	0.0000	1.0000	no	0.0000	1.0000	no
5430407P10Rik	2.8297	0.0008	yes	1.8146	0.0099	yes
5730528L13Rik	2.8298	0.0046	yes	4.2116	0.0004	yes
5730559C18Rik	8.0000	1.0000	no	18.0000	1.0000	no
6030419C18Rik	0.0000	1.0000	no	18.0000	1.0000	no
6030429G01Rik	1.3297	1.0000	no	3.3957	1.0000	no
6230409E13Rik	8.0000	1.0000	no	18.0000	1.0000	no
6330512M04Rik	0.5750	1.0000	no	1.8167	1.0000	no
6430527G18Rik	5.0052	0.0007	yes	2.6252	0.0039	yes
6430548M08Rik	2.6617	0.0069	yes	2.4551	0.0004	yes
6430704M03Rik	-6.0000	1.0000	no	18.0000	1.0000	no
8430427H17Rik	0.3200	0.9502	no	-0.0633	0.9154	no
9030224M15Rik	0.0275	1.0000	no	1.5413	1.0000	no
9030409G11Rik	NA	NA	NA	NA	NA	NA
9030612E09Rik	0.0000	1.0000	no	0.0000	1.0000	no
9130024F11Rik	0.0000	1.0000	no	18.0000	1.0000	no
9130206I24Rik	2.9486	0.0001	yes	3.1465	0.0005	yes
9330182L06Rik	2.5231	0.0460	yes	2.3666	0.0269	yes
9430021M05Rik	0.0000	1.0000	no	0.0000	1.0000	no
9430076C15Rik	0.0000	1.0000	no	0.0000	1.0000	no
9830001H06Rik	-0.6195	0.8117	no	0.6851	0.3980	no
A330050F15Rik	-6.0000	1.0000	no	0.0000	1.0000	no
A430107O13Rik	1.4840	0.9340	no	0.1172	1.0000	no
A4galt	3.9637	1.0000	no	18.0000	1.0000	no
A530013C23Rik	0.0000	1.0000	no	18.0000	1.0000	no
A930011G23Rik	-6.0000	1.0000	no	0.0000	1.0000	no
Abca5	0.3128	0.9997	no	0.6957	1.0000	no
Abcb1b	1.6205	0.2844	no	1.9723	0.0273	yes
Abcg1	1.6980	0.1313	no	1.1503	0.1872	no
Abhd15	0.7326	0.9095	no	1.8455	0.0240	yes
Abhd6	1.0881	0.3586	no	0.4871	0.5060	no
Ablim3	-6.0000	1.0000	no	-12.0000	1.0000	no
Abtb2	1.6817	0.0982	no	-0.4138	0.6636	no
Acan	0.0000	1.0000	no	0.0000	1.0000	no
Accn1	0.0000	1.0000	no	18.0000	1.0000	no
Accn2	0.0300	1.0000	no	1.4876	1.0000	no
Accn4	-0.1368	1.0000	no	18.0000	1.0000	no
Acer2	-0.0068	0.9997	no	0.8214	0.3530	no
Acot1	1.6150	0.2447	no	0.8620	0.3819	no
Acsl6	-0.6700	0.2521	no	2.0060	0.0089	yes

Actl6b	-6.0000	1.0000	no	18.0000	1.0000	no
Actn1	1.2791	0.0093	yes	0.9980	0.0288	yes
Acvr1	1.1918	0.4116	no	1.3183	0.0767	no
Acvr1b	1.5410	0.2498	no	2.4118	0.0034	yes
Acvr2a	0.3556	0.9997	no	0.7420	0.4692	no
Acvr2b	0.0961	0.9997	no	3.0961	0.0388	yes
Adam11	8.0000	0.1243	no	0.6312	1.0000	no
Adam15	2.3720	0.0001	yes	1.4358	0.0016	yes
Adam19	1.0234	0.9311	no	-0.1966	0.8751	no
Adam23	8.0000	1.0000	no	1.9264	1.0000	no
Adamts14	8.0000	1.0000	no	1.3965	1.0000	no
Adamts2	0.5378	1.0000	no	-2.6198	1.0000	no
Adamts20	1.4991	1.0000	no	4.4149	1.0000	no
Adamts7	0.8112	1.0000	no	-0.7591	1.0000	no
Adamts8	8.0000	1.0000	no	0.0000	1.0000	no
Adap1	0.8736	0.2338	no	2.2350	0.0000	yes
Adap2	1.7085	0.0802	no	1.1653	0.0675	no
Adarb1	3.1497	0.0061	yes	-0.1490	1.0000	no
Adc	-1.1885	1.0000	no	18.0000	1.0000	no
Adcy2	1.8382	1.0000	no	0.9588	1.0000	no
Adcy3	0.0415	0.9997	no	1.2235	0.2194	no
Adcy5	1.5158	1.0000	no	0.1456	1.0000	no
Adm	3.0013	1.0000	no	0.2668	1.0000	no
Adora2b	3.8503	1.0000	no	0.0791	1.0000	no
Adra1d	-6.0000	1.0000	no	-1.5821	1.0000	no
Adra2a	8.0000	1.0000	no	2.7254	1.0000	no
Adra2c	0.0000	1.0000	no	18.0000	1.0000	no
Adrb1	2.6492	1.0000	no	-0.5701	1.0000	no
Aebp1	2.2373	0.0029	yes	1.2923	0.0474	yes
Agap1	1.0822	0.2847	no	2.6287	0.0004	yes
Agap2	0.5545	0.9300	no	2.8577	0.0003	yes
Agpat3	1.3363	0.0004	yes	1.8603	0.0000	yes
Agpat9	-0.5009	1.0000	no	0.6969	0.7752	no
Ahdc1	0.0171	0.9997	no	2.2870	0.0031	yes
Ahnak	2.6160	0.0055	yes	2.0885	0.0019	yes
AI118078	0.0000	1.0000	no	0.0000	1.0000	no
AI314831	0.0000	1.0000	no	0.0000	1.0000	no
AI646023	-0.9701	1.0000	no	-1.6321	1.0000	no
AI661453	3.7943	0.0262	yes	1.5398	1.0000	no
AI836003	0.0000	1.0000	no	0.0000	1.0000	no
Aif1l	0.0656	0.9997	no	2.0477	0.1774	no
Aim1	1.8150	0.0202	yes	2.1407	0.0023	yes
Ajap1	0.0000	1.0000	no	0.0000	1.0000	no
AK129341	0.6818	0.9706	no	2.6288	1.0000	no
Ak4	0.2649	0.9997	no	2.7676	0.0000	yes
Ak5	0.0346	1.0000	no	18.0000	1.0000	no
Akap12	1.4669	1.0000	no	0.7100	1.0000	no
Aldh1a2	1.0474	1.0000	no	0.2536	1.0000	no
Aldh5a1	2.0921	0.0756	no	1.5663	0.0852	no

Alox12	1.4359	0.2887	no	0.6508	0.4978	no
Alpl	2.4282	0.0272	yes	-0.5134	0.6208	no
Als2cl	3.0318	0.0000	yes	1.9556	0.0118	yes
Alx3	2.32981000000002e-310	1.0000	no	0.0000	1.0000	no
Alx4	0.0000	1.0000	no	0.0000	1.0000	no
Amigo1	0.3430	0.9997	no	1.2079	1.0000	no
Amigo2	0.3818	1.0000	no	1.0930	1.0000	no
Amn	1.0358	1.0000	no	1.5204	1.0000	no
Amotl2	2.4015	0.0310	yes	0.2897	0.8002	no
Amph	2.3500	1.0000	no	0.7877	1.0000	no
Ank1	0.2631	0.3464	no	-0.7418	0.0208	yes
Ank3	1.8462	0.0008	yes	0.8828	0.1530	no
Ankrd13b	0.3809	0.5455	no	3.5407	0.0000	yes
Ankrd33b	8.0000	1.0000	no	0.3873	1.0000	no
Ankrd34a	3.4424	1.0000	no	0.0000	1.0000	no
Ankrd34b	0.0000	1.0000	no	18.0000	1.0000	no
Ankrd44	1.4118	0.1931	no	2.4379	0.0015	yes
Ankrd56	NA	NA	NA	NA	NA	NA
Ankrd57	NA	NA	NA	NA	NA	NA
Ankrd6	-0.1892	0.9997	no	0.3900	0.7005	no
Anks1b	0.0000	1.0000	no	-12.0000	1.0000	no
Anks6	-0.0030	1.0000	no	2.3905	1.0000	no
Ano6	0.6684	0.5637	no	0.9419	0.0815	no
Ap1m2	8.0000	1.0000	no	-0.0254	1.0000	no
Apba1	2.4818	1.0000	no	2.8055	1.0000	no
Apbb2	2.6607	0.5204	no	0.9013	0.6840	no
Apc2	1.8443	1.0000	no	0.2470	1.0000	no
Apcdd1	8.0000	1.0000	no	18.0000	1.0000	no
Aqp5	0.0000	1.0000	no	0.0000	1.0000	no
Arap2	3.6203	0.1630	no	0.5453	0.5620	no
Arf3	0.2615	0.9733	no	1.6610	0.0040	yes
Arg2	0.5780	1.0000	no	1.5301	1.0000	no
Arhgap20	-6.0000	1.0000	no	-2.2346	1.0000	no
Arhgap26	4.1377	0.0000	yes	1.9621	0.0158	yes
Arhgap29	0.5708	0.6697	no	1.0607	0.0573	no
Arhgap31	1.1863	0.3255	no	1.1329	0.1269	no
Arhgef10l	1.4063	0.0611	no	1.9788	0.0002	yes
Arhgef16	1.1707	1.0000	no	1.8221	0.0174	yes
Arhgef17	1.6113	1.0000	no	1.3396	1.0000	no
Arhgef26	1.0469	1.0000	no	1.5407	1.0000	no
Arhgef37	1.9951	1.0000	no	1.2036	1.0000	no
Arhgef5	2.2534	1.0000	no	2.2635	0.0115	yes
Arhgef7	0.1827	0.9997	no	1.0119	0.1419	no
Arid3c	0.0000	1.0000	no	0.0000	1.0000	no
Arl4c	1.3514	1.0000	no	1.1113	1.0000	no
Arnt2	3.3441	1.0000	no	18.0000	1.0000	no
Arntl	-0.0152	0.9997	no	1.7633	0.0139	yes
Arpp21	0.1433	1.0000	no	3.0052	1.0000	no

Arsb	1.2231	0.3099	no	2.1767	0.0047	yes
Artn	2.4175	0.0007	yes	-0.1540	0.7967	no
Arvcf	-0.8032	0.0282	yes	0.9461	0.0401	yes
Asap2	0.7778	0.5046	no	2.2294	0.0007	yes
Asb4	2.1585	0.0792	no	1.7442	0.0577	no
Asb8	-0.1369	0.9997	no	0.2559	0.6688	no
Ascl2	1.7792	1.0000	no	3.6474	1.0000	no
Atf3	0.6742	1.0000	no	1.3707	0.2337	no
Atn1	1.4083	0.1068	no	1.4013	0.0788	no
Atoh7	0.0000	1.0000	no	0.0000	1.0000	no
Atoh8	2.8812	1.0000	no	18.0000	1.0000	no
Atp11a	0.7417	0.2848	no	1.1918	0.0539	no
Atp6v1c2	2.0836	1.0000	no	18.0000	1.0000	no
Atp8b1	0.4927	1.0000	no	1.1970	1.0000	no
Atp8b2	1.6318	0.0507	no	2.8353	0.0000	yes
Atp9a	-0.5022	0.9758	no	1.2044	0.3138	no
Atrnl1	0.0669	0.9997	no	0.7573	0.4232	no
Atxn1	0.1458	1.0000	no	0.2685	1.0000	no
AU023871	1.4523	0.6956	no	1.5350	0.1468	no
AW011738	6.3688	0.0013	yes	1.8674	0.0333	yes
AW555464	1.9808	0.0067	yes	1.7690	0.0042	yes
Axin2	1.0037	0.7835	no	2.6208	0.0072	yes
B3galnt1	0.2961	1.0000	no	0.1531	0.9097	no
B3gnt3	0.9463	0.6767	no	-0.6293	0.4978	no
B4galnt1	0.5150	0.6800	no	2.9609	0.0000	yes
B4galnt2	0.4425	0.9997	no	0.2320	1.0000	no
B4galnt3	0.4558	1.0000	no	-1.6087	0.0918	no
B4galnt4	0.5677	1.0000	no	1.4687	1.0000	no
B4galt2	0.7047	0.7422	no	0.9230	0.1398	no
B4galt4	1.7409	0.2843	no	0.4142	0.6256	no
B4galt5	1.7096	0.0119	yes	0.8500	0.0922	no
B4galt6	2.8596	0.0018	yes	2.6067	0.0007	yes
B830017H08Rik	NA	NA	NA	NA	NA	NA
B930041F14Rik	3.2564	1.0000	no	1.2439	1.0000	no
Bahcc1	0.8187	0.2468	no	2.0111	0.0029	yes
Bahd1	0.0496	0.9997	no	0.5132	0.2381	no
Bai1	0.0000	1.0000	no	0.0000	1.0000	no
Bai2	8.0000	1.0000	no	18.0000	1.0000	no
Baiap2	1.2410	0.2120	no	1.1644	0.1020	no
Baiap3	0.1934	1.0000	no	1.6951	1.0000	no
Barhl1	-6.0000	1.0000	no	0.0000	1.0000	no
Barhl2	0.0000	1.0000	no	0.0000	1.0000	no
Barx1	8.0000	1.0000	no	18.0000	1.0000	no
Barx2	0.0000	1.0000	no	0.0000	1.0000	no
Batf3	2.3747	1.0000	no	1.4309	0.2092	no
BC005764	0.4575	0.8023	no	2.0629	0.0003	yes
BC022687	1.5020	0.4068	no	1.5927	0.1238	no
BC030476	0.0000	1.0000	no	2.6076	1.0000	no
BC057022	0.0962	1.0000	no	2.6815	1.0000	no

BC061194	0.0000	1.0000	no	18.0000	1.0000	no
BC068157	1.4869	1.0000	no	1.6155	1.0000	no
Bcan	0.0000	1.0000	no	1.9286	1.0000	no
Bcar1	1.5874	0.1537	no	1.1278	0.2458	no
Bcar3	2.1267	1.0000	no	0.7253	1.0000	no
Bcl11b	2.0364	1.0000	no	0.0000	1.0000	no
Bcl2	1.0883	0.6948	no	3.3226	0.0002	yes
Bcl2l11	-0.2020	0.9997	no	0.5949	0.3199	no
Bcl3	2.3942	0.0242	yes	1.2916	0.0950	no
Bcl6	2.7756	1.0000	no	1.2875	0.1886	no
Bcr	2.1090	0.0001	yes	3.1446	0.0000	yes
Bean1	0.0000	1.0000	no	0.0000	1.0000	no
Bend4	2.5043	0.0204	yes	2.3969	0.0059	yes
Bend5	8.0000	1.0000	no	-0.5042	1.0000	no
Bend6	1.1308	1.0000	no	1.1716	1.0000	no
Bend7	2.7798	0.0292	yes	1.6561	0.0294	yes
Bfsp1	1.3897	1.0000	no	2.5546	1.0000	no
Bhlhe22	0.0000	1.0000	no	18.0000	1.0000	no
Bhlhe23	0.0000	1.0000	no	0.0000	1.0000	no
Bhlhe40	2.2738	0.2343	no	1.3214	0.1740	no
Bhlhe41	2.9811	1.0000	no	-0.0892	1.0000	no
Bicc1	1.8434	1.0000	no	1.4812	1.0000	no
Bik	1.8605	0.2983	no	3.3444	0.0185	yes
Bin1	2.0802	0.0082	yes	1.4518	0.0716	no
Blvrb	0.1085	0.9590	no	-1.0710	0.0025	yes
Bmf	1.7718	0.5709	no	0.3132	0.8059	no
Bmi1	0.7186	0.0918	no	2.8412	0.0000	yes
Bmp1	2.1962	0.0022	yes	2.0721	0.0003	yes
Bmp2	3.2571	0.0078	yes	0.4078	1.0000	no
Bmp6	-0.4013	1.0000	no	1.7076	1.0000	no
Bmp7	3.0749	1.0000	no	2.5348	1.0000	no
Bmper	8.0000	1.0000	no	0.0000	1.0000	no
Bmpr1a	1.4912	0.0679	no	1.0659	0.1245	no
Bnc1	0.0000	1.0000	no	18.0000	1.0000	no
Bnc2	0.4089	1.0000	no	1.8196	1.0000	no
Boc	8.0000	1.0000	no	-0.0658	1.0000	no
Bok	4.3562	0.0599	no	0.4461	1.0000	no
Boll	1.7206	1.0000	no	18.0000	0.0619	no
Brsk1	8.0000	1.0000	no	2.4145	1.0000	no
Brsk2	8.0000	1.0000	no	1.8979	1.0000	no
Brwd1	0.1327	0.9997	no	1.6864	0.0030	yes
Bsn	0.1138	0.9997	no	-0.0384	0.9708	no
Bspry	0.2567	1.0000	no	0.0933	1.0000	no
Bves	0.9898	1.0000	no	1.0378	1.0000	no
C030039L03Rik	1.0719	0.6000	no	-0.0784	1.0000	no
C130071C03Rik	8.0000	1.0000	no	18.0000	1.0000	no
C130074G19Rik	2.1332	0.0538	no	1.1148	0.2365	no
C1ql1	0.4417	1.0000	no	1.4941	1.0000	no
C1ql2	0.0000	1.0000	no	18.0000	1.0000	no

C1ql3	-6.0000	1.0000	no	0.0000	1.0000	no
C1ql4	0.0000	1.0000	no	0.0000	1.0000	no
C1qtnf4	1.1216	0.6707	no	-0.0839	0.9498	no
C2cd4b	1.2144	1.0000	no	18.0000	1.0000	no
C2cd4d	0.0000	1.0000	no	0.0000	1.0000	no
C530028O21Rik	8.0000	1.0000	no	0.0000	1.0000	no
C630004H02Rik	1.0742	1.0000	no	0.1135	1.0000	no
C77080	0.9243	0.7107	no	1.9351	0.0145	yes
C77370	8.0000	1.0000	no	1.0292	1.0000	no
Cables1	2.1458	0.0451	yes	2.3689	0.0029	yes
Cabp7	-0.1051	0.9997	no	0.6724	0.5206	no
Cachd1	0.8826	0.4995	no	-0.9323	0.1147	no
Cacna1a	0.9344	0.9842	no	6.9259	0.0060	yes
Cacna1b	8.0000	1.0000	no	18.0000	1.0000	no
Cacna1c	2.0186	0.0310	yes	1.9890	0.0208	yes
Cacna1g	1.7245	0.0001	yes	-0.2374	0.6182	no
Cacna1h	0.4320	0.9997	no	0.9795	1.0000	no
Cacna1i	0.0000	1.0000	no	0.0000	1.0000	no
Cacna1s	0.0000	1.0000	no	0.0000	1.0000	no
Cacna2d1	1.9878	1.0000	no	0.2418	1.0000	no
Cacna2d2	8.0000	1.0000	no	18.0000	1.0000	no
Cacna2d3	8.0000	1.0000	no	2.2414	1.0000	no
Cacnb1	0.0702	1.0000	no	1.6004	1.0000	no
Cacnb2	2.6097	1.0000	no	2.2988	0.0131	yes
Cacnb3	2.3359	1.0000	no	-2.9422	1.0000	no
Cacnb4	-1.1445	0.6494	no	-1.5953	1.0000	no
Cacng4	8.0000	1.0000	no	0.9840	1.0000	no
Cadm1	0.8570	0.7252	no	0.2199	0.7765	no
Cadm3	1.4789	0.2603	no	-1.1626	0.1599	no
Cadm4	2.6538	1.0000	no	3.1110	1.0000	no
Cadps2	-5.7389	1.0000	no	4.4998	1.0000	no
Camk1d	1.4258	0.2318	no	1.4156	0.2413	no
Camk2b	2.5263	1.0000	no	1.3275	1.0000	no
Camk2d	1.0153	0.3637	no	1.5575	0.0332	yes
Camk2n1	2.9480	0.0088	yes	1.4020	0.1406	no
Camk2n2	1.4358	1.0000	no	2.1197	1.0000	no
Camk4	0.4917	1.0000	no	0.6787	1.0000	no
Camkk1	1.4138	0.1827	no	1.7907	0.0558	no
Camkv	3.3535	1.0000	no	18.0000	1.0000	no
Capn2	2.0901	0.0155	yes	1.1439	0.1399	no
Car11	2.2149	1.0000	no	18.0000	1.0000	no
Car14	1.3187	0.4154	no	0.6099	0.5628	no
Car4	8.0000	1.0000	no	18.0000	1.0000	no
Car7	2.5383	0.0158	yes	2.0287	0.0092	yes
Card10	2.8276	0.0032	yes	2.5082	0.0000	yes
Caskin1	0.3260	1.0000	no	2.5897	1.0000	no
Casz1	3.3476	1.0000	no	2.7082	0.0005	yes
Cbfa2t3	0.1313	0.9997	no	0.6583	0.1188	no
Cbfb	1.3014	0.0180	yes	2.1506	0.0000	yes

Cbln1	0.0000	1.0000	no	0.0000	1.0000	no
Cbr3	2.8494	1.0000	no	0.7034	1.0000	no
Cbs	2.8907	0.0001	yes	2.3618	0.0002	yes
Cbx2	0.5287	0.9402	no	2.9552	0.0010	yes
Cbx4	0.8512	0.5082	no	2.2047	0.0005	yes
Cbx7	0.4804	0.8434	no	0.7664	0.1374	no
Cbx8	-1.0577	0.6086	no	2.6641	0.0028	yes
Ccdc102a	-0.1198	0.9997	no	2.3560	0.0067	yes
Ccdc109b	0.3404	0.9460	no	-0.4581	0.3735	no
Ccdc13	0.0000	1.0000	no	0.0000	1.0000	no
Ccdc136	8.0000	1.0000	no	18.0000	1.0000	no
Ccdc3	1.7546	1.0000	no	0.9641	1.0000	no
Ccdc40	-1.7674	0.0538	no	2.3124	0.0605	no
Ccdc48	2.4699	1.0000	no	0.6786	1.0000	no
Ccdc64	0.6549	0.8238	no	0.8559	0.3588	no
Ccdc85c	0.8033	0.8808	no	2.8368	0.0019	yes
Ccdc92	3.8496	0.0022	yes	2.2777	0.1309	no
Ccna1	8.0000	1.0000	no	18.0000	1.0000	no
Ccnd2	0.7751	0.0688	no	3.0731	0.0000	yes
Ccnjl	0.6137	1.0000	no	1.2790	1.0000	no
Ccno	2.0652	1.0000	no	2.1102	1.0000	no
Ccr10	-0.2280	1.0000	no	18.0000	1.0000	no
Cd109	8.0000	1.0000	no	0.5985	1.0000	no
Cd14	1.9460	1.0000	no	0.2805	0.8244	no
Cd302	1.3910	0.3019	no	0.5103	0.5968	no
Cd63	2.4591	0.0008	yes	2.0283	0.0032	yes
Cd70	0.0000	1.0000	no	0.0000	1.0000	no
Cd9	2.3728	0.0011	yes	1.3021	0.0790	no
Cdc14b	1.1300	0.0306	yes	1.6627	0.0172	yes
Cdc42bpb	0.7135	0.5955	no	1.6099	0.0390	yes
Cdc42ep1	2.5731	0.0259	yes	1.3780	0.1422	no
Cdh1	2.6332	0.0043	yes	1.7932	0.0311	yes
Cdh2	2.3616	0.0018	yes	1.4634	0.0293	yes
Cdh22	0.0000	1.0000	no	0.0000	1.0000	no
Cdh4	8.0000	1.0000	no	0.9432	1.0000	no
Cdk14	2.2097	0.0142	yes	0.9537	0.2704	no
Cdk18	1.3660	0.2610	no	1.3886	0.1428	no
Cdk5r2	8.0000	1.0000	no	18.0000	1.0000	no
Cdkl1	1.1037	0.6448	no	-1.2542	0.1319	no
Cdkn1a	2.2601	0.0062	yes	1.9337	0.0047	yes
Cdkn1c	1.6995	0.0162	yes	0.6250	0.4118	no
Cdkn2a	8.0000	1.0000	no	0.0000	1.0000	no
Cdr2l	2.2966	1.0000	no	0.8311	1.0000	no
Cds1	2.0020	0.6457	no	1.2308	0.3974	no
Cdv3	-0.1182	0.8832	no	0.7782	0.0058	yes
Cdx1	-6.0000	1.0000	no	0.0000	1.0000	no
Cdx2	0.0000	1.0000	no	0.0000	1.0000	no
Cdyl2	-0.5078	0.9997	no	0.6228	0.5665	no
Cebpa	2.6451	0.0032	yes	1.5023	0.0642	no

Cebpb	1.0553	0.5817	no	1.0875	0.2332	no
Cebpd	1.3878	0.4447	no	2.3750	0.0056	yes
Cecr6	0.0000	1.0000	no	18.0000	1.0000	no
Celsr1	3.4121	1.0000	no	3.3135	1.0000	no
Celsr2	1.0901	0.1398	no	3.3601	0.0951	no
Celsr3	3.1680	1.0000	no	2.5997	1.0000	no
Cgn	0.5384	0.7858	no	-0.8429	0.1136	no
Cgnl1	0.5915	1.0000	no	0.6142	1.0000	no
Ch25h	8.0000	1.0000	no	18.0000	1.0000	no
Chd3	1.3783	0.0002	yes	1.3414	0.0000	yes
Chd5	0.3591	1.0000	no	1.3951	1.0000	no
Chn1	0.7193	0.6873	no	0.8586	0.4048	no
Chn2	2.4578	0.0011	yes	1.7290	0.0018	yes
Chpf	0.3861	0.8867	no	3.3224	0.0000	yes
Chrd	8.0000	1.0000	no	1.0226	1.0000	no
Chrdl2	0.0000	1.0000	no	0.0000	1.0000	no
Chrm4	1.5921	0.2205	no	4.4111	1.0000	no
Chrna5	8.0000	1.0000	no	0.0000	1.0000	no
Chrnb1	2.8675	1.0000	no	18.0000	0.0756	no
Chst1	8.0000	1.0000	no	18.0000	1.0000	no
Chst15	-0.4717	0.9842	no	1.5958	0.1014	no
Chst2	1.6379	1.0000	no	1.5239	1.0000	no
Chst3	0.8011	1.0000	no	0.9091	1.0000	no
Chsy3	1.2762	1.0000	no	0.1923	1.0000	no
Cidea	8.0000	1.0000	no	0.0000	1.0000	no
Cilp2	-0.9255	1.0000	no	-12.0000	1.0000	no
Cited1	1.9461	0.0021	yes	1.0175	0.1226	no
Ckap4	2.7549	0.0000	yes	1.9651	0.0000	yes
Ckb	1.5289	0.1812	no	0.5923	0.5202	no
Clcf1	8.0000	1.0000	no	4.0350	1.0000	no
Cldn10	-1.4667	0.5060	no	-2.3321	0.0368	yes
Cldn23	8.0000	1.0000	no	0.0000	1.0000	no
Cldn3	0.2560	1.0000	no	18.0000	1.0000	no
Cldn5	1.3294	0.5942	no	0.7273	0.5070	no
Cldn6	0.0000	1.0000	no	0.0000	1.0000	no
Cldn7	8.0000	0.0430	yes	1.8830	0.2545	no
Clec2l	2.3528	1.0000	no	1.2495	1.0000	no
Clgn	1.3047	0.2603	no	1.5168	0.0074	yes
Clic6	4.7368	1.0000	no	4.9061	1.0000	no
Clip1	-0.0044	0.9997	no	0.8445	0.0008	yes
Clock	0.1352	0.9997	no	0.9178	0.0842	no
Clstn1	0.7386	0.6712	no	2.4095	0.0124	yes
Clstn2	1.0414	1.0000	no	0.0443	1.0000	no
Cmtm4	0.5697	0.9997	no	2.8912	0.0019	yes
Cmtm7	1.9118	0.0000	yes	2.5029	0.0000	yes
Cnih3	8.0000	1.0000	no	0.0000	1.0000	no
Cnn1	0.0190	1.0000	no	-0.0173	1.0000	no
Cnn2	2.3840	0.0000	yes	2.1290	0.0000	yes
Cnn3	-0.5342	0.5012	no	1.8345	0.0114	yes

Cnnm1	2.8360	0.0004	yes	18.0000	0.0001	yes
Cnr1	8.0000	1.0000	no	18.0000	1.0000	no
Cntfr	2.0889	1.0000	no	18.0000	1.0000	no
Cntnap1	3.9507	1.0000	no	2.1918	1.0000	no
Cobll1	1.8815	0.2436	no	0.6021	0.5872	no
Coch	-1.9696	1.0000	no	18.0000	1.0000	no
Col18a1	1.4751	0.0038	yes	1.0554	0.0441	yes
Col23a1	0.8086	1.0000	no	4.5081	1.0000	no
Col27a1	3.0983	0.0000	yes	1.3447	0.0170	yes
Col2a1	2.0285	1.0000	no	-2.1175	1.0000	no
Col4a2	0.7159	0.6767	no	0.6824	0.4096	no
Col5a1	-0.3694	0.8764	no	0.7454	0.2234	no
Col8a2	1.0440	1.0000	no	18.0000	1.0000	no
Col9a2	3.1174	1.0000	no	18.0000	1.0000	no
Colec12	0.6994	0.9499	no	0.6482	0.5258	no
Comp	-0.1358	1.0000	no	0.9080	1.0000	no
Copz2	3.2066	0.0560	no	0.6718	0.4226	no
Coro2a	2.5786	0.0009	yes	2.4008	0.0000	yes
Coro6	-0.8974	1.0000	no	18.0000	1.0000	no
Cox8a	-0.0684	0.9997	no	-0.0411	0.9678	no
Cpeb1	8.0000	1.0000	no	18.0000	1.0000	no
Cpeb2	1.7298	0.0108	yes	2.0987	0.0050	yes
Cpm	2.0306	0.0143	yes	1.5734	0.0444	yes
Cpne2	2.0342	0.1807	no	1.8921	0.0531	no
Cpne5	0.1675	1.0000	no	0.7615	1.0000	no
Cpne7	-0.2280	0.9997	no	2.1949	0.0002	yes
Cpxm1	4.1013	0.0081	yes	-0.7000	1.0000	no
Crabp1	8.0000	1.0000	no	18.0000	1.0000	no
Crabp2	-1.5470	1.0000	no	0.1039	1.0000	no
Crb2	-3.5931	1.0000	no	0.9279	1.0000	no
Crb3	1.5644	1.0000	no	2.7104	0.0458	yes
Crhr1	0.0000	1.0000	no	0.0000	1.0000	no
Crim1	-0.3423	0.9997	no	1.5247	0.0886	no
Crlf1	0.4047	0.9997	no	-0.5774	0.5167	no
Crmp1	1.9446	1.0000	no	0.2140	1.0000	no
Crtac1	0.0000	1.0000	no	1.9445	1.0000	no
Crtc3	-0.1371	0.9997	no	1.6180	0.0145	yes
Cry1	0.5887	0.9084	no	2.3797	0.0032	yes
Csf1	1.8489	0.0097	yes	0.4873	0.3901	no
Csnk1e	0.5869	0.5265	no	1.5790	0.0007	yes
Csrnp1	2.0040	0.1412	no	2.1822	0.0168	yes
Csrnp2	0.2602	0.9997	no	1.4923	1.0000	no
Ctbp2	0.2650	0.9712	no	2.9912	0.0000	yes
Ctgf	0.8741	1.0000	no	1.2561	1.0000	no
Cthrc1	0.0000	1.0000	no	0.0000	1.0000	no
Ctnnbip1	0.7194	0.7974	no	1.8714	0.0171	yes
Ctnnd2	2.4294	1.0000	no	2.7907	1.0000	no
Ctsf	1.8404	0.0047	yes	-0.6375	0.4106	no
Cttnbp2	0.9718	0.6523	no	-0.9151	0.2493	no

Cttnbp2nl	1.4863	1.0000	no	0.5110	1.0000	no
Cuedc1	1.3938	0.9629	no	0.1918	1.0000	no
Cul9	3.3511	1.0000	no	1.6499	1.0000	no
Cux1	0.2090	0.7786	no	0.2731	0.3912	no
Cux2	2.1370	1.0000	no	1.6917	1.0000	no
Cwh43	0.0000	1.0000	no	0.0000	1.0000	no
Cx3cl1	8.0000	1.0000	no	-0.6569	1.0000	no
Cxcr4	3.2173	0.0000	yes	2.2734	0.0000	yes
Cxcr7	8.0000	0.0161	yes	1.5841	0.0869	no
Cxxc5	2.5949	0.0143	yes	1.5688	0.0760	no
Cyfip2	0.7774	0.1669	no	2.8330	0.0000	yes
Cygb	8.0000	1.0000	no	18.0000	1.0000	no
Cyp1b1	8.0000	1.0000	no	-12.0000	1.0000	no
Cyp26a1	1.3983	1.0000	no	0.2207	1.0000	no
Cyp27b1	1.8167	1.0000	no	18.0000	1.0000	no
Cyp46a1	8.0000	1.0000	no	18.0000	1.0000	no
Cyr61	1.3675	1.0000	no	0.8921	1.0000	no
Cys1	1.4682	1.0000	no	-0.1796	1.0000	no
D030025P21Rik	0.0000	1.0000	no	0.0000	1.0000	no
D18Ertd653e	3.1807	0.0016	yes	-0.8913	0.2620	no
D19Ertd652e	NA	NA	NA	NA	NA	NA
D430041D05Rik	2.6829	1.0000	no	-2.5392	1.0000	no
D430050G20	NA	NA	NA	NA	NA	NA
D630045J12Rik	-0.2173	0.9997	no	0.2366	1.0000	no
D730039F16Rik	3.2064	0.0113	yes	2.6553	0.0043	yes
D8Ertd82e	1.7580	1.0000	no	1.0652	1.0000	no
D930020B18Rik	0.0000	1.0000	no	18.0000	1.0000	no
D930020E02Rik	NA	NA	NA	NA	NA	NA
D930048N14Rik	0.7860	1.0000	no	-1.4855	1.0000	no
Dab1	0.0000	1.0000	no	-12.0000	1.0000	no
Dab2ip	1.1650	0.3243	no	1.4167	0.0789	no
Dact1	-0.4749	1.0000	no	2.1319	1.0000	no
Dact2	3.2133	0.0129	yes	1.0904	1.0000	no
Dag1	0.0782	0.9997	no	0.8873	0.1201	no
Dapk1	0.1836	0.9997	no	0.9484	0.0598	no
Dbn1	0.7265	0.8177	no	0.6815	0.4632	no
Dbndd1	0.1391	0.9997	no	1.4486	1.0000	no
Dbndd2	0.8466	0.9170	no	1.2323	0.3347	no
Dbx1	0.0000	1.0000	no	0.0000	1.0000	no
Dcbld2	1.0739	0.0792	no	0.2381	0.7187	no
Dcdc2a	-0.9868	1.0000	no	18.0000	1.0000	no
Dchs1	1.9015	1.0000	no	1.4078	1.0000	no
Dclk2	0.5673	0.6354	no	-0.8753	0.0602	no
Ddn	4.1283	1.0000	no	0.6681	1.0000	no
Ddr1	1.5021	1.0000	no	1.9542	0.0630	no
Ddx25	1.0233	1.0000	no	2.0135	1.0000	no
Ddx43	8.0000	1.0000	no	18.0000	1.0000	no
Dennd2a	0.9162	1.0000	no	1.0091	1.0000	no
Dennd5b	1.0991	0.5341	no	1.4429	0.0960	no

Depdc7	0.9134	0.8377	no	1.7240	0.0410	yes
Dgka	1.8713	0.1627	no	2.0198	0.0231	yes
Dgki	8.0000	1.0000	no	18.0000	1.0000	no
Dhh	0.7486	1.0000	no	1.5201	1.0000	no
Dio3	8.0000	1.0000	no	18.0000	1.0000	no
Dio3os	8.0000	1.0000	no	-0.0278	1.0000	no
Dip2b	0.1840	0.9997	no	1.6596	0.0001	yes
Dip2c	0.2585	0.9997	no	1.4076	0.0167	yes
Disc1	3.4843	1.0000	no	4.2891	1.0000	no
Dkkl1	-0.2626	0.9997	no	2.3977	0.0151	yes
Dleu7	8.0000	1.0000	no	18.0000	1.0000	no
Dlg5	1.9469	0.0001	yes	1.9344	0.0034	yes
Dlgap2	0.0000	1.0000	no	0.0000	1.0000	no
Dlgap3	8.0000	1.0000	no	0.9172	1.0000	no
Dlgap4	-0.0626	0.9997	no	1.8854	0.0002	yes
Dlk2	8.0000	1.0000	no	18.0000	1.0000	no
Dll1	0.0621	1.0000	no	1.6845	1.0000	no
Dll4	0.4796	1.0000	no	0.3641	1.0000	no
Dlx1	-0.2660	1.0000	no	-1.9234	1.0000	no
Dlx2	8.0000	1.0000	no	0.0000	1.0000	no
Dlx3	0.0000	1.0000	no	18.0000	1.0000	no
Dlx4	3.7887	1.0000	no	2.7738	1.0000	no
Dlx6	0.7034	1.0000	no	-1.0347	1.0000	no
Dlx6as	NA	NA	NA	NA	NA	NA
Dmbx1	0.0000	1.0000	no	0.0000	1.0000	no
Dmrt2	1.3605	1.0000	no	4.2172	1.0000	no
Dmrt3	0.0000	1.0000	no	0.0000	1.0000	no
Dmrta1	0.0000	1.0000	no	0.0000	1.0000	no
Dmrta2	0.0937	1.0000	no	-0.1300	1.0000	no
Dmrtc2	0.0000	1.0000	no	0.0000	1.0000	no
Dmxl2	1.3134	0.0554	no	1.9557	0.0269	yes
Dnajc22	2.3063	0.0533	no	1.2468	0.1888	no
Dnajc6	3.3482	0.0066	yes	4.7874	1.0000	no
Dnm1	2.1800	0.3126	no	2.3860	0.1202	no
Dnmt3a	0.0048	0.9997	no	1.6739	0.0000	yes
Dnmt3b	0.3188	0.8177	no	2.7483	0.0000	yes
Doc2a	-0.0220	0.9997	no	1.5921	0.0575	no
Doc2b	0.0000	1.0000	no	0.0000	1.0000	no
Dock1	2.1137	0.0532	no	1.4870	0.0915	no
Dock3	0.7218	0.9997	no	2.7948	1.0000	no
Dock4	0.7296	1.0000	no	0.6849	1.0000	no
Dock7	-0.8328	0.0090	yes	1.2092	0.0008	yes
Dock9	0.1852	0.9997	no	2.0971	0.0007	yes
Dok7	8.0000	1.0000	no	2.9407	0.1788	no
Dos	1.1065	0.2468	no	0.8649	0.2992	no
Dpf1	0.3186	0.9997	no	3.3442	0.1256	no
Dpysl5	8.0000	1.0000	no	2.3493	1.0000	no
Drd4	0.0000	1.0000	no	0.0000	1.0000	no
Dscam	0.0000	1.0000	no	0.0000	1.0000	no

Dse	1.0319	0.7139	no	0.4811	0.6515	no
Dsp	1.2842	0.3225	no	0.7622	0.3657	no
Dtx4	2.3751	0.0168	yes	2.6131	0.0009	yes
Duox2	0.0000	1.0000	no	0.0000	1.0000	no
Duoxa2	0.0000	1.0000	no	0.0000	1.0000	no
Dusp14	1.7215	1.0000	no	0.1402	1.0000	no
Dusp2	0.6291	0.9423	no	4.2346	0.0000	yes
Dusp22	1.3017	0.3822	no	0.5612	0.5744	no
Dusp4	0.6375	1.0000	no	0.9267	1.0000	no
Dusp5	1.9561	0.1601	no	1.3579	0.1536	no
Dyrk2	0.2931	0.9997	no	2.3439	0.0062	yes
Dzip1	-0.4744	0.9997	no	-0.6852	0.5150	no
E130012A19Rik	2.3801	0.0152	yes	3.5525	0.0000	yes
E130201H02Rik	0.1224	1.0000	no	-0.8858	1.0000	no
E330009J07Rik	1.3270	0.3792	no	2.1749	0.0087	yes
E330016A19Rik	1.9548	0.0001	yes	3.0848	0.0000	yes
E530011L22Rik	0.0389	1.0000	no	-12.0000	1.0000	no
Ebf1	8.0000	0.3747	no	2.3975	1.0000	no
Ebf2	-0.3993	1.0000	no	-0.6260	1.0000	no
Ebf3	0.0000	1.0000	no	0.0000	1.0000	no
Ebf4	8.0000	1.0000	no	18.0000	1.0000	no
Ece2	-0.3748	0.9824	no	1.7589	0.0348	yes
Ecel1	0.0000	1.0000	no	18.0000	1.0000	no
Echdc3	1.8078	0.1609	no	1.4306	0.1444	no
Efcab4a	0.4938	0.9811	no	1.3996	0.0444	yes
Efemp2	2.9436	0.0000	yes	0.8895	0.1831	no
Efhd1	0.0000	1.0000	no	18.0000	1.0000	no
Efna1	2.4067	0.3234	no	0.5263	1.0000	no
Efna2	2.0651	0.1968	no	18.0000	1.0000	no
Efna3	8.0000	1.0000	no	0.0000	1.0000	no
Efna5	0.6051	1.0000	no	18.0000	1.0000	no
Efnb2	0.1623	1.0000	no	0.3298	1.0000	no
Efr3b	1.3496	1.0000	no	1.9718	1.0000	no
Efs	3.2741	1.0000	no	3.4529	1.0000	no
EG434280	NA	NA	NA	NA	NA	NA
Egln3	3.4800	0.0022	yes	2.2322	0.0098	yes
Egr1	1.5278	0.2888	no	1.5380	0.0919	no
Egr2	0.0000	1.0000	no	18.0000	1.0000	no
Egr3	0.0000	1.0000	no	0.0000	1.0000	no
Egr4	0.0000	1.0000	no	0.0000	1.0000	no
Eid2	1.7417	0.2152	no	2.9716	0.0011	yes
Eif2c4	2.7680	1.0000	no	1.8211	1.0000	no
Eif4e3	1.8627	0.1857	no	1.9260	0.0296	yes
Elac1	0.2219	0.9997	no	1.8970	0.0316	yes
Elavl2	4.8993	0.0065	yes	4.0294	0.0332	yes
Elavl3	8.0000	1.0000	no	2.2930	1.0000	no
Elfn1	8.0000	1.0000	no	-0.4885	1.0000	no
Elk3	1.9374	0.0021	yes	1.6225	0.0001	yes
Elovl2	2.0498	0.0407	yes	0.6519	0.5094	no

Elovl3	1.5927	1.0000	no	18.0000	1.0000	no
Elovl4	8.0000	1.0000	no	0.0000	1.0000	no
Elovl7	2.4602	1.0000	no	2.3289	1.0000	no
Emid1	2.5455	0.0002	yes	2.6298	0.0001	yes
Eml1	-0.7154	0.9820	no	0.0360	1.0000	no
Eml5	0.2469	0.9997	no	1.1912	0.1644	no
Emx1	8.0000	1.0000	no	0.0000	1.0000	no
Emx2	0.0000	1.0000	no	0.0000	1.0000	no
Emx2os	0.7818	1.0000	no	-12.0000	1.0000	no
En1	0.0000	1.0000	no	0.0000	1.0000	no
En2	0.0000	1.0000	no	0.0000	1.0000	no
Enah	2.3184	1.0000	no	1.8074	0.0323	yes
Enc1	0.7998	0.8901	no	2.3743	0.0069	yes
Eno2	8.0000	1.0000	no	1.7556	1.0000	no
Enox1	0.0000	1.0000	no	0.0000	1.0000	no
Enpp1	-0.1097	0.9997	no	1.9152	0.0006	yes
Entpd4	-0.0912	0.9997	no	1.6106	0.0379	yes
Eomes	8.0000	1.0000	no	0.0000	1.0000	no
Epas1	1.3227	0.4872	no	1.3118	1.0000	no
Epb4.1l1	2.2951	0.0000	yes	0.1483	0.7511	no
Epb4.1l4a	0.8490	1.0000	no	1.5678	1.0000	no
Epb4.1l4b	1.7977	0.0097	yes	1.6482	0.0126	yes
Epcam	8.0000	1.0000	no	1.5767	1.0000	no
Epha2	3.5909	1.0000	no	1.4828	0.1714	no
Epha4	2.1914	1.0000	no	0.8214	1.0000	no
Epha7	1.5969	1.0000	no	2.4937	0.0470	yes
Epha8	2.8167	0.0077	yes	0.6262	0.5573	no
Ephb2	4.9048	1.0000	no	1.8752	1.0000	no
Ephb3	3.7660	0.0101	yes	3.1914	1.0000	no
Ephx4	8.0000	1.0000	no	18.0000	1.0000	no
Epn2	0.3558	0.9997	no	1.9752	0.0839	no
Eps8	2.0642	0.2393	no	1.7315	0.1949	no
Erbb2	2.7864	0.0460	yes	1.4735	1.0000	no
Erbb2ip	-0.2276	0.8686	no	0.7291	0.0565	no
Erbb3	0.9606	0.7931	no	1.6724	1.0000	no
Erbb4	0.0000	1.0000	no	-12.0000	1.0000	no
Errfi1	1.8551	0.1211	no	0.9337	0.2801	no
Esam	1.4420	0.3183	no	-0.0343	0.9746	no
Espn	0.9074	0.2672	no	2.5767	0.0505	no
Esr2	8.0000	1.0000	no	0.0000	1.0000	no
Esrp1	8.0000	1.0000	no	18.0000	1.0000	no
Esrp2	0.7775	0.8014	no	0.6624	0.4113	no
Esrrb	8.0000	1.0000	no	0.7907	1.0000	no
Etv4	0.8306	1.0000	no	0.0825	1.0000	no
Etv5	0.4720	0.9295	no	0.9924	0.1956	no
Evl	1.0389	0.0502	no	1.6757	0.0013	yes
Evx2	0.0000	1.0000	no	0.0000	1.0000	no
Exoc6b	0.6203	0.6625	no	-0.2786	0.7136	no
Extl1	1.9573	1.0000	no	-0.3496	1.0000	no

F2rl1	8.0000	1.0000	no	1.2963	1.0000	no
F730043M19Rik	1.0456	0.9342	no	-0.0252	1.0000	no
Fa2h	0.0000	1.0000	no	0.0000	1.0000	no
Faah	2.1369	0.0092	yes	2.3451	0.0002	yes
Fabp3	8.0000	0.0767	no	2.1390	1.0000	no
Fam101b	1.4641	0.2658	no	2.7994	0.0004	yes
Fam102a	1.8277	0.1620	no	1.7647	0.0853	no
Fam113b	0.4195	0.9997	no	-0.5441	0.5670	no
Fam114a1	1.7525	0.0865	no	0.5428	0.6037	no
Fam123a	-1.8491	1.0000	no	18.0000	1.0000	no
Fam131a	1.1835	0.5150	no	0.8712	0.3643	no
Fam131b	-6.0000	1.0000	no	1.2213	1.0000	no
Fam131c	-0.0014	1.0000	no	0.9460	1.0000	no
Fam135a	2.6503	0.0181	yes	2.7742	0.0014	yes
Fam150b	-0.1238	0.9997	no	-0.9156	0.3705	no
Fam159a	8.0000	1.0000	no	0.0000	1.0000	no
Fam163a	8.0000	1.0000	no	0.0000	1.0000	no
Fam169a	0.1077	0.9997	no	0.1666	0.8603	no
Fam171a1	1.5210	0.0243	yes	1.6520	0.0060	yes
Fam171a2	-0.4048	0.9997	no	1.4936	0.1831	no
Fam171b	1.0194	1.0000	no	18.0000	1.0000	no
Fam174b	1.9505	0.1069	no	3.4298	0.0001	yes
Fam176b	2.3269	0.0107	yes	0.8184	0.3328	no
Fam181b	8.0000	1.0000	no	-0.6599	1.0000	no
Fam184a	-1.5060	0.9308	no	3.1717	1.0000	no
Fam189a1	0.0000	1.0000	no	18.0000	1.0000	no
Fam189a2	8.0000	1.0000	no	1.3631	1.0000	no
Fam190a	0.0000	1.0000	no	0.0000	1.0000	no
Fam19a2	-0.9284	1.0000	no	-0.0548	1.0000	no
Fam19a3	0.0000	1.0000	no	0.0000	1.0000	no
Fam19a4	0.0000	1.0000	no	0.0000	1.0000	no
Fam19a5	0.0000	1.0000	no	18.0000	1.0000	no
Fam20c	3.8558	0.0000	yes	1.0038	0.2120	no
Fam43a	2.7316	0.0135	yes	2.1743	0.0132	yes
Fam43b	0.0000	1.0000	no	0.0000	1.0000	no
Fam46b	1.0657	1.0000	no	18.0000	1.0000	no
Fam49b	-0.0495	0.9997	no	1.5451	0.0210	yes
Fam57a	-0.2600	0.9845	no	1.8945	0.0013	yes
Fam59b	8.0000	1.0000	no	18.0000	1.0000	no
Fam65a	-0.0995	0.9997	no	2.6595	0.0002	yes
Fam65b	0.2990	0.9920	no	1.8445	0.0003	yes
Fam69b	0.6716	0.9683	no	2.4825	0.0675	no
Fam69c	0.0000	1.0000	no	0.0000	1.0000	no
Fam78b	1.6573	1.0000	no	1.8097	1.0000	no
Fam83f	8.0000	1.0000	no	1.3062	1.0000	no
Fam83h	2.6140	1.0000	no	1.9878	1.0000	no
Fam89a	1.1105	0.7861	no	3.4641	0.0143	yes
Farp1	1.0028	0.6523	no	0.3713	0.7185	no
Fblim1	0.5839	1.0000	no	0.3839	0.8437	no

Fbll1	0.0000	1.0000	no	0.0000	1.0000	no
Fbn1	1.8584	1.0000	no	0.6060	1.0000	no
Fbxl16	8.0000	1.0000	no	18.0000	1.0000	no
Fbxo43	8.0000	1.0000	no	0.0085	1.0000	no
Fdx1	0.1013	0.9997	no	1.5778	0.0773	no
Fermt2	2.0704	0.0147	yes	0.6671	0.3615	no
Fes	2.9064	0.0001	yes	2.3447	0.0005	yes
Fev	0.0000	1.0000	no	0.0000	1.0000	no
Fgd1	1.2668	0.4031	no	0.6558	0.4877	no
Fgf11	3.1112	0.0034	yes	1.6377	1.0000	no
Fgf12	0.0000	1.0000	no	18.0000	1.0000	no
Fgf15	4.0343	1.0000	no	18.0000	1.0000	no
Fgf16	0.0000	1.0000	no	0.0000	1.0000	no
Fgf17	8.0000	1.0000	no	0.0000	1.0000	no
Fgf18	-6.0000	1.0000	no	18.0000	1.0000	no
Fgf2	-0.3703	0.9997	no	0.8802	1.0000	no
Fgf3	2.8168	1.0000	no	0.2973	0.8215	no
Fgf4	0.0000	1.0000	no	0.0000	1.0000	no
Fgf8	8.0000	1.0000	no	0.0000	1.0000	no
Fgf9	8.0000	1.0000	no	0.0000	1.0000	no
Fgfr1	1.6764	1.0000	no	3.4545	0.0119	yes
Fgfr3	1.4421	0.1013	no	1.6970	0.0431	yes
Fgfr4	3.7679	0.0005	yes	1.6611	0.2195	no
Fhdc1	1.1371	0.0029	yes	-0.9610	0.0006	yes
Fhl3	1.8448	0.0082	yes	2.1825	0.0001	yes
Fhod1	0.4079	0.9303	no	1.7417	0.0061	yes
Fhod3	-0.4220	0.9997	no	0.6563	1.0000	no
Fibcd1	8.0000	1.0000	no	18.0000	1.0000	no
Fign	-1.1713	1.0000	no	0.5376	1.0000	no
Filip1l	1.8140	0.1412	no	0.7458	0.4566	no
Fjx1	2.8898	0.0253	yes	2.3931	1.0000	no
Fkbp1b	1.6595	0.3119	no	2.5911	0.0103	yes
Fkbp5	0.1962	0.9997	no	1.8020	0.0011	yes
Fkbp9	0.5747	0.7772	no	1.6070	0.0500	no
Fli1	2.4666	0.0126	yes	1.8288	0.0268	yes
Flnc	0.9046	1.0000	no	1.5063	1.0000	no
Flt1	2.2184	0.0611	no	1.1344	0.1329	no
Flt3	2.4677	0.0032	yes	2.5867	0.0000	yes
Flt4	1.3876	0.3618	no	0.9383	0.3338	no
Fmnl1	2.6611	0.0000	yes	2.9821	0.0000	yes
Fmnl2	1.5884	0.0417	yes	1.1289	0.0611	no
Fmnl3	1.8767	0.0048	yes	1.6764	0.0002	yes
Fn1	2.4044	0.0000	yes	1.3974	0.0014	yes
Fnbp1	0.2701	0.9842	no	1.7435	0.0001	yes
Fnbp1l	1.1484	0.5280	no	1.4548	0.0952	no
Fndc3a	0.7277	0.3166	no	1.4720	0.0231	yes
Fndc3b	1.7151	0.1149	no	1.8449	0.0234	yes
Fndc4	2.3233	0.0054	yes	3.4144	0.0000	yes
Fndc5	1.4190	0.3881	no	0.9318	0.3497	no

Fndc8	0.2414	1.0000	no	0.9549	1.0000	no
Fosl1	0.2035	1.0000	no	1.5141	1.0000	no
Fosl2	2.7235	0.0161	yes	1.7721	0.0439	yes
Foxa1	2.1064	1.0000	no	1.2893	1.0000	no
Foxb1	0.0000	1.0000	no	0.0000	1.0000	no
Foxb2	0.0000	1.0000	no	0.0000	1.0000	no
Foxc1	8.0000	1.0000	no	18.0000	1.0000	no
Foxc2	-6.0000	1.0000	no	0.0000	1.0000	no
Foxd1	8.0000	1.0000	no	18.0000	1.0000	no
Foxd2	1.6850	1.0000	no	18.0000	1.0000	no
Foxd3	0.0000	1.0000	no	0.0000	1.0000	no
Foxd4	0.0000	1.0000	no	0.0000	1.0000	no
Foxe1	8.0000	1.0000	no	-12.0000	1.0000	no
Foxe3	0.0000	1.0000	no	0.0000	1.0000	no
Foxf1a	8.0000	1.0000	no	18.0000	1.0000	no
Foxf2	0.0000	1.0000	no	0.0000	1.0000	no
Foxg1	0.0000	1.0000	no	0.0000	1.0000	no
Foxi3	0.0000	1.0000	no	0.0000	1.0000	no
Foxj1	1.7263	1.0000	no	0.6135	1.0000	no
Foxl1	0.0000	1.0000	no	0.0000	1.0000	no
Foxl2	0.0000	1.0000	no	0.0000	1.0000	no
Foxl2os	0.0000	1.0000	no	0.0000	1.0000	no
Foxo1	0.6403	0.9558	no	2.3570	0.0059	yes
Foxo6	8.0000	1.0000	no	0.0000	1.0000	no
Foxp4	0.2062	0.9758	no	1.9211	0.0003	yes
Foxq1	8.0000	1.0000	no	18.0000	1.0000	no
Fras1	1.6098	1.0000	no	-0.7451	1.0000	no
Frem3	-2.1621	1.0000	no	-12.0000	1.0000	no
Frmd4a	0.8363	0.0005	yes	-0.5591	0.1022	no
Frmd5	0.5080	0.9712	no	0.9844	1.0000	no
Frmpd1	-0.5392	0.9997	no	1.0702	1.0000	no
Frs3	0.5636	0.9985	no	0.3004	1.0000	no
Frzb	8.0000	1.0000	no	-0.0475	1.0000	no
Fscn1	2.5962	0.0000	yes	1.5619	0.0019	yes
Fsd1l	0.1886	0.9997	no	1.1654	0.3189	no
Fst	1.5769	1.0000	no	1.9421	1.0000	no
Fstl4	0.0000	1.0000	no	0.0000	1.0000	no
Furin	1.8362	0.0002	yes	1.7415	0.0014	yes
Fzd1	2.1747	1.0000	no	-0.0099	1.0000	no
Fzd2	-6.0000	1.0000	no	1.8947	1.0000	no
Fzd3	-0.1572	1.0000	no	18.0000	0.0959	no
Fzd4	1.9947	1.0000	no	0.6686	1.0000	no
Fzd6	1.8315	0.1393	no	2.2990	0.0123	yes
Fzd8	1.3007	0.5354	no	2.5207	0.0080	yes
Fzd9	1.7934	1.0000	no	4.3743	1.0000	no
G530011O06Rik	0.6038	0.9971	no	0.4919	0.6797	no
G630025P09Rik	NA	NA	NA	NA	NA	NA
G6b	NA	NA	NA	NA	NA	NA
Gab1	-0.3651	0.7758	no	-0.0045	0.9960	no

Gabbr1	2.2689	0.0599	no	2.3071	0.0716	no
Gabbr2	-6.0000	1.0000	no	-0.0570	1.0000	no
Gabrb3	0.0000	1.0000	no	0.0000	1.0000	no
Gad1	0.0000	1.0000	no	0.0000	1.0000	no
Gad2	-1.1985	1.0000	no	-3.6398	1.0000	no
Gadd45b	2.8959	0.0241	yes	2.6836	0.0044	yes
Galnt12	3.3468	0.0062	yes	2.9104	0.0030	yes
Galnt3	2.8044	0.2811	no	2.7563	0.0220	yes
Galnt6	2.0290	0.0378	yes	1.3473	0.0509	no
Galntl1	8.0000	1.0000	no	0.0000	1.0000	no
Galr2	-0.5520	1.0000	no	2.2424	1.0000	no
Galr3	NA	NA	NA	NA	NA	NA
Gapdh	-0.1986	0.9637	no	0.8562	0.1583	no
Gas1	0.0940	1.0000	no	2.2975	1.0000	no
Gas6	2.7965	0.0147	yes	1.0357	0.2836	no
Gata2	2.2535	0.0013	yes	2.0430	0.0001	yes
Gata3	3.2781	0.0497	yes	4.2186	0.0257	yes
Gata4	1.5717	0.1285	no	0.1262	0.8918	no
Gata5	1.7700	1.0000	no	18.0000	1.0000	no
Gata6	1.7324	0.2544	no	1.0401	1.0000	no
Gbx1	2.0679	1.0000	no	18.0000	1.0000	no
Gbx2	4.1281	0.0013	yes	3.2604	1.0000	no
Gcgr	2.0446	0.0129	yes	0.8126	0.2218	no
Gcnt4	1.6986	1.0000	no	3.3227	1.0000	no
Gdf10	1.2859	1.0000	no	0.8628	1.0000	no
Gdf11	2.4184	1.0000	no	2.9519	1.0000	no
Gdf6	0.0000	1.0000	no	0.0000	1.0000	no
Gdf7	0.0000	1.0000	no	0.0000	1.0000	no
Gdnf	0.0000	1.0000	no	0.0000	1.0000	no
Gdpd5	0.3203	1.0000	no	0.7731	1.0000	no
Gfi1	2.8568	0.0000	yes	2.8741	0.0000	yes
Gfod1	1.4662	0.3099	no	1.6780	0.0563	no
Gfra1	1.5823	0.4105	no	1.7826	0.0790	no
Gfra3	0.0000	1.0000	no	0.0000	1.0000	no
Gfra4	0.0000	1.0000	no	2.3992	1.0000	no
Ggn	2.7161	1.0000	no	2.0529	1.0000	no
Ggt7	0.4089	0.9997	no	1.3398	1.0000	no
Gipc2	1.3412	0.3475	no	0.7879	0.4441	no
Gipc3	8.0000	1.0000	no	18.0000	1.0000	no
Gja3	0.0000	1.0000	no	0.0000	1.0000	no
Gjb2	-0.2928	0.9997	no	2.9885	0.0007	yes
Gjc1	8.0000	1.0000	no	18.0000	1.0000	no
Gjd3	0.0000	1.0000	no	0.0000	1.0000	no
Gkap1	1.2831	0.2114	no	3.3646	0.0000	yes
Gldc	2.0056	0.0144	yes	1.2631	0.0528	no
Gli1	-3.7740	1.0000	no	1.2532	1.0000	no
Gli3	-0.9276	1.0000	no	1.0196	1.0000	no
Glis1	-0.0107	0.9997	no	0.8309	1.0000	no
Glis2	2.5989	0.0382	yes	1.5098	0.1164	no

Glis3	1.6829	1.0000	no	3.7649	0.0098	yes
Gls2	1.4270	0.0045	yes	3.6538	0.0043	yes
Glt25d2	0.8518	1.0000	no	0.5499	1.0000	no
Gm10125	-0.3848	1.0000	no	0.5557	1.0000	no
Gm10190	0.0000	1.0000	no	0.0000	1.0000	no
Gm10345	0.4401	1.0000	no	0.3926	1.0000	no
Gm10406	8.0000	1.0000	no	18.0000	1.0000	no
Gm106	8.0000	1.0000	no	-0.0234	1.0000	no
Gm11190	0.0000	1.0000	no	0.0000	1.0000	no
Gm11529	0.0000	1.0000	no	0.0000	1.0000	no
Gm12824	8.0000	1.0000	no	18.0000	1.0000	no
Gm1337	3.9180	1.0000	no	2.7957	1.0000	no
Gm13889	-6.0000	1.0000	no	18.0000	1.0000	no
Gm14207	0.8807	1.0000	no	1.8452	1.0000	no
Gm1564	2.3978	1.0000	no	-2.3013	1.0000	no
Gm1568	8.0000	1.0000	no	18.0000	1.0000	no
Gm1673	1.4507	0.7035	no	0.7927	0.5215	no
Gm266	8.0000	1.0000	no	18.0000	1.0000	no
Gm2694	0.8671	1.0000	no	-0.6172	1.0000	no
Gm3230	NA	NA	NA	NA	NA	NA
Gm347	NA	NA	NA	NA	NA	NA
Gm4349	-0.4259	0.9997	no	0.9909	0.3256	no
Gm4980	-6.0000	1.0000	no	0.0000	1.0000	no
Gm5577	0.0871	0.9997	no	0.7750	0.4109	no
Gm581	NA	NA	NA	NA	NA	NA
Gm628	0.0000	1.0000	no	0.0000	1.0000	no
Gm6320	0.0000	1.0000	no	0.0000	1.0000	no
Gm6623	0.0000	1.0000	no	0.0000	1.0000	no
Gm6762	-0.8698	1.0000	no	0.1645	1.0000	no
Gm70	NA	NA	NA	NA	NA	NA
Gm7854	-6.0000	1.0000	no	18.0000	1.0000	no
Gm88	-0.1448	1.0000	no	-1.8602	1.0000	no
Gm8909	-4.2846	1.0000	no	2.3879	1.0000	no
Gm9880	NA	NA	NA	NA	NA	NA
Gm996	3.3685	1.0000	no	18.0000	1.0000	no
Gnai1	1.3395	1.0000	no	-0.3419	1.0000	no
Gnal	0.1653	0.9997	no	-1.2479	0.0807	no
Gnao1	-0.2796	1.0000	no	-0.1584	1.0000	no
Gnaq	1.5973	0.1334	no	2.0913	0.0088	yes
Gnas	-0.0298	0.9997	no	-0.1809	0.5450	no
Gnb4	-0.1719	0.9997	no	1.9766	0.0001	yes
Gng12	0.5833	0.3687	no	1.8623	0.0000	yes
Gng8	0.0000	1.0000	no	0.0000	1.0000	no
Gp1bb	1.5902	0.2444	no	0.2245	0.8351	no
Gp5	0.7013	0.9404	no	1.3602	0.1401	no
Gpc1	2.7434	0.0050	yes	2.5735	0.0011	yes
Gpr124	1.3749	0.4353	no	1.4170	0.1245	no
Gpr135	0.0558	1.0000	no	18.0000	1.0000	no
Gpr137c	0.0873	1.0000	no	-1.5963	1.0000	no

Gpr153	2.6975	1.0000	no	-0.9704	1.0000	no
Gpr156	0.0000	1.0000	no	0.0000	1.0000	no
Gpr160	2.0931	0.0049	yes	2.4611	0.0000	yes
Gpr162	8.0000	1.0000	no	1.5187	1.0000	no
Gpr176	0.6183	1.0000	no	18.0000	1.0000	no
Gpr25	8.0000	1.0000	no	0.0000	1.0000	no
Gpr27	8.0000	1.0000	no	18.0000	1.0000	no
Gpr3	8.0000	1.0000	no	0.0000	1.0000	no
Gpr4	2.1941	1.0000	no	1.4155	1.0000	no
Gpr45	0.0000	1.0000	no	0.0000	1.0000	no
Gpr6	0.0000	1.0000	no	0.0000	1.0000	no
Gpr62	8.0000	1.0000	no	0.0000	1.0000	no
Gpr88	0.0000	1.0000	no	18.0000	1.0000	no
Gpr98	3.9044	0.3786	no	1.2113	1.0000	no
Gprc5b	3.9329	1.0000	no	1.0579	1.0000	no
Gprc5c	1.5502	0.2028	no	1.1205	0.2133	no
Gprin1	8.0000	1.0000	no	18.0000	1.0000	no
Gpt2	0.6431	0.7822	no	1.8216	0.0039	yes
Gpx7	1.6300	1.0000	no	1.6008	0.1250	no
Grasp	3.2348	1.0000	no	2.3821	1.0000	no
Grb10	-0.0584	0.9997	no	1.0829	0.0032	yes
Greb1	3.2152	1.0000	no	2.1562	1.0000	no
Greb1l	0.5160	1.0000	no	0.3973	1.0000	no
Grhl1	0.3755	0.9971	no	-0.8204	0.2346	no
Grhl2	8.0000	1.0000	no	18.0000	1.0000	no
Grid1	1.0260	1.0000	no	-12.0000	1.0000	no
Grid2	0.0000	1.0000	no	0.0000	1.0000	no
Grik3	0.0000	1.0000	no	0.0000	1.0000	no
Grik4	3.5965	1.0000	no	0.2003	1.0000	no
Grin2c	8.0000	1.0000	no	18.0000	1.0000	no
Grin2d	1.9573	1.0000	no	-12.0000	1.0000	no
Grin3b	0.5474	0.9497	no	-0.7972	1.0000	no
Grip1	0.6912	1.0000	no	1.7205	1.0000	no
Grm8	8.0000	1.0000	no	0.0000	1.0000	no
Grwd1	-0.1244	0.9997	no	2.4230	0.0000	yes
Gsc	0.0000	1.0000	no	0.0000	1.0000	no
Gsc2	8.0000	1.0000	no	18.0000	1.0000	no
Gsg1l	1.6106	1.0000	no	0.9441	1.0000	no
Gstt3	1.4260	0.2615	no	2.2659	0.0124	yes
Gsx1	0.0000	1.0000	no	0.0000	1.0000	no
Gsx2	0.0000	1.0000	no	0.0000	1.0000	no
Gucy2e	8.0000	1.0000	no	18.0000	1.0000	no
Gxylt2	8.0000	1.0000	no	-12.0000	1.0000	no
H1f0	1.2117	0.0127	yes	1.8792	0.0086	yes
H1fx	2.1168	0.1235	no	2.0259	0.0323	yes
H2-Bl	0.3436	0.9997	no	1.5102	0.1403	no
H2-K1	0.5388	0.1972	no	1.5929	0.0000	yes
H2-Q10	2.2411	0.0010	yes	0.8336	0.2607	no
H2-Q6	0.8477	0.6669	no	1.8569	0.0145	yes

H2-Q7	1.9352	0.0090	yes	1.2614	0.0325	yes
H2-Q8	NA	NA	NA	NA	NA	NA
H2afy2	2.9113	0.0041	yes	2.6767	0.0048	yes
Hand1	0.0000	1.0000	no	18.0000	1.0000	no
Hand2	1.5263	1.0000	no	0.3415	1.0000	no
Hap1	2.1317	1.0000	no	1.1038	1.0000	no
Hapln4	0.0659	1.0000	no	18.0000	1.0000	no
Has3	-0.2533	0.9997	no	0.9265	0.2980	no
Hbegf	0.4267	1.0000	no	1.8204	0.0712	no
Hcn2	1.9478	0.0527	no	3.0355	0.0109	yes
Hcn3	-0.2907	0.8484	no	-0.5800	0.4643	no
Hcn4	0.0000	1.0000	no	18.0000	1.0000	no
Hcrtr1	-6.0000	1.0000	no	0.0000	1.0000	no
Hdac5	0.6630	0.0282	yes	0.2712	0.3876	no
Hdgfrp3	3.0959	0.0024	yes	2.2861	0.0054	yes
Hectd2	2.3139	0.0067	yes	0.6875	1.0000	no
Hecw2	0.1726	1.0000	no	3.7687	0.0024	yes
Hes1	2.0193	0.0982	no	0.8145	0.4120	no
Hes2	-6.0000	1.0000	no	18.0000	1.0000	no
Hes5	-1.5552	1.0000	no	18.0000	1.0000	no
Hes7	0.0573	1.0000	no	0.9209	1.0000	no
Hey1	0.3264	1.0000	no	-0.0183	1.0000	no
Hey2	3.8556	1.0000	no	-0.0496	0.9707	no
Heyl	2.8413	1.0000	no	18.0000	1.0000	no
Hhex	1.4071	0.1037	no	1.6008	0.0103	yes
Hic1	1.9398	1.0000	no	1.5057	1.0000	no
Hip1r	0.3744	0.8500	no	1.8619	0.0001	yes
Hivep2	2.2428	1.0000	no	0.5462	1.0000	no
Hivep3	1.7742	0.4474	no	1.8628	0.0834	no
Hlx	1.8789	0.1659	no	2.5491	0.0054	yes
Hmga2	2.4101	0.0004	yes	2.6082	0.0003	yes
Hmox1	1.5360	0.0000	yes	0.4458	0.3295	no
Hmx1	0.0000	1.0000	no	0.0000	1.0000	no
Hmx2	0.0000	1.0000	no	18.0000	1.0000	no
Hmx3	0.0000	1.0000	no	0.0000	1.0000	no
Hnf1b	1.6167	1.0000	no	2.2791	1.0000	no
Homer2	0.6837	0.5634	no	1.1800	0.1652	no
Homer3	0.1550	0.9997	no	1.1183	0.0175	yes
Hopx	0.9217	0.8245	no	3.5247	0.0028	yes
Hoxa10	8.0000	1.0000	no	0.2655	1.0000	no
Hoxa11	0.0000	1.0000	no	0.0000	1.0000	no
Hoxa11as	0.0000	1.0000	no	0.0000	1.0000	no
Hoxa13	0.0000	1.0000	no	0.0000	1.0000	no
Hoxa2	0.1766	1.0000	no	18.0000	1.0000	no
Hoxa3	0.0000	1.0000	no	0.0000	1.0000	no
Hoxa4	2.4780	1.0000	no	0.4354	1.0000	no
Hoxa5	2.8105	1.0000	no	2.6323	1.0000	no
Hoxa6	8.0000	1.0000	no	18.0000	1.0000	no
Hoxa7	8.0000	1.0000	no	2.9994	0.2412	no

Hoxa9	1.7187	0.6282	no	2.9284	0.0311	yes
Hoxb13	8.0000	1.0000	no	0.0000	1.0000	no
Hoxb4	2.0444	1.0000	no	1.4615	1.0000	no
Hoxb6	8.0000	1.0000	no	0.0000	1.0000	no
Hoxb7	8.0000	1.0000	no	0.0000	1.0000	no
Hoxb8	0.0000	1.0000	no	0.0000	1.0000	no
Hoxb9	0.0000	1.0000	no	18.0000	1.0000	no
Hoxc10	0.0000	1.0000	no	0.0000	1.0000	no
Hoxc12	0.0000	1.0000	no	0.0000	1.0000	no
Hoxc13	0.0000	1.0000	no	0.0000	1.0000	no
Hoxc5	0.0000	1.0000	no	18.0000	1.0000	no
Hoxc6	0.0148	1.0000	no	0.0000	1.0000	no
Hoxc8	0.0000	1.0000	no	0.0000	1.0000	no
Hoxc9	0.0000	1.0000	no	0.0000	1.0000	no
Hoxd1	0.0000	1.0000	no	0.0000	1.0000	no
Hoxd10	0.0000	1.0000	no	0.0000	1.0000	no
Hoxd11	0.0000	1.0000	no	0.0000	1.0000	no
Hoxd13	0.0000	1.0000	no	0.0000	1.0000	no
Hoxd8	0.0000	1.0000	no	0.0000	1.0000	no
Hoxd9	0.0000	1.0000	no	0.0000	1.0000	no
Hpca	8.0000	1.0000	no	-0.6571	1.0000	no
Hpcal4	0.0000	1.0000	no	0.0000	1.0000	no
Hpdl	0.2382	0.9997	no	3.3819	0.0171	yes
Hr	0.0078	1.0000	no	1.6531	1.0000	no
Hrh3	0.0000	1.0000	no	0.0000	1.0000	no
Hrk	0.0000	1.0000	no	0.0000	1.0000	no
Hs3st3b1	2.6672	0.0100	yes	1.2946	0.1619	no
Hs3st6	0.0000	1.0000	no	-12.0000	1.0000	no
Hs6st3	0.0000	1.0000	no	18.0000	1.0000	no
Hsd11b2	-0.0909	0.9997	no	1.0885	1.0000	no
Hsd17b1	3.4726	1.0000	no	2.8499	0.0192	yes
Hsf4	8.0000	1.0000	no	18.0000	1.0000	no
Hsf5	-6.0000	1.0000	no	-12.0000	1.0000	no
Hspa1a	1.8942	0.1157	no	2.7033	0.0014	yes
Hspa1b	1.8999	0.0497	yes	2.9063	0.0000	yes
Hspa1l	0.0161	0.9997	no	0.7307	0.4840	no
Hspa2	0.3270	0.9997	no	2.1165	0.0171	yes
Hspb1	8.0000	1.0000	no	18.0000	1.0000	no
Htr1d	0.0000	1.0000	no	0.0000	1.0000	no
Htr6	-6.0000	1.0000	no	0.0000	1.0000	no
Htr7	8.0000	1.0000	no	0.0000	1.0000	no
Htra1	0.0000	1.0000	no	-12.0000	1.0000	no
Htra4	-6.0000	1.0000	no	0.0000	1.0000	no
Hunk	1.4707	1.0000	no	1.3300	1.0000	no
Ica1	1.8396	0.0226	yes	1.3867	0.0081	yes
Ica1l	-0.1905	0.9997	no	4.0501	1.0000	no
Icam1	1.9076	0.0856	no	1.1201	0.2145	no
Icam5	0.4960	0.9997	no	-0.3747	0.7467	no
Id1	0.8523	0.6906	no	1.2047	0.1501	no

Id2	2.2498	0.0115	yes	1.4370	0.0692	no
Id3	2.2034	0.0274	yes	1.6559	0.0318	yes
Id4	8.0000	1.0000	no	0.0000	1.0000	no
Ier5l	1.2996	1.0000	no	1.8668	1.0000	no
Iffo2	1.5582	0.0753	no	0.8216	1.0000	no
Igdcc3	8.0000	1.0000	no	18.0000	1.0000	no
Igdcc4	2.0365	0.0679	no	1.3932	0.1157	no
Igf2	2.2370	0.0000	yes	1.1456	0.0001	yes
Igf2as	1.3007	0.9682	no	1.6302	0.1353	no
Igf2bp2	2.0663	0.0002	yes	3.0246	0.0000	yes
Igfbp2	2.5640	1.0000	no	-0.0377	1.0000	no
Igfbp4	2.2986	0.0000	yes	1.8797	0.0000	yes
Igfbp5	0.9743	1.0000	no	0.4923	1.0000	no
Igfbp6	8.0000	1.0000	no	1.9305	1.0000	no
Igfbp7	2.3103	0.0094	yes	0.8022	0.4515	no
Igsf11	8.0000	1.0000	no	18.0000	1.0000	no
Igsf9	0.1586	1.0000	no	2.7604	0.4515	no
Ihh	1.5857	1.0000	no	0.1548	1.0000	no
Ikzf3	0.3518	1.0000	no	2.7863	1.0000	no
Il11	0.2673	1.0000	no	0.0000	1.0000	no
Il17d	0.1355	1.0000	no	-0.2507	1.0000	no
Il17ra	0.4624	0.7883	no	1.0534	0.1627	no
Il17rd	0.8739	1.0000	no	-1.4400	1.0000	no
Il20ra	3.1992	1.0000	no	3.4704	1.0000	no
Il28ra	8.0000	1.0000	no	18.0000	1.0000	no
Il6ra	1.7809	0.1383	no	1.7342	0.0362	yes
Il6st	1.7451	0.1358	no	1.4661	0.0980	no
Ildr2	8.0000	1.0000	no	-12.0000	1.0000	no
Impdh1	0.1968	0.9997	no	2.7946	0.0000	yes
Ina	0.0590	1.0000	no	18.0000	1.0000	no
Inadl	0.6413	0.8874	no	1.2472	0.3140	no
Inf2	1.0044	0.2467	no	1.9518	0.0009	yes
Inhbb	1.6591	1.0000	no	0.7098	1.0000	no
Inppl1	1.7884	0.0390	yes	1.7313	0.0148	yes
Insl3	1.9400	0.7855	no	1.1422	0.4913	no
Insm1	0.0000	1.0000	no	0.0000	1.0000	no
Insm2	0.0000	1.0000	no	18.0000	1.0000	no
Insrr	0.0000	1.0000	no	0.0000	1.0000	no
Iqsec3	0.0000	1.0000	no	0.0000	1.0000	no
Irak3	2.0847	0.0016	yes	2.0928	0.0000	yes
Irf1	1.8716	0.0006	yes	1.4648	0.0106	yes
Irf5	-0.0612	0.9997	no	0.7485	0.2714	no
Irf6	3.0379	0.0587	no	1.8511	0.2414	no
Irs1	1.2480	1.0000	no	0.7931	1.0000	no
Irx2	8.0000	1.0000	no	0.0000	1.0000	no
Irx3	8.0000	1.0000	no	18.0000	1.0000	no
Irx4	8.0000	1.0000	no	0.0000	1.0000	no
Irx5	0.0000	1.0000	no	-0.0547	1.0000	no
Isl2	0.0000	1.0000	no	0.0000	1.0000	no

Islr2	-2.1876	1.0000	no	2.1534	1.0000	no
Ism1	0.0000	1.0000	no	18.0000	1.0000	no
Itga1	2.1640	0.0775	no	0.9202	0.3431	no
Itga3	-0.0786	0.9997	no	1.7512	1.0000	no
Itga5	0.7481	0.3535	no	2.1033	0.0042	yes
Itga6	0.8993	0.1798	no	1.7869	0.0001	yes
Itga9	1.5118	0.0228	yes	1.8398	0.0003	yes
Itgav	1.5785	0.0671	no	1.6244	0.0093	yes
Itgb4	3.0298	1.0000	no	0.7211	1.0000	no
Itgb5	1.5012	0.0602	no	1.1410	0.0505	no
Itpka	1.3578	0.4784	no	1.1196	0.2620	no
Itpr2	0.2650	0.9997	no	0.7596	0.3224	no
Itpr3	2.0819	0.0495	yes	2.1198	0.0091	yes
Itpripl2	2.0800	0.1132	no	1.5587	0.0993	no
Itsn1	1.6470	0.0000	yes	-0.7557	0.0162	yes
Jag1	1.0431	1.0000	no	1.7284	1.0000	no
Jag2	1.5450	1.0000	no	4.5636	0.0008	yes
Jakmip3	-6.0000	1.0000	no	18.0000	1.0000	no
Jazf1	8.0000	1.0000	no	1.3234	1.0000	no
Jdp2	2.6522	0.0245	yes	1.7619	0.0190	yes
Jmjd1c	-0.4714	0.2138	no	1.2575	0.0007	yes
Jph1	2.6431	1.0000	no	18.0000	1.0000	no
Jph3	0.6257	1.0000	no	18.0000	1.0000	no
Jph4	8.0000	1.0000	no	18.0000	1.0000	no
Jub	1.3260	0.5149	no	0.9259	0.3580	no
Jun	2.4242	0.0002	yes	2.5048	0.0000	yes
Kank1	1.1448	0.2735	no	1.0696	0.0960	no
Kank4	8.0000	1.0000	no	0.0000	1.0000	no
Kazald1	0.4670	1.0000	no	0.2549	1.0000	no
Kbtbd13	0.0000	1.0000	no	18.0000	1.0000	no
Kcna3	3.0789	1.0000	no	2.5677	1.0000	no
Kcna7	8.0000	1.0000	no	0.0000	1.0000	no
Kcnb1	8.0000	1.0000	no	18.0000	1.0000	no
Kcnc1	0.0000	1.0000	no	2.3765	1.0000	no
Kcnc3	3.0919	1.0000	no	18.0000	1.0000	no
Kcnc4	0.0000	1.0000	no	0.0000	1.0000	no
Kcnd3	0.0115	1.0000	no	-12.0000	1.0000	no
Kcng2	1.0178	0.7858	no	4.6252	0.0145	yes
Kcng3	8.0000	1.0000	no	18.0000	1.0000	no
Kcnh2	6.0356	0.0035	yes	1.3807	1.0000	no
Kcnh3	2.8024	1.0000	no	2.8996	1.0000	no
Kcnh4	0.0257	1.0000	no	18.0000	1.0000	no
Kcnip2	-0.3117	0.9727	no	-1.2285	0.0300	yes
Kcnip3	1.8240	1.0000	no	2.1920	1.0000	no
Kcnj2	2.5021	1.0000	no	2.4636	1.0000	no
Kcnj4	0.0000	1.0000	no	0.0000	1.0000	no
Kcnk12	5.1330	0.0161	yes	2.4416	0.0110	yes
Kcnk13	1.5043	1.0000	no	0.9338	1.0000	no
Kcnk3	8.0000	1.0000	no	0.0000	1.0000	no

Kcnk4	8.0000	1.0000	no	-0.0649	1.0000	no
Kcnk6	1.6538	0.1313	no	0.9103	0.3402	no
Kcnk9	0.0000	1.0000	no	0.0000	1.0000	no
Kcnma1	0.0000	1.0000	no	0.0000	1.0000	no
Kcnmb4	1.7573	0.1966	no	0.7230	0.7185	no
Kcnq1	0.0117	1.0000	no	18.0000	1.0000	no
Kcnq2	-1.1785	0.5002	no	-0.1830	1.0000	no
Kcnq4	0.3684	1.0000	no	18.0000	1.0000	no
Kcnq5	0.9319	1.0000	no	3.5543	1.0000	no
Kcns3	0.1111	1.0000	no	-12.0000	1.0000	no
Kcnt1	0.0000	1.0000	no	0.0000	1.0000	no
Kcp	5.0391	0.0000	yes	2.1191	0.0960	no
Kctd1	1.9679	0.0116	yes	3.4217	0.0001	yes
Kctd12	2.1166	0.0243	yes	1.3105	0.1052	no
Kctd17	2.4995	0.0094	yes	1.1316	0.1221	no
Kdelc2	1.7708	0.2158	no	1.8636	0.0379	yes
Kdelr3	3.2233	0.0223	yes	2.4470	0.0277	yes
Kdr	2.0588	0.0301	yes	0.5848	0.5314	no
Kif13a	-0.0240	0.9997	no	2.3497	0.0000	yes
Kif17	2.6664	1.0000	no	1.5078	1.0000	no
Kif1b	0.7713	0.2035	no	1.6513	0.0001	yes
Kif1c	0.9179	0.1197	no	1.3999	0.0101	yes
Kif21a	0.5088	0.7366	no	2.3102	0.0000	yes
Kif26a	0.9568	1.0000	no	0.8211	1.0000	no
Kif26b	0.0233	1.0000	no	0.0000	1.0000	no
Kif3c	-0.1158	0.9997	no	0.2295	0.8058	no
Kif5a	8.0000	1.0000	no	18.0000	1.0000	no
Kif5c	-2.0920	0.6578	no	0.0658	1.0000	no
Kifc3	2.1954	0.0039	yes	1.3509	0.0265	yes
Klc2	0.2609	0.9965	no	2.0543	0.0003	yes
Klf14	0.0000	1.0000	no	0.0000	1.0000	no
Klf2	1.9751	0.1519	no	1.3569	0.1536	no
Klf4	2.7754	0.2247	no	1.4613	0.1413	no
Klf5	1.5445	0.2976	no	2.2069	0.0137	yes
Klhdc8a	1.0511	1.0000	no	0.0000	1.0000	no
Klhl14	8.0000	1.0000	no	-12.0000	1.0000	no
Klhl2	-0.1164	0.9997	no	1.3868	0.1143	no
Klhl21	-0.0559	0.9997	no	0.4385	0.6358	no
Klhl22	-0.1817	0.9997	no	1.3898	0.0066	yes
Klhl29	8.0000	1.0000	no	0.0000	1.0000	no
Klhl35	8.0000	1.0000	no	18.0000	1.0000	no
Klhl8	0.4580	0.9997	no	1.2320	0.1291	no
Klrg2	2.3037	1.0000	no	18.0000	1.0000	no
Kras	0.0562	0.9997	no	0.0197	0.9707	no
Kremen1	-0.1669	0.9997	no	2.3073	0.0069	yes
Kremen2	8.0000	1.0000	no	18.0000	1.0000	no
Ksr2	8.0000	1.0000	no	0.7071	1.0000	no
L3mbtl	NA	NA	NA	NA	NA	NA
L3mbtl3	0.4221	0.9441	no	2.0054	0.0008	yes

Lad1	0.0000	1.0000	no	0.0000	1.0000	no
Lama5	3.2049	0.0489	yes	2.7342	0.0556	no
Lamc1	0.6382	0.3739	no	2.5036	0.0000	yes
Laptm4b	2.5452	0.0225	yes	1.4007	0.1296	no
Lass1	8.0000	1.0000	no	18.0000	1.0000	no
Lass6	2.2677	0.0121	yes	2.2563	0.0010	yes
Lats2	0.2104	0.9997	no	0.6474	0.3201	no
Lbx1	0.0000	1.0000	no	0.0000	1.0000	no
Lbx2	8.0000	1.0000	no	18.0000	1.0000	no
Ldlrad3	1.7688	0.1416	no	2.4817	0.0007	yes
Lef1	1.9972	1.0000	no	1.5785	1.0000	no
Lemd1	0.0000	1.0000	no	0.0000	1.0000	no
Lepre1	0.4017	0.8177	no	1.7481	0.0001	yes
Leprel2	2.3022	0.0449	yes	0.2445	1.0000	no
Leprel4	1.9040	0.6563	no	-0.1543	0.9313	no
Lgi2	3.5263	1.0000	no	5.4051	1.0000	no
Lgi3	0.0000	1.0000	no	18.0000	1.0000	no
Lgr4	0.3051	0.9997	no	0.5440	0.3729	no
Lgr6	0.0000	1.0000	no	0.0000	1.0000	no
Lhfp	1.1214	1.0000	no	0.3696	1.0000	no
Lhfpl2	-0.6177	0.7911	no	1.7362	0.0337	yes
Lhfpl3	0.0000	1.0000	no	0.0000	1.0000	no
Lhx1	8.0000	1.0000	no	3.3453	1.0000	no
Lhx2	2.2236	0.4788	no	2.1441	1.0000	no
Lhx3	-6.0000	1.0000	no	0.0000	1.0000	no
Lhx4	0.0000	1.0000	no	0.0000	1.0000	no
Lhx6	1.5525	1.0000	no	0.2669	1.0000	no
Lhx8	0.0000	1.0000	no	0.0000	1.0000	no
Lhx9	8.0000	1.0000	no	0.0000	1.0000	no
Lif	8.0000	1.0000	no	4.6341	1.0000	no
Lifr	2.3830	0.0002	yes	0.6510	0.2745	no
Limd2	2.5496	0.0000	yes	2.0365	0.0000	yes
Lingo3	3.2249	1.0000	no	18.0000	1.0000	no
Lipg	8.0000	1.0000	no	-12.0000	1.0000	no
Lix1l	1.0188	0.7404	no	1.8089	0.0474	yes
Lmo7	0.5351	0.9997	no	2.1297	0.0070	yes
Lmtk3	1.1762	1.0000	no	18.0000	1.0000	no
Lmx1a	5.2270	1.0000	no	2.3022	0.0105	yes
Lmx1b	0.0000	1.0000	no	0.0000	1.0000	no
LOC100034739	NA	NA	NA	NA	NA	NA
LOC100045653	NA	NA	NA	NA	NA	NA
Lor	0.0000	1.0000	no	0.0000	1.0000	no
Loxl2	1.6126	0.2195	no	1.6555	0.0590	no
Lpar1	1.1580	1.0000	no	-1.1071	1.0000	no
Lpar3	0.0000	1.0000	no	0.0000	1.0000	no
Lpgat1	1.8791	0.0014	yes	2.2627	0.0007	yes
Lphn1	0.3531	0.9476	no	2.0304	0.0004	yes
Lpp	1.5675	1.0000	no	0.9052	1.0000	no
Lrfn1	0.8135	1.0000	no	1.5702	0.0890	no

Lrfn4	0.3770	0.9871	no	1.8796	0.0059	yes
Lrig1	0.2348	0.9997	no	0.1290	0.9091	no
Lrp11	1.0115	0.6751	no	2.7959	0.0748	no
Lrp2	0.0000	1.0000	no	18.0000	1.0000	no
Lrp3	1.2259	1.0000	no	2.1011	1.0000	no
Lrp4	1.6661	1.0000	no	2.8345	1.0000	no
Lrp5	0.8475	0.1786	no	2.3562	0.0000	yes
Lrp6	-0.0072	0.9997	no	0.9507	0.2086	no
Lrrc1	-0.6109	0.6618	no	0.9064	0.1415	no
Lrrc10b	2.0844	1.0000	no	18.0000	1.0000	no
Lrrc15	8.0000	1.0000	no	18.0000	1.0000	no
Lrrc16a	3.1868	0.0220	yes	1.5756	0.0389	yes
Lrrc26	0.0000	1.0000	no	0.0000	1.0000	no
Lrrc4	1.9855	1.0000	no	0.3726	1.0000	no
Lrrc4b	-6.0000	1.0000	no	0.0000	1.0000	no
Lrrc8d	-0.0041	0.9997	no	1.0087	0.0492	yes
Lrrk1	0.3337	0.9552	no	2.4673	0.0000	yes
Lrrn2	0.0000	1.0000	no	18.0000	1.0000	no
Ltb4r2	8.0000	1.0000	no	-0.1056	1.0000	no
Ltbp2	1.2211	0.6823	no	-0.6558	0.4423	no
Ltbp3	1.4770	1.0000	no	0.5763	1.0000	no
Ltbp4	1.3028	0.5461	no	0.4723	0.7057	no
Ltk	2.9027	1.0000	no	2.2761	1.0000	no
Luzp1	1.5276	0.0029	yes	1.8029	0.0324	yes
Ly6g6c	0.0000	1.0000	no	0.0079	1.0000	no
Ly6h	0.0000	1.0000	no	18.0000	1.0000	no
Lypd6b	-6.0000	1.0000	no	18.0000	1.0000	no
Lysmd2	1.9275	0.1548	no	2.0034	0.0433	yes
Mab21l2	0.0000	1.0000	no	18.0000	1.0000	no
Madd	0.4382	0.6664	no	0.5633	0.0979	no
Maf	1.5903	0.0376	yes	0.4067	0.5941	no
Mafa	0.0000	1.0000	no	0.0000	1.0000	no
Mafb	1.5612	0.3158	no	0.3987	0.7281	no
Maff	2.0633	0.0682	no	2.2718	0.0348	yes
Magi3	0.5125	0.8853	no	1.1003	0.0753	no
Man1c1	1.9470	0.0002	yes	1.5974	0.0008	yes
Man2a2	1.1728	0.2427	no	2.4321	0.0002	yes
Maneal	0.0000	1.0000	no	0.0000	1.0000	no
Map3k10	-0.0612	0.9997	no	1.2840	0.0284	yes
Map3k3	0.3841	0.7732	no	1.1817	0.0020	yes
Map3k5	0.6984	0.7372	no	2.4499	0.0047	yes
Map3k9	4.3403	1.0000	no	2.2142	1.0000	no
Map4k3	0.8681	0.8177	no	1.3995	0.1274	no
Map4k4	0.9985	0.0113	yes	1.8096	0.0000	yes
Map6d1	2.6189	1.0000	no	-0.0310	1.0000	no
Mapk11	3.9676	1.0000	no	3.9151	1.0000	no
Mapk12	1.7732	1.0000	no	0.9735	1.0000	no
Mapk13	3.1904	0.0023	yes	2.6514	0.0012	yes
Mapk4	8.0000	1.0000	no	-0.3361	1.0000	no

Mapk8ip1	2.3983	1.0000	no	2.2217	1.0000	no
Mapkapk2	0.3383	0.9127	no	1.6366	0.0176	yes
Mapre3	1.6325	0.6342	no	0.5777	1.0000	no
Mapt	0.0403	0.9997	no	1.2274	1.0000	no
Mar11	NA	NA	NA	NA	NA	NA
Mar9	NA	NA	NA	NA	NA	NA
Marcks	1.6610	0.0426	yes	0.4258	0.6373	no
Marcksl1	0.3178	0.9845	no	1.9652	0.0080	yes
Mark1	4.2079	1.0000	no	2.4623	1.0000	no
Marveld1	1.4763	0.3119	no	2.1740	0.0108	yes
Mast1	0.6742	0.9308	no	0.5504	0.5830	no
Mast4	0.0813	0.9997	no	1.6939	0.1253	no
Mboat2	0.7789	0.3491	no	0.3575	0.5238	no
Mcam	0.8178	0.8671	no	0.7611	0.4114	no
Mcc	1.7466	1.0000	no	1.0144	1.0000	no
Mcmbp	-0.1250	0.9997	no	1.1286	0.0006	yes
Mctp1	2.0573	0.0059	yes	2.1843	0.0000	yes
Mdga1	0.3623	0.9682	no	-0.1925	0.7033	no
Mecom	0.5878	1.0000	no	1.3030	1.0000	no
Med12l	1.9852	1.0000	no	2.0495	1.0000	no
Megf10	8.0000	1.0000	no	18.0000	1.0000	no
Megf11	1.5117	1.0000	no	0.9122	1.0000	no
Megf6	-0.1494	1.0000	no	-1.3665	1.0000	no
Megf8	0.6359	0.5150	no	2.6760	0.0000	yes
Mei1	0.0000	1.0000	no	0.0000	1.0000	no
Meis1	2.0751	0.0025	yes	1.9384	0.0002	yes
Meis2	1.9362	0.4541	no	-0.7180	0.7059	no
Mesp1	0.0000	1.0000	no	0.0000	1.0000	no
Mest	1.4148	0.0073	yes	0.6448	0.3245	no
Metrnl	0.9767	0.8113	no	-0.0303	1.0000	no
Mettl1	0.1642	0.9997	no	2.6698	0.0000	yes
Mex3b	0.1712	0.9997	no	2.0258	0.0305	yes
Mfap3l	2.8110	1.0000	no	1.9443	1.0000	no
Mfhas1	1.4025	0.0058	yes	0.4854	0.4675	no
Mfsd4	-0.0098	0.9997	no	0.2452	0.7563	no
Mfsd6	1.9146	0.0535	no	1.5500	0.0343	yes
Mgat3	2.0199	1.0000	no	0.9431	1.0000	no
Mgat5b	0.0000	1.0000	no	0.0000	1.0000	no
Miat	8.0000	1.0000	no	18.0000	1.0000	no
Micall1	0.3269	0.9997	no	2.5256	0.0020	yes
Mier3	0.0000	1.0000	no	-0.0918	0.9091	no
Mir10b	0.0000	1.0000	no	0.0000	1.0000	no
Mir1199	0.0000	1.0000	no	0.0000	1.0000	no
Mir1247	0.0000	1.0000	no	0.0000	1.0000	no
Mir124a-1	2.32982999999999e-310	1.0000	no	2.33616000000002e-310	1.0000	no
Mir124a-3	0.0000	1.0000	no	0.0000	1.0000	no
Mir132	0.0000	1.0000	no	0.0000	1.0000	no
Mir152	0.0000	1.0000	no	0.0000	1.0000	no

Mir1900	2.32983999999998e-310	1.0000	no	2.33604999999999e-310	1.0000	no
Mir1901	0.0000	1.0000	no	0.0000	1.0000	no
Mir193	0.0000	1.0000	no	0.0000	1.0000	no
Mir196b	2.32981000000002e-310	1.0000	no	2.33614e-310	1.0000	no
Mir212	0.0000	1.0000	no	0.0000	1.0000	no
Mir3078	2.32982999999999e-310	1.0000	no	2.33616000000002e-310	1.0000	no
Mir3093	0.0000	1.0000	no	0.0000	1.0000	no
Mir34b	0.0000	1.0000	no	0.0000	1.0000	no
Mir34c	0.0000	1.0000	no	0.0000	1.0000	no
Mir449c	0.0000	1.0000	no	0.0000	1.0000	no
Mir574	0.0000	1.0000	no	0.0000	1.0000	no
Mir615	0.0000	1.0000	no	0.0000	1.0000	no
Mir9-1	NA	NA	NA	NA	NA	NA
Mir9-3	0.0000	1.0000	no	0.0000	1.0000	no
Mir92b	0.0000	1.0000	no	0.0000	1.0000	no
Mixl1	0.0546	1.0000	no	-0.0370	1.0000	no
Mkx	4.4096	1.0000	no	0.2147	1.0000	no
Mllt4	1.4328	0.1400	no	0.5484	0.6489	no
Mllt6	1.0564	0.5690	no	1.1546	0.2426	no
Mmp11	8.0000	1.0000	no	3.0659	1.0000	no
Mmp14	1.5684	0.1306	no	1.4231	0.1032	no
Mmp15	2.0554	1.0000	no	0.6429	1.0000	no
Mmp17	2.0159	0.0850	no	3.3456	0.0006	yes
Mmp23	3.5359	1.0000	no	0.7712	1.0000	no
Mmp24	-0.2255	0.9997	no	1.2490	1.0000	no
Mmp25	8.0000	1.0000	no	3.3370	1.0000	no
Mmp28	2.6691	0.2398	no	2.5490	0.0035	yes
Mms19	0.1306	0.9997	no	0.7180	0.0098	yes
Mn1	3.4413	1.0000	no	1.8245	1.0000	no
Mnx1	0.0000	1.0000	no	0.0000	1.0000	no
Mocos	1.9651	1.0000	no	2.1720	0.0216	yes
Mos	0.0454	1.0000	no	-12.0000	1.0000	no
Moxd1	8.0000	1.0000	no	0.0000	1.0000	no
Mpp3	2.3471	1.0000	no	3.7823	1.0000	no
Mpp6	0.0669	0.9997	no	1.9214	0.0000	yes
Mpped2	0.9596	0.6451	no	2.1554	0.2192	no
Mras	0.1553	0.9997	no	3.3947	0.0874	no
Mrc2	-2.1255	1.0000	no	-2.1136	1.0000	no
Mreg	1.4900	0.4068	no	1.9953	0.0389	yes
Msi1	0.1710	1.0000	no	-0.4873	0.7739	no
Msrb3	1.5326	1.0000	no	0.5643	0.6609	no
Msx1	0.0000	1.0000	no	0.0000	1.0000	no
Msx3	0.0000	1.0000	no	0.0000	1.0000	no
Mtag2	0.0000	1.0000	no	0.0000	1.0000	no
Mtap1a	1.1574	1.0000	no	1.9600	1.0000	no
Mtap1b	1.1832	1.0000	no	-0.2649	1.0000	no

Mtap6	0.0000	1.0000	no	18.0000	1.0000	no
Mtap7	-0.2904	0.9997	no	2.2931	0.0003	yes
Mtap7d2	0.4136	1.0000	no	18.0000	1.0000	no
Mtmr7	-0.1102	1.0000	no	0.8764	1.0000	no
Mtss1l	1.1986	0.4610	no	1.9321	0.0117	yes
Mtus1	3.0887	0.0004	yes	2.3425	0.0000	yes
Mtus2	-1.4361	0.4790	no	2.2432	1.0000	no
Muc1	0.0000	1.0000	no	-3.4962	1.0000	no
Mxra7	0.0345	1.0000	no	-0.4530	1.0000	no
Myb	-0.0954	0.9997	no	2.6736	0.0000	yes
Mybl1	0.3759	0.9997	no	-1.1718	0.0709	no
Mycl1	2.3617	1.0000	no	18.0000	1.0000	no
Mycn	2.0476	0.2823	no	2.4598	0.0104	yes
Myo10	0.8315	0.6236	no	1.5239	0.0405	yes
Myo1b	1.9660	0.0596	no	0.4415	0.6428	no
Myo1e	2.6188	0.0249	yes	2.9649	0.0009	yes
Myo5a	1.4650	0.0001	yes	2.1515	0.0000	yes
Myo5b	0.7883	0.6838	no	0.5256	0.5733	no
Mypop	0.7261	1.0000	no	2.5957	1.0000	no
Myrip	-6.0000	1.0000	no	18.0000	1.0000	no
Myst4	-0.1364	0.9997	no	0.0436	0.9699	no
N28178	2.0425	1.0000	no	-0.3571	1.0000	no
N4bp3	1.4095	0.4537	no	1.5619	0.1059	no
Nab1	0.4294	0.8339	no	1.8557	0.0001	yes
Nab2	2.0422	0.3451	no	1.6871	0.1663	no
Nacad	0.6183	0.9637	no	-1.2668	0.0844	no
Nacc2	0.1944	0.9997	no	1.3290	0.1598	no
Nags	0.3963	0.8177	no	2.2552	0.0000	yes
Nanos1	0.9847	0.5923	no	-0.2424	0.8342	no
Nat8l	3.3095	1.0000	no	2.3921	0.0079	yes
Nav1	1.5169	1.0000	no	1.9387	1.0000	no
Nav2	1.8182	1.0000	no	2.1765	1.0000	no
Nbea	1.2596	0.1552	no	2.4026	0.0001	yes
Nbl1	-0.0210	1.0000	no	-0.6259	1.0000	no
Ncald	2.2931	0.1954	no	1.0466	1.0000	no
Ncoa1	0.8566	0.6098	no	1.7930	0.0374	yes
Ncoa2	-0.2707	0.9284	no	0.4733	0.3047	no
Ncoa3	0.7760	0.1493	no	1.6321	0.0006	yes
Ncs1	1.4340	0.5468	no	2.6484	0.0036	yes
Ndrg1	2.3894	0.0003	yes	1.1511	0.0304	yes
Necab2	-1.3254	1.0000	no	18.0000	1.0000	no
Nedd4l	0.5419	0.8219	no	2.0146	0.0026	yes
Nefh	1.3646	0.1719	no	4.0218	1.0000	no
Nefm	0.0000	1.0000	no	0.0000	1.0000	no
Nek6	0.2016	0.9997	no	1.6657	0.0009	yes
Neo1	2.6009	0.0115	yes	1.1302	1.0000	no
Nes	2.3627	0.0002	yes	1.7660	0.0012	yes
Neurl1a	1.4436	1.0000	no	0.9703	1.0000	no
Neurl1b	8.0000	1.0000	no	1.5217	1.0000	no

Neurod2	0.0000	1.0000	no	0.0000	1.0000	no
Neurog1	0.0000	1.0000	no	0.0000	1.0000	no
Neurog2	0.0000	1.0000	no	0.0000	1.0000	no
Nexn	1.0194	1.0000	no	1.8093	1.0000	no
Nfatc1	0.7852	0.3141	no	2.3896	0.0000	yes
Nfatc4	1.2525	1.0000	no	2.5713	1.0000	no
Nfe2l3	-1.0909	1.0000	no	-0.6649	1.0000	no
Nfia	2.5378	0.0035	yes	3.2250	0.0831	no
Nfib	0.3084	1.0000	no	1.8675	1.0000	no
Nfic	2.1886	0.0030	yes	1.9505	0.0042	yes
Nfil3	3.1706	0.0065	yes	2.6033	0.0026	yes
Nfix	0.8156	0.2868	no	-0.1209	0.8995	no
Nfkb1	-0.0645	0.9997	no	2.0818	0.0000	yes
Nfkbiz	0.7585	0.8463	no	1.4559	0.0877	no
Ngef	3.1078	0.0046	yes	1.1898	1.0000	no
Ngfr	0.6299	1.0000	no	-0.0698	1.0000	no
Nhlrc1	0.8242	1.0000	no	3.9709	1.0000	no
Nin	0.4763	0.3439	no	2.4846	0.0000	yes
Nkain1	3.0040	0.0045	yes	4.5446	0.0001	yes
Nkain2	0.0000	1.0000	no	0.0000	1.0000	no
Nkd1	1.1736	1.0000	no	1.9753	1.0000	no
Nkpd1	1.0653	1.0000	no	18.0000	1.0000	no
Nkx1-2	8.0000	1.0000	no	18.0000	1.0000	no
Nkx2-1	0.0000	1.0000	no	0.0000	1.0000	no
Nkx2-2	0.0000	1.0000	no	0.0000	1.0000	no
Nkx2-3	8.0000	1.0000	no	-12.0000	1.0000	no
Nkx2-4	0.0000	1.0000	no	0.0000	1.0000	no
Nkx2-5	0.0000	1.0000	no	0.0000	1.0000	no
Nkx3-1	8.0000	1.0000	no	0.0000	1.0000	no
Nkx3-2	0.0000	1.0000	no	0.0000	1.0000	no
Nkx6-1	0.0000	1.0000	no	18.0000	1.0000	no
Nkx6-2	1.0546	1.0000	no	0.5586	1.0000	no
Nlgn2	1.0473	0.2413	no	3.2475	0.0001	yes
Nlrp6	2.2909	0.0164	yes	1.0604	0.0899	no
NM_001145974	NA	NA	NA	NA	NA	NA
NM_001172117	NA	NA	NA	NA	NA	NA
Nod1	0.9962	0.5535	no	0.4315	0.6230	no
Nodal	0.0400	1.0000	no	18.0000	1.0000	no
Nog	8.0000	1.0000	no	18.0000	1.0000	no
Nol3	0.6738	1.0000	no	2.2016	1.0000	no
Nos1ap	2.6665	0.0011	yes	0.1427	0.8458	no
Notch1	1.5830	0.4186	no	1.5922	0.0177	yes
Notch3	0.7682	1.0000	no	0.4960	1.0000	no
Notum	8.0000	1.0000	no	18.0000	1.0000	no
Nova1	1.5937	0.2719	no	2.4762	1.0000	no
Npas1	-1.0031	0.7974	no	0.7988	1.0000	no
Npas3	0.0000	1.0000	no	-1.0551	1.0000	no
Npdc1	2.5173	0.1241	no	1.5170	0.1246	no
Npnt	1.2386	1.0000	no	0.6551	1.0000	no

Nppc	0.0000	1.0000	no	0.0000	1.0000	no
Npr1	1.4324	0.1149	no	1.4597	0.0089	yes
Npr2	1.1721	0.6563	no	0.3232	0.8186	no
Nptx1	0.0000	1.0000	no	0.0000	1.0000	no
Nptxr	8.0000	1.0000	no	18.0000	1.0000	no
Npw	2.6200	1.0000	no	18.0000	1.0000	no
Npy	0.0000	1.0000	no	0.0000	1.0000	no
NR_003258	NA	NA	NA	NA	NA	NA
NR_027352	NA	NA	NA	NA	NA	NA
NR_028280	NA	NA	NA	NA	NA	NA
NR_029460	NA	NA	NA	NA	NA	NA
NR_033135	NA	NA	NA	NA	NA	NA
NR_036582	NA	NA	NA	NA	NA	NA
NR_036665	NA	NA	NA	NA	NA	NA
Nr2e1	0.0000	1.0000	no	0.0000	1.0000	no
Nr2f1	2.6386	1.0000	no	1.8251	1.0000	no
Nr2f2	1.9104	0.2278	no	0.9236	0.3119	no
Nr2f6	0.9683	0.1416	no	1.0572	0.0481	yes
Nr4a2	0.7264	0.6491	no	2.7732	1.0000	no
Nr4a3	-0.5555	1.0000	no	18.0000	1.0000	no
Nr6a1	-0.4612	0.9539	no	2.0709	0.0442	yes
Nrarp	-0.1395	0.9997	no	1.9463	0.0220	yes
Nrbp2	1.9504	0.0714	no	1.9226	0.0269	yes
Nrg2	2.4110	0.1596	no	3.4830	0.0003	yes
Nrg3	0.0000	1.0000	no	0.0000	1.0000	no
Nrip3	2.8730	0.0032	yes	1.0504	0.2087	no
Nrp2	1.7397	1.0000	no	0.6521	1.0000	no
Nrtn	1.3622	0.4746	no	0.7262	0.5052	no
Nrxn2	8.0000	1.0000	no	1.9157	1.0000	no
Nsg1	-0.0412	1.0000	no	1.0980	1.0000	no
Nt5c1a	0.0000	1.0000	no	0.0000	1.0000	no
Nt5c2	-0.4121	0.4055	no	1.0512	0.0425	yes
Ntf5	8.0000	1.0000	no	18.0000	1.0000	no
Ntn1	2.0503	1.0000	no	-12.0000	1.0000	no
Ntn4	1.3406	0.2604	no	2.3020	0.0715	no
Ntng2	3.0453	0.3460	no	18.0000	0.0015	yes
Ntrk1	8.0000	1.0000	no	1.5033	1.0000	no
Nuak1	0.1033	1.0000	no	1.1597	0.5109	no
Nuak2	2.5790	0.0122	yes	1.8448	0.0145	yes
Nxph3	0.0000	1.0000	no	0.0000	1.0000	no
Nxph4	0.0000	1.0000	no	18.0000	1.0000	no
Obsl1	2.8216	0.0000	yes	1.5703	0.0442	yes
Ociad2	0.0506	0.9997	no	1.0141	0.2810	no
Ocln	1.0336	0.7863	no	1.7470	0.0066	yes
Odf3b	1.3297	0.5144	no	3.1323	0.0296	yes
Odz4	0.1357	1.0000	no	-0.8314	1.0000	no
Olfm1	2.2292	0.0082	yes	3.1809	0.0000	yes
Olfm2	8.0000	1.0000	no	-0.0502	1.0000	no
Olfml2b	2.2977	1.0000	no	1.5807	0.0954	no

Olig2	0.0000	1.0000	no	0.0000	1.0000	no
Onecut1	1.7715	1.0000	no	0.8361	1.0000	no
Onecut2	2.9497	1.0000	no	1.7484	1.0000	no
Onecut3	8.0000	1.0000	no	-12.0000	1.0000	no
Oprd1	0.0000	1.0000	no	-12.0000	1.0000	no
Osbpl6	8.0000	1.0000	no	1.5291	1.0000	no
Osr2	8.0000	1.0000	no	18.0000	1.0000	no
Otop1	2.0398	1.0000	no	0.0000	1.0000	no
Otp	0.0000	1.0000	no	0.0000	1.0000	no
OTTMUSG00000010105	NA	NA	NA	NA	NA	NA
Otud1	1.3697	0.4361	no	0.4624	0.6809	no
Otud7a	8.0000	1.0000	no	0.0000	1.0000	no
Otx1	8.0000	1.0000	no	0.0000	1.0000	no
Otx2	0.0000	1.0000	no	0.0000	1.0000	no
Ovol1	0.2508	1.0000	no	-0.4940	1.0000	no
Ovol2	0.0000	1.0000	no	18.0000	1.0000	no
Oxr1	-0.0908	0.9997	no	0.7254	0.2156	no
Oxt	8.0000	1.0000	no	0.0000	1.0000	no
P2rx5	-1.1960	1.0000	no	18.0000	1.0000	no
P2rx6	-1.3132	1.0000	no	0.0000	1.0000	no
P2ry2	1.5000	0.3882	no	2.9675	0.0015	yes
P4ha2	1.7834	0.0477	yes	1.1947	0.4158	no
P4ha3	0.5144	1.0000	no	1.5094	1.0000	no
Pacsin1	8.0000	1.0000	no	18.0000	1.0000	no
Pacsin3	1.1395	0.5358	no	0.5161	0.4678	no
Pak6	0.9748	0.2447	no	1.9684	0.0070	yes
Panx2	0.0000	1.0000	no	0.0000	1.0000	no
Papolb	0.0000	1.0000	no	18.0000	1.0000	no
Paqr4	0.6282	0.6566	no	0.5886	0.5207	no
Paqr8	1.2054	1.0000	no	1.4670	0.1862	no
Paqr9	2.3418	0.0000	yes	2.0693	0.0051	yes
Pard3	0.8309	0.7943	no	0.3500	0.6746	no
Pard6b	0.6187	0.9590	no	1.4733	0.1104	no
Parp12	1.2128	0.3452	no	0.6604	0.4376	no
Parp14	0.7474	0.6751	no	1.0933	0.1996	no
Parp8	3.3500	0.0000	yes	2.6480	0.0000	yes
Pawr	0.7063	0.8515	no	1.9908	0.0077	yes
Pax2	0.0000	1.0000	no	0.0000	1.0000	no
Pax6	-0.2159	0.9997	no	0.6991	0.4988	no
Pax6os1	0.0000	1.0000	no	0.0000	1.0000	no
Pax9	0.5244	1.0000	no	-0.9986	1.0000	no
Pcdh1	2.5060	0.0092	yes	1.9691	0.0042	yes
Pcdh12	1.1316	1.0000	no	0.5447	1.0000	no
Pcdh7	0.3119	1.0000	no	2.5281	1.0000	no
Pcdh8	8.0000	1.0000	no	0.0000	1.0000	no
Pcdhac2	NA	NA	NA	NA	NA	NA
Pcdhgc3	NA	NA	NA	NA	NA	NA
Pcgf2	0.3590	0.9997	no	1.1453	0.1046	no
Pcnx	0.9440	0.1132	no	2.1885	0.0000	yes

Pcolce2	3.6216	0.0080	yes	2.7660	0.0100	yes
Pcp4l1	3.3260	1.0000	no	0.8087	1.0000	no
Pcsk6	2.7766	0.0000	yes	3.9664	0.0000	yes
Pcsk9	2.1313	0.0033	yes	1.2542	0.1080	no
Pde10a	3.1184	1.0000	no	0.5509	1.0000	no
Pde2a	1.5006	0.0078	yes	1.8914	0.0009	yes
Pde3b	0.0379	0.9997	no	2.3823	0.0001	yes
Pde4a	0.2045	0.9997	no	2.8870	0.0000	yes
Pde4dip	0.3567	0.9970	no	1.0995	0.0956	no
Pde5a	1.4593	0.3115	no	1.6672	0.0587	no
Pde8a	2.3699	0.0019	yes	2.7581	0.0002	yes
Pde8b	0.3568	1.0000	no	0.3384	1.0000	no
Pdgfa	4.3582	1.0000	no	18.0000	0.0086	yes
Pdgfb	2.3161	0.0876	no	0.9203	0.3698	no
Pdgfra	2.6146	1.0000	no	-0.6892	1.0000	no
Pdlim4	1.7573	0.1511	no	1.6537	0.0478	yes
Pdp1	0.1178	0.9997	no	0.2207	0.8060	no
Peli2	2.7516	1.0000	no	1.8454	0.0374	yes
Perp	1.8348	0.1501	no	1.2183	0.1837	no
Pfkfb3	2.1807	0.0011	yes	2.6398	0.0000	yes
Pfn2	2.5847	0.1378	no	-1.0533	0.3908	no
Pgbd5	0.1007	1.0000	no	0.0000	1.0000	no
Phactr2	0.6785	0.7931	no	1.7414	0.0095	yes
Phc2	-0.1714	0.9916	no	0.6933	0.2427	no
Phf13	0.4987	0.9741	no	-0.5956	0.5223	no
Phf15	0.0309	0.9997	no	1.1068	0.0842	no
Phf21b	2.1035	0.3439	no	6.1688	0.0082	yes
Phlda1	2.2612	0.1119	no	4.1689	1.0000	no
Phlda3	0.4654	0.9585	no	1.8427	0.0174	yes
Phldb1	1.6715	0.0024	yes	2.4551	0.0029	yes
Phldb2	1.1617	0.2542	no	0.4722	0.5064	no
Phox2a	0.7773	1.0000	no	0.9228	1.0000	no
Phyhip	-0.0219	0.9997	no	0.5825	0.5724	no
Phyhipl	8.0000	1.0000	no	18.0000	1.0000	no
Pigz	4.0465	0.0918	no	-0.0597	1.0000	no
Pik3c2b	1.1338	1.0000	no	2.0724	1.0000	no
Pik3ip1	0.7628	0.8725	no	2.5227	0.0298	yes
Pitpnm1	1.7102	0.0000	yes	2.1662	0.0000	yes
Pitpnm3	0.0000	1.0000	no	0.0000	1.0000	no
Pitx1	0.0000	1.0000	no	0.0000	1.0000	no
Pitx2	0.0000	1.0000	no	18.0000	1.0000	no
Pitx3	0.0000	1.0000	no	0.0000	1.0000	no
Pkd2	3.3043	0.0002	yes	2.9148	0.0007	yes
Pkdcc	2.2555	0.0005	yes	1.9947	0.0037	yes
Pkdrej	0.9441	1.0000	no	2.1534	1.0000	no
Pknox2	2.9889	1.0000	no	18.0000	1.0000	no
Pkp1	8.0000	1.0000	no	0.3791	1.0000	no
Pkp2	1.2128	0.5552	no	1.4049	0.1299	no
Pkp4	-0.0006	0.9999	no	0.9213	0.0069	yes

Plagl1	1.6346	0.1258	no	0.0818	0.9336	no
Plbd1	1.8360	0.0739	no	1.4460	0.0312	yes
Plcg1	0.4408	0.8517	no	2.0847	0.0001	yes
Plcl1	8.0000	1.0000	no	2.5805	1.0000	no
Pld2	-0.3167	0.9997	no	1.6086	0.3743	no
Plec	0.9221	0.0041	yes	2.0199	0.0000	yes
Plekha1	2.3673	0.0000	yes	1.2019	0.0215	yes
Plekha2	2.9472	0.0004	yes	2.0627	0.0005	yes
Plekha5	0.8260	0.3200	no	2.2400	0.0000	yes
Plekhg1	1.2138	1.0000	no	-0.1504	1.0000	no
Plekhg3	3.2341	0.0001	yes	1.8978	0.0162	yes
Plekhg6	1.8970	1.0000	no	2.7619	1.0000	no
Plekhh1	0.3711	0.9997	no	1.8287	0.0249	yes
Plekhh2	2.6022	1.0000	no	1.5834	1.0000	no
Plekhh3	1.5630	1.0000	no	-0.5861	1.0000	no
Plekho1	1.3245	0.0209	yes	1.3148	0.0166	yes
Plk2	1.8615	0.1827	no	1.0442	0.2944	no
Plk3	1.5628	0.0127	yes	2.3118	0.0027	yes
Plk5	8.0000	1.0000	no	18.0000	1.0000	no
Pllp	1.6313	1.0000	no	-1.6191	1.0000	no
Pls1	1.6572	0.3724	no	1.2982	0.1869	no
Pltp	0.4822	0.9811	no	0.2855	0.6742	no
Plxdc1	-0.8990	0.6767	no	3.0896	0.0012	yes
Plxna1	-0.0567	0.9997	no	2.6018	0.0008	yes
Plxna4	0.4526	1.0000	no	-0.1944	1.0000	no
Plxnb1	1.8613	0.2069	no	1.4283	0.1020	no
Plxnb2	2.0272	0.0000	yes	1.1630	0.0089	yes
Plxnc1	0.2299	0.9997	no	1.4926	0.0427	yes
Plxnd1	2.0193	0.0031	yes	1.9122	0.0055	yes
Pm20d2	1.7772	0.3106	no	3.6342	1.0000	no
Pmepa1	8.0000	1.0000	no	18.0000	1.0000	no
Pnma2	8.0000	1.0000	no	0.0000	1.0000	no
Pnmal2	-6.0000	1.0000	no	18.0000	1.0000	no
Podn	1.0033	0.3923	no	0.0771	0.9387	no
Podxl2	8.0000	0.1849	no	0.5952	0.7090	no
Pom121l2	0.0000	1.0000	no	0.0000	1.0000	no
Popdc3	2.9735	1.0000	no	-1.0258	1.0000	no
Pou2f3	0.0000	1.0000	no	0.0000	1.0000	no
Pou3f1	0.0000	1.0000	no	0.0000	1.0000	no
Pou3f2	0.0000	1.0000	no	0.0000	1.0000	no
Pou3f3	8.0000	1.0000	no	0.0000	1.0000	no
Pou4f1	2.2867	0.4324	no	18.0000	1.0000	no
Pou4f2	0.0000	1.0000	no	0.0000	1.0000	no
Pou4f3	8.0000	1.0000	no	0.0000	1.0000	no
Ppapdc1a	0.0000	1.0000	no	0.0000	1.0000	no
Ppapdc2	0.7497	0.9285	no	1.7790	0.0508	no
Pparg	3.3904	0.0028	yes	1.3657	0.0965	no
Ppargc1b	0.4076	0.9997	no	3.2227	0.0003	yes
Ppfia3	0.2757	0.9997	no	2.1522	0.1607	no

Ppig	-0.0373	0.9997	no	0.4608	0.1296	no
Ppl	2.6053	1.0000	no	1.1737	1.0000	no
Ppm1e	0.0375	0.9997	no	0.0576	0.9498	no
Ppm1h	1.6260	0.0336	yes	2.3985	0.0012	yes
Ppm1j	2.2046	1.0000	no	18.0000	1.0000	no
Ppm1n	0.0362	1.0000	no	0.0000	1.0000	no
Ppp1r16b	0.8226	1.0000	no	0.9327	1.0000	no
Ppp1r1b	8.0000	1.0000	no	0.0000	1.0000	no
Ppp2r2c	8.0000	1.0000	no	18.0000	1.0000	no
Ppp3cc	1.8854	0.0540	no	1.7772	0.0201	yes
Ppp4r1	0.1018	0.9997	no	0.6836	0.1033	no
Ppp4r4	1.9418	1.0000	no	2.0910	0.0294	yes
Ppy	0.0000	1.0000	no	0.0000	1.0000	no
Prdm12	0.0000	1.0000	no	0.0000	1.0000	no
Prdm13	0.0000	1.0000	no	0.0000	1.0000	no
Prdm14	0.0000	1.0000	no	0.0000	1.0000	no
Prdm16	1.1964	0.3680	no	1.7183	0.2409	no
Prdm6	0.0000	1.0000	no	0.0000	1.0000	no
Prdm9	0.2579	0.9997	no	1.1749	0.1760	no
Prkaa2	8.0000	1.0000	no	18.0000	1.0000	no
Prkar2a	0.7502	0.2334	no	2.2854	0.0015	yes
Prkca	1.0554	0.0759	no	1.2289	0.0082	yes
Prkce	0.5880	0.9765	no	0.1682	1.0000	no
Prkch	2.0834	0.1255	no	1.1960	0.2019	no
Prkcz	0.7987	0.7835	no	1.1094	0.3664	no
Prkd3	0.0410	0.9997	no	1.6493	0.0000	yes
Prkg1	1.6375	1.0000	no	18.0000	1.0000	no
Prkg2	8.0000	1.0000	no	-12.0000	1.0000	no
Prox1	2.5207	0.0122	yes	1.2198	0.1361	no
Prph	8.0000	1.0000	no	18.0000	1.0000	no
Prr18	8.0000	1.0000	no	18.0000	1.0000	no
Prr7	1.5217	1.0000	no	1.7662	1.0000	no
Prrt1	8.0000	1.0000	no	18.0000	1.0000	no
Prrt4	-0.9551	1.0000	no	18.0000	1.0000	no
Prrx2	2.6635	1.0000	no	0.0000	1.0000	no
Prrxl1	0.0000	1.0000	no	0.0000	1.0000	no
Prss12	0.4663	1.0000	no	-1.3997	1.0000	no
Prss16	3.2540	0.0517	no	2.0544	0.0201	yes
Prss23	-0.9784	1.0000	no	0.9833	1.0000	no
Prtg	8.0000	1.0000	no	0.9723	1.0000	no
Psd	-0.0187	0.9997	no	-0.6033	0.5109	no
Pstpip2	2.0673	0.0005	yes	1.9989	0.0000	yes
Ptch2	-0.0448	0.9997	no	0.5201	1.0000	no
Ptger3	1.8315	0.0016	yes	2.8564	0.0000	yes
Ptgfrn	2.5661	1.0000	no	1.9749	1.0000	no
Pth1r	1.5589	0.3822	no	0.7823	0.4678	no
Pth2	0.0000	1.0000	no	0.0000	1.0000	no
Ptms	2.2667	0.0011	yes	1.2063	0.0650	no
Ptpn14	-0.0617	0.9997	no	1.5986	1.0000	no

Ptpn21	0.7836	0.7179	no	2.1525	0.0064	yes
Ptpn3	2.8687	1.0000	no	-0.4199	0.8440	no
Ptpn5	0.0000	1.0000	no	18.0000	1.0000	no
Ptpn9	0.3444	0.9997	no	1.9373	0.0181	yes
Ptprf	2.7050	0.0003	yes	1.2299	0.0237	yes
Ptprg	2.4918	0.1185	no	1.0488	0.5762	no
Ptprj	0.2348	0.9997	no	1.2434	0.0715	no
Ptprn	0.0387	1.0000	no	18.0000	1.0000	no
Ptprs	1.1340	0.0115	yes	2.2694	0.0000	yes
Ptprt	8.0000	1.0000	no	-2.0362	1.0000	no
Ptpru	1.3925	0.0001	yes	1.3417	0.0089	yes
Ptrf	0.1427	0.9997	no	1.7266	0.0423	yes
Pura	0.3670	0.9770	no	1.4667	0.0744	no
Pus3	-0.3768	0.9105	no	1.1703	0.0369	yes
Pvrl1	2.1138	0.0792	no	2.0142	0.0257	yes
Pvrl3	0.8330	0.8859	no	1.8344	0.0327	yes
Pygo1	-6.0000	1.0000	no	18.0000	1.0000	no
Pyy	0.0000	1.0000	no	0.0000	1.0000	no
Rab11fip3	1.4937	0.0159	yes	1.8490	0.0013	yes
Rab11fip4	3.0225	0.3439	no	2.0154	0.0508	no
Rab15	-0.5979	1.0000	no	18.0000	1.0000	no
Rab19	3.0029	1.0000	no	-0.2407	1.0000	no
Rab20	2.0588	0.1643	no	0.0939	0.9447	no
Rab27b	1.2518	0.2675	no	0.8242	0.2481	no
Rab31	2.6457	0.0073	yes	1.8510	0.0251	yes
Rab34	0.3391	0.9997	no	1.1179	0.0536	no
Rab6b	2.6040	1.0000	no	2.9795	1.0000	no
Rac3	0.3981	0.9997	no	1.9257	0.0467	yes
Radil	3.8468	0.0406	yes	1.0747	1.0000	no
Ralgds	1.9946	0.0765	no	1.2530	0.0952	no
Ralgps2	0.0831	0.9997	no	0.6838	0.3995	no
Ralyl	0.0000	1.0000	no	0.0000	1.0000	no
Ramp2	2.1275	0.0115	yes	0.8904	0.1680	no
Ranbp9	-0.0349	0.9997	no	0.2897	0.6316	no
Rap1gap2	2.0172	0.0314	yes	1.4964	0.3456	no
Rap2a	0.5118	0.9705	no	1.5038	0.0187	yes
Rapgef3	2.3119	0.0016	yes	1.1245	0.2446	no
Rapgef4	3.7811	0.0000	yes	0.6155	0.1522	no
Rapgefl1	1.2437	1.0000	no	18.0000	1.0000	no
Raph1	1.9270	0.0015	yes	0.8812	0.0749	no
Rara	2.0469	0.0012	yes	1.4805	0.1257	no
Rarg	2.0318	0.1163	no	1.7119	0.0522	no
Rarres1	1.0206	1.0000	no	0.1183	1.0000	no
Rasa2	0.3408	0.9985	no	2.5811	0.0005	yes
Rasal2	0.2984	0.9997	no	0.9085	0.3402	no
Rasd1	1.8306	1.0000	no	1.3062	1.0000	no
Rasd2	8.0000	1.0000	no	2.8509	1.0000	no
Rasgef1c	0.0000	1.0000	no	18.0000	1.0000	no
Rasgrp2	2.5309	0.0000	yes	1.9062	0.0000	yes

Rasip1	1.4027	0.0989	no	0.8976	0.1476	no
Rasl10a	8.0000	1.0000	no	-12.0000	1.0000	no
Rasl10b	1.6948	1.0000	no	1.4002	1.0000	no
Rasl11a	1.4039	0.4675	no	2.8557	0.0522	no
Rasl11b	0.9261	1.0000	no	1.7358	1.0000	no
Rassf5	1.6729	0.1380	no	1.9711	0.0140	yes
Raver2	2.1607	1.0000	no	1.4750	1.0000	no
Rax	0.0000	1.0000	no	0.0000	1.0000	no
Rbfox2	2.0014	0.0013	yes	1.2258	0.0162	yes
Rbfox3	8.0000	1.0000	no	-0.8871	1.0000	no
Rbm20	-1.8860	1.0000	no	0.5646	1.0000	no
Rbm24	0.0606	1.0000	no	18.0000	1.0000	no
Rbm46	0.0000	1.0000	no	0.0000	1.0000	no
Rbm47	1.1678	0.9856	no	1.5276	0.0865	no
Rbms1	0.1604	0.9997	no	-0.5330	0.1095	no
Rbpms	2.2871	0.0018	yes	1.4983	0.0067	yes
Rbpms2	2.9021	0.0115	yes	1.5251	0.0604	no
Rcor2	0.9891	0.2712	no	3.0147	0.0021	yes
Rcsd1	2.3501	0.0000	yes	1.8201	0.0021	yes
Reep1	0.4741	0.9997	no	1.7376	0.0534	no
Reep2	0.8236	1.0000	no	0.6503	1.0000	no
Rel	2.9101	0.0240	yes	2.4890	0.0094	yes
Relb	1.2237	0.3676	no	1.2882	0.1056	no
Reln	3.3317	0.0000	yes	0.0000	1.0000	no
Rem1	0.0000	1.0000	no	1.5791	1.0000	no
Rem2	0.0000	1.0000	no	0.0000	1.0000	no
Ret	2.5537	1.0000	no	18.0000	1.0000	no
Rftn1	0.4382	0.9502	no	2.6407	0.0000	yes
Rfx4	0.0000	1.0000	no	0.0000	1.0000	no
Rgl1	1.8944	0.0241	yes	0.4117	0.5772	no
Rgl3	8.0000	1.0000	no	18.0000	1.0000	no
Rgma	-6.0000	1.0000	no	-12.0000	1.0000	no
Rgmb	3.7309	1.0000	no	1.2039	1.0000	no
Rgnef	-0.2578	1.0000	no	3.7094	1.0000	no
Rgs6	-6.0000	1.0000	no	0.5960	1.0000	no
Rgs7bp	1.0314	1.0000	no	1.1034	1.0000	no
Rhbdf1	4.0770	0.0000	yes	3.3521	0.0000	yes
Rhbdl3	8.0000	1.0000	no	-0.0726	1.0000	no
Rhobtb1	-0.0594	0.9997	no	1.3113	0.1676	no
Rhobtb3	0.9825	0.4232	no	2.1855	0.0076	yes
Rhoc	2.2530	0.0078	yes	0.5765	0.3814	no
Rhod	1.5415	0.5149	no	-0.3154	0.7455	no
Rhoq	1.1559	0.5625	no	1.6691	0.0394	yes
Rhou	3.1124	0.0146	yes	2.0278	0.0180	yes
Rhpn1	8.0000	1.0000	no	0.0661	1.0000	no
Rilpl1	0.5114	0.9997	no	0.8922	0.3860	no
Rimkla	8.0000	1.0000	no	0.0000	1.0000	no
Rimklb	0.0000	1.0000	no	18.0000	1.0000	no
Rims2	8.0000	1.0000	no	18.0000	1.0000	no

Rims4	2.6076	1.0000	no	0.6839	1.0000	no
Rin3	3.4593	0.0000	yes	2.1257	0.0000	yes
Ripply3	0.8252	0.9068	no	0.8771	1.0000	no
Rln1	0.0000	1.0000	no	-12.0000	1.0000	no
Rnd2	0.2702	0.9997	no	2.6018	0.0001	yes
Rnf130	0.5006	0.7523	no	2.0415	0.0014	yes
Rnf144a	2.2545	0.0002	yes	3.3994	0.0001	yes
Rnf144b	2.7952	0.0021	yes	1.9051	0.0189	yes
Rnf150	0.8064	1.0000	no	1.2267	1.0000	no
Rnf152	8.0000	1.0000	no	2.0090	1.0000	no
Rnf157	0.5358	0.8957	no	0.6807	0.5750	no
Rnf165	2.0218	1.0000	no	-0.0064	1.0000	no
Rnf182	-1.0942	1.0000	no	18.0000	1.0000	no
Rnf208	0.8121	0.7246	no	2.6451	0.0162	yes
Rnf216	-0.1490	0.9997	no	0.4059	0.6331	no
Rnf217	2.4634	0.0975	no	2.1608	0.0275	yes
Rnf220	-0.3281	0.8035	no	1.0009	0.0092	yes
Rnf39	2.4986	1.0000	no	18.0000	1.0000	no
Rpp25	1.6120	1.0000	no	-12.0000	1.0000	no
Rps6ka1	0.3972	0.3698	no	0.0905	0.8497	no
Rragd	2.7722	0.0000	yes	0.7080	0.2363	no
Rras2	0.4544	0.9997	no	1.6331	0.0623	no
Rspo1	8.0000	1.0000	no	18.0000	1.0000	no
Rspo3	0.0430	1.0000	no	0.2672	1.0000	no
Rspo4	8.0000	1.0000	no	0.0000	1.0000	no
Rsrc1	-0.3884	0.6658	no	1.4799	0.0003	yes
Rtbdn	-0.1178	0.9997	no	-0.2812	0.8164	no
Rtkn	1.6173	0.1036	no	1.2048	0.0643	no
Rtn1	-0.1442	0.9997	no	1.8797	0.0410	yes
Rtn2	-0.4130	0.9997	no	0.5904	0.4615	no
Rtn4r	1.0566	1.0000	no	2.6288	1.0000	no
Rtn4rl1	1.2751	1.0000	no	1.3272	1.0000	no
Rtn4rl2	0.0000	1.0000	no	0.0000	1.0000	no
Rufy4	2.0149	1.0000	no	0.3398	1.0000	no
Rundc3a	1.6189	0.0374	yes	-0.4585	0.4034	no
Rundc3b	0.1601	1.0000	no	4.1316	1.0000	no
Runx1t1	1.4872	0.0375	yes	-1.4284	0.0004	yes
Runx2	4.7315	0.0911	no	2.4758	0.0806	no
Rusc1	0.1036	0.9997	no	1.5248	0.0798	no
Rusc2	1.1991	0.9028	no	-1.5097	0.3010	no
Ryr2	1.3451	1.0000	no	-1.0098	1.0000	no
S1pr5	8.0000	1.0000	no	18.0000	1.0000	no
Sall1	3.3501	1.0000	no	3.6118	1.0000	no
Sall3	0.0000	1.0000	no	18.0000	1.0000	no
Sall4	2.7713	0.0589	no	0.4773	0.7991	no
Samd10	1.1123	0.3568	no	2.3390	0.0031	yes
Samd4	2.4194	1.0000	no	-0.2558	1.0000	no
Samd5	8.0000	1.0000	no	18.0000	1.0000	no
Sap30l	0.2499	0.9997	no	0.0494	0.9666	no

Sarm1	8.0000	1.0000	no	18.0000	1.0000	no
Satb1	2.2710	0.0000	yes	2.0584	0.0001	yes
Satb2	1.4710	1.0000	no	4.1518	1.0000	no
Sbf2	1.6375	0.0155	yes	0.8090	0.1723	no
Sbk1	1.1925	0.5659	no	3.3546	0.0002	yes
Scamp5	1.2181	0.5698	no	0.4380	0.6964	no
Scarf2	2.0222	1.0000	no	0.6394	1.0000	no
Sccpdh	1.2297	0.2951	no	2.0548	0.0005	yes
Scn1b	2.1264	1.0000	no	0.9598	1.0000	no
Scn5a	-6.0000	1.0000	no	18.0000	1.0000	no
Scn8a	8.0000	1.0000	no	-2.3425	1.0000	no
Scrn1	8.0000	1.0000	no	18.0000	1.0000	no
Scrt1	0.4073	1.0000	no	0.0000	1.0000	no
Scrt2	0.0000	1.0000	no	0.0000	1.0000	no
Sct	8.0000	1.0000	no	18.0000	1.0000	no
Scube1	-0.7628	1.0000	no	1.1814	1.0000	no
Scube2	-0.5917	1.0000	no	18.0000	1.0000	no
Scube3	1.6925	1.0000	no	0.9293	1.0000	no
Sdc1	0.5603	0.3693	no	2.1214	0.0000	yes
Sdc3	1.1346	0.0870	no	0.6618	0.3717	no
Sdk1	0.7065	1.0000	no	-0.2756	1.0000	no
Sdk2	3.7314	1.0000	no	1.0988	1.0000	no
Sec14l2	1.1189	0.0510	no	1.8355	0.0020	yes
Sec24d	2.0482	0.0486	yes	1.7089	0.0412	yes
Sel1l3	0.0000	1.0000	no	0.0000	1.0000	no
Sema3f	1.7449	1.0000	no	1.3871	1.0000	no
Sema4c	1.0197	0.4478	no	1.2214	0.0416	yes
Sema4f	8.0000	1.0000	no	18.0000	1.0000	no
Sema4g	2.7252	0.0000	yes	1.7967	0.0015	yes
Sema5b	0.0428	1.0000	no	-12.0000	1.0000	no
Sema6a	2.4879	1.0000	no	0.1472	1.0000	no
Sema6b	0.7614	0.8177	no	1.8471	0.0102	yes
Sema6d	1.4971	0.1954	no	0.5212	0.4758	no
Sema7a	3.1985	1.0000	no	2.3959	1.0000	no
Sepn1	-0.2659	0.9997	no	1.7956	0.0160	yes
Sept10	NA	NA	NA	NA	NA	NA
Sept3	NA	NA	NA	NA	NA	NA
Sept5	NA	NA	NA	NA	NA	NA
Serinc2	5.2975	0.0000	yes	4.5953	0.0000	yes
Serp2	0.1025	0.9997	no	0.1780	1.0000	no
Serpine2	3.6088	0.0021	yes	3.0143	0.0004	yes
Sertad4	0.5000	1.0000	no	0.2134	1.0000	no
Sesn3	2.5761	1.0000	no	2.5182	1.0000	no
Sestd1	1.6274	1.0000	no	3.0973	0.0025	yes
Setbp1	4.4091	1.0000	no	18.0000	1.0000	no
Sez6	-6.0000	1.0000	no	0.0000	1.0000	no
Sfmbt1	-0.1724	0.9682	no	0.1557	0.7185	no
Sfmbt2	2.2252	0.3325	no	2.7402	0.0426	yes
Sfn	0.9811	0.7974	no	3.1182	1.0000	no

Sfrp1	1.5020	1.0000	no	-0.5370	1.0000	no
Sfrp2	8.0000	1.0000	no	1.7163	1.0000	no
Sfrp5	0.0556	1.0000	no	18.0000	1.0000	no
Sgcb	1.2909	0.1709	no	2.1745	0.0008	yes
Sgk1	0.5143	0.9272	no	0.2931	0.7080	no
Sgk3	0.1078	0.9997	no	-1.0020	0.0311	yes
Sgms1	0.2684	0.9997	no	-0.9280	0.0638	no
Sh2d5	2.3250	0.0239	yes	1.6157	0.0082	yes
Sh3bp4	1.0813	1.0000	no	0.1471	1.0000	no
Sh3bp5	1.7497	0.0133	yes	1.4124	0.0206	yes
Sh3d20	NA	NA	NA	NA	NA	NA
Sh3pxd2a	0.1264	0.9997	no	0.2106	0.7993	no
Sh3pxd2b	0.4773	0.9997	no	1.8774	0.0299	yes
Sh3rf1	1.0112	0.7131	no	2.5751	0.0042	yes
Sh3rf3	0.0000	1.0000	no	18.0000	1.0000	no
Shank3	-0.1556	0.9997	no	2.7951	0.0002	yes
Shc2	8.0000	1.0000	no	2.6556	1.0000	no
Shc3	0.0000	1.0000	no	0.0000	1.0000	no
She	1.6086	1.0000	no	1.0937	1.0000	no
Shisa2	8.0000	1.0000	no	1.7169	1.0000	no
Shisa3	0.0888	1.0000	no	0.4390	0.7054	no
Shisa6	-1.3715	1.0000	no	0.0000	1.0000	no
Shisa7	0.0000	1.0000	no	18.0000	1.0000	no
Shisa9	8.0000	1.0000	no	0.0000	1.0000	no
Shox2	8.0000	1.0000	no	18.0000	1.0000	no
Shroom1	2.6615	1.0000	no	1.2455	1.0000	no
Shroom3	-0.8778	1.0000	no	-1.2101	1.0000	no
Siah2	0.5029	0.9142	no	1.9855	0.0003	yes
Sim1	0.0000	1.0000	no	0.0000	1.0000	no
Sim2	-6.0000	1.0000	no	0.0000	1.0000	no
Sirpa	1.7750	0.0001	yes	1.3049	0.0000	yes
Six1	-6.0000	1.0000	no	18.0000	1.0000	no
Six2	0.0000	1.0000	no	18.0000	1.0000	no
Six3	0.0000	1.0000	no	0.0000	1.0000	no
Six3os1	0.0000	1.0000	no	0.0000	1.0000	no
Six4	8.0000	1.0000	no	18.0000	1.0000	no
Six5	1.2102	0.5455	no	2.2097	0.0168	yes
Six6	0.0000	1.0000	no	0.0000	1.0000	no
Skap1	2.2786	0.1992	no	1.1907	1.0000	no
Ski	0.4893	0.2313	no	1.8882	0.0000	yes
Skor1	0.0000	1.0000	no	0.0000	1.0000	no
Slain1	2.0699	0.0345	yes	3.7889	0.0001	yes
Slain2	0.0604	0.9997	no	2.2676	0.0000	yes
Slc10a4	0.0000	1.0000	no	18.0000	1.0000	no
Slc12a2	0.1093	0.9997	no	2.0713	0.0107	yes
Slc16a11	0.8289	0.8132	no	-0.7517	0.2904	no
Slc16a12	2.0916	0.0963	no	1.1067	0.2573	no
Slc16a9	8.0000	1.0000	no	1.4464	1.0000	no
Slc17a7	2.0477	1.0000	no	18.0000	1.0000	no

Slc18a3	NA	NA	NA	NA	NA	NA
Slc22a15	1.5183	1.0000	no	3.3779	0.0000	yes
Slc22a17	2.2771	0.0891	no	1.8178	0.0195	yes
Slc23a2	0.0889	0.9997	no	2.2043	0.0009	yes
Slc25a23	0.2339	0.9997	no	1.8804	0.0062	yes
Slc25a33	0.2645	0.9997	no	2.1623	0.0115	yes
Slc26a10	0.4770	0.9583	no	2.9330	0.0001	yes
Slc26a4	0.0000	1.0000	no	0.0000	1.0000	no
Slc27a2	2.2162	0.0002	yes	0.6833	0.2426	no
Slc29a4	1.0425	1.0000	no	1.5034	1.0000	no
Slc2a13	1.6351	1.0000	no	18.0000	1.0000	no
Slc30a2	8.0000	1.0000	no	1.1473	1.0000	no
Slc30a3	1.6389	1.0000	no	1.5156	1.0000	no
Slc30a4	2.3429	0.0611	no	2.2856	0.0084	yes
Slc32a1	2.0534	1.0000	no	-1.0058	1.0000	no
Slc35d3	4.3764	0.0005	yes	1.2727	0.1834	no
Slc35e4	1.6385	1.0000	no	18.0000	1.0000	no
Slc37a3	0.3263	0.9962	no	0.9916	0.1052	no
Slc38a3	1.9987	0.0862	no	0.5833	0.5633	no
Slc41a2	8.0000	1.0000	no	0.9793	1.0000	no
Slc44a1	0.3794	0.9098	no	0.5626	0.4599	no
Slc44a5	0.4341	0.9997	no	0.4254	0.6887	no
Slc45a3	2.3038	0.0476	yes	2.4126	0.0051	yes
Slc47a2	0.0000	1.0000	no	-0.0314	1.0000	no
Slc4a11	3.4589	1.0000	no	18.0000	1.0000	no
Slc4a4	3.8996	1.0000	no	0.7809	1.0000	no
Slc4a8	4.0384	1.0000	no	3.3671	0.0546	no
Slc5a5	0.0435	1.0000	no	1.5110	1.0000	no
Slc6a17	0.0000	1.0000	no	0.0000	1.0000	no
Slc6a20a	2.4717	0.0002	yes	0.6562	0.4472	no
Slc6a4	1.8576	1.0000	no	1.5173	1.0000	no
Slc7a10	8.0000	1.0000	no	-1.9757	1.0000	no
Slc7a8	1.8834	0.0551	no	1.0291	0.2160	no
Slc9a2	0.0000	1.0000	no	0.0000	1.0000	no
Slc9a3	0.0000	1.0000	no	18.0000	1.0000	no
Slc9a3r2	2.5079	0.0020	yes	1.4875	0.0493	yes
Slc9a5	1.4807	1.0000	no	3.0623	1.0000	no
Slco3a1	3.3423	0.0204	yes	2.5389	0.0001	yes
Slmo1	1.0743	0.7157	no	1.5019	1.0000	no
Smad1	2.7367	0.0116	yes	1.7885	0.0426	yes
Smad4	0.3278	0.8886	no	1.7450	0.0000	yes
Smad6	2.0217	0.0352	yes	0.9587	0.2897	no
Smad7	1.4776	0.4611	no	1.9418	0.0113	yes
Smad9	2.2010	1.0000	no	1.3728	1.0000	no
Smagp	1.1088	0.5040	no	1.2964	0.1495	no
Smarca2	1.4121	0.0000	yes	2.1858	0.0000	yes
Smarcd3	0.1658	0.9997	no	0.8920	0.2991	no
Smo	0.1505	0.9997	no	2.4160	0.0016	yes
Smok2a	0.0000	1.0000	no	0.0000	1.0000	no

Smpdl3b	2.6091	1.0000	no	-0.7364	1.0000	no
Smtnl1	1.9435	1.0000	no	-1.0292	1.0000	no
Smurf1	1.2332	0.3812	no	2.2536	0.0072	yes
Snai1	1.2456	1.0000	no	0.4364	1.0000	no
Snai3	8.0000	1.0000	no	18.0000	1.0000	no
Snap91	0.0000	1.0000	no	18.0000	1.0000	no
Sncaip	2.0194	1.0000	no	1.1430	1.0000	no
Sncb	0.0000	1.0000	no	0.0000	1.0000	no
Snhg11	3.3865	1.0000	no	1.3162	1.0000	no
Snn	1.4213	0.4660	no	0.7879	0.4528	no
Snph	0.0000	1.0000	no	0.0000	1.0000	no
Snta1	1.3727	0.4017	no	0.2983	0.8044	no
Sntb2	0.8114	0.8519	no	2.6156	0.0057	yes
Snx10	2.0239	0.0133	yes	0.9751	0.1082	no
Snx18	0.2581	0.9997	no	1.4293	0.0823	no
Snx21	0.7978	0.2307	no	-0.2087	0.7523	no
Snx24	1.7613	0.0679	no	0.5441	0.5584	no
Sobp	0.0000	1.0000	no	18.0000	1.0000	no
Socs1	3.2627	1.0000	no	2.1869	1.0000	no
Socs2	0.8593	0.3072	no	1.7636	0.0079	yes
Socs3	2.8829	0.0000	yes	-0.4010	0.4792	no
Sort1	1.5612	0.0047	yes	2.3539	0.0000	yes
Sox1	NA	NA	NA	NA	NA	NA
Sox11	2.4161	1.0000	no	-1.0960	1.0000	no
Sox13	2.7202	0.0007	yes	2.4833	0.0004	yes
Sox18	1.3282	0.5595	no	0.9846	0.3615	no
Sox2	0.0000	1.0000	no	0.0000	1.0000	no
Sox21	0.0000	1.0000	no	18.0000	1.0000	no
Sox30	0.0000	1.0000	no	0.0000	1.0000	no
Sox4	0.5768	0.8917	no	2.5332	0.0004	yes
Sox6	0.6446	0.0040	yes	-0.7765	0.0081	yes
Sox7	3.0319	1.0000	no	0.1286	1.0000	no
Sox8	0.0400	1.0000	no	0.0000	1.0000	no
Sp5	0.0000	1.0000	no	0.0000	1.0000	no
Sp7	0.0000	1.0000	no	18.0000	1.0000	no
Sp9	-0.0198	0.9997	no	-0.7585	0.4242	no
Spata18	8.0000	1.0000	no	18.0000	1.0000	no
Spats2	0.0733	0.9997	no	1.6646	0.0485	yes
Spats2l	3.5254	0.0021	yes	3.2295	0.0674	no
Spdya	-0.0221	0.9997	no	1.4352	0.1536	no
Speg	1.3377	0.4004	no	0.0649	0.9507	no
Spint1	8.0000	1.0000	no	18.0000	1.0000	no
Spint2	0.2076	0.9997	no	2.1909	0.0003	yes
Spna2	1.9678	0.0001	yes	1.8196	0.0000	yes
Spnb2	1.4026	0.0005	yes	1.8098	0.0004	yes
Spnb3	0.9276	1.0000	no	0.1375	1.0000	no
Spnb4	2.2342	1.0000	no	1.9966	0.4057	no
Spns2	0.5329	0.2425	no	2.8712	0.0000	yes
Spock2	-0.2127	1.0000	no	3.0837	1.0000	no

Spred1	-0.1330	0.9997	no	1.4978	0.0670	no
Spred3	1.2748	1.0000	no	1.4296	1.0000	no
Spsb1	2.4325	0.4727	no	18.0000	1.0000	no
Spsb4	2.0608	1.0000	no	1.5374	1.0000	no
Src	0.5719	0.9997	no	2.0134	0.1245	no
Srcin1	-0.3751	1.0000	no	18.0000	1.0000	no
Srgap1	1.7130	1.0000	no	0.6502	1.0000	no
Srms	1.1607	1.0000	no	1.8530	1.0000	no
Srsf13b	NA	NA	NA	NA	NA	NA
St14	2.9581	0.1609	no	0.6245	0.5670	no
St8sia6	8.0000	1.0000	no	4.4008	1.0000	no
Stac2	2.0353	1.0000	no	18.0000	1.0000	no
Stat5b	-0.4129	0.5520	no	1.4041	0.0182	yes
Stau2	0.8972	0.1941	no	2.8653	0.0000	yes
Steap2	1.6828	0.0782	no	1.8868	0.0018	yes
Stk33	0.0000	1.0000	no	0.0000	1.0000	no
Stk39	1.9893	0.0023	yes	1.4564	0.0582	no
Stmn3	8.0000	1.0000	no	0.0000	1.0000	no
Stox1	1.0395	1.0000	no	0.5553	1.0000	no
Stox2	1.3928	1.0000	no	1.2814	1.0000	no
Stx3	-0.3375	0.9997	no	1.0177	0.0780	no
Stxbp5l	0.0000	1.0000	no	0.0000	1.0000	no
Sulf2	2.0587	1.0000	no	3.9124	0.0001	yes
Susd3	1.4372	0.4309	no	0.9896	0.3067	no
Susd5	0.0000	1.0000	no	0.0000	1.0000	no
Sv2c	-1.0079	1.0000	no	-12.0000	1.0000	no
Syde2	0.4847	0.9997	no	3.7340	0.0000	yes
Syn2	8.0000	1.0000	no	-1.5129	1.0000	no
Sync	0.0271	0.9997	no	-0.9620	0.1675	no
Syncrip	-0.1672	0.8122	no	1.2236	0.0000	yes
Syne2	0.9177	0.6767	no	1.0454	0.1875	no
Syngr3	-6.0000	1.0000	no	-0.0588	1.0000	no
Synj2	2.0476	0.0030	yes	1.8729	0.1725	no
Synm	0.4944	1.0000	no	2.2242	1.0000	no
Synpo	0.3264	1.0000	no	2.5559	1.0000	no
Sypl2	8.0000	1.0000	no	-12.0000	1.0000	no
Syt12	0.7034	1.0000	no	1.9838	1.0000	no
Syt13	8.0000	1.0000	no	1.9574	1.0000	no
Syt2	-0.7630	1.0000	no	2.8012	1.0000	no
Syt7	1.4851	1.0000	no	1.2957	1.0000	no
Syt9	1.1197	1.0000	no	0.0000	1.0000	no
T	0.0000	1.0000	no	18.0000	1.0000	no
Tanc1	1.1448	0.7065	no	2.2226	1.0000	no
Tbc1d16	0.6216	0.9997	no	1.8112	0.0333	yes
Tbc1d30	1.4406	1.0000	no	3.5436	1.0000	no
Tbc1d9	-0.1900	0.9997	no	-0.2461	0.7705	no
Tbkbp1	2.2964	0.0206	yes	1.8786	0.0003	yes
Tbr1	0.0000	1.0000	no	0.0000	1.0000	no
Tbx1	8.0000	1.0000	no	0.0000	1.0000	no

Tbx15	2.6089	1.0000	no	18.0000	1.0000	no
Tbx18	0.0000	1.0000	no	0.0000	1.0000	no
Tbx2	1.1771	1.0000	no	-0.5923	1.0000	no
Tbx20	0.0407	1.0000	no	18.0000	1.0000	no
Tbx21	0.0000	1.0000	no	18.0000	1.0000	no
Tbx3	2.3629	0.1366	no	0.7776	0.4161	no
Tbx4	0.0000	1.0000	no	0.0000	1.0000	no
Tcea3	1.1933	0.5200	no	0.9935	0.2846	no
Tcf15	0.7115	1.0000	no	1.5056	1.0000	no
Tcf7	2.1559	0.0097	yes	2.1809	0.0001	yes
Tcf7l1	2.9356	0.0325	yes	2.4907	0.0236	yes
Tcf7l2	0.2999	0.9275	no	-1.1973	0.0003	yes
Tcfap2a	NA	NA	NA	NA	NA	NA
Tcfap2c	NA	NA	NA	NA	NA	NA
Tcfap2e	NA	NA	NA	NA	NA	NA
Tcfeb	NA	NA	NA	NA	NA	NA
Tcfl5	8.0000	1.0000	no	18.0000	1.0000	no
Tcp11l1	1.0898	0.6641	no	2.0600	0.0092	yes
Tcte2	0.1526	1.0000	no	-0.9817	1.0000	no
Tdrd5	1.4640	1.0000	no	1.6029	1.0000	no
Tead1	2.0864	1.0000	no	0.0712	1.0000	no
Tead2	1.1469	0.4231	no	0.6823	0.4869	no
Tead4	1.4031	1.0000	no	-0.4951	1.0000	no
Tec	2.4836	0.0005	yes	1.8132	0.0000	yes
Tesc	4.1693	0.2498	no	1.8730	0.1720	no
Tex14	-1.7018	1.0000	no	2.7877	1.0000	no
Tgfa	2.6408	0.0383	yes	1.6213	1.0000	no
Tgfb2	1.0265	1.0000	no	0.7218	1.0000	no
Tgif1	0.7698	0.3306	no	2.3726	0.0000	yes
Thpo	2.0840	1.0000	no	1.3686	0.1948	no
Thrb	0.5532	1.0000	no	0.2814	1.0000	no
Tiam2	-0.4161	0.9997	no	1.3013	1.0000	no
Timp3	1.2304	0.4912	no	1.4611	0.1145	no
Tipin	-0.2916	0.8222	no	-0.2250	0.8084	no
Tjp1	1.6121	0.0008	yes	2.8937	0.0000	yes
Tjp2	0.8272	0.2837	no	1.8180	0.0047	yes
Tle2	2.0273	0.0729	no	0.5835	0.5159	no
Tll1	0.0000	1.0000	no	0.0000	1.0000	no
Tlx1	0.0000	1.0000	no	0.0000	1.0000	no
Tlx2	8.0000	1.0000	no	2.2131	1.0000	no
Tlx3	0.0000	1.0000	no	0.0000	1.0000	no
Tm6sf1	2.6985	0.0000	yes	1.8131	0.0000	yes
Tmcc3	2.3295	0.0101	yes	0.9398	0.4020	no
Tmed8	-0.1787	0.9997	no	2.5128	0.0025	yes
Tmeff1	1.2266	0.5239	no	1.6530	0.1262	no
Tmem102	2.6302	1.0000	no	3.5486	1.0000	no
Tmem108	3.2010	1.0000	no	2.3469	1.0000	no
Tmem117	8.0000	1.0000	no	18.0000	1.0000	no
Tmem121	1.0559	1.0000	no	2.5056	1.0000	no

Tmem132b	0.0000	1.0000	no	0.0000	1.0000	no
Tmem132e	1.1064	1.0000	no	1.6576	1.0000	no
Tmem145	0.0000	1.0000	no	18.0000	1.0000	no
Tmem150a	1.7118	0.1659	no	1.4789	0.0948	no
Tmem150c	0.8651	1.0000	no	4.1651	1.0000	no
Tmem151a	-1.9901	1.0000	no	18.0000	1.0000	no
Tmem151b	0.0000	1.0000	no	18.0000	1.0000	no
Tmem158	0.7097	0.9504	no	2.5162	0.0085	yes
Tmem163	8.0000	1.0000	no	3.9164	1.0000	no
Tmem22	1.0268	1.0000	no	0.0057	1.0000	no
Tmem229a	3.5182	1.0000	no	0.5107	1.0000	no
Tmem229b	1.5544	0.0108	yes	2.1329	0.0000	yes
Tmem28	8.0000	1.0000	no	0.0000	1.0000	no
Tmem30b	4.1409	1.0000	no	0.5037	1.0000	no
Tmem44	1.0228	0.3980	no	2.9047	1.0000	no
Tmem54	8.0000	0.0561	no	2.3684	0.3454	no
Tmem59l	8.0000	1.0000	no	18.0000	1.0000	no
Tmem8	0.4735	0.9300	no	1.9281	0.0184	yes
Tmem90a	0.0000	1.0000	no	0.9494	1.0000	no
Tmem91	0.0401	0.9997	no	-0.1240	1.0000	no
Tmem98	1.6449	0.1843	no	1.8342	0.0395	yes
Tmie	2.3006	1.0000	no	1.1212	1.0000	no
Tmod2	8.0000	1.0000	no	18.0000	1.0000	no
Tmtc1	1.3924	1.0000	no	0.6615	1.0000	no
Tnfrsf11a	1.3016	1.0000	no	0.6822	1.0000	no
Tnfsf11	0.0350	1.0000	no	2.0260	1.0000	no
Tnrc18	0.7859	0.3455	no	-0.0480	0.9512	no
Tns1	-0.7740	0.0208	yes	0.0689	0.9272	no
Tns3	0.9531	0.3556	no	1.7684	0.0123	yes
Tnxb	2.2087	1.0000	no	18.0000	1.0000	no
Tpbg	8.0000	1.0000	no	18.0000	1.0000	no
Tpd52	0.7535	0.1719	no	1.3732	0.0002	yes
Tpm1	-0.0903	0.9985	no	-0.5244	0.0191	yes
Tpm2	1.5900	0.0986	no	1.9761	0.0021	yes
Tpm4	1.5253	0.0138	yes	0.8811	0.1270	no
Tppp	0.6104	0.9997	no	1.7348	0.4061	no
Trank1	8.0000	1.0000	no	18.0000	1.0000	no
Trib1	1.8995	1.0000	no	0.4855	0.6662	no
Tril	8.0000	1.0000	no	0.9202	1.0000	no
Trim14	1.8271	0.0414	yes	1.1692	0.0755	no
Trim36	0.7026	1.0000	no	2.2831	1.0000	no
Trim47	1.6263	0.0409	yes	-0.2790	0.7305	no
Trim62	0.9407	1.0000	no	4.4291	1.0000	no
Trim67	0.0000	1.0000	no	-12.0000	1.0000	no
Trim7	-0.0282	0.9997	no	0.7103	0.4988	no
Trim71	2.6705	1.0000	no	1.2321	1.0000	no
Trio	1.0561	0.4216	no	2.0283	0.0114	yes
Triobp	0.3826	0.8484	no	-0.0287	0.9611	no
Trnp1	0.0000	1.0000	no	2.2092	1.0000	no

Trp53i11	2.4617	0.0787	no	0.9526	0.3250	no
Trp73	0.3476	1.0000	no	18.0000	1.0000	no
Trpc1	0.8407	1.0000	no	1.6240	1.0000	no
Trpc3	8.0000	1.0000	no	2.2707	1.0000	no
Trpm8	0.0000	1.0000	no	0.0000	1.0000	no
Trps1	1.3862	1.0000	no	1.6030	1.0000	no
Tsc22d1	-0.2027	0.9774	no	-0.3646	0.5515	no
Tshr	8.0000	1.0000	no	1.9351	1.0000	no
Tshz3	2.6013	1.0000	no	0.5395	1.0000	no
Tsku	1.7139	1.0000	no	1.1077	1.0000	no
Tspan18	0.9376	0.4343	no	0.7831	0.2567	no
Tspan2	2.2905	0.0204	yes	2.1914	0.0029	yes
Tspan5	-0.2826	0.9629	no	1.8219	0.0030	yes
Ttbk1	0.0000	1.0000	no	18.0000	1.0000	no
Ttc34	0.0000	1.0000	no	0.0000	1.0000	no
Ttc39c	2.2772	0.2269	no	2.2471	0.0009	yes
Ttc9	8.0000	1.0000	no	18.0000	1.0000	no
Ttc9b	0.0000	1.0000	no	0.0000	1.0000	no
Ttll11	0.2325	1.0000	no	0.0784	1.0000	no
Ttpa	1.1803	0.4472	no	0.3817	0.7286	no
Ttyh1	0.2971	1.0000	no	0.0863	1.0000	no
Tub	8.0000	1.0000	no	18.0000	1.0000	no
Tubb2b	0.2012	0.9997	no	0.0135	0.9908	no
Tubb6	1.9084	0.0792	no	0.7921	0.4042	no
Tulp1	2.6859	0.1971	no	-12.0000	1.0000	no
Tulp4	-0.2309	0.9606	no	1.7243	0.0028	yes
Twist1	2.0415	1.0000	no	-0.6401	1.0000	no
Txndc16	0.9746	0.4365	no	0.7242	0.2359	no
Tyro3	3.4878	0.0004	yes	1.4939	0.2554	no
Uap1l1	1.3929	0.0338	yes	1.1532	0.0131	yes
Ube2j1	-0.0254	0.9997	no	-0.2173	0.7073	no
Ube2ql1	8.0000	1.0000	no	0.4645	1.0000	no
Ubl3	0.1460	0.9997	no	1.5010	0.0021	yes
Ubtd1	1.3837	0.4513	no	1.4890	0.1042	no
Ubtd2	0.2630	0.9997	no	1.6035	0.0827	no
Ucn	0.0000	1.0000	no	0.0000	1.0000	no
Ucp1	0.0000	1.0000	no	18.0000	1.0000	no
Ulk2	0.2732	0.9997	no	0.7939	0.1655	no
Unc13b	0.2499	0.9997	no	3.0889	0.0017	yes
Unc5a	3.5823	0.1236	no	4.9207	0.0022	yes
Unc5b	3.2344	1.0000	no	0.1776	1.0000	no
Unc80	8.0000	1.0000	no	0.0000	1.0000	no
Uncx	0.0000	1.0000	no	0.0000	1.0000	no
Usp2	0.2353	0.9997	no	1.7416	0.1799	no
Usp35	-0.5305	1.0000	no	18.0000	1.0000	no
Usp43	0.0000	1.0000	no	18.0000	1.0000	no
Ust	0.9268	1.0000	no	0.5889	1.0000	no
Utf1	8.0000	1.0000	no	0.0000	1.0000	no
Vangl1	0.1518	0.9997	no	-0.8807	0.1110	no

Vash1	2.2048	0.0068	yes	1.4875	0.0319	yes
Vash2	1.3524	1.0000	no	2.3810	1.0000	no
Vat1	0.9605	0.3249	no	1.7114	0.0226	yes
Vav2	0.2897	0.9997	no	1.2468	0.1015	no
Vav3	1.3969	0.2961	no	1.9778	0.0034	yes
Vax1	8.0000	1.0000	no	0.0000	1.0000	no
Vax2	8.0000	1.0000	no	0.0000	1.0000	no
Vax2os1	0.0000	1.0000	no	0.0000	1.0000	no
Vax2os2	0.0000	1.0000	no	0.0000	1.0000	no
Vgf	4.2903	1.0000	no	1.7947	1.0000	no
Vgll3	-6.0000	1.0000	no	-12.0000	1.0000	no
Vim	2.5133	0.0000	yes	2.1227	0.0000	yes
Vipr1	8.0000	1.0000	no	3.0527	0.0618	no
Vldlr	2.4213	1.0000	no	2.0883	1.0000	no
Vmn1r90	0.3381	1.0000	no	2.5845	1.0000	no
Vmn2r-ps14	NA	NA	NA	NA	NA	NA
Vrtn	8.0000	1.0000	no	0.0000	1.0000	no
Vsig10	2.0012	1.0000	no	1.7823	1.0000	no
Vstm2l	0.0000	1.0000	no	0.0000	1.0000	no
Vsx1	0.0000	1.0000	no	0.0000	1.0000	no
Vsx2	0.0000	1.0000	no	0.0000	1.0000	no
Vwa2	0.0000	1.0000	no	0.0000	1.0000	no
Vwa5b2	1.3821	0.0762	no	3.3639	1.0000	no
Wasf1	1.3242	1.0000	no	4.2401	1.0000	no
Wasf3	8.0000	1.0000	no	18.0000	1.0000	no
Wdfy3	0.2597	0.9186	no	0.5411	0.1274	no
Wdr8	-0.1080	0.9997	no	0.4623	0.4330	no
Wdr86	0.0989	1.0000	no	1.0462	1.0000	no
Whrn	4.5019	1.0000	no	1.9204	1.0000	no
Wipf1	0.0179	0.9997	no	1.6434	0.0001	yes
Wnk2	0.3937	1.0000	no	1.0601	1.0000	no
Wnt1	0.0000	1.0000	no	0.0000	1.0000	no
Wnt10a	0.0000	1.0000	no	0.0000	1.0000	no
Wnt10b	8.0000	1.0000	no	18.0000	1.0000	no
Wnt11	0.0000	1.0000	no	-1.2277	1.0000	no
Wnt2b	1.0390	1.0000	no	-0.8780	1.0000	no
Wnt3	0.0000	1.0000	no	0.0000	1.0000	no
Wnt3a	0.0447	1.0000	no	-1.3327	1.0000	no
Wnt4	0.3885	1.0000	no	-0.4004	1.0000	no
Wnt5b	1.0412	1.0000	no	-0.0565	1.0000	no
Wnt6	0.0000	1.0000	no	18.0000	1.0000	no
Wnt7a	0.0000	1.0000	no	0.0000	1.0000	no
Wnt7b	0.0000	1.0000	no	0.0000	1.0000	no
Wnt9a	0.0000	1.0000	no	18.0000	1.0000	no
Wnt9b	8.0000	1.0000	no	18.0000	1.0000	no
Wscd2	0.0000	1.0000	no	0.0000	1.0000	no
Wt1	1.9087	1.0000	no	18.0000	1.0000	no
Wtip	3.6916	0.0001	yes	1.7556	0.0324	yes
Wwc1	3.9352	0.0010	yes	0.4952	0.8041	no

Wwtr1	1.5569	1.0000	no	1.6008	1.0000	no
X99384	1.1521	0.6016	no	0.8638	0.3754	no
Xkr4	0.0000	1.0000	no	0.0000	1.0000	no
Xkr6	1.4478	1.0000	no	2.2365	1.0000	no
Xkr7	0.0000	1.0000	no	18.0000	1.0000	no
Xlr	-1.5189	0.1346	no	-2.2148	0.0044	yes
Xylt1	0.2733	0.9997	no	2.7980	0.0074	yes
Yap1	1.6879	0.7515	no	1.0253	0.2335	no
Ybx2	5.3486	0.0982	no	-0.0813	0.9494	no
Yes1	0.9767	0.3351	no	1.0466	0.1282	no
Ypel1	0.2264	0.9997	no	0.2402	0.8319	no
Zar1	0.0000	1.0000	no	0.0000	1.0000	no
Zbed3	1.2349	0.5420	no	2.4447	0.0044	yes
Zbtb10	0.9741	0.4171	no	2.8972	0.0016	yes
Zbtb16	0.8229	1.0000	no	2.8928	0.0013	yes
Zbtb42	1.0350	0.7491	no	3.0242	0.0095	yes
Zbtb7c	8.0000	1.0000	no	-0.9677	1.0000	no
Zbtb8b	4.4052	1.0000	no	-2.0184	1.0000	no
Zc3h12c	0.5871	0.9986	no	2.6470	1.0000	no
Zcchc14	1.2225	0.2838	no	0.9146	1.0000	no
Zdbf2	2.8345	1.0000	no	-2.4303	1.0000	no
Zdhhc2	0.4627	0.8201	no	1.1353	0.0151	yes
Zdhhc23	1.3753	0.4746	no	18.0000	1.0000	no
Zdhhc8	1.5866	0.2362	no	2.5079	0.0031	yes
Zfp105	1.5297	0.2579	no	2.3056	0.0144	yes
Zfp277	-0.1297	0.9997	no	1.1541	0.0221	yes
Zfp318	0.4440	0.7683	no	1.1938	0.0714	no
Zfp358	0.1520	0.9997	no	2.1327	0.0170	yes
Zfp385b	0.5622	1.0000	no	1.0479	0.3932	no
Zfp395	-0.0899	0.9997	no	1.6408	0.0427	yes
Zfp423	8.0000	1.0000	no	-5.0401	1.0000	no
Zfp503	1.8497	1.0000	no	1.2548	1.0000	no
Zfp516	2.7142	0.0082	yes	2.0475	0.0126	yes
Zfp521	1.1573	1.0000	no	4.3944	1.0000	no
Zfp580	2.0377	0.1736	no	1.5439	0.1489	no
Zfp608	1.0979	0.5650	no	2.4060	0.0034	yes
Zfp618	1.7337	1.0000	no	1.2698	1.0000	no
Zfp623	0.2969	0.9997	no	2.2148	0.0126	yes
Zfp651	2.3413	1.0000	no	0.7186	1.0000	no
Zfp664	-0.0226	0.9997	no	0.6678	0.1900	no
Zfp703	0.9104	0.6778	no	1.3956	0.0779	no
Zfp704	0.1288	0.9997	no	1.7142	0.0289	yes
Zfp710	1.0425	0.3321	no	1.8713	0.0008	yes
Zfp777	-0.1112	0.9997	no	2.7284	0.0000	yes
Zfp810	-0.1420	0.9997	no	1.6521	0.1078	no
Zfp827	1.5315	0.0307	yes	2.5775	0.0026	yes
Zfp964	2.3274	1.0000	no	18.0000	1.0000	no
Zfpm2	0.2006	1.0000	no	-0.4280	1.0000	no
Zfyve28	0.5803	1.0000	no	3.1112	1.0000	no

Zhx2	-0.1910	0.9997	no	-9.1172	1.0000	no
Zic1	0.0000	1.0000	no	0.0000	1.0000	no
Zic2	0.0000	1.0000	no	0.0000	1.0000	no
Zic5	0.0000	1.0000	no	18.0000	1.0000	no
Zkscan16	8.0000	1.0000	no	0.0000	1.0000	no
Zkscan17	0.2589	0.9871	no	1.4054	0.0184	yes
Zkscan2	3.3912	1.0000	no	18.0000	1.0000	no
Zmat3	0.0257	0.9997	no	1.1631	0.4398	no
Zmiz1	0.9519	0.0374	yes	1.6725	0.0007	yes
Zmynd11	-0.2611	0.8177	no	0.8412	0.0065	yes
Znrf4	0.0000	1.0000	no	18.0000	1.0000	no
Zswim5	1.5850	1.0000	no	3.7505	1.0000	no
Zswim6	1.1000	0.6767	no	1.1740	0.2157	no
Zyg11a	-0.9673	1.0000	no	2.1595	1.0000	no

Table S2. Genes contained in the Mtf2-PRC2 erythroid-specific gene regulatory network

Gene Name	log2 Fold Change
Acsl6	2.3106
Actn1	1.39382
Acvr1	1.82458
Acvr1b	2.44087
Adam15	1.90754
Adap1	2.63643
Adc	1.79769e+308
Agap1	2.77345
Agap2	2.96827
Agpat3	2.35275
Ahnak	2.0414
Aim1	2.41919
Ak4	2.54939
Ankrd13b	3.79421
Ankrd44	2.64606
Arf3	1.97697
Arhgef10l	1.98416
Arsb	2.46866
Asap2	2.3364
Atp11a	1.57917
Atp8b2	2.8691
AW011738	2.01983
AW555464	2.23256
B4galnt1	3.12791
B4galt5	1.157
B4galt6	2.73133
Bahcc1	1.93575
BC005764	2.13385
Bcr	3.47984
Bend4	2.31495
Bend7	2.01608
Bin1	1.93024
Bmi1	2.8787
Bmp1	2.34436
Bmpr1a	1.51743
Brwd1	1.82602
Cables1	2.12916
Camk2d	1.65181
Camkk1	2.55516
Card10	2.89161
Casz1	2.8976
Cbfb	2.34785
Cbs	2.52744
Cbx2	3.4014
Cbx4	2.56136
Cbx7	1.19618

Cbx8	2.72465
Ccdc85c	3.00989
Ccdc92	3.50689
Ccnd2	3.06765
Cd63	2.37898
Cd9	1.73468
Cdc14b	1.70367
Cdc42bpb	2.01637
Cdh1	2.37681
Cdh2	1.74543
Cdk18	1.87656
Cdkn1a	1.83109
Cebpa	2.0635
Cebpd	2.49204
Chd3	1.42096
Chn2	1.93083
Chpf	3.21552
Cited1	1.65424
Ckap4	2.31578
Clgn	1.75111
Clstn1	3.06789
Cmtm4	3.17668
Cmtm7	2.72361
Cnn2	2.40825
Cnn3	2.10438
Cnnm1	3.54487
Col18a1	1.50364
Col27a1	2.1921
Coro2a	2.72176
Cpeb2	2.04865
Cpm	2.17436
Cpne7	2.47633
Crtc3	1.64223
Cry1	2.40869
Csf1	1.10538
Csnk1e	1.86429
Csrnp1	2.15097
Ctbp2	2.58461
Ctnnbip1	2.14207
Cxcr4	2.55437
Cyfip2	3.15987
D730039F16Rik	2.61233
Dab2ip	2.87829
Dapk1	1.0891
Dip2b	1.60719
Dip2c	1.65976
Dkkl1	2.74449
Dlg5	2.34881
Dlgap4	2.21047

Dlx4	3.79879
Dmxl2	2.64677
Dnmt3a	2.03249
Dnmt3b	3.13864
Dock3	3.31071
Dock7	1.09716
Dock9	2.10356
Dtx4	2.92202
Dusp2	3.1277
Dyrk2	2.74666
E130012A19Rik	3.94097
E330009J07Rik	2.59478
E330016A19Rik	3.1213
Efcab4a	1.95855
Efemp2	1.73444
Egln3	2.36207
Eid2	3.53919
Elk3	1.68747
Emid1	3.02237
Enc1	2.43163
Enpp1	2.00294
Epb4.1l4b	2.50988
Ephb3	4.62555
Etv5	1.57466
Evl	1.86984
Faah	2.57183
Fam101b	3.0987
Fam135a	2.93953
Fam171a1	2.10314
Fam174b	3.08017
Fam43a	2.3476
Fam49b	1.5926
Fam57a	1.94918
Fam65a	2.73112
Fam65b	2.24606
Fes	2.66342
Fgfr1	2.89634
Fgfr3	2.67952
Fhl3	2.48859
Fhod1	1.64919
Fkbp5	1.83528
Fli1	2.18855
Flt3	2.59442
Fmnl1	2.8386
Fmnl3	2.01061
Fn1	1.84421
Fnbp1	2.2098
Fnbp1l	1.83292
Fndc3a	1.50609

Fndc3b	2.12114
Fndc4	3.53764
Fosl2	2.14213
Foxo1	2.23987
Foxp4	2.29997
Furin	2.12522
Fzd6	2.81728
Gadd45b	2.73846
Galnt12	3.54246
Galnt3	3.20934
Galnt6	1.87689
Gata2	2.32442
Gfi1	3.0311
Gjb2	3.23886
Gkap1	3.41237
Gldc	1.69956
Gls2	4.23873
Gnaq	1.92937
Gnb4	2.0392
Gng12	2.11977
Gpc1	3.10088
Gpr160	2.42711
Gpt2	1.76635
Grb10	1.12843
Grwd1	2.54208
H1f0	2.01501
H1fx	2.49154
H2-K1	2.01047
H2-Q6	2.23193
H2afy2	3.3536
Hcn2	3.10571
Hdgfrp3	2.47076
Hhex	2.02505
Hip1r	1.92211
Hivep3	3.06165
Hlx	2.31703
Hmga2	2.85397
Homer3	1.34529
Hoxa9	3.96371
Hspa1a	2.44652
Hspa1b	2.46644
Ica1	1.88431
Id3	1.98319
Igf2bp2	3.07421
Igfbp4	2.41189
Impdh1	3.01498
Inf2	2.24384
Inppl1	1.91671
Irak3	2.44434

Irf1	1.81397
Itga5	2.48914
Itga6	2.05143
Itga9	1.73069
Itgav	2.07196
Itgb5	1.30501
Itpr3	2.35546
Jdp2	2.05608
Jun	1.49371
Kcnk12	3.10943
Kctd1	3.52632
Kif13a	2.44963
Kif1b	1.50274
Kif1c	1.66642
Kif21a	2.77857
Kifc3	1.75002
Klc2	1.64325
Klf5	2.16088
Klhl22	1.59962
Kremen1	2.46737
L3mbtl3	2.10165
Lamc1	2.81635
Lass6	2.39443
Ldlrad3	2.77601
Lepre1	2.33353
Limd2	2.37856
Lmx1a	2.19729
Lpgat1	2.59693
Lphn1	2.55667
Lrfn4	1.63607
Lrp5	2.44057
Lrrk1	3.28081
Luzp1	1.9805
Man1c1	2.00826
Man2a2	2.82994
Map3k10	1.21885
Map3k3	1.47636
Map3k5	2.46772
Map4k4	2.15295
Mapk13	2.62303
Mapkapk2	1.7307
Marcksl1	2.27067
Marveld1	2.63953
Mcmbp	1.17489
Mctp1	2.29171
Megf8	2.87007
Meis1	2.24103
Mettl1	2.55341
Micall1	2.56752

Mllt6	2.26098
Mmp17	3.78338
Mpp6	1.68955
Mtap7	2.58987
Mtss1l	2.2463
Mtus1	2.41041
Myb	2.95785
Mycn	2.8102
Myo10	2.08608
Myo1e	2.46561
Myo5a	1.97753
Nab1	1.46547
Nacc2	2.30058
Nags	2.44405
Nat8l	2.91964
Nbea	2.67776
Ncoa1	1.58101
Ncoa3	1.39342
Nedd4l	2.24045
Nefh	4.02304
Nek6	1.51116
Nes	2.28995
Nfatc1	2.58107
Nfia	3.54124
Nfic	1.9736
Nfil3	2.88473
Nfkb1	2.5299
Nin	2.8118
Nkain1	4.23709
Nlgn2	3.04826
Nlrp6	2.53456
Notch1	1.89117
Npr1	1.73029
Nr2f6	1.40843
Nrbp2	2.07304
Nrg2	3.19851
Ntn4	2.61676
Ntng2	4.59946
Nuak2	2.3626
Obsl1	2.191
Odf3b	3.78173
Olfm1	3.66639
P2ry2	2.89775
Paqr9	2.29772
Parp8	2.78085
Pawr	2.26174
Pcnx	2.45495
Pcolce2	2.94074
Pcsk6	3.92379

Pde2a	2.16477
Pde3b	2.60438
Pde4a	3.01221
Pde8a	2.7082
Peli2	2.33195
Pfkfb3	2.94413
Phactr2	1.96303
Phf15	1.45292
Phf21b	5.8015
Phldb1	2.33718
Pitpnm1	2.25427
Pkd2	3.23842
Pkdcc	2.35081
Plbd1	1.72047
Plcg1	2.5269
Pld2	2.53146
Plec	1.93863
Plekha1	1.55507
Plekha2	2.6754
Plekha5	2.52388
Plekhg3	2.21088
Plekhh1	1.78939
Plekho1	1.27598
Plk3	2.3664
Plxdc1	3.57297
Plxna1	2.86102
Plxnb2	1.63072
Plxnc1	1.55712
Plxnd1	2.44376
Ppargc1b	3.362
Ppm1h	2.31213
Prkar2a	2.35424
Prkca	1.49501
Pstpip2	2.09833
Ptger3	2.73883
Ptms	1.87093
Ptpn21	2.82238
Ptpn9	2.10298
Ptprf	1.89957
Ptprj	1.39987
Ptprs	2.75307
Ptpru	1.87802
Rab11fip3	1.92261
Rab31	2.18594
Rapgef4	1.96191
Rara	2.21229
Rasa2	2.23024
Rasgrp2	2.43691
Rassf5	2.16505

Rbfox2	1.56623
Rbpms	1.72527
Rcor2	2.94044
Rcsd1	2.20954
Rftn1	2.56772
Rhbdf1	4.38461
Rhobtb3	2.03686
Rhou	2.2017
Rin3	2.48226
Rnd2	2.42383
Rnf130	2.01679
Rnf144a	3.66583
Rnf144b	2.10782
Rnf208	2.72266
Rnf217	2.47131
Rragd	1.17313
Rsrc1	1.71999
Rtkn	1.56675
Samd10	2.78476
Satb1	2.24113
Sbk1	3.13338
Sccpdh	2.47747
Sdc1	2.2958
Sec14l2	1.94317
Sec24d	1.90432
Sema4g	2.20961
Sema6b	2.25561
Sepn1	2.20868
Serinc2	4.97386
Serpine2	3.46582
Sfmbt2	3.09049
Sgcb	2.68952
Sh2d5	1.44978
Sh3bp5	1.71268
Sh3pxd2b	2.04943
Shank3	3.00793
Siah2	2.40141
Sirpa	1.579
Six5	2.62066
Slain1	4.02134
Slain2	2.24301
Slc12a2	2.07343
Slc22a17	2.4903
Slc23a2	2.33143
Slc25a23	2.29157
Slc25a33	2.37869
Slc26a10	3.17706
Slc45a3	2.92951
Slc6a20a	1.39649

Slco3a1	2.96092
Smad1	2.25849
Smad4	1.72925
Smad6	1.58806
Smad7	2.62724
Smarca2	2.02346
Smo	2.51753
Smurf1	2.47057
Snx10	1.38084
Socs2	1.67738
Sort1	2.68478
Sox13	2.52651
Sox4	2.8873
Spint2	2.51995
Spna2	2.19905
Spnb2	2.30683
Spns2	2.85566
Stat5b	1.48598
Stau2	2.55237
Steap2	2.40027
Sulf2	3.42897
Syde2	4.27837
Tbc1d16	2.12063
Tbkbp1	2.14947
Tcf7	2.34245
Tcp11l1	2.03235
Tec	2.03051
Tgif1	2.40434
Tjp1	2.5026
Tjp2	2.15596
Tm6sf1	2.1312
Tmed8	2.31789
Tmeff1	2.65362
Tmem158	2.60432
Tmem229b	2.53672
Tmem8	1.91027
Tmem98	2.2471
Tns3	2.03582
Tpd52	1.60959
Tpm2	2.44311
Tpm4	1.36508
Trim14	1.44185
Trio	2.34278
Tspan2	2.59616
Tspan5	1.90803
Ttc39c	2.70402
Tulp4	1.41992
Uap1l1	1.35795
Ubl3	1.48231

Unc13b	3.0104
Vash1	2.11324
Vat1	1.98523
Vav3	2.25623
Vim	2.3889
Vipr1	3.19434
Wipf1	1.77483
Xylt1	3.20516
Zbed3	2.77365
Zbtb16	3.04578
Zbtb42	2.98786
Zdhhc8	2.53715
Zfp105	2.49563
Zfp358	2.32256
Zfp516	2.38026
Zfp608	2.49227
Zfp623	2.49968
Zfp703	1.68371
Zfp710	2.14146
Zfp777	2.64552
Zfp827	2.25219
Zkscan17	2.07478
Zmiz1	1.49095

Table S3. Genes contained in the Mtf2-PRC2 HSPC-specific gene regulatory network

Gene Name	log2 Fold Change
1110032F04Rik	0.596984
1700019N12Rik	2.77822
1700025G04Rik	0.369169
1700054N08Rik	0.42941
2010107G23Rik	1.38476
2810025M15Rik	0.345494
3830403N18Rik	1.12636
4732471D19Rik	0.579762
4933439C10Rik	0.613551
8430427H17Rik	0.327769
Abcb1b	1.00875
Abcg1	0.69361
Adam15	0.416335
Adam23	1.4927
Adap1	0.50235
Adcy3	0.93569
Agap2	0.669611
Ahnak	0.565285
Aim1	0.637959
AK129341	0.933629
Ank1	0.510119
Ankrd13b	0.701277
Ankrd44	0.884323
Anks6	2.00874
Apba1	1.46999
Apcdd1	0.883579
Arf3	0.158787
Arhgap26	0.496678
Arhgap31	0.410187
Arl4c	0.380435
Ascl2	1.00915
Atf3	0.44565
Atp11a	1.10246
Atp8b2	0.393437
Atrnl1	0.310991
B4galnt1	0.988442
B4galnt4	0.69906
B4galt4	0.453143
B4galt6	1.27871
Bahcc1	0.226768
Bahd1	0.462717
Baiap3	0.94305
BC005764	0.949485
Bcl2	0.746562
Bcl2l11	0.434143

Bcr	0.122189
Bend4	1.1622
Bend5	1.06281
Blvrb	0.265401
Bmi1	1.13201
Bsn	0.531578
Cables1	0.995651
Cacnb2	0.592766
Camkv	1.39891
Casz1	1.01739
Cbfa2t3	0.678457
Cbfb	0.452824
Cbr3	1.93485
Cbx4	0.353275
Cbx7	1.19188
Ccdc102a	0.527193
Ccdc109b	1.50108
Ccnd2	1.0686
Ccno	2.49537
Cd14	1.54592
Cd63	0.269857
Cdkn1a	0.579259
Cdv3	0.235232
Cdyl2	0.541025
Cebpb	0.256051
Cebpd	0.748729
Celsr1	1.7623
Celsr2	1.31972
Celsr3	1.81852
Chrm4	1.59378
Chst15	0.390709
Clstn1	0.660526
Cmtm7	0.699628
Cnnm1	4.04667
Coro2a	0.767949
Cpne7	1.04957
Crim1	0.423279
Crtc3	0.724657
Cry1	0.286763
Csnk1e	0.38579
Csrnp1	0.436275
Ctbp2	0.483165
Cul9	0.907799
Cux1	0.45905
Cxcr4	1.24815
Cyfip2	1.03402
Dclk2	0.978662
Ddx43	2.4761
Dip2b	0.657785

Dip2c	0.584543
Dkkl1	0.881977
Dmxl2	1.12333
Dnajc6	2.09762
Dnmt3b	0.603054
Doc2a	0.429301
Dtx4	0.475136
Dusp2	0.751088
Dusp4	0.687585
Dusp5	0.473015
E130012A19Rik	1.43591
E330009J07Rik	0.83092
Ece2	0.388973
Efcab4a	0.485332
Efna2	0.827909
Efs	0.929814
Egln3	0.764725
Egr2	1.00514
Egr4	0.99284
Eid2	0.775879
Eif2c4	1.36769
Eif4e3	0.543602
Elac1	0.50967
Elavl2	3.7614
Elk3	0.383924
Emid1	0.533034
Eml5	0.540702
Epha7	0.970443
Ephb2	1.63102
Erbb2ip	0.320921
Evl	0.458179
Fam101b	0.779005
Fam113b	0.816132
Fam169a	1.00325
Fam174b	0.515297
Fam43a	0.383645
Fam49b	0.608099
Fam65a	0.543073
Fam65b	0.490141
Fam69b	0.458385
Fes	0.70904
Fgf11	0.648979
Fgf3	1.37629
Fhod3	0.808028
Filip1l	0.280555
Fjx1	1.21751
Fli1	0.376685
Flt3	1.21146
Fmnl1	0.650555

Fnbp1	0.438574
Fndc3a	0.308176
Fndc5	1.3234
Fosl1	1.44951
Fosl2	0.651031
Frmd4a	0.331996
Fzd6	1.14816
Fzd9	0.890406
Gabbr1	1.30837
Galnt12	2.31455
Galnt3	1.24459
Galnt6	0.986417
Gapdh	0.0944826
Gata2	0.647641
Gbx2	0.386211
Gfi1	1.48311
Gfod1	0.512935
Gkap1	0.400455
Gli3	1.11714
Gm1337	2.07168
Gm1673	0.542521
Gm4349	0.980659
Gnai1	0.546772
Gnal	0.47729
Gnb4	0.332264
Gpc1	1.16025
Gpr160	1.05183
Grwd1	0.263211
H2afy2	1.00865
Hcn2	1.42314
Hdgfrp3	0.890819
Hectd2	0.980415
Hmga2	0.555505
Homer2	0.847842
Hoxa6	1.32581
Hoxa7	1.30554
Hoxa9	0.931457
Hpdl	1.38219
Hsd17b1	1.26263
Hspa1a	2.10266
Hspa1b	2.24609
Hspa1l	2.04045
Hspa2	1.00043
Hspb1	2.67992
Ica1l	0.728368
Igfbp5	0.883399
Ikzf3	1.87456
Il17ra	0.642347
Il6ra	0.712239

Impdh1	0.706229
Inhbb	0.908493
Irak3	1.10207
Irf1	0.38869
Irf5	0.302046
Itpr3	0.292097
Itpripl2	0.865106
Jag2	0.833593
Jdp2	0.405326
Jmjd1c	0.584299
Jph1	0.947203
Jun	0.484493
Kcna3	0.720911
Kcnc3	1.55282
Kcng2	0.645986
Kcnip3	0.59787
Kcnj2	0.726794
Kcnk12	1.17762
Kcnmb4	1.437
Kcnq5	1.36195
Kctd1	0.671968
Kctd12	0.676143
Kif13a	0.308959
Kif17	0.699832
Klf2	0.163094
Klf4	0.885229
Klf5	1.71991
Klhl21	0.386075
L3mbtl3	0.165516
Lgi2	2.1814
Lhfpl2	0.774403
Lhx6	1.14621
Lphn1	0.407579
Lrp11	1.12671
Lrrc1	0.240115
Lysmd2	0.63978
Madd	0.428046
Man2a2	0.752346
Map3k3	0.404352
Mapk11	0.565754
Mapkapk2	0.370902
Marcksl1	0.187197
Mast1	0.722887
Mcmbp	0.274043
Mctp1	0.588014
Mdga1	0.58461
Med12l	0.201801
Megf8	0.659471
Mettl1	0.340137

Mex3b	0.365706
Mfsd4	0.557911
Micall1	0.281827
Mier3	0.468162
Mllt6	0.773713
Mmp17	1.22561
Mmp28	1.12042
Mms19	0.417277
Msrb3	0.607406
Mtap1b	0.495067
Mtus1	0.695283
Myb	0.85959
Myo5a	1.09997
Myst4	0.432182
Nanos1	0.845025
Nat8l	1.29607
Nbea	0.5106
Ncoa1	0.25129
Ncoa2	0.481854
Ncs1	0.795252
Nefh	1.72804
Nes	0.352939
Nfatc1	0.451266
Nfil3	0.755334
Nfix	0.629524
Nfkb1	0.434788
Nfkbiz	0.337247
Nin	1.08689
Nkain1	1.11868
Nlgn2	0.666181
Notch1	0.513861
Notch3	0.627827
Nova1	1.5628
Npas1	1.73812
Nptxr	1.79769e+308
Npy	1.79769e+308
Nr4a2	0.74805
Nrarp	0.551525
Nrbp2	0.899849
Nrg2	1.23467
Nt5c2	0.495974
Ntn4	1.2038
Ntng2	1.60532
Nuak2	0.571893
Odf3b	1.16503
Olfm1	0.6521
Otud1	1.07967
P2ry2	0.922423
Paqr4	0.253776

Paqr8	0.545977
Parp14	0.927319
Parp8	0.974325
Pde4a	0.632341
Phactr2	0.324479
Phf15	1.07084
Phf21b	1.84552
Pik3ip1	1.41646
Pitpnm1	0.706809
Plcg1	0.533299
Plec	0.803119
Plekha2	0.618317
Plekhh1	0.330875
Plk2	0.319541
Plxdc1	2.08472
Plxna1	0.381676
Plxnc1	0.455638
Plxnd1	0.222949
Pparg	0.681406
Ppargc1b	0.814351
Ppig	0.561982
Ppm1e	0.4322
Ppm1h	0.758569
Ppp3cc	0.719213
Ppp4r1	0.251529
Prdm9	0.312765
Prkd3	0.326617
Prss16	1.25827
Psd	0.473372
Pstpip2	0.227297
Ptger3	0.713511
Ptpn14	0.63956
Ptprn	0.558288
Ptprs	0.428869
Ptpru	2.21125
Pus3	0.368762
Rab15	2.11025
Rab31	0.679957
Ranbp9	0.287819
Rasa2	0.7738
Rasal2	0.532698
Rasd1	1.03206
Rasd2	1.63336
Rassf5	0.695487
Rcor2	0.514247
Rcsd1	0.731331
Rel	1.05967
Rftn1	0.56606
Rgs7bp	0.495686

Rin3	0.671186
Rnf130	0.294703
Rnf144a	0.765027
Rnf150	0.604639
Rnf208	1.11221
Rnf216	0.338675
Rnf217	0.79814
Rnf220	0.451419
Rps6ka1	0.595918
Rsrc1	0.448381
Runx2	1.41943
Rusc1	0.404922
Sap30l	0.213704
Satb1	0.797058
Sema6b	0.682575
Serpine2	0.173573
Sestd1	0.949066
Sfmbt2	1.77756
Sfn	0.781225
Sgcb	0.515546
Sh2d5	0.937009
Sh3pxd2b	0.26831
Sh3rf1	0.390657
Shank3	0.496008
Sirpa	0.449951
Slc12a2	0.725834
Slc23a2	0.600916
Slc26a10	0.723476
Slc7a8	0.307971
Slc9a5	0.852114
Slco3a1	1.09556
Slmo1	1.06962
Smad4	0.265071
Smarca2	0.476499
Smo	0.263279
Snx18	0.142227
Socs2	1.28736
Sort1	0.343392
Sox4	0.936409
Sp9	0.479714
Spns2	0.453645
Spred3	0.739581
St14	1.41206
Stat5b	0.239446
Stx3	0.830399
Syde2	0.362441
Sync	0.618353
Syncrip	0.602443
Tbc1d30	0.669889

Tbkbp1	0.544675
Tdrd5	1.96615
Tgif1	0.3816
Tipin	0.373334
Tm6sf1	0.931424
Tmed8	0.750263
Tmeff1	0.605613
Tmem229b	0.781929
Tmem8	0.35631
Tnrc18	0.549027
Tns1	0.300917
Trib1	0.35129
Trps1	0.836957
Tspan5	0.658671
Tulp4	0.323828
Txndc16	0.542034
Ube2j1	0.302122
Unc13b	1.09969
Unc5a	1.6913
Uncx	-1.79769e+308
Vash1	0.29301
Vash2	1.37813
Vat1	0.463774
Vav3	0.459758
Vim	0.465586
Wipf1	0.363252
Xylt1	1.36716
Zbed3	0.45356
Zbtb10	0.657627
Zbtb16	1.04427
Zc3h12c	0.526073
Zdhhc2	0.687817
Zfp277	0.191121
Zfp318	0.364284
Zfp516	0.293717
Zfp521	0.802465
Zfp580	1.22001
Zfp608	0.741005
Zfp664	0.337144
Zfp703	0.564838
Zfp704	0.800308
Zfp777	0.540296
Zkscan17	0.4531
Zmiz1	0.793909
Zmynd11	0.183295
Zswim5	1.31019
0610010O12Rik	-2.2915
1110067D22Rik	-0.600458
1300014I06Rik	-2.08462

1600021P15Rik	-0.91287
1810027O10Rik	-0.328309
2510009E07Rik	-0.549331
2610109H07Rik	-0.902282
2700046G09Rik	-0.939663
2810030E01Rik	-1.30671
2810055F11Rik	-1.26008
2810459M11Rik	-2.926
4430402I18Rik	-2.75717
4930420K17Rik	-1.10412
5430407P10Rik	-0.468623
6430548M08Rik	-0.922416
A430107O13Rik	-1.56983
Abhd6	-1.44031
Abtb2	-1.59596
Acot1	-2.135
Actn1	-0.560826
Acvr1	-1.33203
Acvr2a	-0.888228
Adap2	-1.57562
Aebp1	-1.76681
Agpat3	-0.811375
Agpat9	-1.14646
AI661453	-0.578525
Aif1l	-1.00513
Ak4	-0.811845
Akap12	-0.335693
Aldh1a2	-2.68297
Aldh5a1	-1.85767
Alox12	-1.11819
Alpl	-2.75888
Als2cl	-1.57937
Amigo1	-0.930385
Amn	-2.62025
Amotl2	-0.478197
Ank3	-0.882399
Arhgap29	-0.439193
Arhgef10l	-0.694164
Arhgef16	-2.52879
Arhgef17	-0.710594
Arhgef5	-0.721866
Arhgef7	-0.172559
Asap2	-0.252115
Asb4	-0.991551
Atp8b1	-1.68863
Atp9a	-0.798153
AU023871	-0.705808
AW555464	-1.94678
B3galnt1	-0.981768

B4galt2	-0.998777
Baiap2	-0.738836
BC057022	-1.7131
Bcar1	-1.17615
Bcar3	-2.31242
Bcl3	-0.639934
Bend6	-2.33796
Bend7	-1.68904
Bhlhe40	-1.17526
Bicc1	-2.22512
Bin1	-0.628551
Bmp1	-1.78074
Bmp7	-2.55311
Bmpr1a	-2.011
Brsk1	-0.875273
C130074G19Rik	-2.4667
C77080	-0.649904
Cacna1h	-1.44951
Cadm1	-1.88455
Cadm4	-1.15957
Camk2n1	-2.34433
Capn2	-0.852695
Car14	-2.24833
Car7	-1.16057
Card10	-1.5745
Cbs	-2.11129
Ccdc3	-1.00114
Ccdc85c	-0.498751
Cd302	-1.99079
Cd9	-0.753929
Cdc14b	-0.966983
Cdc42bpb	-0.703748
Cdc42ep1	-1.48579
Cdh1	-2.13053
Cdh2	-2.53375
Cdk18	-0.899643
Cdkn1c	-2.28354
Cebpa	-0.435223
Cgn	-2.19923
Cgnl1	-1.08765
Chpf	-0.548361
Chrd	-2.6378
Chsy3	-0.724871
Cited1	-2.84964
Ckb	-0.408499
Cldn5	-0.356232
Cmtm4	-0.617264
Cnn2	-0.209615
Cnn3	-0.426191

Cobll1	-1.88518
Col18a1	-2.47934
Col27a1	-2.22414
Col4a2	-0.181194
Colec12	-0.559063
Comp	-0.844605
Copz2	-1.42738
Cpm	-3.07767
Cpne2	-0.554059
Crb3	-2.48345
Ctsf	-0.447199
Cttnbp2nl	-0.390021
Cuedc1	-0.704119
Cux2	-0.875737
Cxcr7	-0.810065
Cxxc5	-0.699861
Cyr61	-2.95116
Cys1	-2.32961
D730039F16Rik	-3.06529
D8Ertd82e	-1.29132
Dab2ip	-0.582907
Dact2	-1.54169
Dag1	-0.823578
Dapk1	-0.695258
Dcbld2	-0.759595
Dcdc2a	-2.50584
Ddr1	-1.16649
Dennd5b	-1.81403
Depdc7	-1.87676
Dio3os	-2.89594
Dlgap3	-2.29132
Dnajc22	-2.41525
Dnm1	-1.7365
Dock1	-0.274948
Dse	-0.231635
Dsp	-1.79717
Dusp14	-0.737205
Dusp22	-1.13525
Echdc3	-2.53595
Efemp2	-1.25548
Efna1	-0.414427
Elovl2	-2.62056
Enc1	-0.365207
Epas1	-0.797527
Epb4.1l1	-1.43949
Epb4.1l4b	-1.09195
Epha2	-0.896877
Erbb2	-1.4672
Erbb3	-1.4311

Errfi1	-1.68934
Esam	-0.373771
Espn	-0.838375
Esrp2	-2.30655
Exoc6b	-0.626081
F2rl1	-1.37574
Faah	-0.888341
Fam114a1	-2.16706
Fam135a	-0.902581
Fam176b	-0.954317
Fam189a2	-0.959994
Fam20c	-3.04392
Fam83f	-1.61255
Fam83h	-1.70713
Fam89a	-1.50454
Farp1	-1.53708
Fdx1	-0.198768
Fermt2	-1.79145
Fgd1	-1.52326
Fgfr3	-1.13493
Fgfr4	-2.60626
Fhl3	-0.345431
Fign	-2.24069
Fkbp5	-0.155342
Fkbp9	-0.885432
Fmnl3	-0.27896
Fn1	-2.41442
Fndc3b	-0.771403
Fndc4	-1.09697
Foxa1	-2.75146
Foxj1	-2.63608
Foxp4	-0.759905
Fras1	-3.03685
Frs3	-1.10906
Fscn1	-0.915762
Fst	-2.39323
Furin	-0.94188
Fzd1	-1.13691
Fzd4	-0.309057
G530011O06Rik	-0.869684
Gab1	-0.266176
Gata4	-0.430592
Gata6	-2.01664
Gcgr	-2.58256
Gcnt4	-1.75762
Gdf10	-0.930772
Gdf11	-1.32379
Gfra1	-2.64087
Gipc2	-2.35802

Gjb2	-0.642954
Gldc	-2.98049
Glis2	-0.755152
Gnas	-0.287089
Gp1bb	-0.750293
Gp5	-0.601997
Gpr153	-0.724439
Gpr176	-2.45341
Gprc5c	-2.21375
Gpt2	-2.04363
Gpx7	-2.16689
Grb10	-0.972009
Greb1	-1.75999
Greb1l	-1.27801
Grik4	-3.3325
Grip1	-2.21769
Gstt3	-1.28084
H1f0	-0.258608
H2-K1	-0.297418
H2-Q10	-2.63141
H2-Q6	-1.85565
H2-Q7	-2.46394
Hdac5	-0.189299
Hes1	-1.09408
Hip1r	-1.3065
Hmox1	-0.88226
Hnf1b	-2.39184
Hs3st3b1	-2.25274
Hsd11b2	-1.28916
Hunk	-2.26205
Icam1	-0.365517
Id2	-1.38878
Iffo2	-0.869794
Igdcc4	-2.20758
Igf2	-2.33257
Igf2as	-2.05203
Igfbp2	-1.62442
Igfbp4	-0.545574
Igfbp6	-1.69227
Igsf9	-1.37119
Ihh	-2.69226
Inadl	-1.28543
Inf2	-0.241028
Irf6	-1.4059
Irs1	-2.26733
Itga1	-0.624684
Itga3	-2.37588
Itga5	-0.751996
Itgb5	-1.56415

Itpka	-1.8873
Itsn1	-1.30259
Jazf1	-0.643945
Jub	-1.24772
Kank1	-1.96149
Kcp	-1.03428
Kctd17	-0.544356
Kdelc2	-0.802333
Kdr	-0.160344
Kif1b	-0.337264
Kif1c	-1.56803
Kif21a	-0.501497
Kifc3	-0.954244
Kras	-0.194885
Lamc1	-0.394987
Laptm4b	-0.661718
Ldlrad3	-0.393562
Lepre1	-0.648898
Leprel4	-1.18353
Lgr4	-0.933382
Lhx2	-1.29692
Lifr	-2.35499
Lmo7	-2.19747
Loxl2	-1.65576
Lpgat1	-0.398501
Lpp	-1.13897
Lrfn4	-0.367592
Lrig1	-1.31904
Lrp3	-1.52013
Lrp4	-0.896232
Lrp5	-0.805278
Lrrc16a	-1.14905
Ltb4r2	-0.781216
Maf	-0.306843
Mafb	-0.578295
Maff	-0.47275
Magi3	-0.88031
Map4k3	-0.949055
Map4k4	-0.0804581
Mapk8ip1	-1.1428
Mapre3	-1.24748
Marcks	-1.14222
Mark1	-0.804753
Marveld1	-0.237433
Mcc	-2.4326
Meis2	-0.720401
Mfap3l	-0.619793
Mfhas1	-0.85094
Mgat3	-2.64966

Mixl1	-2.58141
Mllt4	-0.881936
Mmp14	-1.37592
Mmp15	-0.747341
Mocos	-1.97444
Mras	-1.66979
Mreg	-2.05425
Msi1	-2.19767
Mtmr7	-1.36139
Mtss1l	-0.583303
Myo10	-0.446821
Myo1b	-1.51348
Myo1e	-1.18275
Myo5b	-2.32649
Nab1	-0.326125
Nab2	-0.80577
Nacc2	-0.842013
Nags	-1.19252
Nav2	-1.32999
Ncald	-1.94608
Ndrg1	-2.19424
Nedd4l	-0.349076
Nek6	-1.35027
Neo1	-1.16757
Nfib	-0.950236
Nfic	-0.659077
Ngef	-2.72262
Ngfr	-1.06318
Nlrp6	-2.24029
Nodal	-2.49865
Npdc1	-0.649516
Npnt	-0.814056
Npr1	-0.361481
Nr2f1	-1.06231
Nr2f2	-0.809823
Nr2f6	-1.68335
Obsl1	-0.604909
Ocln	-1.99402
Onecut1	-2.31137
Onecut2	-1.81614
Oxr1	-0.188432
P4ha3	-1.75737
Pacsin3	-2.15112
Paqr9	-2.25491
Pard3	-2.57201
Pard6b	-0.739786
Parp12	-0.332405
Pawr	-0.373118
Pax2	-3.41668

Pcdh1	-2.19348
Pcolce2	-2.88624
Pcp4l1	-1.46594
Pcsk6	-1.16322
Pcsk9	-2.82373
Pde4dip	-1.22795
Pde5a	-0.410425
Pdgfra	-0.957908
Perp	-0.554769
Pfn2	-1.46251
Phldb1	-0.431009
Phldb2	-1.58473
Pkd2	-0.3658
Pkdcc	-1.42505
Pkp2	-1.86074
Pkp4	-0.200344
Plbd1	-0.824361
Pld2	-1.50299
Plekha1	-0.62097
Plekhg3	-0.861942
Plekhg6	-1.90819
Pllp	-1.80045
Pls1	-1.11469
Pltp	-0.743093
Plxna4	-0.428415
Plxnb1	-2.5585
Plxnb2	-1.12768
Ppl	-2.64512
Ppp4r4	-2.11769
Prkaa2	-1.22907
Prkar2a	-0.240627
Prkca	-0.19874
Prkcz	-1.33992
Prox1	-2.2199
Prph	-1.42289
Prss23	-1.47343
Ptgfrn	-2.22699
Pth1r	-2.37999
Ptms	-1.38118
Ptpn21	-0.837539
Ptprf	-2.02411
Ptprg	-1.54026
Ptrf	-0.277066
Pvrl1	-1.00279
Pvrl3	-1.67235
Rab11fip3	-0.606343
Rab11fip4	-0.636126
Rab20	-0.83305
Rab27b	-0.340571

Rab34	-0.518528
Ramp2	-0.388349
Rap2a	-0.326091
Rapgef4	-1.84614
Rapgefl1	-1.0555
Raph1	-1.58439
Rarres1	-1.79699
Rasgrp2	-0.199974
Rasl10b	-2.35882
Rasl11b	-1.18747
Rbfox2	-1.52367
Rbm47	-1.71843
Rbpms	-0.943137
Rbpms2	-0.606206
Reep2	-0.421728
Rgl1	-0.795305
Rhbdf1	-1.00091
Rhobtb1	-1.16916
Rhoc	-1.26181
Rhod	-1.88681
Rhou	-0.969977
Rims2	-1.4908
Rras2	-0.562681
Rtkn	-0.785626
Rtn2	-0.583342
Rtn4rl1	-1.67999
Sall1	-2.47807
Sall4	-2.89074
Sbf2	-0.814504
Scamp5	-0.932592
Scube3	-1.30425
Sdc1	-1.28419
Sdc3	-0.298434
Sdk1	-2.45797
Sec14l2	-2.30678
Sec24d	-0.892654
Sema4g	-2.53791
Sema6d	-0.322443
Sesn3	-0.660978
Sfmbt1	-0.483785
Sfrp1	-1.04323
Sgk1	-0.329237
Sgms1	-0.398433
Sh3bp5	-1.02537
Sh3pxd2a	-0.857581
Shisa3	-0.895602
Shroom1	-1.69083
Siah2	-0.32899
Six2	-4.07868

Six5	-0.579251
Ski	-0.414604
Slc16a12	-2.61672
Slc25a23	-0.845827
Slc25a33	-0.888545
Slc27a2	-2.70614
Slc30a3	-1.28457
Slc37a3	-1.48118
Slc38a3	-2.27257
Slc44a1	-0.907575
Slc4a4	-2.55211
Slc6a4	-0.910246
Slc9a3r2	-0.667777
Smad1	-0.542056
Smagp	-0.896806
Smarcd3	-0.327007
Smpdl3b	-1.15403
Snai1	-1.43468
Snta1	-1.38834
Snx21	-0.817766
Snx24	-1.68712
Socs3	-1.113
Sox13	-0.618662
Spats2	-0.727632
Spats2l	-1.55493
Speg	-2.33201
Spna2	-0.18607
Src	-0.761818
Srgap1	-0.548641
Steap2	-2.46627
Synj2	-1.60918
Synpo	-1.46085
Syt12	-2.04064
Syt7	-1.01617
Tbx3	-2.30395
Tcea3	-2.50946
Tcf7l1	-1.34735
Tcf7l2	-0.952843
Tead1	-1.4315
Tead2	-1.17067
Tgfa	-1.39635
Thpo	-2.14067
Thrb	-2.18315
Tjp1	-0.916755
Tjp2	-0.3634
Tle2	-1.0338
Tmcc3	-1.59239
Tmem150a	-2.49937
Tmem150c	-2.27276

Tmem158	-0.77891
Tmem22	-0.946511
Tmem30b	-2.31328
Tmem54	-2.0183
Tmie	-2.64622
Tpm1	-0.295641
Tpm2	-0.791412
Tpm4	-0.578644
Trim71	-2.16276
Trpc1	-0.760216
Tsc22d1	-1.02916
Tsku	-1.01678
Tspan18	-0.78669
Ttc39c	-0.787891
Ttll11	-1.37154
Ttpa	-0.960743
Tubb2b	-0.503512
Tubb6	-1.27444
Ube2ql1	-2.51699
Ubl3	-0.190878
Ulk2	-0.232659
Vav2	-0.502284
Vldlr	-2.28492
Wtip	-0.52073
Wwc1	-2.36215
Wwtr1	-0.546361
X99384	-1.57704
Xlr	-2.09493
Yap1	-2.00591
Yes1	-1.06119
Zcchc14	-0.741352
Zfp385b	-2.1479
Zfp395	-0.269615
Zfp623	-0.48409
Zfp651	-1.56819
Zyg11a	-1.94094

Table S4. Primer List

PRIMER SEQUENCE	GENE	DIRECTION
CTGCCCGGACGGACTGATAA	Myb	Forward
CGTCTGGCTGGCTTTGGAAG	Myb	Reverse
CACCGTGCTGTGGGACAATG	Stat5b	Forward
TGTGCCAGGAACACGAGGTT	Stat5b	Reverse
GCCTAGCAAACCCTGGGAGT	Fli1	Forward
CACCTCATCAGGGTCCGTCA	Fli1	Reverse
CATCAGGTGAACCGCCCACT	Gata1	Forward
GCTGCTACCAGCTACCACCA	Gata1	Reverse
CCCGCAACTAGAGGGACAGG	Tal1	Forward
GCCGTTGAGCAGGACTAGGT	Tal1	Reverse
GAGTCGTGCAGCACACCAAG	Crebbp	Forward
TGTTGAGGCAGAAGGGCACA	Crebbp	Reverse
TGATGCCATGGCTGACTGGT	Cxcr4	Forward
GACGCCCACATAGACTGCCT	Cxcr4	Reverse
ATTCAGAGCCACAGGCACCA	Cdkn1a	Forward
ATGAGCGCATCGCAATCACG	Cdkn1a	Reverse
TGGACCAAATGCCTGACTC	Cdkn1b	Forward
GGGAACCGTCTGAAACATTTTC	Cdkn1b	Reverse
GTCTGATGGAGAAGCTGATGG	Spi1	Forward
AGATGCTGTCCTTCATGTCG	Spi1	Reverse
GCACCTGACTGATGCTGAGAA	β1-globin	Forward
TTCATCGGCGTTCACCTTTCC	β1-globin	Reverse
TGGCCTGTGGAGTAAGGTCAA	εY-globin	Forward
GAAGCAGAGGACAAGTTCCCA	εY-globin	Reverse
CAAGCGGTCTCCTTTACGTC	Mtf2	Forward
CCATTTCATTGGGAGCTTCT	Mtf2	Reverse
AGTGACTTGGATTTTCCAGCAC	Ezh2	Forward
AATTCTGTTGTAAGGGCGACC	Ezh2	Reverse
AACTCGAAATCTTATCGCACCAA	Suz12	Forward
TGCAAATGTGCAGACAAGCTAT	Suz12	Reverse
CATGACCCAGAACTTTTGTGAA	Ezh1	Forward
GACAACCAGGAAAGCGATTC	Ezh1	Reverse
GAAGGCGGTAAATGGGCTTCT	Jarid2	Forward
TCGTTGCTAGTAGAGGACACTT	Jarid2	Reverse
ACCGCCACCACCTACTACAC	E2f1	Forward
CCTCCAGGTCCAACTTCCTT	E2f1	Reverse
ATGCTGTCAGTATTGAGAGTGGC	Eed	Forward
GAGGCTGTTCACACATTTGAAAG	Eed	Reverse
ACGGCGCAACCTACAAAGAG	E2f2	Forward
GTCTGCGTGTAAAGCGAAGT	E2f2	Reverse
TTTTCTGAGCCACATAAAAGGGG	E2f8	Forward
CTTCCTTGGGCTTGGTTGGT	E2f8	Reverse
GCCAGACCTTGGAAACCTCA	Dnmt3b	Forward
TTGTTTCCTGAAAGAAGGCCC	Dnmt3b	Reverse
ATGGCTGCCACTCGATATGAA	Cdk4	Forward

TCCTCCATTAGGAACTCTCACAC	Cdk4	Reverse
TTTCAGATGGCCCTTACCTCG	Cdk6	Forward
GAACTTCCACGAAAAAGAGGCT	Cdk6	Reverse
GGGACAGCCAAGTCTGTTATG	p53	Forward
GGCAGAATAGCTTATTGAGGGG	p53	Reverse
AAGGATGGCGTCAAGTACCAA	Gata2	Forward
TATCGGGTGGTGTGTTGCAG	Gata2	Reverse
CGTCCTAGTAAGCACTCGCA	Reln	Forward
AGGGACACATTGTACGCTGG	Reln	Reverse
AGGTCGGTGTGAACGGATTTG	Gapdh	Forward
TGTAGACCATGTAGTTGAGGTCA	Gapdh	Reverse
TCCTCCTCAGACCGCTTTT	Hprt	Forward
CCTGGTTCATCATCGCTAATC	Hprt	Reverse
Genotyping		
GACACCATAACCAGGACAGCTT	Mtf2	Forward
GGAACTTCGGAATAGGAACTTCGG	Mtf2	Reverse
TCAGAAGCTCAAGCCAGACAAGAC	Mtf2	Reverse
ChIP-qPCR		
CTTACCTTGGATATGGAGCTGG	Gata2	Forward
TTTGTGTACTCAGAAGGCAGAG	Gata2	Reverse
GGGCGAAGTTTCTCCGG	Myb	Forward
CTCCTCCTTCTCCTCCTTCTC	Myb	Reverse
CAGCCAACACATCTAAACACAG	Stat5b	Forward
GTGAGCAGTGAACGAGTGTAG	Stat5b	Reverse
CTCGTAGCCCCTTCAGATTAG	Fli1	Forward
AGTTTCATCCGGTTAACTGTCTC	Fli1	Reverse
TTGGGAATCAAGACTGACCTG	Gata1	Forward
ATCACCCTGAACTCGTCATAC	Gata1	Reverse
CTGGGTGTTGAGATACGGAAA	Tal1	Forward
GCCGTTGTCTAGCCTCTTAAG	Tal1	Reverse
CCCAGAAGGGAAACGATTTT	Lhx1	Forward
GACAGTTTGGGTGGGAGCTA	Lhx1	Reverse
TCCATGCAGTAGCCAGTGAG	Klf1	Forward
TCCTCCTTGAGCAGAAGAGC	Klf1	Reverse
AACTGCCGGTACTGCTCACT	E2F4	Forward
CCAGGGTATCTGGTGCAACT	E2F4	Reverse
CGTATTAGGTCCATCTTGAGAGTAC	Actb	Forward
GCCACGATTATTGTAGGCGTGATCGTAGC	Actb	Reverse
CAGAGCATGGTGTAGGAGCA	Oct-4	Forward
GCTGGCGGAAAGACACTAAG	Oct-4	Reverse
GTACCCCATCAGTTGACTTGAG	Dnmt3b	Forward
TTGATCTTTCCCCACACGAG	Dnmt3b	Reverse
GGACTTTATGAGGGTACTGGC	Dnmt3a	Forward
GATGTCCCTCTTGTCACTAACG	Dnmt3a	Reverse
GACCTACTTGAGAGCATCCAG	DNMT1	Forward
TTCCCTTTCCCTTTGTTCCC	DNMT1	Reverse
Methyl-qPCR		
CACAGAGTCTGAGAGTTTGGG	MST1-CpG1	Forward
TTAAGGGCACGCATCCG	MST1-CpG1	Reverse

TCTTCGGCTTTCTGACTTCTG	MST1-CpG2	Forward
ACTGCCTCAATGCTCCATC	MST1-CpG2	Reverse
CAGGGATAGTGAACAGGATGC	MST2-CpG1	Forward
CTCACTCTGGTAGCAAGACATC	MST2-CpG1	Reverse
shRNA	**Gene**	**Type**
GCCTTTACTTTCAACATCAAAGTGGCTAG	DNMT1	Knock Down
ATATGGCTACCGTCTTCGTTCAACATAGA	DNMT1	Scramble
AACAAGGAAGTGCTGTATGAGCTCATTGA	TAZ	Knock Down
ATGGTTATCGACGATGCGATATAACGAAG	TAZ	Scramble

Table S5. Clinical characteristics of responders Vs non-responders within local AML cohort

	Responder (n=20)	Non-responder (n-12)
Median age (years) [range]	57.3 [28.2-71.1]	62.7 [22.4-67.9]
WBC at diagnosis [range]	11.2 [1.4-138.4]	5.5 [0.7-122]
Median bone marrow blast % at diagnosis [range]	90 [29-100]	71.5 [22-95]
Cytogenetic Risk group Favorable/intermediate/adverse	7/12/1	2/5/5
MTF2 Basal/low	14/6	1/11
% Complete remission	100	0
# alloHCT	5	9
# deaths	7	11
Median overall survival (days)	771 [149-1951]	322 [41-972]

Table S6. Clinical characteristics of MTF2 Basal Vs MTF2 Low patients within local AML cohort

	All (n=32)	MTF2 Basal (n=15)	MTF2 Low (n=17)
age	58.4 [22.4-71.1]	58.8 [28.2-68]	56.1 [22.4-71.1]
WBC at diagnosis [range]	8.05 [0.7-138.4]	10.8 [1.4-138.4]	5.5 [0.7-122]
Median bone marrow blast % at diagnosis [range]	85 [22-100]	85 [29-100]	85 [22-95]
Cytogenetic risk group (fav/inter/adverse)	9/17/6	5/10/0	4/7/6
Response to first induction n(%)	20 (62.5)	14 (93.3)	6 (35.3)
# alloHCT (%)	14 (43.8)	7 (46.6)	7 (41.2)
# of deaths (%)	18 (56.3)	6 (40)	12 (70.6)
Died from leukemia n(%)	15 (46.7)	3 (20)	12 (70.6)
Median Overall Survival (days)	729 [41-1951]	1548 [41-1951]	519 [53-1030]

Table S7. Clinical data of patients belonging to local cohort

Patient #	age at diagnosis	date of diagnosis	WBC at diagnosis	% bone marrow blasts at diagnosis	molecular	genetic risk group	treatment	responder	MTF2 status	H3k27me3 Status	BMT (y/n)	date of BMT	date of relapse	date of death	date of last f/u	OS	dead/alive (1/0)	cause
1	63.0	15-Dec-11	114.6	69	-y, add(14)	inter	I	y	b	b	y	22-Dec-14	17-Sep-14	11-Mar-16	11-Mar-16	1548.0	1	other
2	60.6	23-Apr-14	18	95	del(11)	inter	I	y	b	b	y	15-Oct-14	n/a	15-Jul-16	15-Jul-16	814.0	1	other
3	22.4	30-Jun-14	4.2	95	11q23	adverse	I	n	L	L	y	02-Oct-14	n/a	11-Mar-15	11-Mar-15	254.0	1	leuk
4	66.1	05-Nov-12	10.8	95	del(13)	inter	I	y	b	b	y	04-Apr-13	n/a	n/a	21-Nov-16	1477.0	0	n/a
5	62.6	13-Jun-11	5.3	95	-7	adverse	I	n	L	L	n	n/a	1-Nov-11	27-Nov-11	27-Nov-11	167.0	1	leuk
6	28.2	29-May-14	113.6	70	inv(16)	fav - cbf	I	y	b	b	n	n/a	n/a	n/a	21-Mar-17	1027.0	0	n/a
7	56.1	25-May-12	6.9	30	complex	adverse	I	n	L	L	n	n/a	n/a	17-Jul-12	17-Jul-12	53.0	1	leuk
8	31.9	15-Oct-12	122	80	npm	fav - npm	I	n	L	L	y	31-May-13	4-Sep-13	14-Sep-13	14-Sep-13	334.0	1	leuk
9	41.4	13-Mar-14	1.2	90	t(15;17)	fav -apl	I	y	L	L	n	n/a	n/a	n/a	06-Jan-17	1030.0	0	n/a
10	59.5	23-Oct-12	2.6	33	normal	inter	I	y	b	L	y	02-May-13	3-Oct-13	27-Feb-14	27-Feb-14	492.0	1	leuk
11	71.1	16-Jul-13	2.4	50	normal	inter	I	y	L	L	n	n/a	15-May-14	15-Jul-15	15-Jul-15	729.0	1	leuk
12	65.5	06-Jul-12	5.7	40	complex	adverse	I	n	L	L	n	n/a	n/a	23-Feb-13	23-Feb-13	232.0	1	leuk
13	66.2	27-Jun-11	12	85	normal	inter	I	n	L	L	y	28-Feb-12	n/a	23-Jun-03	23-Jun-13	727.0	1	leuk
14	50.5	12-Sep-11	15.5	90	npm	fav - npm	I	y	L	L	n	n/a	22-Sep-12	12-Feb-13	12-Feb-13	519.0	1	leuk
15	58.8	08-Nov-11	1.9	85	npm	fav - npm	I	y	b	b	n	n/a	n/a	n/a	12-Mar-17	1951.0	0	n/a
16	64.5	22-Jul-13	57	90	npm	fav - npm	I	n	L	L	n	n/a	n/a	12-Jan-15	12-Jan-15	539.0	1	leuk
17	51.1	25-Oct-12	11.5	90	npm	fav - npm	I	y	b	b	n	n/a	n/a	n/a	22-Feb-17	1581.0	0	n/a
18	34.2	16-May-11	9.2	70	t(6;22)	inter	I	y	b	b	y	07-Sep-11	n/a	n/a	21-Feb-16	1742.0	0	n/a
19	52.1	10-Jul-12	4.1	22	complex	adverse	I	n	L	L	y	13-Dec-12	9-Jul-14	15-Aug-14	15-Aug-14	766.0	1	leuk
20	67.9	20-Dec-13	3.4	26	del(12)	inter	I	n	L	L	y	05-Jun-14	6-Jul-14	26-Oct-14	26-Oct-14	310.0	1	leuk
21	29.5	21-Nov-13	2.1	95	-y	inter	I	y	b	b	y	26-Mar-14	n/a	n/a	19-Dec-16	1124.0	0	n/a
22	68.0	25-Nov-13	14.6	68	inv(16)	fav - cbf	I	y	b	b	n	n/a	n/a	n/a	27-Mar-17	1218.0	0	n/a
24	32.9	16-Jun-15	26	90	normal	inter	i	y	L	L	y	06-Nov-15	n/a	n/a	20-Mar-17	643.0	0	n/a
31	62.9	26-May-15	0.7	63	normal	inter	i	n	L	L	n	n/a	n/a	25-May-16	25-May-16	365.0	1	leuk

32	46.1	29-May-15	2.7	38	t(8;21)	fav - cbf	i	y	b	b	n	n/a	n/a	n/a	29-Nov-16	550.0	0	n/a
23	42.1	14-Mar-16	81.3	95	del(5q)	adverse	I	y	L	L	y	04-Aug-16	n/a	n/a	06-Mar-17	357.0	0	n/a
25	69.8	26-Sep-16	17.5	86	add(2)	inter	i	y	L	L	n	n/a	n/a	n/a	22-Mar-17	177.0	0	n/a
26	57.9	11-Mar-16	1.4	90	add(15)	inter	i	y	b	b	y	aug 3 2016	n/a	n/a	13-Mar-17	367.0	0	n/a
27	53.5	24-Jul-14	0.8	63	normal	inter	i	n	L	L	n	n/a	n/a	n/a	19-Mar-17	969.0	0	n/a
28	68.0	11-Apr-16	138.4	100	normal	inter	i	y	b	b	n	n/a	8-Sep-16	09-Jun-16	14-Nov-16	217.0	1	leuk
29	63.8	14-Apr-16	88.6	92	-y	inter	i	n	b	b	n	n/a	n/a	25-May-16	25-May-16	41.0	1	other
30	56.7	22-Apr-16	1.8	29	normal	inter	i	y	b	b	n	n/a	30-Aug-16	18-Sep-16	18-Sep-16	149.0	1	leuk

Table S8. Clinical characteristics of TCGA AML cohort

	All (n=165)	Basal (n=83)	Low (n=82)
Median age (years)[range]	58 [18-88]	61 [22-81]	55 [18-88]
WBC at diagnosis [range]	14.3 [0.4-297.4]	11.5 [0.5-297.4]	18.9 [0.4-137.2]
Median bone marrow blast % at diagnosis [range]	73 [30-100]	64 [30-100]	79.5 [30-98]
Cytogenetic risk* group (fav/inter/adverse)	33/95/37	24/37/22	9/58/15
# alloHSCT (%)	72 (43.6)	42 (50.6)	30 (36.5)
# deaths (%)	104 (63)	44 (53)	60 (73.2)
Median Overall Survival (days)	578 [28-2859]	822 [28-2859]	335 [30-2099]

Table S9. Multivariate Overall Survival Analysis using TCGA P53 WT AML Patients

Overall Survival Covariates	Hazard Ratio (95% CI)	P- Value (calculated using Wald Test)
Age	1.040 (1.023 to 1.058)	<0.001
Adverse Cytogenetics	1.707 (1.023 to 2.848)	0.041
Favorable Cytogenetics	0.453 (0.206 to 0.998)	0.049
BM Count	1.003 (0.993 to 1.014)	0.544
MTF2 Low	1.867 (1.193 to 2.924)	0.006

Table S10. Multivariate Disease Free Survival Analysis using TCGA P53WT AML Patients

Disease Free Survival Covariates	Hazard Ratio (95% CI)	P- Value (calculated using Wald Test)
Age	1.008 (0.989 to 1.027)	0.407
Adverse Cytogenetics	0.600 (0.266 to 1.353)	0.218
Favorable Cytogenetics	0.407 (0.198 to 0.877)	0.022
BM Count	0.995 (0.983 to 1.008)	0.462
MTF2 Low	1.686 (0.976 to 2.114)	0.031

Table S11. Primer sequences

CHIP-qPCR		
GGATGATTCTGGACGACACTAC	AKT3	Forward
ACAGTGACACAACCTGGAATAA	AKT3	Reverse
CATGACCGGGTTGTACCTAAAT	FZD3	Forward
CTCTCTGTGATCCCATCTCTCT	FZD3	Reverse
CAGGCCGCGTTGTTTATTTAG	MET	Forward
GGAGAGTCACATAGCTGGTTAG	MET	Reverse
CCCTGTGCTGTGATGTGAATA	LRP2	Forward
GGTGATAGGAAGGGCAGTAAAC	LRP2	Reverse
GGCATCCACACAGCTACTAAA	GLI3	Forward
AAGCCCACATAGTGGGAATAAA	GLI3	Reverse
GAACACACCTGCAAAGGAAAC	ROCK2	Forward
CTGGCCTACTGATAGACTGAAAC	ROCK2	Reverse
Methyl-ChIP-qPCR		
AAATCGGCCAGCAAGAT	MTF2 (R1)	Forward
CGAATGGCAGCTCTCCAAA	MTF2 (R1)	Reverse
TTGGAGAGCTGCCATTCG	MTF2 (R2)	Forward
TGCCAACCGCTTCATACA	MTF2 (R2)	Reverse
RT-qPCR		
TGCCAAGCTTCTCTGTGAAAG	MDM2	Forward
TCCTTTTGATCACTCCCACC	MDM2	Reverse
AGGAAATCTTGGGCTTGATGG	MITF	Forward
TGTTGGGAAGGTTGGCTG	MITF	Reverse
CATCTACACCGACAACTCCATC	CCND1	Forward
TCTGGCATTTTGGAGAGGAAG	CCND1	Reverse
TGTCACTGTCTTGTACCCTTG	CDKN1A	Forward
GGCGTTTGGAGTGGTAGAA	CDKN1A	Reverse
GCCATCTACAAGCAGTCACAG	TP53	Forward
TCATCCAAATACTCCACACGC	TP53	Reverse
AGACCGTTTGTGTTTTGTGATG	AKT3	Forward
GAATGTAGATAGTCCAAGGCAGAG	AKT3	Reverse
CTCTGTATTTTGGGTTGGAAGC	FZD3	Forward
GGAGTATTTGGATCCCTCAGG	FZD3	Reverse
GACTCCTACAACCCGAATACTG	MET	Forward
ATAGTGCTCCCCAATGAAAGTAG	MET	Reverse
GTATCCCTCGTGCTTATGTCTG	LRP2	Forward
CTTCTCCATCACAAACCCAGT	LRP2	Reverse
TCTGTGAGCACGAAGGTTG	GLI3	Forward
TTGGGTCTGTGTAACGCTTAG	GLI3	Reverse
TGATGGTTTCTATGGGCGAG	ROCK2	Forward
TGTTCCTACAAGTGAATCCGC	ROCK2	Reverse
GGCTTTTGACTCAAGGAAACG	FLT3	Forward
TGTTTTGGTAGGTGTGAGGAC	FLT3	Reverse
TCGATGAACTAGGCAAAGACC	CDK6	Forward
AGGTGGGAATCCAGGTTTTC	CDK6	Reverse
GGTGAATCTGGGCTTATGGG	RAC1	Forward
TCAGGATACCACTTTGCACG	RAC1	Reverse
GGCTTGTTTTATCTTGGCACTATC	MTF2	Forward
TACAGACCATTTCCCCACTTC	MTF2	Reverse
CGGTAAATCCAAACTGCTATGC	EZH2	Forward
ACATACTTCAGGGCATCAGC	EZH2	Reverse
CAAGAAAAGAGCAACATGGGAG	SUZ12	Forward
AGAGGTTTGGCAATAGGAGC	SUZ12	Reverse